Theses and Dissertations

December 2017

Short Synthesis and Biological Evaluation of 5-chloro-7-benzoyl 2,3-dihydrobenzo[b]furan -3-carboxylic Acid(brl-37959) and Its Analogs.

Shamsul Arefin Ahmed
University of Wisconsin-Milwaukee

Recommended Citation

SHORT SYNTHESIS AND BIOLOGICAL EVALUATION OF 5-CHLORO-7-BENZOYL 2,3-

DIHYDROBENZO[b]FURAN -3-CARBOXYLIC ACID(BRL-37959) AND ITS ANALOGS.

by

Shamsul Arefin Ahmed

A Dissertation Submitted in

Partial Fulfillment of the

Requirements for the Degree of

Doctor of Philosophy

in Chemistry

at

The University of Wisconsin-Milwaukee

December 2017

ABSTRACT

SHORT SYNTHESIS AND BIOLOGICAL EVALUATION OF 5-CHLORO-7-BENZOYL 2,3-DIHYDROBENZO[b]FURAN -3-CARBOXYLIC ACID(BRL-37959) AND ITS ANALOGS.

by

Shamsul Arefin Ahmed

The University of Wisconsin-Milwaukee, 2017
Under the Supervision of Professor M. Mahmun Hossain

The synthesis of BRL-37959 has previously been reported. As an NSAID, the compound was tested for and found that it had very low gastric irritancy. Commercially available NSAIDs are non-selective COX inhibitors that enhance the risk of gastric, duodenal mucosal injury or erosions and ulcer problems as well as lead to nephrotoxicity. The COX-2 selective inhibitor Celecoxib (Celebrex) increases the risk of serious cardiovascular (CV) thrombotic events, myocardial infarction and stroke as well as increased nephrotoxicity. COX inhibitors are active against inflammation, pain, fever and different types of cancers. Considering the enormous potential benefits and side effects of non-selective COX inhibitors and selective COX-2 inhibitor. Our research goal was to

find a COX inhibitor that binds with both COX-1 and COX-2 in such a ratio that it would be a safer drug. Another aim was to develop a synthesis method of the target inhibitor that will be simple, cost-effective and ensure high yield. Benzofuran is an important building block of BRL- 37959. In Dr. Hossain's lab, Matt Dudley had developed a novel, unprecedented, one pot procedure to synthesize various benzofuran derivatives. We have followed the efficient, large scale potential, high yield and simple process to synthesize benzofuran. Based on the synthesis of benzofuran, we have developed a short and more cost-effective procedure for the synthesis of BRL-37959. The older method was tedious and resulted in very low yields (≤ 5%). This new method is simple and uses inexpensive starting materials, as well as giving high overall yields (62%). In enzyme screening, we found that BRL-37959 selectively binds with COX-1. We followed our improved method and successfully made some analogs with higher yield.

To

My beloved Father & Mother who always inspired me for the Ph.D.

and who passed away in 2005 and 2014, respectively.

TABLE OF CONTENTS

Page

LIST OF FIGURES

LIST OF TABLES

LIST OF SCHEMES

ACKNOWLEDGEMENTS

Introduction

Benzofuran, an important class of heterocyclic compound is present in as a core moiety in different natural products and pharmaceuticals as well as polymers. Many derivatives of benzofuran of natural and synthetic sources have biological properties such as anti-inflammatory, antimicrobial, antifungal, antihyperglycemic, analgesic, antiparasitic, and antitumor activities.[1-7] Several Non-steroidal anti-inflammation drugs (NSAIDs) possess the benzofuran scaffold such as morphine, codeine, oxycodone, BRL-37959, naltrexone and naloxone (Figure-1).

1.2. NSAIDs

NSAIDs are used mostly in the treatment of inflammation, pain, and edema, as well as of osteoarthritis, rheumatoid arthritis, and musculoskeletal disorders. Because of selectivity to cyclooxygenase (COX) enzymes, all available NSAIDs are classified into two categories. (Table-1)

1.2.1 NASIDs and their Function

NSAIDs block the active sites of both COX1 and COX2 and thus prevents prostaglandin formation. Almost all NSAIDs are non-selective and bind to both enzymes, but relieve patients from inflammation, pain, and fever as well as create gastric irritancy, ulcers and
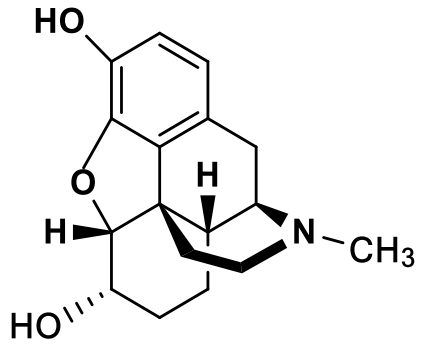
Morphine
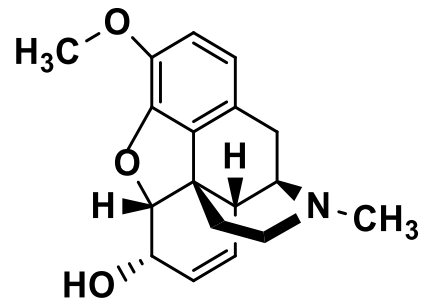
Codeine
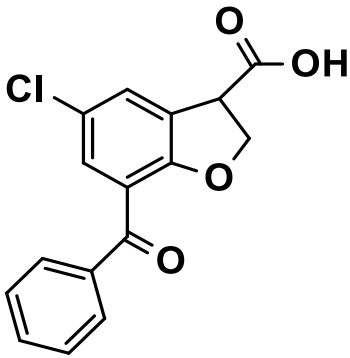
BRL-37959
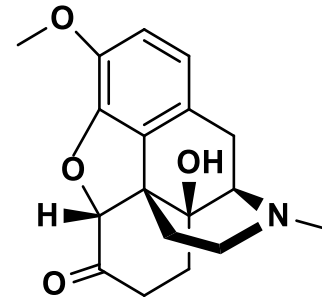
Oxycodone
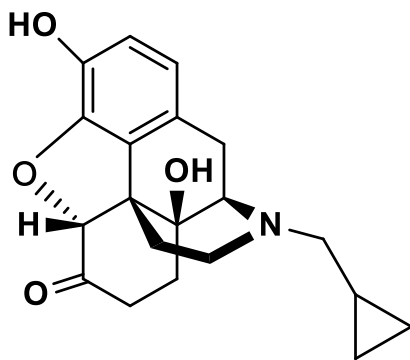
Naltrexone,
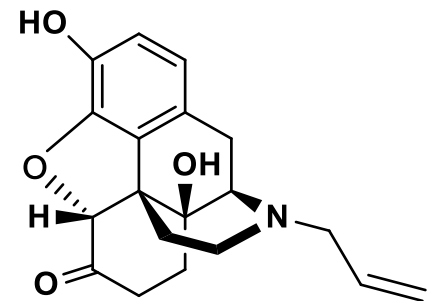
Naloxone

Figure 1- Different types of NSAIDs and Opioids.

Table 1 - Different Nonsteroidal anti-inflammatory drugs

Non-selective (COX-1 and 2) (traditional, conventional)	Selective (COX-2)
Aspirin	Celebrex (Celecoxib)
Acetaminophen	Rofecoxib
Indomethacin (Indocin)	Valdecoxib
Ibuprofen (Advil, Motrin)	Parecoxib
Naproxen (Aleve, Naprosyn)	Celecoxib
Sulindac (Clinoril)	Etoricoxib
Diclofenac (Voltaren, Cataflam)	Lumiracoxib
Piroxicam (Feldene)	Selectives (COX-2)
β- Piroxicam (Cycladol)	COXIBs
Meloxicam (Movatec)	Rofecoxib
	Valdecoxib
Ketoprofen (Profenid)	Parecoxib

renal failure over long term use. The COX, non-selective NSAIDs inhibit the secretion of prostaglandins in the gastrointestinal mucosa and produce gastroduodenitis, gastric ulcers, and digestive bleeding. Since non-selective NSAIDs block COX-1 in the gastrointestinal mucosa and they consequently inhibit the production of prostacyclin, PGE2, and PGD2 in the stomach[8-13] but cause adverse side effects. These effects prostaglandins act as cytoprotective agents of the gastrointestinal mucosa; they inhibit the acid secretion by the stomach, increase the blood flow and the production of the protective mucus. However, COX1 enzymes releases prostaglandins, prostacyclin, PGE2 and PGD2 in kidneys, dilate the vasculature, reduce the renal vascular resistance and boost the organ perfusion(Figure-2).[14] These effects lead to the redistribution of the blood flow from the renal cortex to the nephrons in the intramedullary region.[15,16]The inhibition of these mechanisms tends to decrease the total renal perfusion and rearrange the blood flow to the cortex; a

progression that ends in severe renal vasoconstriction, medullary ischemia and, under certain conditions, acute kidney failure.COX1 enzyme releases thromboxane that aggregates platelet and COX2 enzyme synthesizes prostaglandins that act as a vasodilators. This prostaglandin keeps blood vessel free from clogging. There is a dynamic balance between the platelet aggregation and vasodilation. The selective COX-2 inhibition in the heart creates a tendency to thrombosis, due to the shift in the pro-thrombotic/anti-thrombotic balance on the endothelial surface and damage of the protecting effect of the up- regulation of COX-2 in cardiac ischemia and myocardial infarction[18-20] (Figure- 3).
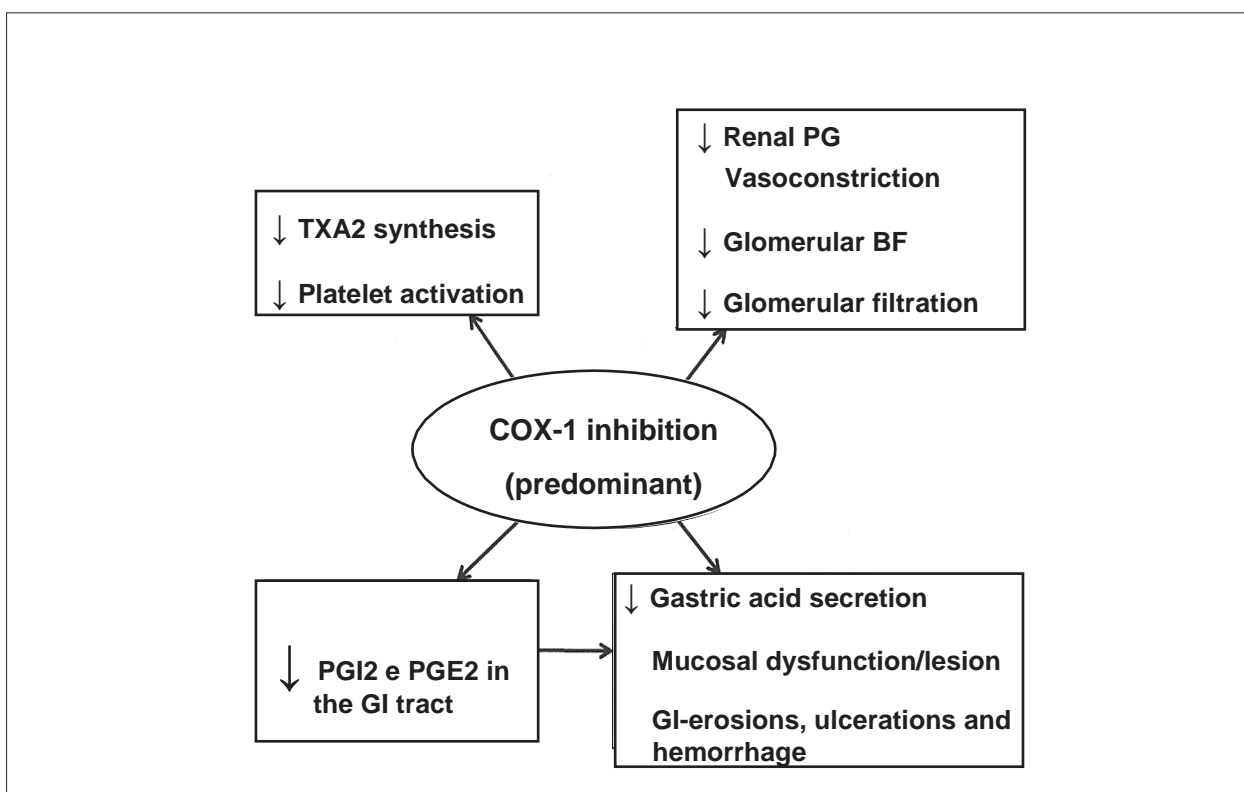
Figure 2 - Representation of the effects related to COX-1 inhibition. COX - cyclooxygenase; PG - prostaglandin; TX - thromboxane; GI - gastrointestinal.
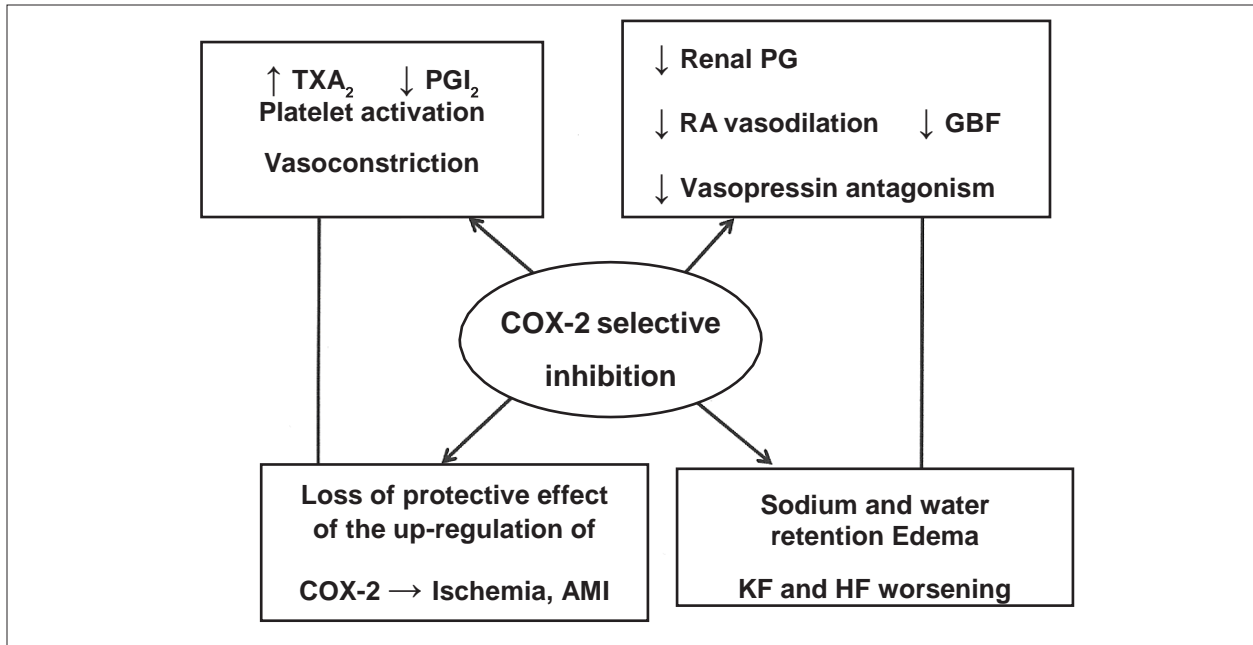
Figure 3 - Schematic representation of the effects related to COX-2 inhibition. COX - cyclooxygenase; PG - prostaglandin; TX - thromboxane; GI - gastrointestinal; RA - renal arteriole; GBF - glomerular blood flow; AMI - acute myocardial infarction; HF - heart failure; KF - kidney failure

Celebrex, the only COX2 selective inhibitor is available on the market, because of cardiovascular problems, the FDA applied restriction on its use. Moreover, at present, there are no non-opioids safe drugs for inflammation and pain.

Opioids are a group of medications that include the illegal drug heroin, synthetic opioids such as fentanyl, and prescription pain relief drugs such as oxycodone (OxyContin®), hydrocodone (Vicodin®), codeine, morphine, and many others. These drugs are chemically associated and act on opioid receptors on nerve cells in the body and brain. Chronic pain affects about 100 million people in the USA, or one-third of the U.S. population, and it is the prime reason of disability. While many treatments are recommended for pain, the number of prescription opioids has increased immensely in recent years.

1.2.2. Global market of NSAIDs

Up-to-date treatments for pain principally include non-steroidal anti-inflammatory drugs ("NSAIDs") for mild to moderate pain and opioids for moderate to severe and chronic pain. The opioids are disreputable related to tolerance and dependence, whereas safety issues with Cox-2 inhibitors, a significant class of NSAIDs, have limited their use. In 2014, the global pain management market for pharmaceuticals and medical devices was worth $36.6 billion[21] and for NSAID drugs segment was $11.4 billion in 2014[22]. An aging world population has prompted the growth in this sector, in addition to an increased incidence of obesity and osteoarthritis, as well as changing views towards pain management. Aged people are more susceptible to illness such as arthritis, joint or bone pain, epilepsy, depression, nerve damage, diabetic neuropathy, and different types of injuries due to low resistance levels. The global population of geriatrics (people aged 65 years or more) is expected to rise to 2 billion by 2050, accounting for nearly 22% of the projected global population. This demographic will lead to a substantial increase in the overall world demand for different pain management medications, thereby driving the global pain management therapeutics market[23]. Allied Market Research has estimated that the anti-inflammatory therapeutics market will reach $106.1bn, globally in 2020. In regard to product types, the global pain management drugs market is presently dominated by opioids and non-steroidal anti-inflammatory drugs (NSAIDs), whose total share was over 52% of the market's overall revenues in 2015. North America led the market, accounting for over 56% of the overall market in the same year.

1.2.3. Opioids market size and abuse

Opioids are used as anesthetics, cough suppressants, diarrhea suppressants and to reduce surgical pain, injury or trauma, cancer pain, as well as pain intensifying from other diseases. Opioids are primly used in cancer pain management and end-stage diseases in which supportive care is required. The worldwide opioids market was approximately US$ 339.24 billion in 2014.

By product, the morphine and codeine sections together accounted for around 62% of the overall market in 2014. North America was the top market for opioids, and it had approximately 65% of the revenue share in 2014, followed by Europe with around a 20% share in 2014. Some factors such as increasing palliative care facilities, reformed regulations for prescription of opioids, and increased attention of generic manufacturers towards Abuse-Deterrent Formulation (ADF) have driven the growth of the opioid market in North America and Europe. By 2021, the global opioids market revenue is postulated to be about US$ 421.6 billion.

Prescription opioid pain relievers are usually safe if used for a short time, but because they create elation in addition to pain relief, people abuse these (taken in a different way or a larger quantity than prescribed, or taken without a doctor's prescription). Logical use even as prescribed by a doctor can lead to dependence and, once misused, opioid pain relievers can lead to overdose incidents and deaths.

More than 90 people in the United States die in a day because of opioids overdose.[25] The misuse of and addiction to opioids together with prescription pain relievers, heroin, and synthetic opioids such as fentanyl is an acute national crisis that influences public health as well as social and economic welfare. The Centers for Disease Control and Prevention estimates that the total "economic burden" of prescription opioid abuse only in the United States is $78.5 billion a year, including the cost of healthcare, lost productivity, addiction treatment, and involvement of the criminal justice.[26]

In 2015, more than 33,000 persons in the united states died in the aftermath of an opioid overdose, including prescription opioids, heroin, and illicitly manufactured fentanyl, a powerful synthetic opioid.[25] Approximately 2 million people in the United States agonized from substance use disorders related to prescription opioid pain relievers, and 591,000 suffered from a heroin use disorder (not mutually exclusive) in 2015.[27] For more information about the opioid crisis:

- About 21 to 29 percent of chronic pain patients misuse prescribed opioids.[28]
- Among 8 and 12 percent build up an opioid use disorder.[29-31]
- 4 to 6 percent who misuse prescription opioids switch to heroin.[29-31]
- Roughly 80 percent of people who use heroin, first abused prescription opioids.[29]
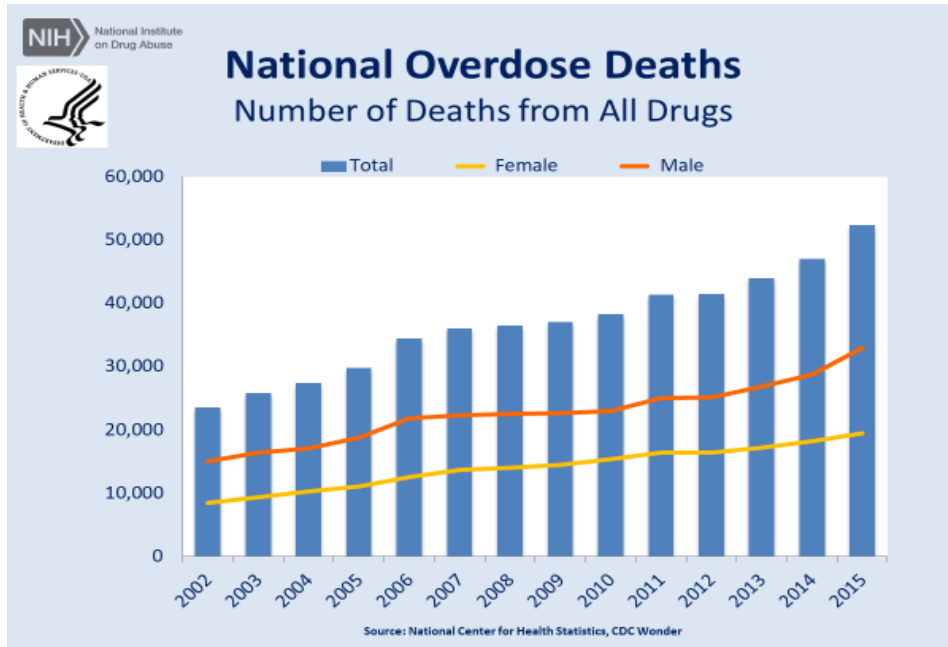
Figure 4 - National Overdose Deaths—Number of Deaths from All Drugs.
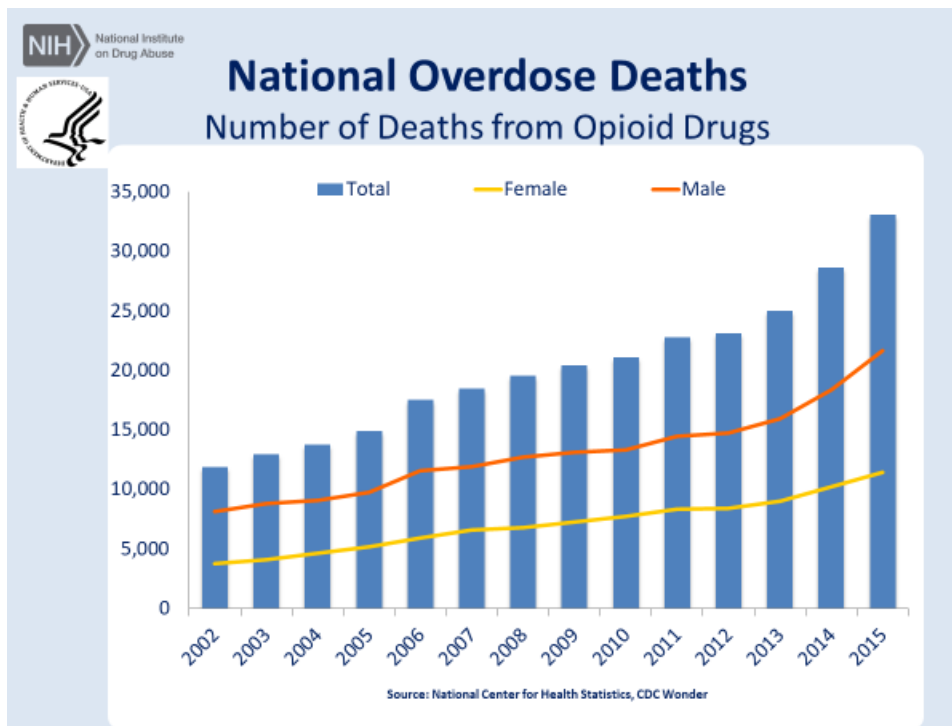
Figure 5 - National Overdose Deaths—Number of Deaths from Opioid Drugs.

Figure 6- National Overdose Deaths—Number of Deaths from Prescription Opioid
Pain Relievers (excluding non-methadone synthetics).
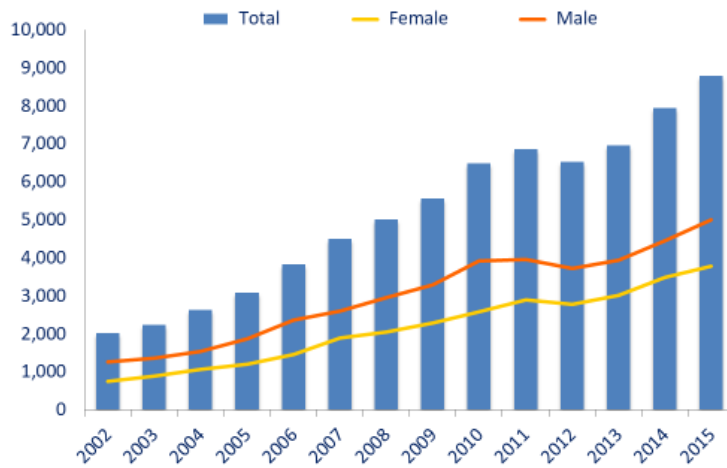
Figure 7- National Overdose Deaths—Number of Deaths from Benzodiazepines.
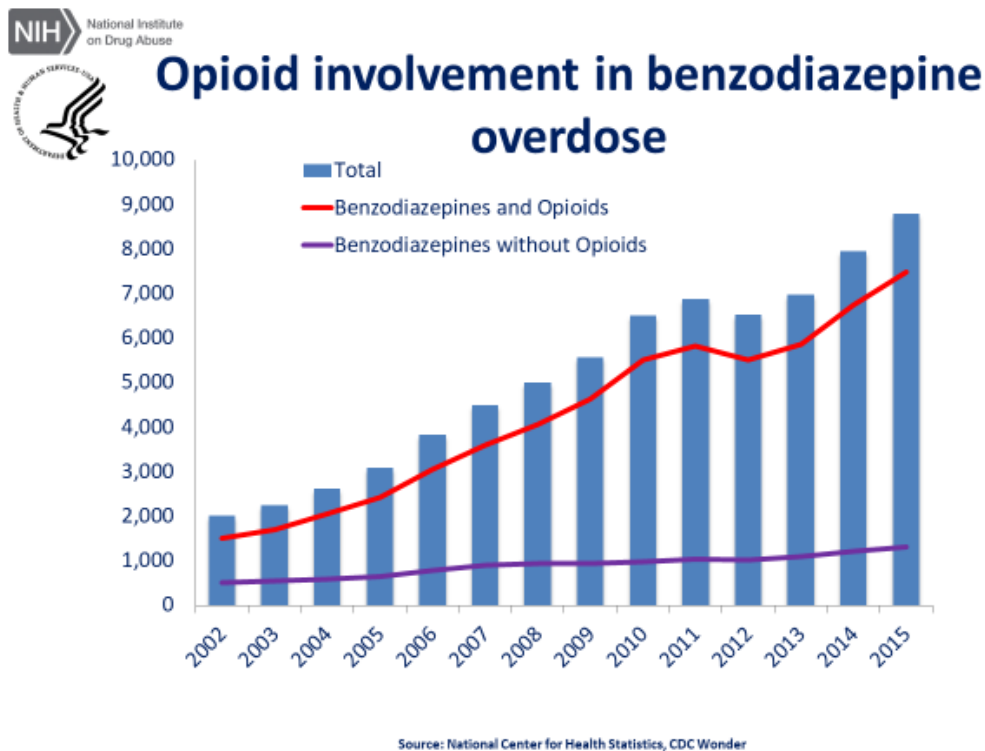
Figure 8- National Overdose Deaths—Number of Deaths from Benzodiazepines, with and without opioids.

1.3 Background

In 1986, Boyle[32] and her co-worker synthesized BRL-37959 (5) and found that the compound was active as a Non-Steroidal Anti- Inflammatory Drug (NSAID). Zomepirac (brand name Zomax), an equipotent drug as BRL-37959, was used as a reference compound(Table-1). Zomax replaced morphine for relieving postoperative pain. It is not addictive but was withdrawn from the market in 1983 because it caused anaphylaxis, a severe allergic reaction, in patients**.**

Figure 9-Structural analysis of BRL 37959
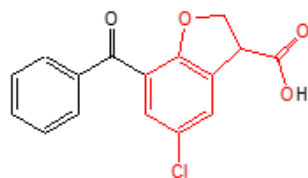
BRL 37959 (analgesic,
low gastric irritancy)

Since 1983, no reasonable non-opiate drug is available for postoperative pain. BRL 37959 may be used as an alternative NSAID, like VIOXX (Rofecoxib), which causes little gastric irritation, but has been withdrawn from the market because it increases the risk of heart attack.

Table-2: Biological data of racemic BRL-37959 vs Zomax.

Compound	Analgesia (ED_{50})	PG Synthase (ID_{50})	Gastric irritancy(ED_{50})
Zomepirac(Zomax)	0.6 (0.4-1.0)	0.6	8 (4.2-15.4)
Racemic BRL-37959	0.8 (0.5-1.3)	0.25	150 (87.2-258.0)

Note: ED_{50} = Effective dose in mg/kg with 95% confidence limits in parentheses.
ID_{50} = inhibitory dose of prostaglandin synthetase (PG) in mg/ml

1.4 Aim of the Project:

Non-selective commercially available COX inhibitors enhance the risk of gastric and or duodenal mucosal injury or erosions, ulcers and ulcer problems including bleeding as well as lead to nephrotoxicity.[18,19.] The COX-2 selective inhibitor Celecoxib (Celebrex) increases the risk of serious cardiovascular (CV) thrombotic events, myocardial infarction and stroke as well as increased nephrotoxicity.

It is well known that COX1 enzyme releases thromboxane that aggregate platelets and COX2 enzyme synthesize prostaglandins that act as a vasodilator. This prostaglandin keeps blood vessel free from clogging. There is a dynamic balance between the platelet aggregation and vasodilation. Therefore, COX inhibitors are active against inflammation, pain, and fever as well as different types of cancers. Considering the enormous potential benefits and side effects of non-selective COX inhibitors and selective COX-2 inhibitors, our research goal was to find out a COX inhibitor that binds with both COX1 and COX2 in such a ratio that it would be a safer drug. Also, another aim was to develop a synthesis method of the target inhibitor that would be simple, cost efficient and ensure a high yield.

Boyle and her colleges found that BRL-37959 had less gastric irritancy than zomepirac. But this drug is not available on the market, in search of its reason we have found that the overall yield of Boyle's method is a meager (≤ 5%).

Benzofuran is an essential building block of BRL 37959. In Dr. Hossain's lab, Matt Dudley[33] had developed a novel, unprecedented, one pot procedure to synthesize various benzofuran derivatives. We have followed this efficient, more economical, large scale

potential, selective, high yield and simple process to synthesize benzofuran and designed a synthetic route to synthesize BRL-37959 with higher yield.

1.5. Binding mode of NSAIDs with Cyclooxygenase (COX) enzymes

1.5.1. Cyclooxygenase (COX) enzymes and their function

Phospholipase(PLAs) of plasma membranes release arachidonic acid and cyclooxygenase enzymes convert this into prostaglandins. Prostaglandins are signaling molecules that facilitate a different group of physiological actions throughout the body. Various types of tissues specific prostaglandins such as PGD2, PGE2, PGI2, PGF2, TxA2 are formed. Prostanoids then exert their effects by signaling through separate G-protein coupled receptors (GPCRs).[34-35] Prostaglandin signaling is involved in a variety of biological functions. For example, prostanoids play a significant role in the maintenance of vascular homeostasis. Vascular endothelium-derived PGI2, a vasodilator, and an anti-thrombotic agent are thought to counterbalance the effects of TXA2, which induces vasoconstriction and thrombosis.[36-39] PGE2 and PGI2 are also important regulators of kidney function and gastric cytoprotection.[41-42]Pathophysiological responses mediated by prostanoid signaling include pain, fever, inflammation, and tumorigenesis[37,43,45] and has been in reference in.[45-47] Phospholipase (PLAs) of plasma membranes releases arachidonic acid, and cyclooxygenase enzymes convert it into prostaglandin PGF and thromboxane A2 (TXA2), together termed as prostanoids. There are four principal bioactive PGs generated in vivo: prostaglandin E2 (PGE2), prostacyclin (PGI2), prostaglandin D2 (PGD2), and prostaglandin F2 (PGF2)

Prostaglandin E2

Prostaglandin E2 (PGE2) is generated in large amounts in the body and has a broad range of biological functions such as regulation of immune responses, blood pressure, gastrointestinal integrity, and fertility. PGE2 plays an important role in causing inflammation, redness and pain. PGE2 contributes to the growth of arterial dilation and enhanced microvascular permeability that increases blood flow to the inflamed tissue, as well as leads to the common sign of inflammation: redness, swelling, and pain. Pain is the result of the action of PGE2 on peripheral sensory neurons and on central sites within the spinal cord and the brain.[48]

PGI2 and Inflammation

PGI2 regulates cardiovascular homeostasis. PGI2 is found in vascular cells, including endothelial cells, VSMCs, and endothelial progenitor cells[49-50] PGI2 is produced by the consecutive action of COX and PGIS, a member of the cytochrome P450 superfamily that positively transforms PGH2 to PGI2. PGIS localizes with COX in the endoplasmic reticulum, plasma membrane, and nuclear membrane.[41-52] PGIS is initially expressed in endothelial cells, where it combines with COX-1,[25] although the COX-2-dependent PGI2 generation by endothelial cells has been stated to be modified in vivo. This is done to thrombin, shear stress, oxidized low-density lipoprotein, hypoxia, and inflammatory cytokines, as well as upregulation of COX-2[53-54] which harmonizes it. PGI2 is an effective vasodilator and an inhibitor of platelet aggregation, leukocyte adhesion, and VSMC proliferatio.[47] PGI2 is also antimitogenic and inhibits DNA synthesis in the VSMC.[55] These

actions of PGI2 are facilitated through specific IP receptors (Table). This receptor is expressed in the kidney, liver, lung, platelets, heart, and aorta.[56]

Besides its cardiovascular effects, PGI2 is a vital mediator of the edema and pain that accompany acute inflammation. PGI2 quickly forms following tissue injury or inflammation, and it is present at high concentrations in inflammatory milieus[57] PGI2 is the most abundant prostanoid in synovial fluid in human arthritic knee joints, as well as in peritoneal cavity fluid from mice injected with irritants.[58-59]

PGD2 and Inflammation

PGD2 is produced in both the central nervous system and peripheral tissues and appears to function in both an inflammatory and homeostatic capacity.[60] In the brain, PGD2 regulates sleep and other central nervous system activities, including pain perception. [51-62] In peripheral tissues, PGD2 is synthesized mainly by mast cells but also by other leukocytes, such as DCs and Th2 cells.[63-64]Two genetically distinctive PGD2-producing enzymes have been recognized, including hematopoietic- and lipocalin-type PGD synthases (H-PGDS and L-PGDS, respectively). H-PGDS is usually confined to the cytosol of immune and inflammatory cells, while L-PGDS is more reserved to tissue-based expression.[64-65]

PGF2α and Inflammation

PGF2, originated mostly from COX-1 in the female reproductive system, plays a significant role in ovulation, luteolysis, contraction of the uterine smooth muscle, and

initiation of parturition.[66-67] Recent studies have revealed that PGF2 also plays a major role in renal function[68], contraction of arteries[69], myocardial dysfunction,[70-71] brain injury,[72] and pain.[73] Administration of PGF2 produces acute inflammation, and NSAIDs inhibit PGF2 biosynthesis both in vitro and in vivo.[74] Elevated biosynthesis of PGF2 has been found in patients suffering from RA, psoriatic arthritis, reactive arthritis, and osteoarthritis.

Cardiovascular risk factors, such as diabetes, obesity, smoking, and thickening of the intima-media ratio in the carotid artery, have been randomly related with elevations in PGF2 metabolites, together with IL-6 and acute phase proteins in body fluids.[76—77] The sprouting role of PGF2α in acute and chronic inflammation opens up opportunities for the design of new anti-inflammatory drugs.

Thromboxane and Inflammation

Thromboxane A2 (TXA2) is a type of thromboxane, synthesized from PGH2 via thromboxane synthase, and it is non-enzymatically degraded into biologically inactive TXB2. TXA2 is principally derived from platelet COX-1, but it can also be made by other cell types, including macrophage COX-2.[78-79] TXA2 activity is mainly mediated through the TP, which couples with GQ, G12/13, and multiple small G proteins, which in turn control several effectors, including phospholipase C, small G protein Rho, and adenylyl cyclase (Table-3).[92] TP and TP,2 spliced isoforms of TP in humans, communicate with different G proteins and undergo hetero-dimerization, which results in alteration to intracellular traffic and receptor protein conformations. Only the TP protein is expressed
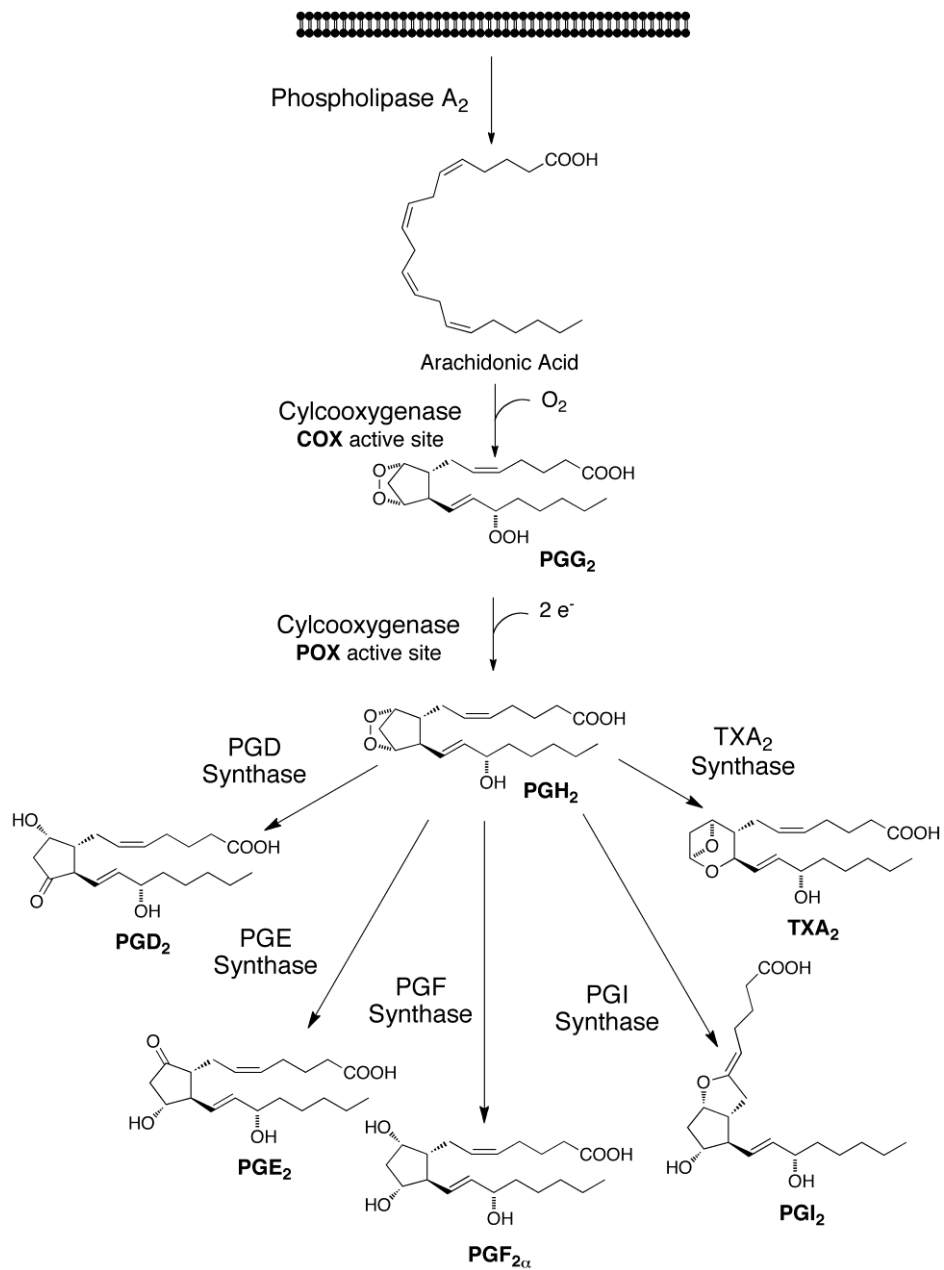
Figure 10- Biosynthesis of prostanoids.

in mice. TP activation arbitrates several physiological and pathophysiological responses, with platelet adhesion and aggregation, smooth muscle contraction and pro-function is controlled by several factors, such as oligomerization, desensitization, internalization, glycosylation, and crosstalk with receptor tyrosine kinases[94] TP and TP, spliced iso-forms of TP in humans, communicate with different G proteins and undergo hetero-dimerization, which results in alteration to intracellular traffic and receptor protein conformations. While TXA2 is the favored physiological ligand of the TP receptor, PGH2, in specific, can also activate this receptor94.The cutting of TP decreases vascular proliferation and platelet activation in response to vascular injury, which delays atherogenesis, and prevents angiotensin II– and L-NAME induced hypertension and the associated cardiac hypertrophy.[95-96]

1.5.2. COX reaction

The transformation of AA to the parental prostaglandin, PGH2, takes place at two specifically unique but functionally coupled active sites within the COX enzymes.

The bis-deoxygenation of AA occurs in the L-shaped cavity of the COX active site, leading to the formation of the hydroperoxy endoperoxide, prostaglandin G2 (PGG2).[85]PGG2 then moves out of the COX site to the peroxidase (POX) active site, where it rapidly is reduced by accepting two-electrons to form the hydroxy endoperoxide, PGH2[43]. Hydroperoxides except PGG2 can be reduced in the POX active site, and commencement of the COX reaction is dependent upon a two-electron oxidation of the heme moiety at the POX site. The requirement for heme oxidation at the POX active site

to initiate COX catalysis is best described by a branched-chain mechanism, as shown in Figure 11. The two-electron oxidation of heme takes place in conjunction with the two-electron reduction of a hydroperoxide substrate, and results in the formation of a ferryl-oxo protoporphyrin radical cation ((PPIX•) +Fe4+O) designated Compound I.[86-87] In the presence of a reducing co-substrate, two subsequent one-electron reductions restore the heme moiety to its original state.[88-89]Otherwise, Compound I can abstract a hydrogen from Tyr-385 in the COX active site, which results in the formation of a tyrosyl radical, thus commencing the oxygenase reaction.

1.5.3. Structure of COX enzymes

1.5.3.1. General COX structure

In 1994, the first three-dimensional structure of COX-1 was made, and two years later the crystal structure of COX-2 was obtained.[89,90] Subsequent cleavage of the signal sequence, mature COX-1 contains amino acid residues 25-600, with residues 33-586 displaying clear electron density in crystallographic analysis89. Also, residues 33-583 were determined in the first crystal structure of COX-2; 35 amino acids at the C-terminus could not be traced.[90] A 14-amino acid elimination at the N-terminus of COX-2 results in the numbers of most COX-2 amino acids to be 14 units lower than those of COX-1, but by convention, the amino acids of both isoforms are referred to by the numbering of the initial COX-1 translation product. Comparison of the crystal structures of COX-1 and
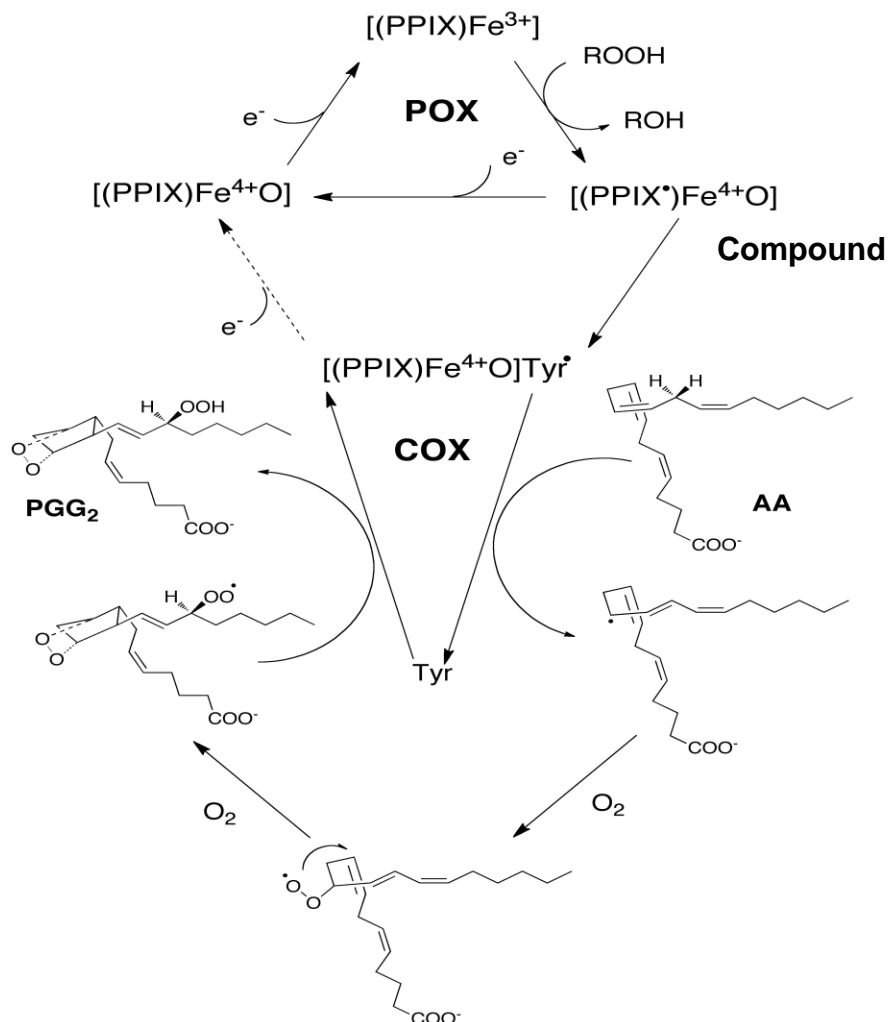
Figure 11- Branched chain mechanism for COX catalysis. In the POX, active site, the heme moiety, (PPIX)Fe3+, undergoes a two-electron oxidation to form Compound I, (PPIX•) Fe4+O, whereas the hydroperoxide substrate (ROOH) undergoes a two-electron reduction. The enzyme can return to its original state by two subsequent one- electron reductions or the radical can be transferred to a tyrosine residue in the COX active site. While AA is bound within the COX active site, the newly formed tyrosyl radical can abstract the 13-pro-(S) hydrogen from the fatty acid substrate. AA undergoes several radical rearrangements in addition to two oxygenation reactions to provide the development of the hydroperoxy endoperoxide, PGG2. The radical is then shifted back to the tyrosine residue to allow the initiation of subsequent catalytic cycles.

discloses that the two isoforms have virtually superimposable structures with each. COX monomer consists of three domains: an epidermal growth factor (EGF)-like domain, a membrane binding domain, and a large globular catalytic domain, which holds the cyclooxygenase (COX) and peroxidase (POX) active sites.[89-91] The COX enzymes are found as homodimers with an extensive dimer interface created by the EGF-like and catalytic domains.[92]

Table 3: Summary of the structure, distribution and regulation of COX-1 and COX-2

	COX1	COX2
cDNA	Chromosome 9; 22kB	Chromosome 1; 8.3kB
mRNA	2.8kB	4.5kB
Protein	72kDa;599 amino acids	72kDa;604 amino acids
	Amino acids: 90% between species for both isoforms; similar Vmax and Km values for arachidonic acid	
Differences	Glucocorticoids inhibit expression of COX-2, not COX-1; the active site of COX-2 is larger than that of COX-1	
Regulation	Predominantly constitutive. Increased 2- to 4-fold by inflammatory stimuli	Predominantly inducible (10- to 20-fold) Constitutive in certain tissues
Tissue Expression	Most tissues, but particularly platelets, stomach, kidney	Induced by inflammatory stimuli and mitogens in macrophages/ monocytes, synoviocyes, chondrocytes, fibroblasts, endothelial cells. Induced by hormones in the ovaries and foetal membranes. Constitutive expression in the CNS, kidney, testes, tracheal epithelial cells.

Domain construction

COX, a monotopic membrane protein that binds with phospholipid bilayer of the plasma membrane as if it was a basic membrane protein.

The membrane-binding domain (residues 73-116) consists of four short amphipathic α-helices (A-D). The helices are placed approximately orthogonal to one another forming a hydrophobic surface model for introduction into a single face of the membrane bilayer. The helices of the membrane binding domain are also surrounded by a somewhat large open area that has been termed the "lobby," as it is assumed that substrates and inhibitors must travel through this zone to enter the active site located within the catalytic domain.

The catalytic domain is physically homologous to mammalian myeloperoxidase, indicating that the COX enzymes evolved from soluble heme-dependent peroxidases[93]. This main domain of the COX monomer largely consists of a α-helical secondary structure. The POX active site is located in a solvent-accessible trench at the top of the catalytic domain while the COX active site lies at the vertex of a large, L- shaped hydrophobic channel that ranges from the membrane-binding domain into the catalytic domain. Inside the COX channel, the catalytic and membrane binding domains are separated by a compression formed by three residues: Arg-120, Tyr-355, and Glu-524.

The EGF-like domain is composed of a short sequence of amino acids at the N- terminus (residues 34-72) of the protein, and its particular function remains unknown. However, it has recommended that this domain may start and retain interactions necessary for the insertion of COX into the membrane bilayer[93].

POX active site:

The peroxidase active site (shown in Fig-12) is the position of heme binding where His-388 serves as the proximal heme ligand. Gln-203 and His-207 are located on the distal side of the heme, approximately 5 Å from the heme iron, but do not coordinate the metal[88]. It is assumed that these residues play a key role in the two-electron reduction of the hydroperoxide substrate.[45] Mutation of His-388, Gln-203, or His-207 results in a dramatic reduction in peroxidase activity.[44,94] Recent studies confirm that, while the kcat/Km for peroxidase activity of G203V oCOX-1 is 17% that of WT enzyme, the mutant enzyme holds full COX activity and has a specific activity corresponding to that of WT proposing that this Glu-203 is not needed for the initiation of COX catalysis.[95]

In contrary to the majority of peroxidases, the POX active site of COX enzymes is exposed to solvent and can, therefore, hold large alkyl peroxide substrates. The opening of the POX active site also permits for relatively easy dissociation of small ligands, including heme, in and out of the active site cavity. Due to the nature of

POX active site and the reactivity of the heme moiety, crystallization of substrates or products attached to the peroxidase active site has been difficult. Lately, the 2.0 Å crystal structure of oCOX-1 in complex with an analog of the non-steroidal anti- inflammatory drug (NSAID) flurbiprofen presented the first view of a ligand bound to the POX active site (PDB ID: 1Q4G).[96] A detailed explanation of NSAIDs as COX inhibitors is provided below. Though, in this specific structure, a glycerol molecule, used as a cryoprotectant, lies between Gln-203 and His-207 with the 1-hydroxyl group located roughly above the heme iron (Figure 12)[96]. The 3-hydroxyl group forms hydrogen bonding interactions with a water molecule coordinated to His-20794. The position of this glycerol molecule is likely to mimic the binding conformation of the peroxide moiety of alkyl hydroperoxide substrates. This structure was used as the basis for docking and molecular dynamics studies for predicting the productive binding mode of the hydroperoxy endoperoxide intermediate, PGG2, within the POX active site[97].
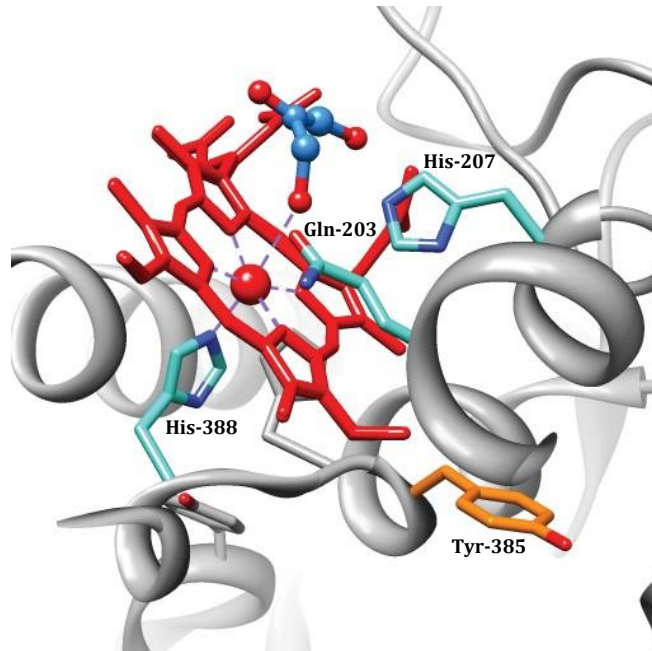
Figure 12- Glycerol molecule bound within the POX active site of COX-1. Heme (red stick structure) is shown bound in the POX active site in addition to a glycerol molecule (blue and red) shown in ball-and-stick mode. Key residues for peroxidase activity are shown in turquoise. The catalytic tyrosine is shown in orange. PDB ID: 1Q4G.

1.6 COX active site

The COX active site channel ranges 25 Å from the membrane binding domain to the interior of the catalytic domain; the catalytic center is placed on the upper half of the channel from Arg-120 to Tyr-385. Although the COX-1 and COX-2 active sites are somewhat similar, the COX-2 active site is about 20-30% larger than that of COX-1(Figure 13). The size variation is rather assigned to a single amino acid change (Ile-523 in COX-1, Val in COX-2) that limits the gateway to a pocket of the main active site channel [99]. Substitution of secondary shell residues, Ile-434 and His-513, in COX-1 for Val-434 and Arg-513 in COX-2 also makes the change in active site size.

Figure 13- Solvent accessible surfaces in the cyclooxygenase active site of COX-1 and COX-2. The catalytic domains of the COX proteins are shown as red in a ribbon diagram with the membrane binding domains (predominantly helix D) shown in green. Residues lining the COX active site of both proteins are shown in white with the solvent accessible surfaces in the active site designated as translucent light-blue.

It is confirmed from Crystal structures and molecular models of ovine COX-1 (oCOX-1) and murine COX-2 (mCOX-2) that the carboxylic acid of the arachidonic acid ion-pairs to the guanidinium group of Arg-120 and hydrogen bonds to Tyr-355. The aliphatic backbone stirs up into the top of the cyclooxygenase active site from the hydrophobic channel and then forms a distinct bend in the proximity to Tyr385 (Figure 14).[100-104] In these structures, because of van der Waals interactions, all most all the of contacts are formed between the substrate and various protein residues in the active site. The ω-end

Figure 14- Arachidonic acid bound in the active site of oCOX-1.[32]

The carboxylate of the substrate ion-pairs with Arg-120 and hydrogen
-bonds with Tyr-355 at the construction site, projects up the hydrophobic
channel, and makes an L-shaped bend around Tyr-385. The heme
prosthetic group is designated in red. Residues that are in contact with
arachidonic acid in the active site channel are shown in yellow.

of arachidonic acid links, up in a narrow channel at the top of the active site and is
surrounded by six aromatic amino acids. Mutation of Gly-533 at the top of this channel
caps off the channel and ends the oxygenation of arachidonic acid but not that of fatty
acids with shorter carbon chains[104].

1.7 Binding mode of NSAIDs to COX enzymes

1.7.1 Aspirin

Aspirin covalently alters both COX-1 and COX-2 over acetylation of Ser-530, it is 10-100 times more potent against COX-1 than against COX-2.[105-107]The cause for this variance in inhibitor potency against the two cyclooxygenase isoforms is ambiguous. Without acetylation, both COX enzymes predominantly create PGG2 and small amounts of lipoxygenase-type products (hydroperoxy fatty acids), with either R or S stereochemistry for the peroxide group at C-15.[107-108] Acetylation of Ser-530 entirely stops arachidonate catalysis and product formation in COX-1 but permits the synthesis of 15(R)-hydroxyeicosatetranoic acid and 11(R)-hydroxyeicosatetranoic acid in COX-2. [103-104] This disparity inhibition of the COX enzymes by aspirin is due to the larger volume of the COX-2 active site produced by the Val-523 substitution at the mouth of the side pocket 109.Mutation of Val-523, Arg-513, and Val-434 in COX-2 to their COX-1 equivalents (Ile-523, His513, Ile-434) consequences in the inhibition of 15- and 11(R)-hydroxyeicosatetranoic acid formation subsequent treatment with aspirin.[110]

The crystal structure of COX-1 bound with 2-bromoacetoxybenzoic acid (an aspirin analog) shows the integration of the bromoacetyl group at Ser-530 (Figure 15).[111] Two rotamers of the bromoacetyl group exist that blockade the active site channel to different degrees; this may assist to clarify the different results of acetylation of COX-1 and COX-2. In this structure, salicylic acid is also connected to the active site, which explains the
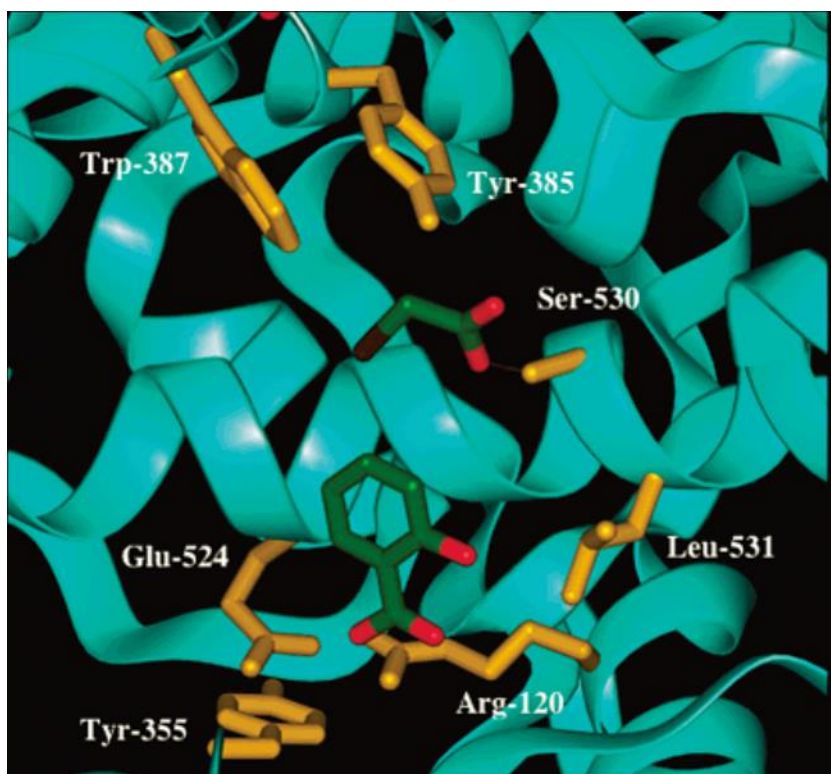
Figure 15- Crystal structure of an aspirin analogue in the active site of oCOX-1.[57] The bromoacetyl group of the aspirin analogue 2-bromoacetoxy-benzoic acid is shown covalently bound to Ser-530 in the COX active site (red and orange linker). The product of the reaction, salicylic acid, is shown in the active site with its carboxylate making hydrogen bonds with Arg-120 and Tyr-355 at the construction site. The bromoacetyl group of the inhibitor and the salicylic acid product are shown in green and are colored by atom. Key active site residues are shown in yellow.

selective delivery of the acetyl group to Ser-530. The salicylate carboxyl group ion-pairs to Arg-120, which is positioned immediately below Ser-530. Mutation of Arg-120 to Gln or Ala removes ion-pairing and hydrogen bonding interactions with the salicylate group and significantly reduces aspirin acetylation of Ser-530.[112] Another aspirin analog, o-acetylsalicylhydroxamic acid[113] also binds in the COX-1 active site channel, acetylates Ser-530, and hydrogen-bonds with Arg-120 at the construction site. The acetyl group on Ser-530 propels into the active site instantly below Tyr-385, shut down the top of the channel and blocking the entrance of substrate to the catalytic tyrosyl radical. In the

30

crystal structures of COX with aspirin analogs, a hydrogen bond is present between the carbonyl oxygen of the acetyl adduct and the phenolic hydrogen of Tyr385.[112,113] The presence of Tyr-385 across the active site from Ser-530 plays a significant role of acetylation.[114] Mutation of Tyr-385 to Phe decreases aspirin acetylation of the serine hydroxyl by 93%.[112] The hydrogen-bonds between Tyr-385 and the acetyl group of aspirin, which increases its reactivity by stabilizing the negative charge of the tetrahedral intermediate of acetylation. This action of Tyr-385 is like the stimulation of substrate acylation of serine proteases through the oxyanion hole in the active site.[115]Remarkably, aspirin acetylates heme-reconstituted enzyme 100-fold more rapidly than apoenzyme.[116]One probable clarification for this consequence is that the heme group restricts protein conformational mobility and easiness enzyme-aspirin interactions. The inhibition of COX enzymes by aspirin is also based on the oxidative state of the enzymes; activation of COX with peroxides to form the Tyr-385 tyrosyl radical reduces acetylation by aspirin.[117]The necessity of Tyr-385 and the heme prosthetic group for acetylation of Ser-530 underlines the dynamic roles of the different parts of the cyclooxygenase active site in the overall inhibition of its enzymatic activity by aspirin.

1.7.2. Flurbiprofen and Ibuprofen

X-ray crystallography of COX-inhibitor complexes and site focused mutagenesis studies have assisted revealing the molecular basis for the time-dependent inhibition of some aryl propionic and aryl acetic acid inhibitors. COX-1 crystal structures of competitive reversible (ibuprofen and methyl flurbiprofen) and time-dependent (flurbiprofen and alclofenac (2-(4-(allyloxy)-3-chlorophenyl) ethanoic acid)) inhibitors disclose the same binding conformation of inhibitor in the active site. It indicates that the mechanism of time-

dependent inhibition of COX thru NSAIDs does not include broad conformational changes in the enzyme structure or the binding of the inhibitor to diverse, active sites. In the crystal structure of COX-1 with flurbiprofen, the inhibitor binds to the cyclooxygenase active site with the carboxylate of the inhibitor. Then it makes hydrogen-bond that links with Arg-120 and Tyr-355 at the constriction site (Figure 16A)[118,] The structurally alike, but kinetically different, ibuprofen binds in an almost same style in the COX-1 active site, creating an ion pair with Arg-120 and a hydrogen bond with Tyr-355 (Figure 17B).[118]These crystallographic results recommend that the kinetic dissimilarities between competitive, reversible and time-dependent, functionally irreversible inhibitors cannot entirely clarify through the binding modes exhibited by these inhibitors.
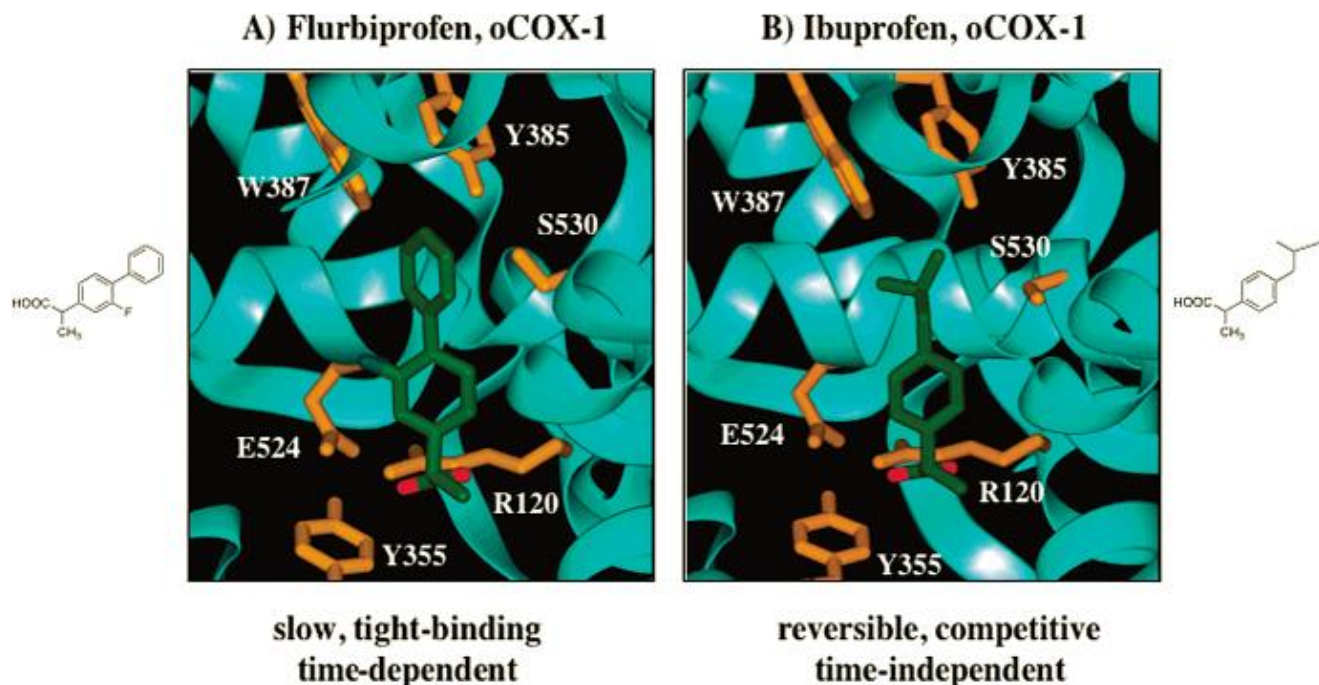
Figure 16- Flurbiprofen and ibuprofen bound in the active site of ovine COX-1. Panel **A** shows a time-dependent and functionally irreversible inhibitor, flurbiprofen (green), in the oCOX-1 active site with its carboxylate coordinated to Arg-120 and Tyr-355 at the constriction site. Panel **B** shows a competitive reversible inhibitor, ibuprofen (green), bound in a similar conformation. Key active site residues are shown in yellow.

1.7.3. Indomethacin

Crystal structure of indomethacin and COX-2 demonstrates that indomethacin binds intensely within the cyclooxygenase active site (Figure 17A).[119] The p-chlorobenzoyl group progresses up into the active site channel, and the chlorine atom interacts with Leu-384 at the top of the active site, whereas the benzoyl oxygen interacts with Ser-530. The benzoyl group itself is stabilized by hydrophobic interactions with Leu-384, Tyr-385, Phe-381, and Trp387. The carboxylate of indomethacin creates a salt bridge with Arg-120 and builds additional interactions with Tyr-355 at the constriction site. The o-methoxy group makes a large cavity provided by Ser-353, Tyr-355, and Val-523. The indole ring interacts with Val-349, and the 2′-methyl group impels into a small hydrophobic pocket formed by Val-349, Ala-527, Ser-530, and Leu-531 (Figure 17B).[119] Mutagenesis of Val-
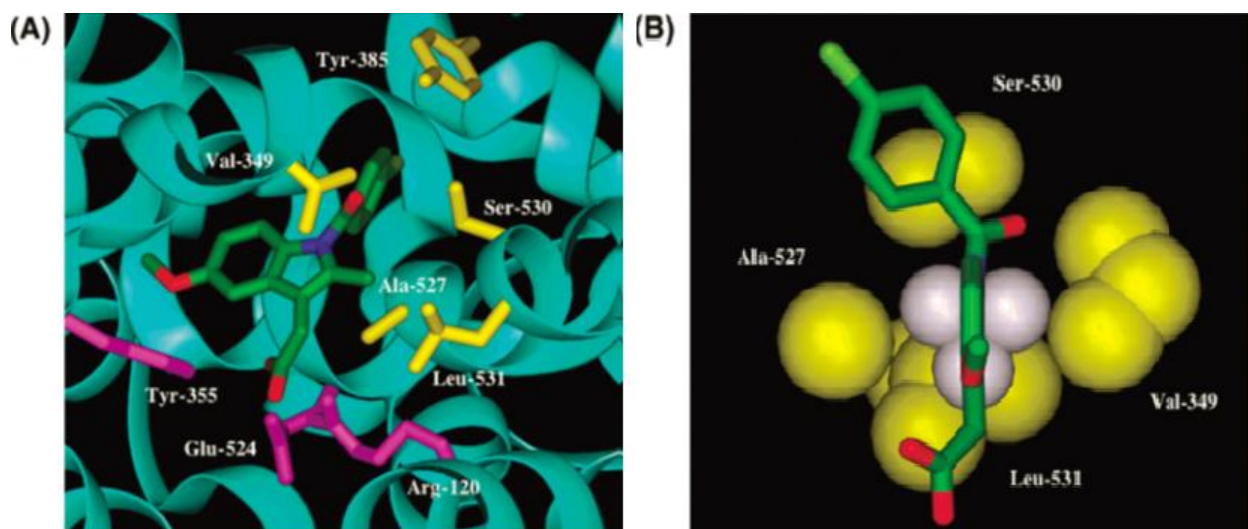
Figure 17 - Crystal structure of indomethacin in the active site of murine COX-2.[60] Panel A shows key active site residues important for inhibitor binding. Indomethacin is shown in green and is colored by atom. Arg-120, Tyr-355, and Glu-524 at the constriction site are shown in purple. Residues that constitute the small hydrophobic binding pocket (Val-349, Leu-531, Ala-527, and Ser-530), as well as additional active site residues (Tyr-385), are shown in yellow. Panel B is a space-filling model of the 2α-methyl group of indomethacin (green) inserted into the hydrophobic binding pocket (yellow).[104]

349 to alanine or leucine shows that introduction of the 2′-methyl group of indomethacin into this small pocket is a crucial interaction responsible for the time-dependent inhibition of COX enzymes by this inhibitor.[120] A V349 A mutant enlarges the pocket size and raises the potency of indomethacin compared to wild type mCOX-2 (0.08 vs. 0.25 μM), while a V349L mutant cuts the pocket size and decreases the potency of the inhibitor (4.0 μM). The K_I of V349A for indomethacin association is almost 4-fold lower than wild-type mCOX-2 with a slight increase in k_2 (0.074 vs. 0.052 s-1), while V349L shows a 3-fold increase in KI that accompanies a k_2 of 0.074 s-1. Indomethacin reveals slow, time-dependent, and functionally irreversible inhibition of both wild-type mCOX-2 and the V349A mutant with no significant reverse rate constant (k_{-2}) for the second inhibitory step (eq 2). However, indomethacin exhibits reversible inhibition with the V349L mutant with a measurable k_{-2} of 0.01 s-1. A2 ′-des-methyl analogue of indomethacin is a poor inhibitor of mCOX-2 and the V349 mutants and is quickly competed off the enzymes by arachidonic acid. 2-Des-methyl indomethacin does not inhibit COX-1 at all. Hence, a critical factor of the time-dependent inhibition of COX by indomethacin is endorsed to the binding of the 2′methyl group of the inhibitor into this small hydrophobic pocket.

1.7.4. Diclofenac

Diclofenac inhibition of COX-2 is not affected by mutation of Arg-120 to alanine or of Tyr-355 to phenylalanine, with IC_{50} values for inhibition that is comparable to that of wild-type mCOX-2 (wt, 77 nM; R120A, 257 nM; Y355F, 137 nM).[60] However, a S530A COX-2 mutant is resistant to diclofenac inhibition (IC_{50} > 50 μM), proposing that Ser-530 is important for inhibitor binding in the COX-2 active site. In support of this hypothesis, a

S530M COX-2 mutant shows a greater than 240-fold growth in IC_{50} for diclofenac over wild-type enzyme[121].Also, diclofenac quenches the internal protein fluorescence of apo COX-1 but does not quench the fluorescence of the aspirin-acetylated enzyme, recommending that diclofenac must interact with Ser-530 in the COX active site for binding and inhibition[81].Most crystal structures of COX enzymes with carboxylic acid-containing NSAIDs demonstrate the inhibitors located with their carboxylates coordinated to Arg-120 and their aromatic functional groups stir up into the cyclooxygenase active site. In contrary to diclofenac binds in the active site of COX-2 in a distinctive inverted binding mode with its carboxylic acid moiety hydrogen-bonded to Ser-530 and Tyr-385 (Figure 18).[104, 105] The inhibitor also builds great van der Waals interactions with several hydrophobic residues inside the active site. For example, the phenyl acetic acid ring is enclosed by the side chains of Tyr-385, Trp-387, Leu-384, and Leu-352. The dichlorophenyl group makes van der Waals interaction with Val-349, Ala-527, Leu-531 (the indomethacin binding pocket), and Val-523. Unlike most other NSAIDs with carboxylic acid moieties, neither Tyr-355 nor Arg120 creates contact with the inhibitor. The unique binding mode of diclofenac is like the structure of the nonproductive complex of arachidonic acid. COX-2 in which the substrate binds in an inverted conformation with its carboxylate coordinated to Ser-530 and Tyr-385.[41]This positioning contrasts with most structures resolved for fatty acid substrates attached to COX, including arachidonic acid, where the carboxylate of the substrate forms hydrogen bonds or ion pairs with Tyr-355 and Arg-120. The novel, inverted binding of diclofenac and the nonproductive
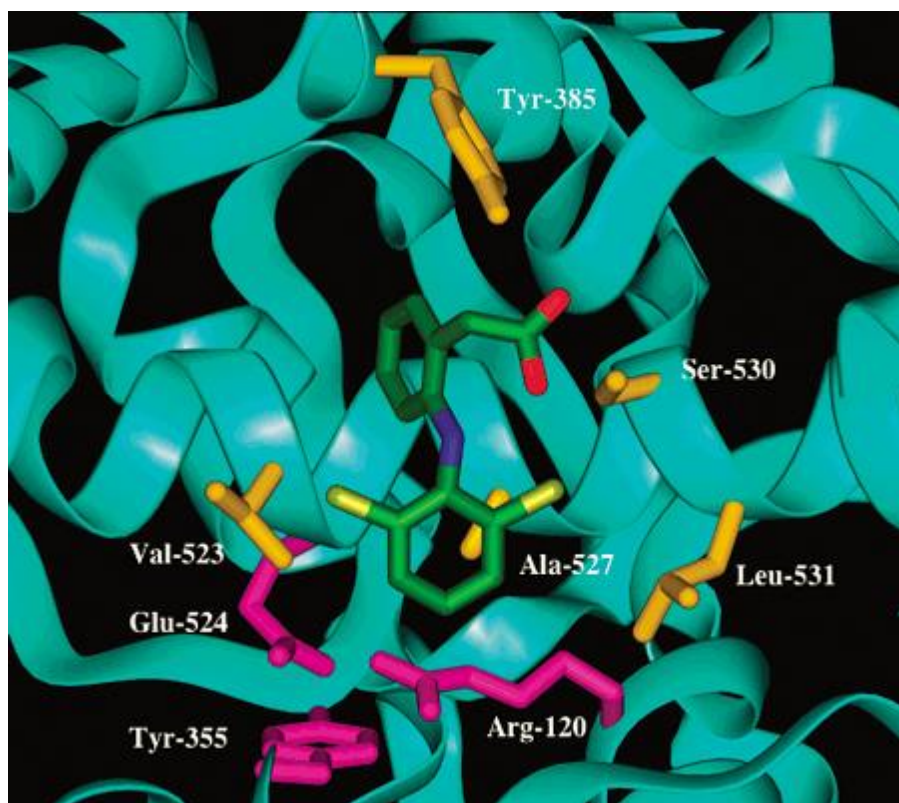
Figure 18- Crystal structure of diclofenac in the active site of murine COX-2.[60] Diclofenac binds in a novel, inverted orientation with its carboxylate coordinated by Tyr-385 and Ser-530 at the top of the active site. Diclofenac is shown in green and is colored by atom with each chlorine atom colored in light-green. Arg-120, Tyr-355, and Glu-524 at the construction site are shown in purple. Additional key active site residues are shown in yellow.[104]

conformation of arachidonic acid in COX-2 highlight the significance of Ser-530 and Tyr-385 in ligand association and the chelation of negative charges in COX-2 and may characterize a new binding mode demonstrated by some classes of NSAIDs.

1.7.5. Celecoxib analogue

The first crystal structure of human COX-2 (hCOX-2) displays that there is an overall variance in the size and shape of the COX-2 active site compared to that of COX-1[30]. Almost 25% larger active site of COX-2 is due to the single Val-523 substitution (Ile in

COX-1) in the active site and by the Arg-513 and Val-434 substitutions (His-513 and Ile-434 in COX-1) in the secondary shell. The crystal structure of mouse COX-2 with the celecoxib analog 4-(5-(4-bromophenyl)-3(trifluoromethyl)-1H-pyrazol-1-yl) benzene-sulfonamide (SC558) discloses that the sulfonamide group of the inhibitor binds in the side pocket adjacent to Val-523 in COX-2 (Figure 19).[31] Access to this pocket is constrained in COX-1 because of the extra steric bulk of Ile at this location. The binding of the sulfonamide group of SC558 in this side pocket is expedited by the additional substitutions of Val-434 and Arg-513.[31] The sulfonamide group of SC558 interacts with His-90, Gln-192, and Arg-513. The Arg-513 is preserved in all COX-2 enzymes and provides a positive charge in the side pocket. SC558 forms hydrogen bonds between its sulfonyl oxygens and His-90 and Arg-513, and the sulfonamide nitrogen hydrogen-bonds to the backbone carbonyl oxygen of Phe-518. The bromophenyl ring of 4 binds in a hydrophobic cavity formed by Ser-530, Leu-359, Trp-387, Tyr-385, Leu-384, and Phe-381, and the trifluoromethyl group of the pyrazole ring binds in a small pocket provided by Met113, Val-116, Val-349, Tyr-355, Leu-359, and Leu-531. Confirming the prior mutagenesis studies on human COX-2, the crystal structure of mouse COX-2 and compound 4 exhibits that the selective, time-dependent step in diaryl heterocycle inhibition of COX-2 is probably the placing of the methyl sulfonyl or sulfonamide group of the inhibitor past Val523 in COX-2 and into the side pocket. Val523 is replaced in COX-1 by the extra steric bulk of Ile-523.[122-125]
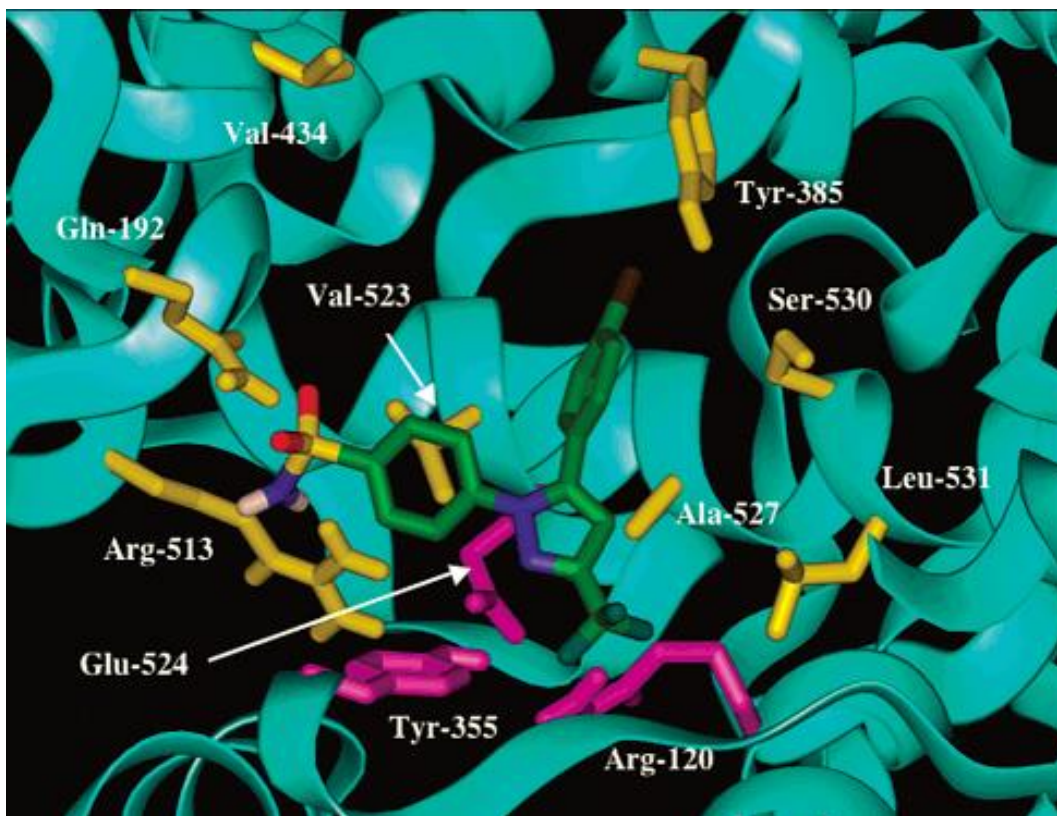
Figure 19- Crystal structure of the celecoxib analogue, SC558, in the active site of murine COX-2.[31]Compound SC558 is shown in green and is colored by atom. The key active site residues important   inhibitor binding is highlighted. Arg-120, Tyr-355, and Glu-524 at the constriction site are shown in purple. Residues that constitute the small hydrophobic binding pocket (Val-349, Leu-531, Ala-527, and Ser-530) and the COX-2 side pocket (Val-523, Arg-513, and Gln-192) are shown in yellow. Tyr-385 and Val-434 are also designated in yellow.

1.7.6. Naproxen and its analogs

Naproxen, a NSAIDs widely used for analgesic, anti-pyretic, and anti-inflammatory activity (Fig. 20). It has been stated that it is active in the prevention of bladder cancer growth even when administered several weeks after the tumor-initiating agent.[126] Naproxen, is non-selective COX inhibitor that binds both COX-1 and COX-2 and have gastrointestinal side effects. In recent growing evidence suggests that it has no cardio vascular side

38

effects when administered in the higher doses that deliver continued inhibition of platelet COX-1 during the dosing interval (e.g.500 mg twice daily).[127-129]

A

Naproxen   Flurbiprofen

Diclofenac   Indomethacin
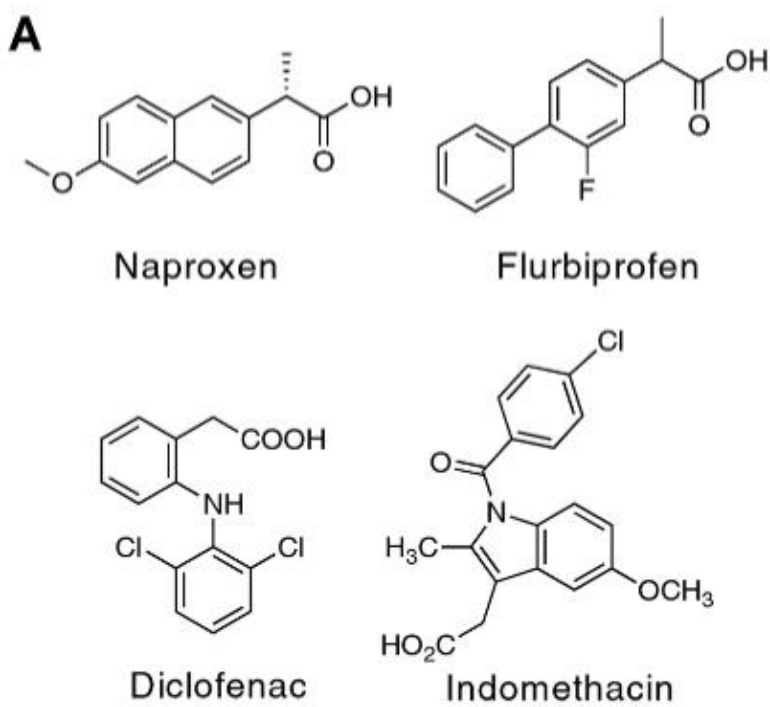
Naproxen inhibited oCOX-1 with an IC_{50} value of 340 nM and mCOX-2 with an IC_{50} value of 180 nM and showed greater than 80% inhibition in the presence of 500 nM AA (Fig. 21). Binding of Naproxen with COX — Aryl carboxylic acid inhibitors bind in one of two orientations in the COX active site (Fig.20).[130] Flurbiprofen attach canonically with its carboxylate moiety ion-paired and hydrogen-bonded to the constriction site residues Arg-120 and Tyr-355 (Fig. 20B).[131-138] In contrast, diclofenac binds in a reversed orientation in which its carboxylate is hydrogen-bonded to the side chains of Tyr-385 and Ser-530 (Fig.20B).[139]These two orientations can be differentiated by mutations of constriction site residues
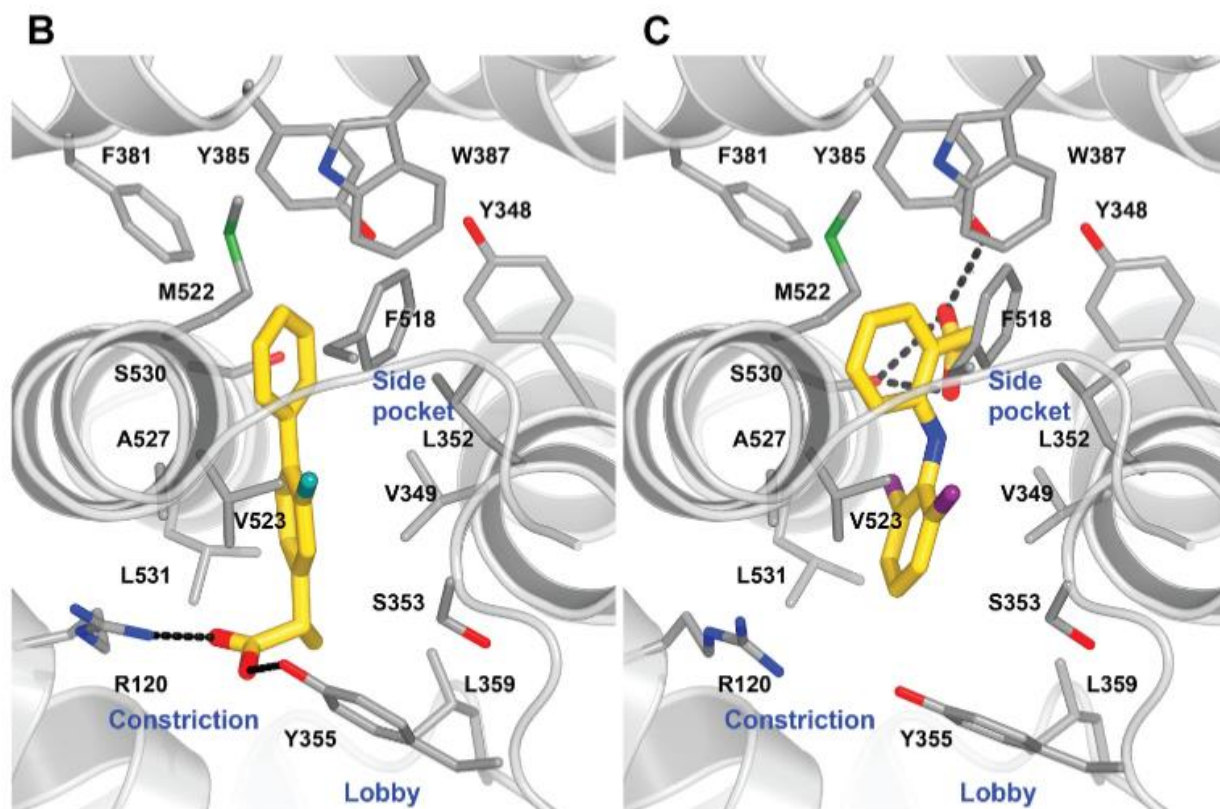
FIGURE 20. Chemical structures of NSAIDs and crystal structures of flurbiprofen and diclofenac bound in mCOX-2 active site. **A**, chemical structures of naproxen, flurbiprofen, diclofenac, and indomethacin. The structures of flurbiprofen (Protein Data Bank entry 3PGH; inhibitor carbon atoms colored gold) (**B**) and diclofenac (Protein Data Bank entry 1PXX) (**C**) bound at the COX-2 active site show the opposing binding modes that position their acidic groups either coordinated to the constriction residues Arg-120 and Tyr-355 at the base of the active site or to the catalytic Tyr-385 as well as Ser-530 at the top of the pocket.[130]

Mutation of Tyr-355 to Phe in mCOX-2 ceased inhibition by naproxen (Fig.22A),[130] while mutation of Arg-120 to Gln slightly amplified the potency of inhibition as displayed by an improved IC_{50} and a greater extent of inhibition (90%).Mutation of Arg-120 to Ala lead to a complete loss of enzyme inhibition by naproxen (Fig. 22A). In concert, these outcomes suggest that the carboxylate group of naproxen binds at the construction site in the canonical orientation, coordinated to Tyr-355 and Arg-120. To thoroughly inspect the

binding mode predicted from this studies Duggan and his co-worker.[130] determined the

co-crystal structure of naproxen bound to mCOX-2 at 1.7 Å resolution, the highest
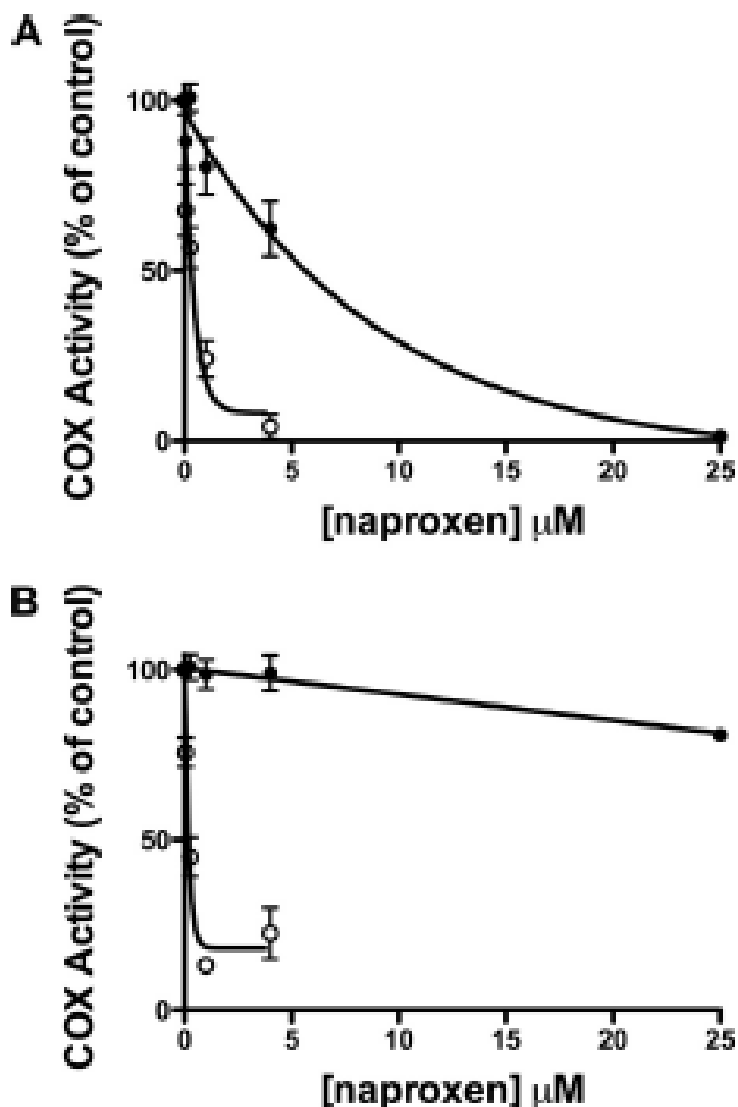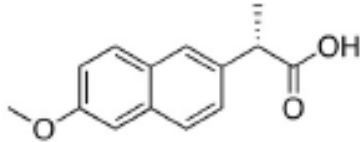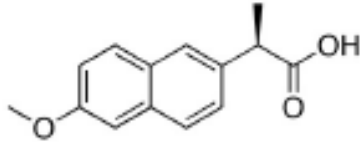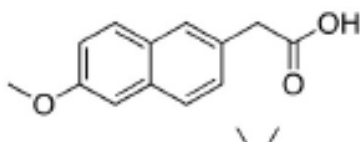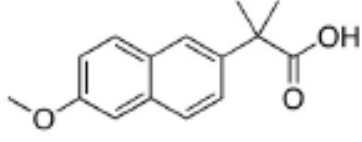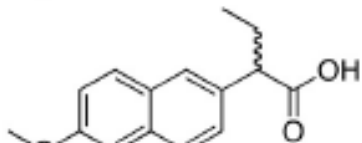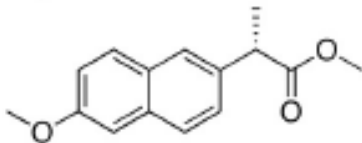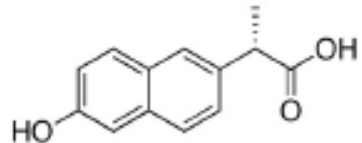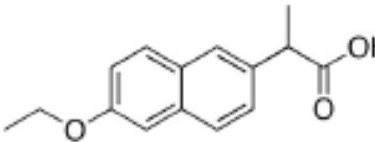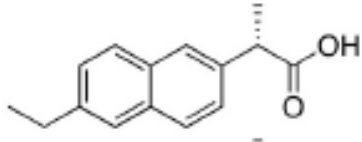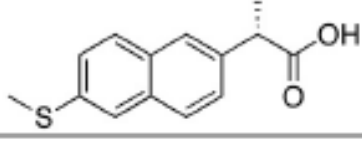
FIGURE 21. Effect of preincubation of enzyme and inhibitor on COX inhibition by naproxen. Closed circles (F) represent incubations in which (0.05–25 nM) and AA (500 nM) were added simultaneously to COX. For the incubations represented by open circles (E), COX was preincubated with naproxen (0.05nM) for 5 min before the addition of 500 nM AA. A is representative of incubations with oCOX-1, and B represents reactions withmCOX-2. The reaction with substrate was allowed to proceed for 8 s before quenching. Substrate consumption was analyzed by TLC as described. Each data point is the mean of at least two experiments in duplicate. Error bars, S.E. which eradicate inhibition by flurbiprofen but have no effect on inhibition by diclofenac.[130]

Table. 3a.COX inhibition studies of Naproxen.

Analog	COX-1	COX-2
	>25 μM (50%)	0.9 μM (70%)
	>25 μM (20%)	>25 μM (10%)
	>25 μM (10%)	>25 μM (20%)
	no inhib.	>25 μM (10%)
	no inhib.	no inhib.
	>25 μM (20%)	>25 μM (10%)
	>25 μM (30%)	>25 μM (30%)
	>25 μM (10%)	>25 μM (25%)
	>25 μM (45%)	0.77 μM (65%)
	>25 μM (40%)	0.67 μM (70%)
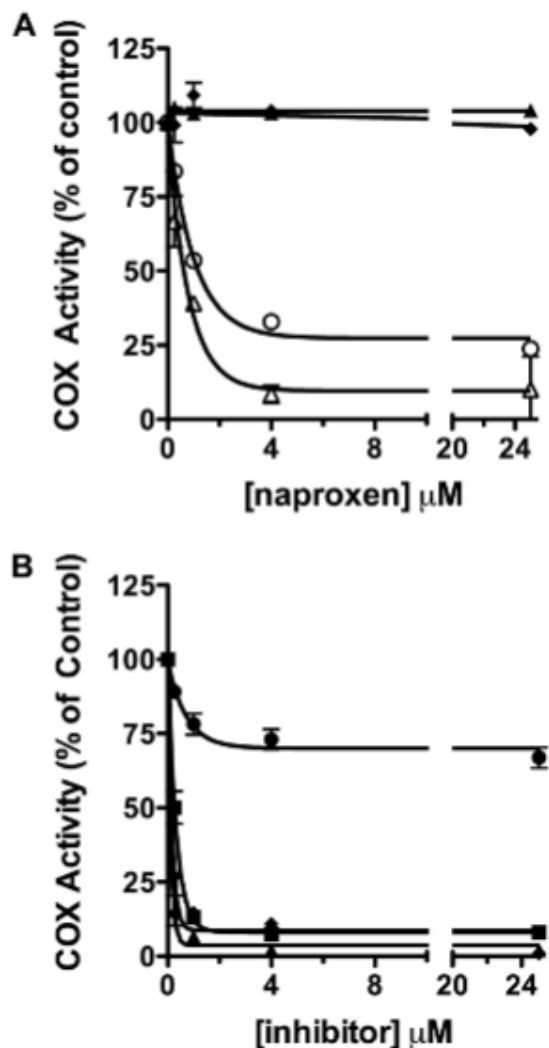
Figure 22- Inhibition of mCOX-2 active site mutants by naproxen and non-selective NSAIDs. *A*, naproxen (0.25–25 μM) was preincubated with WT mCOX-2 (○) or R120A (▲), R120Q (△), and Y355F (◆) mCOX-2 mutant enzymes for 20 min prior to the addition of substrate (50 μM) for 30 s at 37 °C. *B*, naproxen (●), indomethacin (■), diclofenac (▲), or flurbiprofen (◆) was preincubated with mCOX-2 W387F for 20 min prior to the addition of substrate (50 μM). Inhibitor concentrations ranged from 0.25 to 25 μM. Each reaction was terminated and substrate consumption was analyzed by TLC as described. Data points represent the mean of duplicate determinations. Data points for naproxen against W387F represent the mean of five independent experiments in duplicate. *Error bars*, S.E.
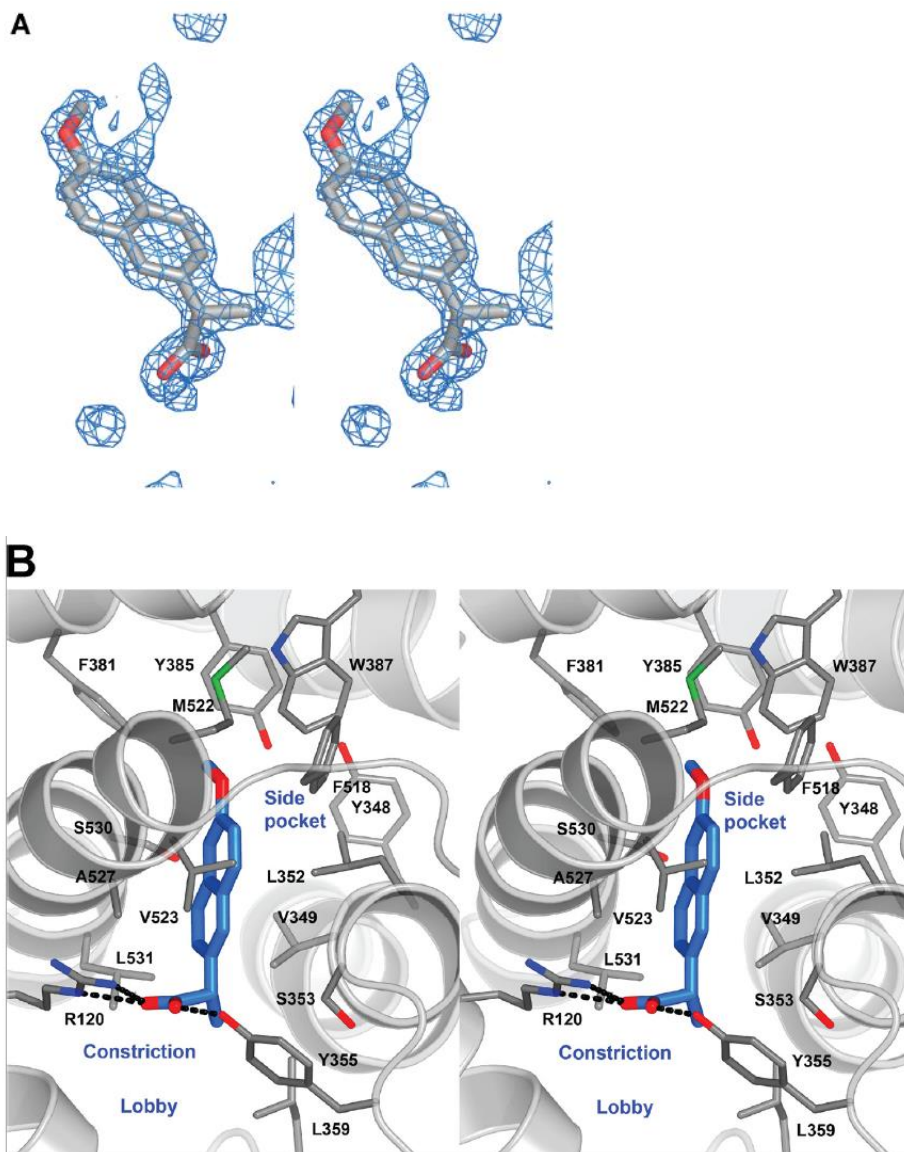
Figure 23- Crystal structure of naproxen bound to mCOX-2. A, difference electron density map (F$_0$Fc) contoured at 3.5α of the COX-2 active site prior to the addition of naproxen to the model or modification of side chain positions in the binding pocket.[130]

resolution COX structure to date and among the highest resolution membrane. The topology of the COX dimer and active site are like those of previous studies. To some extent, amazingly, the residues lining the active site were exposed in single conformations, even though the fact that many of them were surrounded only by solvent. The resolution of this structure allowed the detection of a β-OG molecule lying on the external side of the constriction, at the base of the funnel-shaped entrance to the active site (lobby region), like to high resolution structures of COX-1(e.g. Protein Data Bank entry 2AYL).[140] A solvent molecule is frequently observed hydrogen-bonded toTyr-385 and Ser-530 in the active site; nevertheless, when this density was fitted with a water molecule in the current structure, a 5α residual electron density peak kept on at that position. When equipped with a chlorine atom, the residual peak gone, and the atom polished to a temperature factor like neighboring protein and inhibitor atoms. A peak in the great difference map at the same location delivered further indication that the peak was a chlorine atom. While the physiological consequence of chloride binds in gat this position is unknown, chloride ions have been used earlier to recognize the binding site of molecular oxygen in various proteins, including dioxygenases.[141-142] This increases the probability that the Chloride ion may be revealing of the position of molecular oxygen before assimilation into COX substrates. Strong electron density was detected for a single orientation of naproxen binding within the COX-2 active site, making no contacts in the COX-2 side pocket or lobby region (Fig. 23). As projected by the mutagenesis data, the.

45
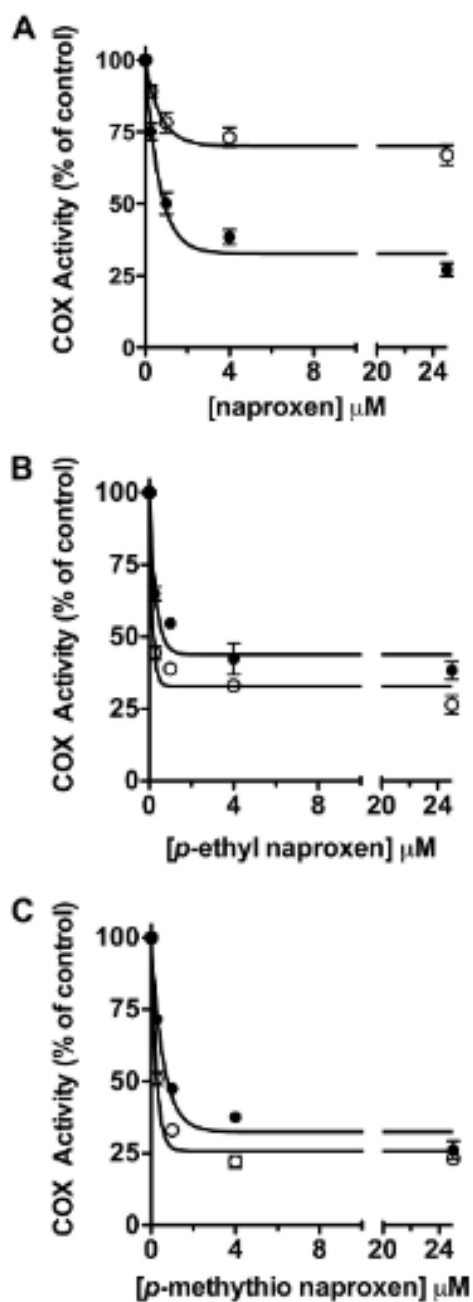
Figure 24. Inhibition of WT and W387F mCOX-2 by naproxen and naproxen analogs. Following a 20-min preincubation of naproxen **(A),** *p*-naproxen **(B),** or a p-methylthio naproxen**(C)** with mCOX-2(●) Or W387F mCOX-2(O), [1-^{14}C] AA(50µM) was added and allowed to react for 30s prior to termination with organic solvent. Concentrations of inhibitors ranged from 0.25 µM. Product formation was measure, by TLC as described. Each data point is the mean of at least two independent experiments. Error bars, S.E

binding mode of naproxen is alike that of other members of the 2-aryl propionic acid family of NSAIDs with the carboxylate group of naproxen participating in hydrogen-bonding inter-actions with Arg-120 (2.8 and 2.9 Å) and Tyr-355 (2.5 Å) at the base of the active site. The remains of the interactions between the compound and protein were van der Waals contacts. The (S)--methyl group of naproxen puts in the hydrophobic cleft adjacent to Val-349, whereas the naphthyl backbone of naproxen makes hydrophobic contacts with Ala-527, Gly-526, and Leu-352. Remarkably, the side chain of Leu-352 accepts an alternate conformation from that observed in the co-crystal structures of flurbiprofen, indomethacin, and diclofenac bound to mCOX-2. The p-methoxy group of naproxen is focused on the apex of the COX active site and forms van der Waals interactions with Trp-387 and Tyr-385. As mentioned above, the mCOX-2 naproxen crystal structure shows that the (S)--methyl group of naproxen is oriented in a conformation like that of the -methyl group of flurbiprofen and creates hydrophobic contacts with Val-349 as well as Leu-359.[131] Naproxen inhibited V349A mCOX-2 with a potency and extent of inhibition similar to those of WT mCOX-2(IC50 3.5M, 75% inhibition), but the V349I and V349L mutants were both more sensitive to inhibition (IC50 0.28 and 0.35 M, greater than 95% inhibition. The rise in inhibition detected when naproxen was tested against V349I or V349L could result from amplified hydrophobic interactions between the-methyl group and residue 349.To trial this hypothesis, 2-des-methyl naproxen was tested against the WT and V349I/L mutant enzymes. Elimination of the methyl group led to a substantial reduction in inhibition of WT COX and the V349I/L mCOX-2 mutants (maximum inhibition of 20% at concentrations up to 25 M) (Table 3a and data not shown). The accumulation

of bulk at the-position also caused to a loss of potency because the-ethyl analog of naproxen showed no inhibition of either wild-type COX-1 or COX-2 enzymes in our standard IC_{50} assay (Table 1). Likewise, bulkier substitutions at the-position of flurbiprofen impart a complete loss of inhibition of COX-1[31]. Hence, the (S)-methyl group is a vital determinant of naproxen efficacy, and it cannot be substituted with smaller (hydrogen) or larger (ethyl) substituents. The naproxen-COX-2 crystal structure displays that the p-methoxy group interacts with Trp-387 by van der Waals associates with two carbon atoms of the side chain, C2 (3.4 Å) and C 2(3.6 Å), the latter being the position of the side chain unique spatially to tryptophans. Trp-387 is positioned at the top of the COX active site near the catalytic residue, Tyr-385, and has been exposed to be an important residue for the proper locating of AA within the active site to yield the cyclooxygenase product, PGG 2. The W387F mCOX-2 mutant enzyme procedures relatively little amounts of PGG 2 but grown amounts of the uncyclized product, 11-hydroxyeicosatetraenoic acid.[144] We verified the W387F mutant for sensitivity to naproxen inhibition. A higher protein concentration was applied as the mutant's decreased catalytic activity. Naproxen had a negligible inhibitory effect on W387F, displaying only 25% inhibition at 25M (Fig.22B). The W387F mutation has not been studied with other inhibitors, so it was examined against several other carboxylate-containing NSAIDs. Amazingly, the IC_{50} values for diclofenac, flurbiprofen, and indomethacin against the W387F mutant enzyme were similar to earlier reported values against wild-type enzyme (87,120, and 250 n, respectively) (Fig. 22B).

Diclofenac and indomethacin only form a single contact point to the Trp side chain, to the C 2 position, one strictly imitated by phenylalanine.[144]While flurbiprofen also crates interactions with both carbon atoms of the Trp residue, they originate from a phenyl ring of the inhibitor that is earlier strengthened by other interactions, making the one with the Trp possibly less important for binding. In naproxen, the oxygen of the p-methoxy group lies within van der Waals contact range only of the Trp side chain. Thus, the interaction between Trp-387 and naproxen appears to be unique among carboxylate-containing NSAIDs.

To more investigation, the interaction between the methoxy group and Trp-387, two naproxen analogs, were synthesized in which an ethyl or methyl thio group was replaced for p-methoxy to present variations in size and polarity as well as to eliminate the possibility of hydrogen-bonding interactions. The methyl-thio analog has been stated to exhibit anti-inflammatory activity in vivo but has not been verified in vitro. The ethyl analog has not been testified. Both the p-ethyl and p-methyl thio analogs could inhibit wild-type mCOX-2 to the same extent as naproxen (IC$_{50}$ 0.67 and 0.77 M in our standard IC$_{50}$ assay) (Table 3a). Remarkably, both analogs displayed a loss of potency compared with naproxen when tested against oCOX-1 so that no IC$_{50}$ value could be determined at inhibitor concentrations up to 25 M. (Table 1). An increase in COX-2 selectivity at reduced substrate concentrations (500 nM and 5M AA). More notable yet, both analogs inhibited W387F as well as they inhibited wild-type enzyme (Fig. 24). The variance in sensitivity of W387F mCOX-2 to naproxen and the p-ethyl and p-methyl thio analogs facilitate to crystallize the complex of mCOX-2 with the p-methyl thio naproxen derivative. A structure

of this complex was purified at 2.3 Å resolution (Fig.25). Like naproxen, the inhibitor is

bound completely within the main channel of the COX active site. The
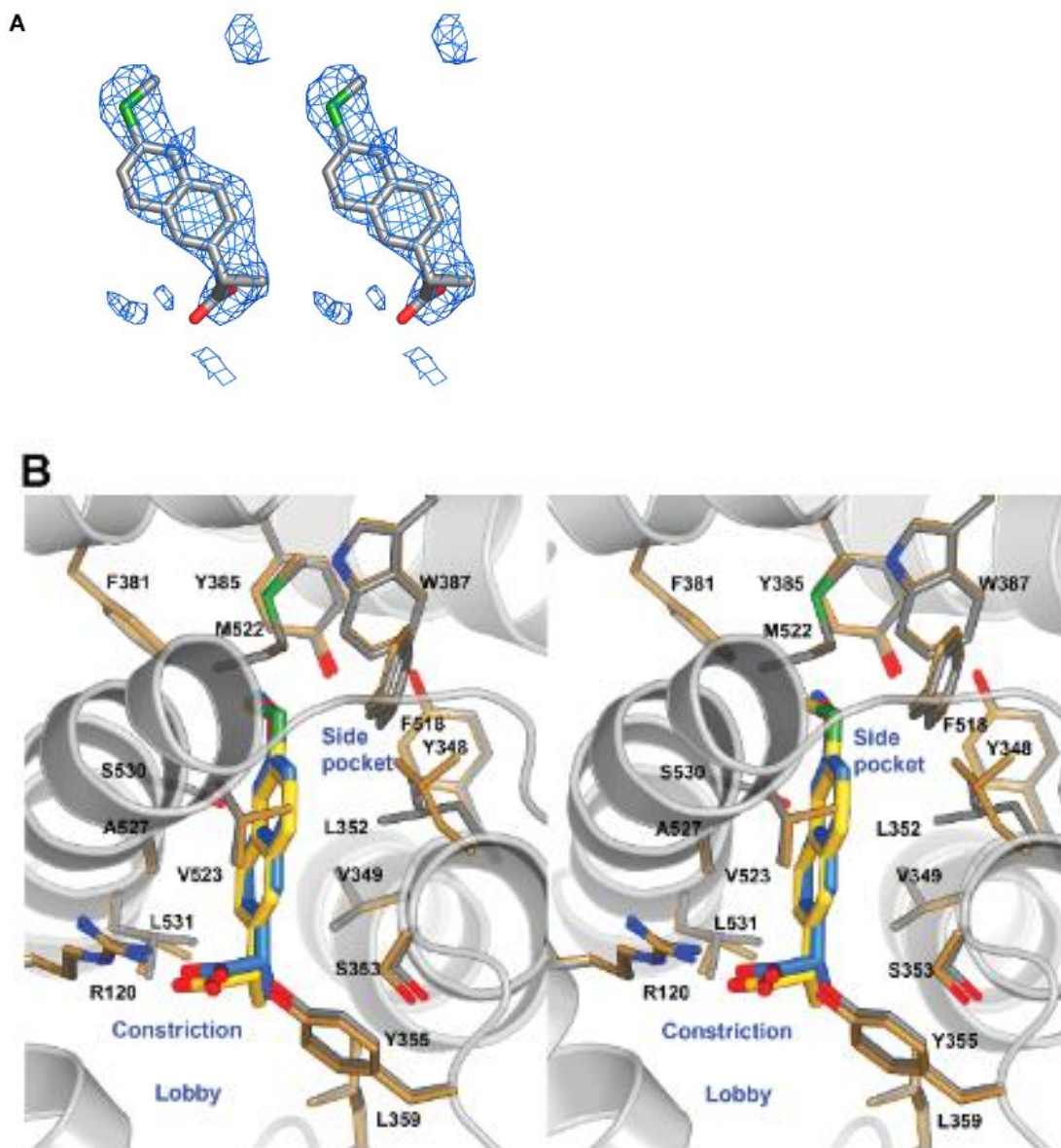
Figure 25 Crystal structure of *p*-methylthio naproxen bound to mCOX-2. A,stereoview of the($F_o F_c$) difference electron map contoured at 3.0δ prior to the addition of the inhibitor to the model.B,ste-review of the *p*-methylthio naproxen analog bound within the mCOX-2 active site.The carboxylate partici-pates in hydrogen-bonding interactions with Arg-120 and Tyr-355 at the base of the active site; this interaction is represented by the dashed yellow lines.[130]

nearest equivalent atoms (distance 0.2 Å) between the two compounds are the sulfur and oxygen atoms of the p-methyl thio and p-methoxy groups, respectively. The carboxylate tails of the compounds vary greatest in position, with the p-methyl thio-substituted compound extending 0.5 Å less deeply into the binding site. The p-methyl thio naproxen analog adopts a binding conformation similar to that of naproxen, maintaining many of the same interactions with surrounding residues. For instance, the carboxylate makes hydrogen-bonding interactions with Arg-120 (2.9 and 3.0 Å) and Tyr-355 (2.5 Å), and the(S)--methyl group builds hydrophobic contacts with Val-349 and Leu-359. The naphthyl backbone participates in van der Waals interactions with Ala-527 and Gly-526, whereas the methyl thio substituent at the 6-position contacts Tyr-385 and Trp-387. In contrast to naproxen, the p -methyl thio naproxen analog is not within van der Waals distances of Leu-352. This difference arises from the Leu side chain exhibiting different side chain conformation in the two structures, with that observed in the methyl thio analog being consistent with that seen in the previously published NSAID mCOX-2 co-crystal structures (three of four monomers). No explanation for the rotation of the residue in the naproxen structure or its failure to rotate in the methyl thio derivative structure is readily apparent. Comparison of the two crystal structures also indicates that Val-523 makes hydrophobic contacts with the naphthyl backbone of the p-methyl thio naproxen analog but does not contact naproxen. This observation results from the relative shift of the compounds within the active site. kinetic studies as well as an extensive mutagenesis study, exploration of the structure-activity relationship, and x-ray crystallography were carried out to find out the molecular determinants of COX inhibition by naproxen. Key interactions between the inhibitor and constriction site residues as well as a novel

interaction with Trp-387 (Fig. 22) was identified. Substitution of an ethyl or methyl-thio group for the p-methoxy substituent created COX-2- favoring naproxen analogs that were unchanged by mutation of Trp-387 to Phe (Fig.24). X-ray crystal structures of both naproxen and the p-methyl thio analog bound to mCOX-2. The combination of mutagenesis, chemical elaboration of naproxen analogs and structural studies clearly defined the contribution of protein and inhibitor atoms to affinity (Figs.23 and 25).

Naproxen is a comparatively simple molecule with only three functional groups dispersed on opposite ends of the naphthyl scaffold. Obtained data specify that each of these substituents is essential for potent inhibition of both COX isoforms and that very slight structural disparity is endured. Mutagenesis data indicate that one probability about the nature of the interaction between the carboxylate moiety of naproxen and mCOX-2 is that the carboxylate interacts with Arg-120 via hydrogen bonding rather than ion-pairing interactions (Fig.22A). In divergence, the crystal structure of flurbiprofen in complex with mCOX-2 shows that the carboxylate makes a salt bridge with the guanidinium group of Arg-120.[141] Besides, prior studies have revealed a 1000-fold increase in the IC_{50} value or flurbiprofen against R120Q oCOX-1 compared with wild-type enzyme, signifying that ion-pairing interactions are more vital for inhibition by flurbiprofen than naproxen.[145]

The-methyl group of naproxen looks to be involved in key interactions with the COX enzymes. Initiation of a range of substituents of variable size and stereochemistry at the -position recommends that the steric requirements for this interaction are rigorous, while removal of the-methyl group also causes a remarkable loss of potency (Table 3a) The-methyl group leads to a small hydrophobic cleft below Val-349, which may help to anchor naproxen within the mCOX-2 active site and thus strengthen the canonical binding

orientation. The x-ray crystal structures of other 2-arylpropionic acids and the diaryl heterocyclic compound, SC-558, bound to the COX enzymes direct that the-methyl group (or 4-trifluoromethyl, in the case of SC-558) is bound in a similar style to the naproxen structure. [131,146] Carboxylate-containing COX inhibitors without a methyl group in the-position applies alternative interactions to bolster binding within the COX active site. For instance, the indolyl-2-methyl group of indomethacin introduces into a hydro-phobic pocket above Val-349 lined by Ala-527, Ser-530, and Leu-531 to form a firmly bound complex. [131,147] Likewise, whereas diclofenac binds in an inverted orientation with the carboxylate coordinated to Ser-530 and Tyr-385, a chlorine atom on the lower aniline ring also supplements into the hydrophobic pocket above Val-349. A key interaction between naproxen and Trp-387 was revealed during the mutagenesis screen by the indicating that the W387F mutant was mostly insensitive to naproxen inhibition. This interaction seems to be exclusive to naproxen as the same mutation had no considerable effect on inhibition of mCOX-2 by diclofenac, flurbiprofen, or indomethacin (Fig.22B). The interaction with Trp-387 may consequence from an amalgamation of hydrophobic packing of the methyl group and electro-static interactions with the polarized methoxy group. This area of the enzyme looks to be stable in its ability to bind functional groups; the p-hydroxy and p-ethoxy analogs were very weak inhibitors, however a methylene or sulfur substitution for the oxygen atom of the p-methoxy group of naproxen created effective inhibitors of WT mCOX-2. Contrasting naproxen, the p-ethyl and p-methyl thio analogs are potent inhibitors of W387F mCOX-2. This recommends that either the interaction with Trp-387 is not essential to inhibition by the naproxen analogs or that they can interact more efficiently with W387F COX-2 than is naproxen. Crystal structures of naproxen and the p-

methyl thio naproxen analog display the substituents at the 6-position oriented in a very like fashion at the top of the COX active site, delivering no definitive basis for differential inhibition of W387F mCOX-2. Additionally, with the exemption of Leu-352, there are no intensely different interactions through the rest of the active site. The substitution of Phe for Trp at position 387 generates a larger active site for the mutant enzyme related with WT mCOX-2. The capability of the p-ethyl and p-methyl thio naproxen analogs to inhibit W387F mCOX-2as well as WT recommends that the analogs may be able to accept an alternate conformation in the larger active site of W387F mCOX-2, rewarding for the loss of the interaction with Trp-387 in the wild-type enzyme.

1.7.7. Oxicam and its analogs

Oxicams are a group of NSAIDs structurally related to 2-methyl-1,2-benzothiazine-enolamide-1,1-dioxides and different types of substituted oxicams such as meloxicam, droxicam and ampiroxicam are available in market. Oxicams are NSAIDs, containing a fused thiazine dioxide ring and an extended carboxamide substitution (Fig. 26C).[142] The oxicam scaffold displays substantial flexibility and occurs as several protonation tautomers throughout the keto/enol equilibrium.[149] Isoxicam attaches to the COX-2 active site using a remarkable binding pose—the murine COX-2isoxicam complex was crystallized in the space group P21212 and diffracted to 2.0 Å applying earlier described conditions.[150] The electron density map of the COX-2 isoxicam complex was of exceptional
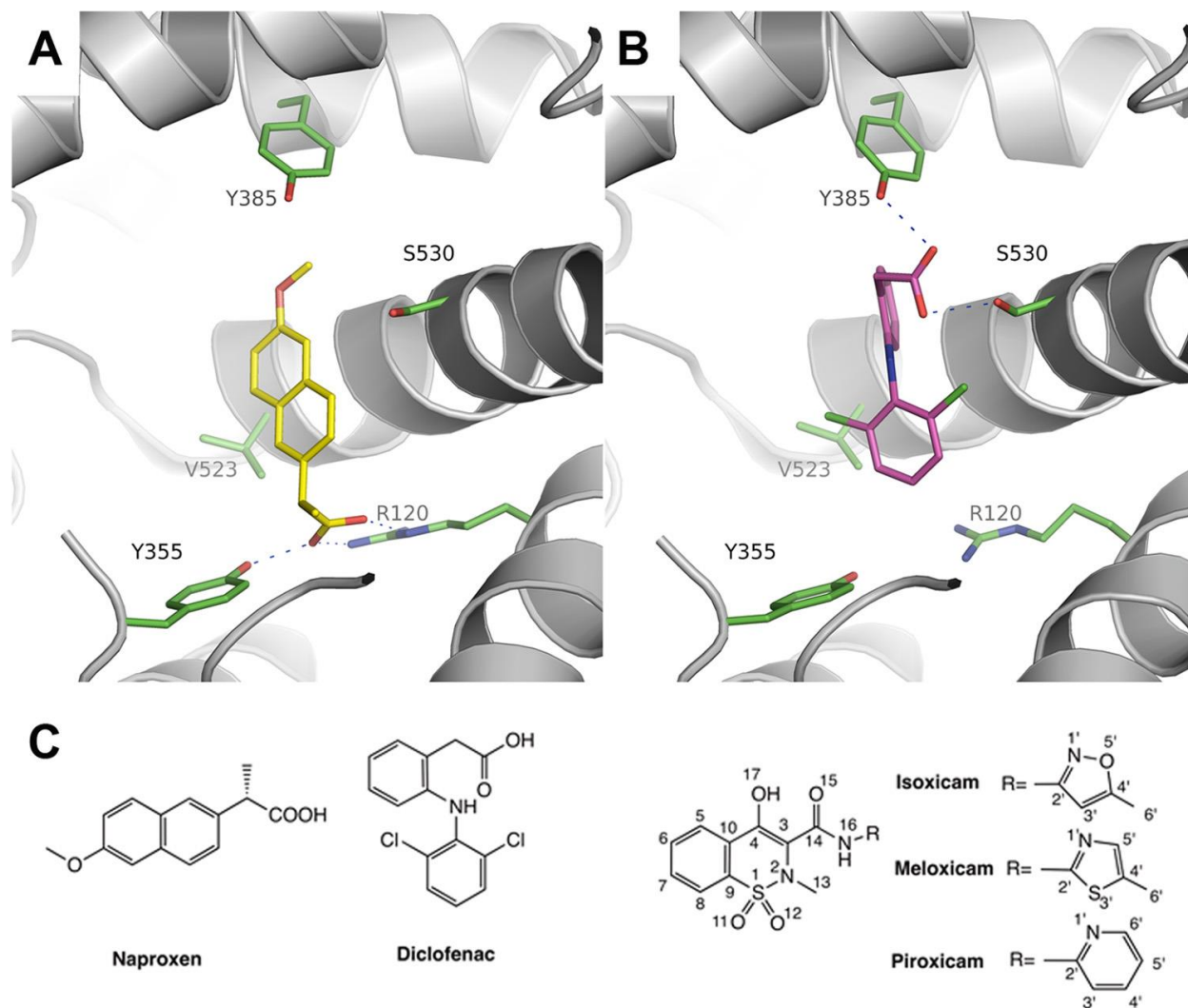
Figure 26. Binding modes of NSAIDs in the COX-2 active site.A,mCOX-2 naproxen complex(PDB ID 3NT1) reveals the H-bonding interactions(dashes) between naproxen(yellow) and the constriction site of mcox-2.B, COX-2 diclofenac complex(PDB ID 1PXX) showing the H-bonding interactions(dashes) between diclofenac(magneta) and Ser-530 and Tyr-385.C,chemical structure of oxicams and other representative NSAIDs.[148]

quality to build in significant amounts of COX-2 (residues 33–583) and other protein sub-structural elements including protoporphyrin IX, the glycosylation sites at Asn-68, Asn-144, Asn-410, and four -OG detergent molecules after molecular switch and structural modification. Four detergent molecules are placed in the outer shell of the protein. There are four molecules next to Lys-180 on the side of each monomer, which are shared with

four other monomers from symmetric mates, counting as two detergent molecules for each asymmetric unit. The other two detergent molecules are outside of Tyr-91 in helix B in monomers B and C. No detergent molecules were observed in the lobby region or close to helix D. The overall structure, consisted of the epidermal growth factor domain, membrane binding domain, and the larger catalytic
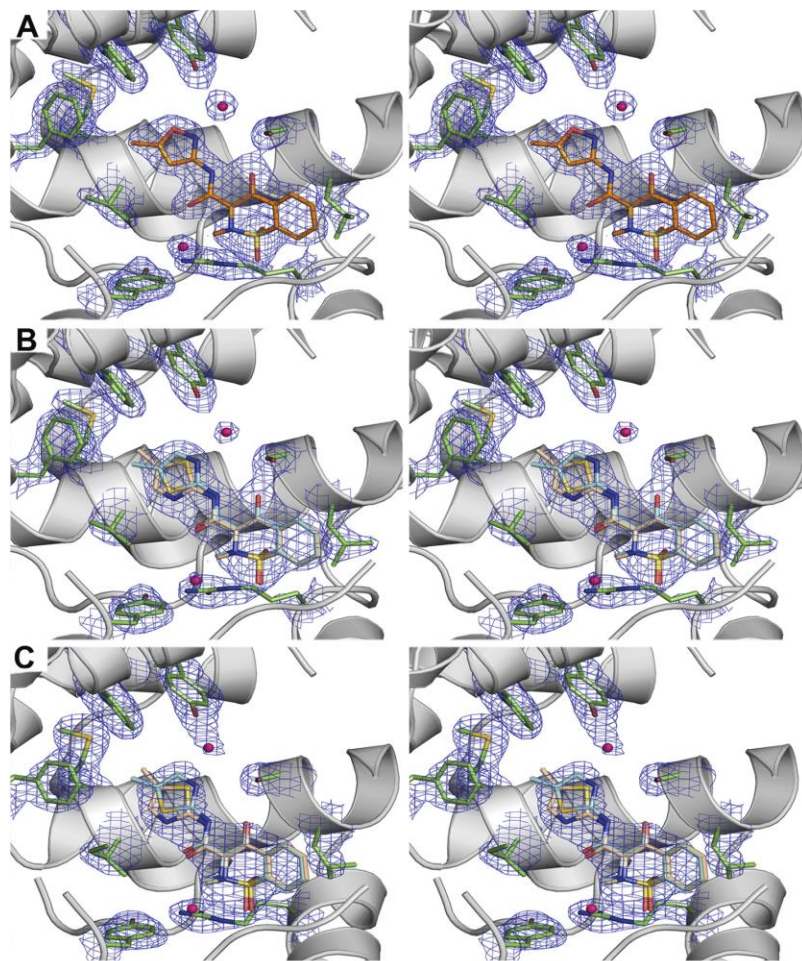
Figure 27. **Stereo-diagram of the electron density maps around isoxicam and meloxicam**. A, a simulated annealing composite omit map in the active site of mCOX-2, isoxicam complex. B, a simulated annealing composite omit map in the active site of mCOX-2, meloxicam complex. C, a simulated annealing composite omit map in the active site of mCOX-1, meloxicam complex. The simulated annealing omits maps (34) are contoured at 1.5 in blue mesh; the key residues are illustrated with a stick representation of the final modal (carbon in green, oxygen in red, isoxicam in orange); the molecule of isoxicam is colored in orange and meloxicam is colored in wheat and yellow.[148]

domain, is like to the high-resolution crystal structure of the mCOX-2 naproxen complex (PDB ID 3NT1), and few variations were observed among the four monomers in the asymmetric unit with a root mean square deviation from 0.16 to 0.21 Å for the backbone atoms. As such, the conformation of isoxicam in monomer A was used to designate the facts associated with COX interactions and comparisons with other COX complexes. The residues are categorized as the ovine COX-1 numbering system for clarity.[131] Well classified electron densities accounting for isoxicam were observed in the COX active site of all four monomers in one asymmetric unit (Fig. 27A). Isoxicam binds in the COX channel in an amazingly unique manner compared with other reported conformation between helix 6 and helix 17 in the active site, adjusting a configuration with an intramolecular hydrogen bond between the nitrogen atom from the carboxamide and the 4-hydroxyl oxygen of the benzothiazine. The drug interfaces with the hydrophobic COX channel, primarily by van der Waals interactions. The only instant polar interaction between isoxicam and COX is a hydrogen bond between the 4-hydroxyl group from benzothiazine ring and Ser-530 with an actual distance of approximately 2.7 Å.

Figure 28. Isoxicam binds to COX-2 in a novel pose via a two-water-mediated network (stereo-diagram). The H-bonds are illustrated as dashes, the key residue is in green sticks, water are in deep pink, and isoxicam is in orange.[148]

Remarkably, two finely ordered water molecules in the active site deliver additional polar bridges between isoxicam and COX residues besides the 4-OH–Ser-530 interaction (Figs. 27 and 28).[148] The first water, which is positioned immediately above the constriction site of COX, is approximately 3.0 Å away from both the oxygen of Tyr-355 and the guanidino nitrogen of Arg- 120, demonstrating that two hydrogen bonds are formed. In the meantime, the same water molecule is within H-bond distances of the oxygen of the carboxamide and the nitrogen atom in the thiazine ring of the inhibitor. At the top of the active site, another water lies between Tyr-385 and Ser-530 and the nitrogen atom of the isoxazole ring from isoxicam. The Binding of Isoxicam to COX-2 takes in Side Chain Rotation of Leu-531 and Structural Movement of Helix D—The isoxicam complex discloses a small difference in the backbones of helices C and D in the membrane binding domain and the side chain of Leu-531 in helix 17 compared with the

1.7 Å resolution mCOX-2naproxen complex (PDB ID 3NT1).[148] Because of steric

hindrance between Val-116 and one oxygen of the dioxide of isoxicam, helix D of COX-2
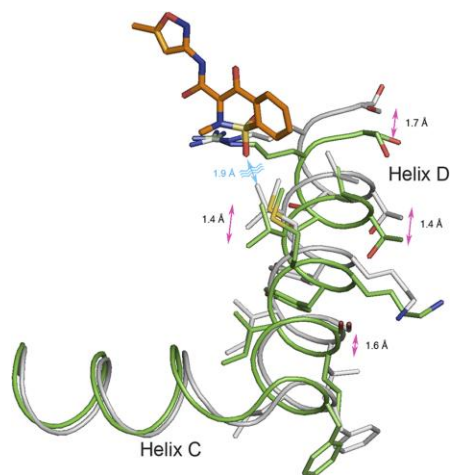
FIGURE 29. Structural changes in helices C and D of COX-2 upon the binding of isoxicam. The backbone atoms of monomer A from mCOX-2 naproxen (PDB ID 3NT1) and isoxicam complexes are aligned. The helices are in a tube representation, with the naproxen complex in gray and the isoxicam complex in green.[148]

travels over 1.0 Å to hold the benzyl ring of the benzothiazine without further modifications

in the orientation of the corresponding residues in the helix (Fig.29). This kind of

movement was detected in the complexes of COX- 2AA and COX-21-AG (3MDL) but to

a lesser degree. This accommodation is also found in helix C, which undergoes a 0.5 Å

shift of the backbone from the original position. This flexibility of membrane binding

domain helices is steady with the observations made in the complex of human COX-2

with a zomepirac derivative, RS57067.[151] In compare, helix 17, which also co-relates with

isoxicam, does not move. Though, the side chain of Leu-531 in this helix shows a different

rotamers (Fig. 30).[148] The C atom of Leu-531 shifts approximately 3.5 Å away from the

active site toward the dimer interface, causing a possible CH- interaction between the C

atom of Leu-531 and the aromatic ring of the inhibitor with approximately 4.2 Å. This

movement releases a new hydrophobic pocket consists of Met-113, Val-116, Leu-117, Ile-345, Val-349, Leu-531, Leu-534, and Met-535, which put up the rigid fused benzyl ring of isoxicam (Fig. 30). Meloxicam Shows Two Conformations upon Binding to COX-2—Meloxicam, an analog of isoxicam, is a 5-fold preferential inhibitor of COX-2 over COX-1.[152] To study why meloxicam is a favored COX-2 inhibitor whereas isoxicam is a nonselective one, the mCOX-2meloxicam complex was determined by x-ray crystallography.The 2.45 Å resolution structure is of appropriate value to include most of the components including the EGF domain, membrane binding domain, the catalytic domain, and glycosylation sites at Asn-68, Asn-144, and Asn-410. Yet, the detailed orientation of the carboxamide moiety of meloxicam could not be determined. Both the sulfur and nitrogen atoms of the thiazole ring are good candidates to make an alike hydrogen bonding network between the coordinated water and the catalytic apex. The electron density around the methyl group on the thiazole ring is inadequate to distinguish the conformation in the complex (Fig.27).[148]

This statement recommends that two conformations are existing in the m COX-2 meloxicam complex. In the first conformation, the methyl group points down toward the entry of the active site. The nitrogen of the thiazole ring is approximately 2.8 Å away from the water, while the sulfur atom interacts with Val-523 and Phe-518 in this conformation. In the second conformation, the methyl group points up and binds in a hydrophobic pocket comprising Leu-384, Trp-387, Phe-518, and Met-522. In this conformation, the sulfur of
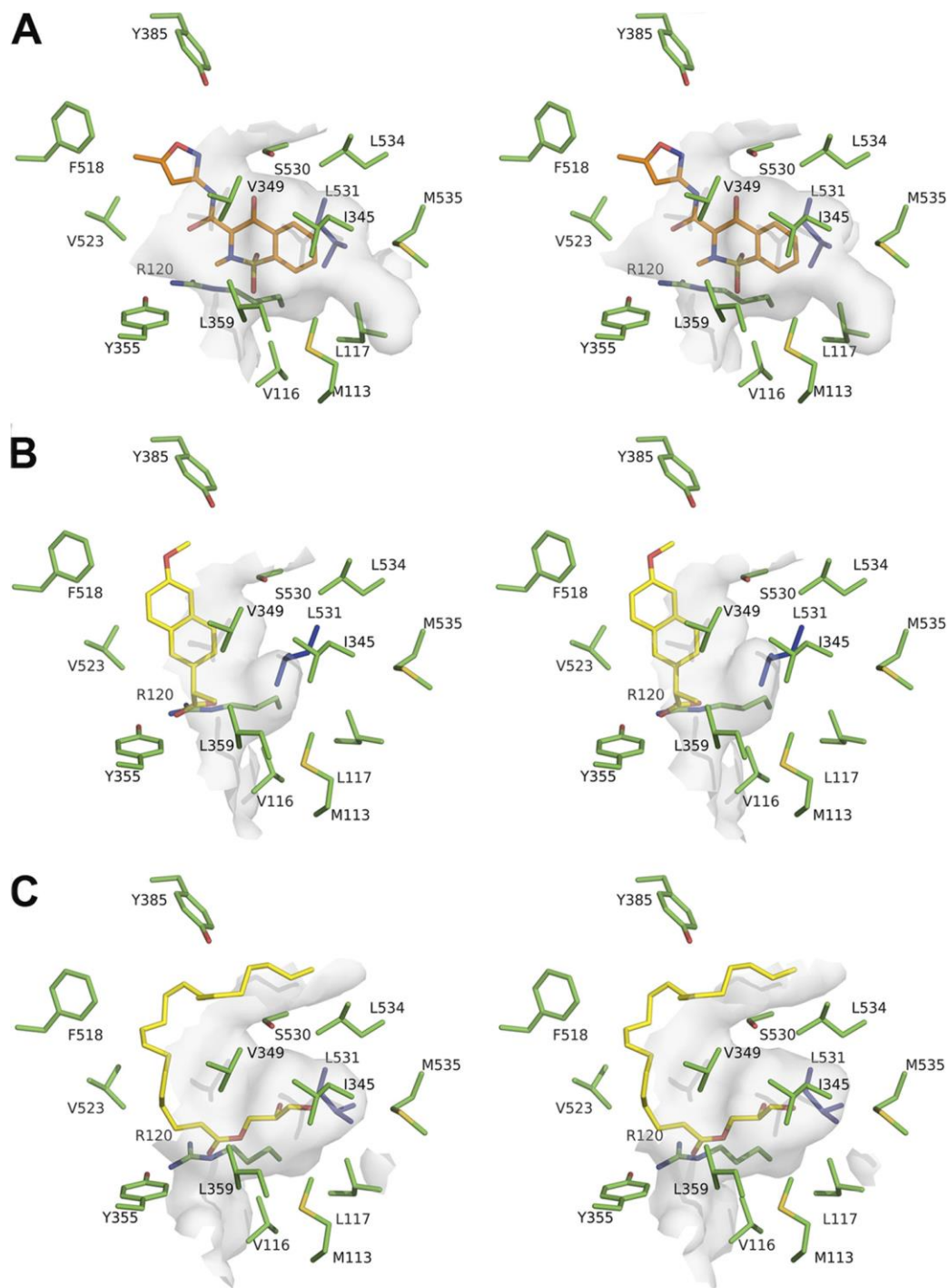
FIGURE 30. Leu-531 opens a new binding pocket for isoxicam in the mCOX-2 active site. A, stereo-diagram of the surface representation around isoxicam (orange sticks and balls). B, same view of the binding pocket around the naproxen (yellow sticks and balls) complex (PDB ID 3NT1). C, binding pocket around 1-AG (yellow sticks and balls) complex (PDB ID 3MDL). The interacting residues are in green, and Leu-531 is highlighted in blue; the surrounding surfaces are shown in semi-transparent gray.[148]
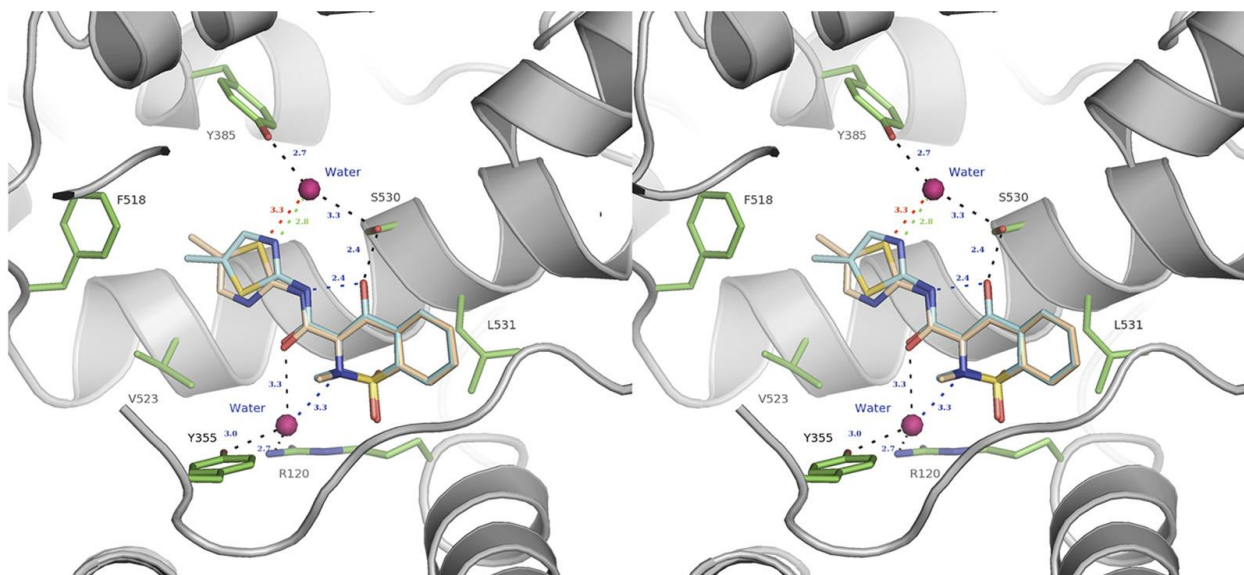
FIGURE 31. Stereo-diagram of meloxicam bound to the mCOX-2 active site. The protein residues are shown as green sticks and balls, the coordinated waters are in spheres, and the methyl-pointing-down conformation of meloxicam is colored in cyan and a green dash for the interaction with the water; the methyl-pointing-up conformation is in wheat with the corresponding H-bond in red. Other hydrogen bonds are illustrated as black dashes.[148]

the thiazole group interacts with the water molecule at an effective distance of 3.3 Å. Based on the quality of the electron density map or the chemical plausibility for satisfying hydrogen bonding and hydrophobic interactions it is not possible to eliminate any confirmation. Therefore, both conformations are counted in in the final structure (Fig. 30). Other than this conformational flexibility, meloxicam binds to the COX active site in the same mode as isoxicam with hydrogen bonding to Ser-530, hydrogen bonding to two coordinated waters complexed to Tyr- 385/Ser-530 and Arg-120/Tyr-355, and the new hydrophobic pocket generated by the movement of Leu-531. Subtle Structural Features around Phe-518 distinct the selectivity of meloxicam for COX-2 over COX-1, Provided that New Structural Insights on Selectivity—The structure of ovine COX-1 in complex with meloxicam was solved at 2.4 Å resolution. The binding pose of meloxicam in the COX-1 active was similar to that of meloxicam bound to COX-2 (Figs.27 and 32). In vitro assay,
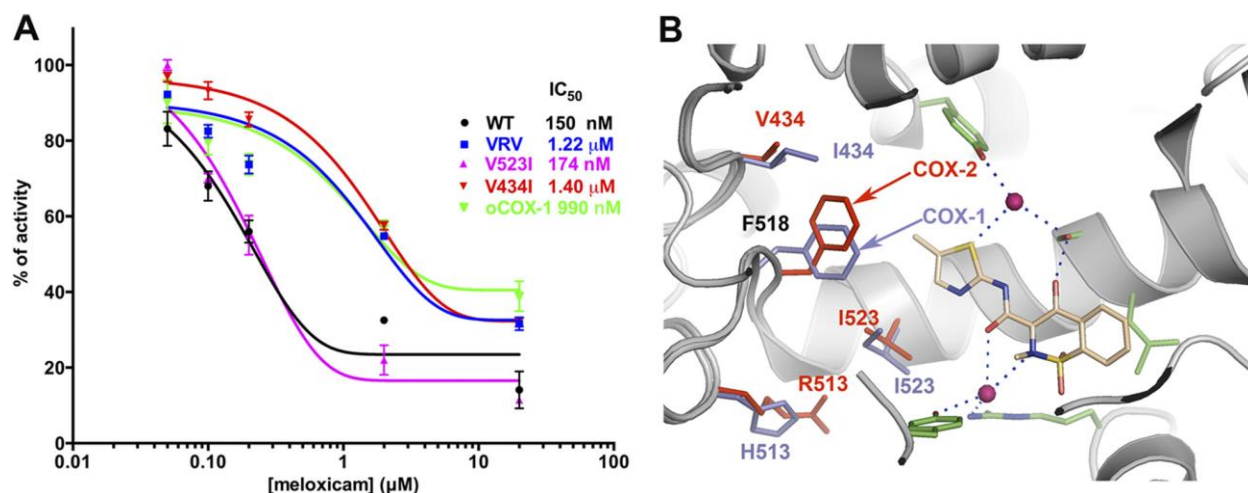
FIGURE 32. Inhibition of mCOX-2 and mutants by meloxicam. A, inhibition profiles of meloxicam toward oCOX-1, mCOX-2, and its mutants. B, structural difference in the active site between oCOX-1 (slate sticks) and mCOX-2 (red sticks) highlighting the changes in residues 434, 518, 513, and 523. Points in A are from triplicate measurements and are depicted as the mean S.E. (error bars). The backbone atoms of oCOX-1 meloxicam structure are aligned with those of the mCOX-2 meloxicam complex. Only the up conformation of meloxicam from mCOX-2 complex is represented for clarity.[148]

meloxicam displays an IC_{50} of 150 nM toward wild-type recombinant mouse COX-2 while

it shows an IC_{50} of 990 nM for native ovine COX-1 (Fig. 32), Physically, COX-1 and COX-

2 share most secondary characteristics with slight changes in the active site that include

I434V, H513R, and I523V COX-13COX-2 substitutions. [131,147] The triple COX-2 mutant of

V434I/R513H/V523I exhibited a reduced inhibition by meloxicam with an IC_{50} of 1.22 M,

which is like wild type ovine COX-1 (Fig. 32). As Arg-513 is placed in the side pocket of

COX-2 and hardly interacts with meloxicam in the crystal structure, then inhibition studies

on the mCOX-2 mutants of V434I and V523I was concentrated. The V523I mutant

displayed potent inhibition by meloxicam with an IC50 of 174 nM. But, meloxicam inhibited

the V434I mutant with an IC_{50} of 1.4 M. This study discloses that mutation of Val-434 to

Ile at position 434 in murine COX-2 is sufficient to decrease the potency of meloxicam

COX-2 inhibition to that of ovine COX-1 (Fig. 32). The extra carbon in the side chain of

Ile- 434 in the secondary shell in COX-1 initiates Phe-518 to move toward the main

63

channel further than in COX-2 in which a valine is located at the same position[131]. Therefore, the selectivity of meloxicam for COX-2 is due to the subtle structural features about Phe-518, wherever several rotamers of Phe-518 are bestowed in COX-1 and COX-2 structures because of the difference of secondary shell residues Ile-434 for COX-1 and Val-434 for COX-2.

Oxicams bind in the cyclooxygenase channel with an innovative pose compared with earlier described NSAID binding modes, in which the carboxylic acid of the inhibitor interacts either in the canonical mode with Arg-120 and Tyr-355[131,147] or in the inverted binding mode with Tyr-385 and Ser-530.[131] On the other hand, oxicams interact with all four of these residues, Arg-120, Tyr-355, Tyr-385, and Ser-530. Nevertheless, apart from a direct hydrogen bond between the 4-hydroxyl group of the benzothiazine moiety and Ser-530, the oxicams do not openly interact with any of these residues by ion pairing or hydrogen bonding. But, they interact indirectly by bridging with two tightly bound waters: a tetrahedrally coordinated water bound to Arg-120 and Tyr-355 and a trigonally coordinated water bound to Tyr-385 and Ser-530. Besides, the water bridge between the carboxamide and Ser-530 and Tyr-385 delivers the first structural clarification for the study that all oxicam drugs contain a heteroatom at the 1position in the carboxamide moiety. The binding of oxicams is go together with by variations in protein conformation, explaining an induced fit mechanism, which is unusual in the interaction between COX and NSAIDs. This comprises the rotation of the side chain of Leu-531 and a modest movement of helix D. The rotamer of Leu-531 in the oxicam complexes is like that detected in the nonproductive conformations of mCOX-2AA mCOX-21-AG (36), and G533V-AA complexes[153], but such a rotation has not been noticed in the binding of any

NSAIDs. For isoxicam, it opens a completely new sub-pocket in the COX active site (Fig. 28), which may characterize a target region for drug discovery. It is an important remarking that the variance in orientation of Leu-531 in the complexes of oxicams or 1-AG is mainly a result of structural fluctuations among the complexes and changes in quality of the electron densities around the region in the two complexes. The second isoxicam-induced protein conformation is the over 1.0 Å movement of helix D as a retort to steric hindrance between the oxygen of the sulfonyl dioxide and the side chain of Val-116. This extra confirms the flexibility of the membrane-binding domain of COX-2.[147] The identification of this novel binding approach offers exact interactions between oxicams and COX-2 and atonements the prior computational models for oxicams.[152] The strain of forecasting the oxicam-protein interactions arises for several reasons: the oxicams may exist in several tautomers; the two highly coordinated water molecules in the active site are nearly impossible to predict, as the representation and role that water plays in ligand-protein interactions reduces the effective ness of docking predictions[154]; and the recognition of the movement of Leu-531 in COX-2 complexes was only recently reported.[154] These complex trepidations in the COX-2 active site existing an array of computational problems that complicate the forecast of oxicam binding modes. Even though most structure-activity relationship studies of oxicams were finished before the discovery of COX-2 and before the recognition of the importance of COX-2 in inflammation, several lines of sign show that the binding mode labelled here fits well with available studies and the pharmacological characterizations of oxicams. The methyl substituent at the 2 position of the benzothiazine is optimal for anti-inflammatory activity. This methyl group interacts with residues Leu-359, Tyr-355, and Val-349. Replacement

of this methyl group with any other substituent (e.g. H, benzyl, allyl, ethyl, propyl) either removes the interaction between the protein residues or introduces steric bulk that prevents binding in this region. Thus, such substituents were less active than the 2-methyl compounds. Among analogs of 3-carboxamides with anilide substituents, meta-substituted anilides display more potent activity than para-substituted anilides. The meta-substitution pattern mimics the methyl-up conformation of meloxicam and fits quite well within the pocket formed by Leu-384, Tyr-385, Met-522, Phe- 518, and Trp-387 in the crystal structures. Finally, in a study of thieno [2,3, -e] thiazine analogs, the 2-pyridyl carboxamide (tenoxicam) presented better activity compared with isomeric 3- or 4-pyridyl amides, consistent with the essential role of a H-bond acceptor for ligand binding to the water coordinated to Tyr-385 and Ser-530. Meloxicam displays modest COX-2 selectivity with an IC_{50} of 150 nM for COX-2 and an IC_{50} of 990 nM for COX-1 in our in vitro assay. In mutagenesis experiments recommend that the preference of meloxicam for COX-2 is not because of the substitution of Ile-523 in COX-1 for Val-523 in COX-2, which responsible for the selectivity of inhibition by rofecoxib and celecoxib, but somewhat subtle changes around Phe-518 produced by the substitution of isoleucine to valine at residue 434 in COX-2 (Fig.33). The added methylene group of Ile-434 in oCOX-1 drives Phe-518 into the main channel of the cyclooxygenase active site and shrinks the available space close to the thiazole ring of meloxicam. This modification of the orientation of Phe-518 between COX-1 and COX-2 structures was first defined in the complex of COX-2 with SC-558, a diaryl heterocyclic COX-2 selective inhibitor.[131]It was recommended that the addition of the phenyl sulfonamide group into the side pocket of COX-2 is helped by the movement of Phe-518 to accommodate the movement of Val-523. This hypothesis

was not verified with mutagenesis experiments. The probable bangs between the 4-methyl group of meloxicam and Phe-518 propose a direct interaction of Phe-518 with inhibitor in the case of meloxicam as resisted to protein movement in the case SC-558. Thus, subtle environmental differences around Phe-518 adjust the COX-2 selectivity of different classes of inhibitors. Together, the crystal structure of recombinant murine COX-2 in complex with isoxicam and meloxicam existing here delivers the first structural description for the binding mode of the oxicam class of NSAIDs and discloses a novel binding mode in the cyclooxygenase channel via a two-water-mediated network characterized by interactions with formerly recognized binding residues all over the main channel of the active site. Additionally, this binding mode involves the movement of Leu-531 to accommodate the inhibitor. This is the first time Leu-531 has been known as an interacting residue in NSAID binding although it is involved in binding certain substrates. Moreover, mutagenesis studies direct that the molecular basis for the preferential inhibition of COX-2 by meloxicam is because of the subtle differences around Phe-518 in the active site. In conclusion, this structural description of COX-2oxicam complexes clarifies previous structure-activity studies of oxicams, directs new substitutions within the oxicam scaffold, and finds a new pocket around Leu-531 for development of novel NSAIDs.

1.7.8 NSAIDs as anti-cancer agent

Infections and inflammation link to cancer. A possible relation between inflammation and the growth of pre-cancerous trauma in different cells have been recognized. The

researcher has found that inflammation in prostate, colon, and pancreas will increase 14%, 25% and 20% risk of prostate, colon and pancreatic cancer respectively.[155] Therefore, inflammation seems to initiate or induce growth of tumor cells. Chronic inflammation depicted by infiltration of mononuclear immune cells (including macrophages, lymphocytes, and plasma cells), tissue destruction, fibrosis, and increased angiogenesis. Due to Chronic inflammation, the initiation and propagation of tumor cells such as intensified genomic damage, augmentation of DNA synthesis, cellular proliferation, disruption of DNA repair pathways, inhibition of apoptosis, and the promotion of angiogenesis and invasion occur in cells. Pro-inflammatory molecules, such as cytokines, inducible nitric oxide synthase (iNOS), reactive oxygen species (ROS), and NF-kB are upregulated in chronic inflammation. All these processes simultaneously ensure a suitable microenvironment for the exponential growth of tumor cells. So, inflammation may give both the key mutations and the compatible environment to enhance tumor growth.

In Chavey et al., it is mentioned that some cytokines, including IL-6, IL-8, G-CSF (granulocyte colony stimulating factor), IFN-γ (interferon-γ), and MIP-1β (macrophage inflammatory protein- 1β), were found to be more abundant in breast carcinoma than in normal breast tissue. Nowadays, Researchers also have found that COX1 and COX2 enzymes are overexpressed in different tumor cells, for example colorectal, gastric, esophageal, hepatocellular, pancreatic, head and neck, non-small cell Lung, ovarian, breast, bladder, cervical, endometrial and skin Cancer cells.[156]

Long term use of aspirin (a Non-selective NSAID) and other NSAIDs reduce the incidence of colorectal esophageal, breast, lung and bladder cancers. In 1990, indomethacin was

used as an anti-tumor agent in over hundred patients in an advanced stage of colorectal cancer and liver, Pancreatic cancer and primary gastric cancers and found that patient survived six months more than the expected. Hong-Mei Wang et.al mentioned that Indomethacin suppressed the growth of colon cancer via inhibition of angiogenesis in vivo.[157]

Selective COX-2 inhibitor celecoxib Inhibits AKT signaling and induces apoptosis of human colorectal and prostate cancer cells in vitro.[158] Researchers also have found that COX2 inhibitors also reduce the growth of human breast & lungs cancer and COX1 inhibitors inhibit the progression of human ovarian as well as colon cancer. Sue-Lin Fu et.al[159] have found that COX-2 inhibitors have anticancer effects on gastric cancer. Inhibitors show significant roles in angiogenesis and infiltration or metastasis of stomach carcinoma. The anticancer effects of COX-2 inhibitors may involve inducing apoptosis, suppressing proliferation, reducing angiogenesis and weakening invasiveness. Researchers have identified that selective COX-2 inhibitor, Celecoxib active against breast cancer in vitro and vivo.[160-161] In a combination of NSAIDs and chemotherapeutic agents, the scientist has obtained synergetic effects on tumor development and progression in vitro models 3. In 1994, Teicher et al. performed a Lewis lung carcinoma model and identified a positive effect of using nonsteroidal anti-inflammatory drugs with chemotherapy in the primary and last stage of non-small cell lung cancer. It is proven that in combinations of a COX inhibitor with chemotherapeutic agents such as cisplatin and cyclophosphamide led to tumor growth delay and a decreased number of lung metastases.[162]Moreover, researchers have found a synergistic effect on human NSCLC cell lines by using sulindac sulfide (COX-1 and -2 inhibitor) with the cytotoxic agents

paclitaxel and docetaxel.[163]In mouse model study, it is found that non-selective COX inhibitor SC-236 drug prevents tumor growth and increases the effect of radiotherapy without affecting the radio response of the standard tissue.[122]Pyro et al. studied and identified the radiation-enhancing effect of COX-2 inhibitors in vitro as well as in vivo in human lung and colon cancer.[164]

COX inhibitor, nimesulide showed inhibition of proliferation and decreased the doses of different anti-tumor drugs such as cisplatin, VP-16, and docetaxel.[165]

NSAIDs can also use for reduction of side effects associated with chemotherapy. When celecoxib applied with capecitabine for metastatic colorectal cancer chemotherapy, the side effects (such as diarrhea and the hand–foot syndrome) decreased in greater extent.[166] In colorectal cancer xenograft mouse model (HT29 cells and Colon-26 cells in nude mice and BALB/c mice) studies, it was found that Celecoxib enhanced CPT-11 cytotoxicity and also reduced the difficulty of CPT-11 induced diarrhea.[167]

Celecoxib increases CPT-11 cytotoxicity in colorectal cancer xenograft mouse models (HT29 cells and Colon-26 cells in nude mice and BALB/c mice), but it can also decrease the severity of CPT-induced diarrhea. The remission of diarrhea recommends an inflammatory part of the pathogenesis of CPT-11 induced delayed diarrhea. Trifan et.al identified that COX-2 enzyme was expressed after treatment of rat colon cancer cells with CPT-11 and PGE2 synthesis was enhanced.[168]

Through cell line model study, it is clear that NSAIDs are also active against the tumor. NSAIDs can do prevention of angiogenesis, proliferation, invasive growth, and induce apoptosis in cells in a COX2 dependent or independent manner. Anti-cancer activities of

NSAIDs follow verities of the mechanism. But, the key mechanisms are the prevention of prostaglandin E2 (PGE2) formation and transcriptional activity of COX2 inhibition. Moreover, by clinical trials, the required doses of NSAIDs that induce COX2 free path for causing anti-tumor activities are not found yet.

EGFR (epidermal growth factor receptor) has a significant role in the regulation of normal cell growth, apoptosis, and other cellular activities. Different types of cancers such as non-small-cell lung cancer, pancreatic cancer, breast cancer, colon cancer and some other cancers that are caused by upregulation of EGFR. The receptors are continuously and abnormally activated by mutation of EGFRs. EGFR inhibitors used as anti-cancer agents. Since COX produces PGE2 which activates the EGFR, in combination therapy both inhibitors play a synergetic role in cancer treatment. When Celecoxib was used with Herceptin (a monoclonal antibody against the ErbB receptor HER-2/neu) in vitro and in the vivo cell proliferation assay, Mann et al. found a positive effect on control of colorectal carcinoma cell growth. In colorectal cancer cell growth reduction, COX-2 and HER2/neu inhibitors work together more efficiently. In a murine model study of human FAP, it is identified that in a combination of sulindac (a COX inhibitor) with EKI-569(an irreversible inhibitor of EGFRK) furnish protection to intestinal neoplasia.[169]

1.7.9. NSAIDs to circumvent resistance to conventional chemotherapy

At First, NSAIDs were combined with traditional chemotherapeutic agents to overcome cancer chemotherapy resistance mechanism and found that NSAIDs increased the efficacy of the chemotherapeutic agents. In the mitochondrial level, Bcl-2 family of pro and anti-apoptotic proteins stimulates or inhibits apoptosis. Bcl-2 family members impart a clinically important resistance to chemotherapeutic agents in some hematologic and

solid malignancies, including acute myeloid leukemia, acute lymphoblastic leukemia, chronic myeloid leukemia, chronic lymphoblastic leukemia, multiple myeloma, prostate cancer, malignant brain tumors, and neuroblastoma.[170-175] Downregulation of Bcl-2 amplifies toxicity for chemotherapeutic agents in some tumor cell lines.[176-177]COX-2 selective NSAIDs such as SC-58125 and NS-398 can down-regulate Bcl-2 and consequently induce apoptosis in colon and prostate cancer cell lines.[178] In HCT116 colorectal carcinoma cells, it is found that an increase in pro-apoptotic Bax protein and a decrease in Bcl-XL protein induces apoptosis.[179] Through Bak and Bax up-regulation, mitochondrial membrane potential loss and activation of caspase-3.[180-181](Fig-26) Celecoxib, aspirin, and indomethacin might induce apoptosis. Bcl-2 family of anti-apoptosis proteins can also be downregulated by inhibiting Akt signaling. Akt/PKB is a serine/threonine protein kinase that works as an important regulator of cell survival and proliferation. It has been revealed that PI3K/Akt signaling components are frequently altered in human cancers. Another mechanism of amplified Akt signaling is the reduced activity of Akt regulatory proteins. Akt phosphorylation is linked with phosphorylation and thus inactivation of the pro-apoptotic proteins Bad and caspase-9. Phosphorylated Bad cannot bind to Bcl-2, whereas phosphorylated caspase-9 cannot be activated lead to a reduced activity of mitochondrial apoptosis[182-183]. Celecoxib and aspirin inhibit Akt phosphorylation and resulting in apoptosis in the human A549 non-small cell lung cancer cell line.[184] In an in vivo model of spontaneous metastatic breast cancer, it is found that celecoxib-induced apoptosis correlated with a significant decrease in Akt activation.[185] Celecoxib also blocked Akt phosphorylation and kinase activity in cultured human C611B cholangio carcinoma cells, which associated with Bax translocation to mitochondria,

cytochrome c release into the cytosol, followed by activation of caspase-9 and caspase-3. The addition of PGE2 to these cells suppressed the apoptotic activities of celecoxib.[186-187] The epidermal growth factor receptor (EGFR; erbB1), a member of the tyrosine kinase receptor family composed of HER-2/neu (erbB2), erbB3, and erbB4.[188-189] The ErbB receptors are located at the cell surface and connect to a common structure constituted of an extracellular ligand binding domain, the transmembrane segment, and an intracellular tyrosine kinase domain.[190] When LS-174T colorectal carcinoma cells exposed to PGE2 and display rapid induction of Akt signaling, Akt activation can be stopped by EGFR-specific tyrosine kinase inhibitors. This rapid transactivation of the EGFR appears through an intracellular pathway because inactivation of EGFR ligands with inhibitory antibodies did not inhibit PGE2-mediated Akt activation (Fig. 33).[191] In Caco-2, LoVo and HT-29 colon cancer cell lines PGE2 expression induces phosphorylation and consequently activation of downstream targets of the EGFR pathway such as ERK2. When selective inhibitors activated EGFR activation, PGE2 induced ERK2 activation reduced extensively.[192] PGE2, still, can also directly activate EGFR signaling and thus promote cell proliferation.[190,191] The mechanism involves PGE2-mediated metalloproteinase activation resulting in shedding of EGFR ligand from the plasma membrane and consequently, stimulated EGFR signaling. Another mechanism includes activation of the cAMP/protein kinase A pathway directing to enhanced expression of amphiregulin, a ligand of EGFR.[193] The TNF family of death receptors and ligands is a family of apoptosis-inducing proteins. Several human death receptors have been recognized.[194,195] Apoptosis is activated upon binding of specific TNF superfamily ligands, such as TNF, FasL (CD95L/APO-1L) or TNF- related apoptosis-inducing ligand (TRAIL),
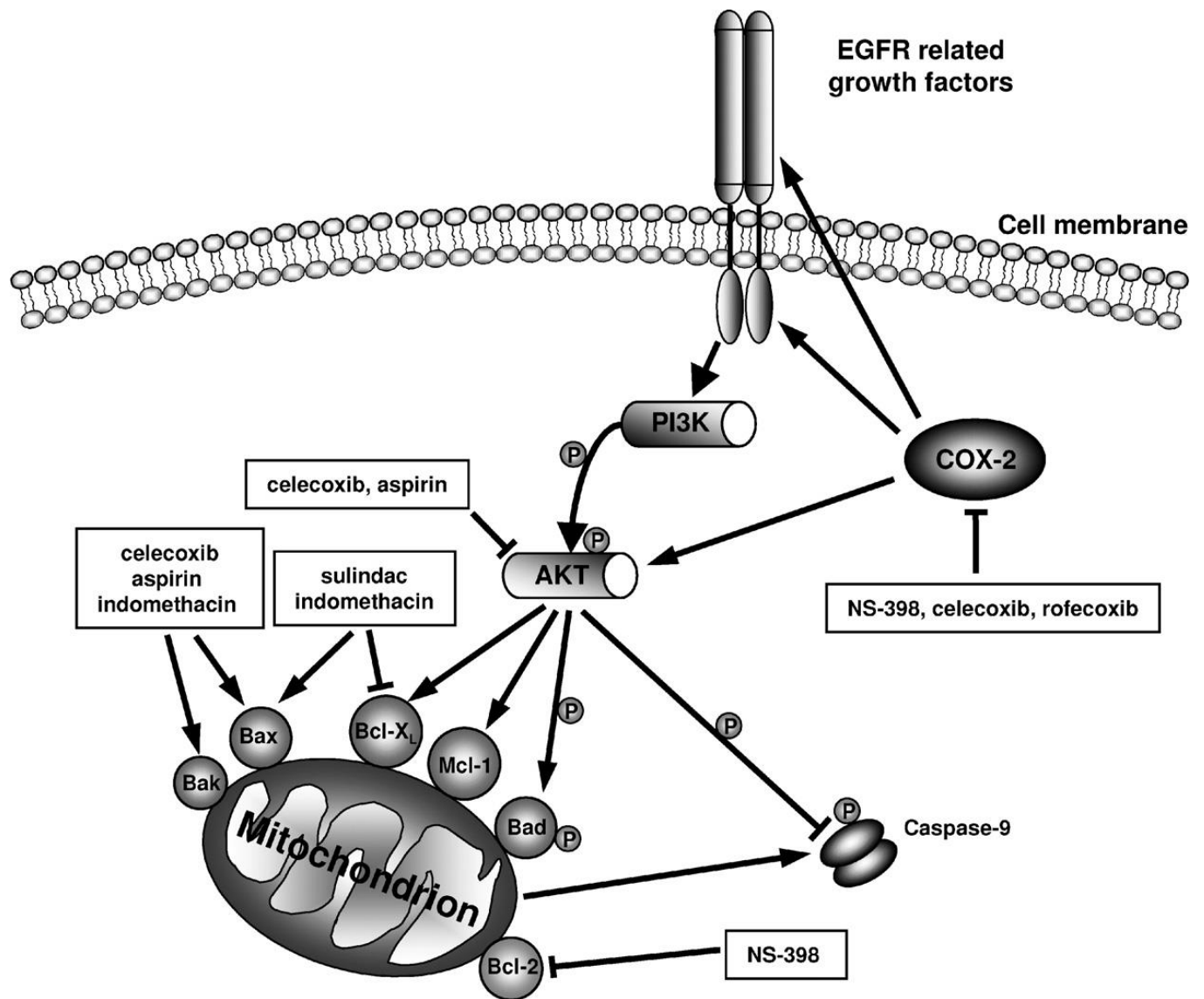
Figure 33- Akt can be upregulated by COX-2, while both Akt and COX-2 are inhibited by NSAIDs. Inhibition of Akt prevents phosphorylation and inactivation of Bad and caspase-9 resulting in decreased apoptosis. Different NSAIDs can modulate expression of Bcl-2 family members. Modulation of Bcl-2 family members involves downregulation of anti-apoptotic members and upregulation of pro-apoptotic members.

to a receptor TNFR1, TNFR2, Fas or DR4 (TRAIL-R1/APO-2)/DR5 (TRAILR2/ KILLER/ TRICK2), respectively. Moreover, attaching to the agonistic receptors TNFR1, TNFR2, Fas, DR4, and DR5, FasL can also bind to the soluble inhibitory decoy receptor, DcR3,

74

whereas TRAIL can bind to membrane-bound DcR1 (TRAIL-R3) and DcR2 (TRAIL-R4), which both lack functional death domains and are thus unable to induce apoptosis. TRAIL also attaches to a soluble TNF family receptor, osteoprotegerin. But, the physiological importance of this interaction appears to be nominal. Upon trimerization of the death receptors, an intracellular death inducing signaling complex (DISC) is produced that consists of trimerized receptor molecules and recruited TNF receptor associated death domain (TRADD) or Fas-associated death domain (FADD) and procaspase-8 molecules. Subsequent DISC gathering a cascade of effector caspases and substrates are triggered. The nucleus is compressed and split, the cytoplasm is reduced, and apoptosis induction is completed.[196, 197]

Many studies discovered that death receptor apoptosis pathways are involved in chemotherapy-induced apoptosis. NSAIDs are also able to induce apoptosis via the TRAIL and Fas signaling pathways as was identified by Han et al. They presented that FADD is required to induce apoptosis with indomethacin in Jurkat cells.[198] Indomethacin also induces apoptosis in a developed doxorubicin resistant SCLC cell line via death receptor signaling.[199] In a hepatocellular cell line model, exposure to NS-398 caused Fas ligand upregulation and Fas-mediated apoptosis in COX-2 overexpressing cell lines.[200] TRAIL receptor DR5 was upregulated in colon, prostate, and NSCLC cell lines after contact to sulindac sulfide and celecoxib, respectively. These NSAIDs induced apoptosis, which was further enlarged in combination with TRAIL[201,202] (Fig. 27). COX-2 inhibition can be straightway involved in enhancing TRAIL-mediated apoptosis as demonstrated in HT29 colon cancer cells. Both COX-2 inhibition and COX-2 downregulation induced

clustering of DR5 at the cell surface and reorganization of the death-inducing signaling

complex components (DR5, FADD, and procaspase-8) into cholesterol-rich and

ceramide-rich domains.[203] Also, the upregulation of DR5, NSAIDs especially, sulindac

might also increase TRAIL-sensitivity by down-regulating surviving expression.[204–207]

Other downstream components of the apoptosis pathway such as anti-apoptotic

members of the Bcl-2 family can be disturbed NSAIDs as well. For example, the reduction
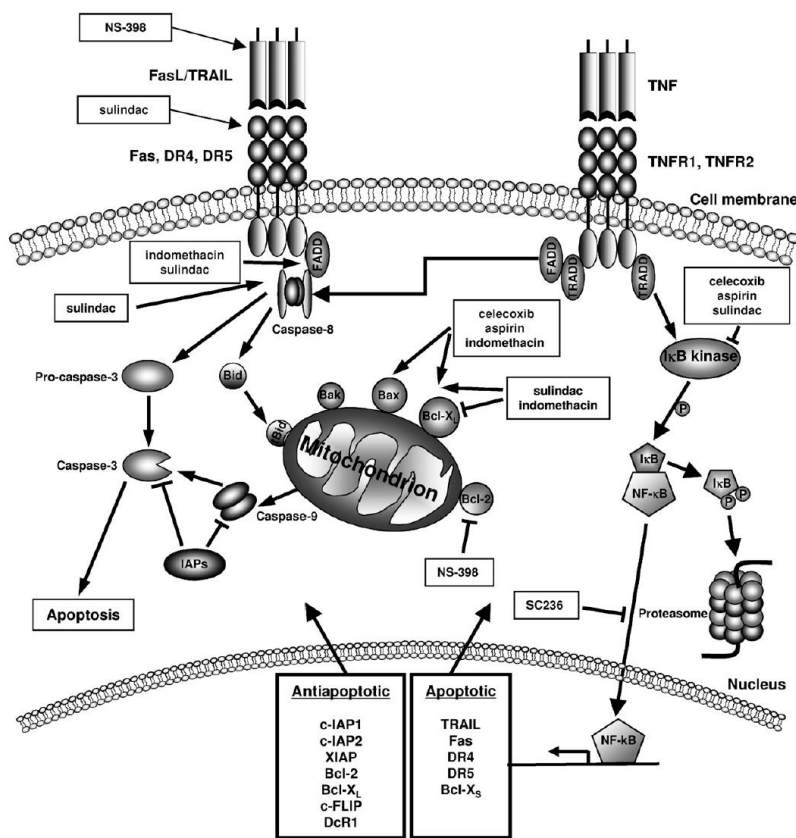
Figure 34- Death receptor-mediated apoptosis is facilitated at different levels by NSAIDs. NS-398 increases FasL expression, sulindac sulfide increases DR5 expression and indomethacin and sulindac sulfide can activate the intracellular part of the death-inducing signaling complex. Inhibition of I_B kinases by selective and non-selective COX inhibitors results in decreased NF-_B in the nucleus and subsequently in a decreased transcription of pro- and anti-apoptosis proteins in expression of the anti-apoptotic protein Bcl-XL in Bax-proficient HCT116 cells by sulindac sulfide enlarged TRAIL induced apoptosis. The impact of sulindac sulfide on Bcl-XL is probably due to a reduction in NF-_B activity[208].

1.8 Synthesis of BRL-37959

BRL-37959 was synthesized by Boyle and his coworkers of using expensive starting material and overall yield of the process was only 5%. This synthetic method is shown in Scheme 1.

Scheme 1: First Method for Synthesis of BRL-37959 by Boyle
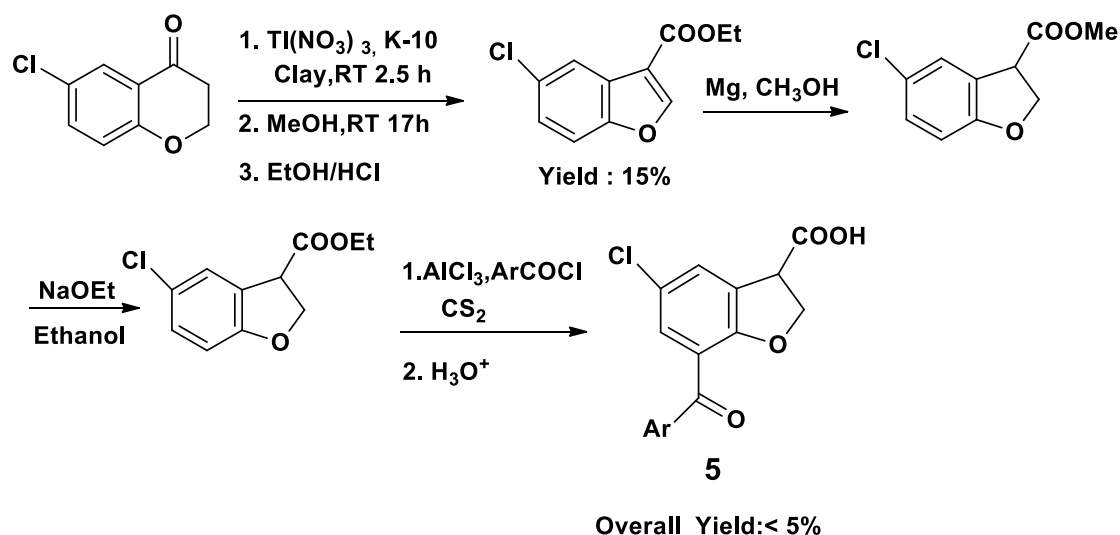
Since the compound seemed a potent NSAID, Becham Research Laboratory (BRL) developed second method(scheme-2) to produce BRL-37595. The overall yield of the method was also ≤ 5%. Then they developed also third method to (scheme-3) synthesize the compound but yield was not improved.

1.8.1. Direct Friedel-Crafts benzoylation of 5-chlorobenzofuran-3-ethyl ester (3)

Friedel-Crafts benzoylation was done on 5-chlorobenzofuran-3-ethyl ester directly (scheme-4) gave benzoylation exclusively at the Ortho-position (i.e., 33) in 20% yield and

was not investigated further. This result is supported by previous researchers.[217] A long with the method above, the method of Sharghi[182] et al. was used ZnO as a catalyst (Scheme: 5). This process was unsuccessful, and only starting materials were recovered.

1.8.2. Attempts to benzoylate 5-chloro salicyalldehyde (1)

A Fries method was also tested to benzoylate 5-chlorosalicylaldehyde as shown in (Scheme 4) below. This method also proved failed when 5-chloro salicylaldehyde was used. When only salicylaldehyde was used, the reaction gave low yields (i.e., < 5%) of salicylaldehyde benzoylated at the para position.

1.8.3. Exploration of other methods

While direct benzoylation of 5-chlorobenzofuran was not feasible due to the above result, investigation of previous work, other than that presented earlier, disclosed two interesting methods that might have likely in forming the elusive 3-formyl-2-hydroxy benzophenone as shown in Figure 35. Synthesis of 3-formyl-hydroxy benzophenone would tolerate for subsequent transformation into a benzofuran-3-ethyl ester derivative. Since this compound could be proposed through only two possible methods, an approach was made to synthesize 3-formyl-2-hydroxybenzophenone. The first method included a novel Mg-mediated formylation of 2-hydroxybenzophenone and the second method involved either a Duff formylation of salicylic acid as shown in Scheme 6.[217]

Scheme 2:

X= Me,Cl,Br

Overall Yield:< 5%

Scheme 3:

X = Cl, H, Br, F, CH₃

Overall Yield:< 5%
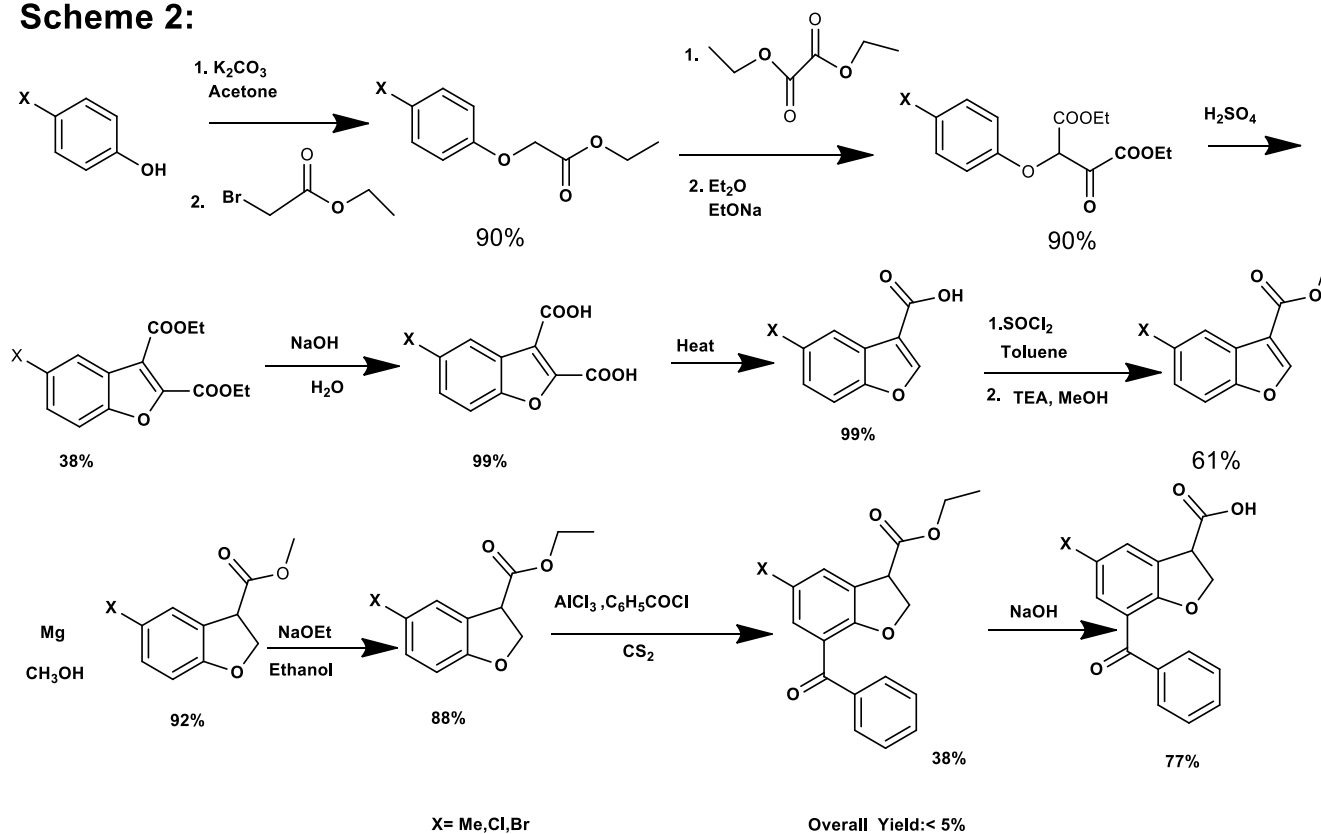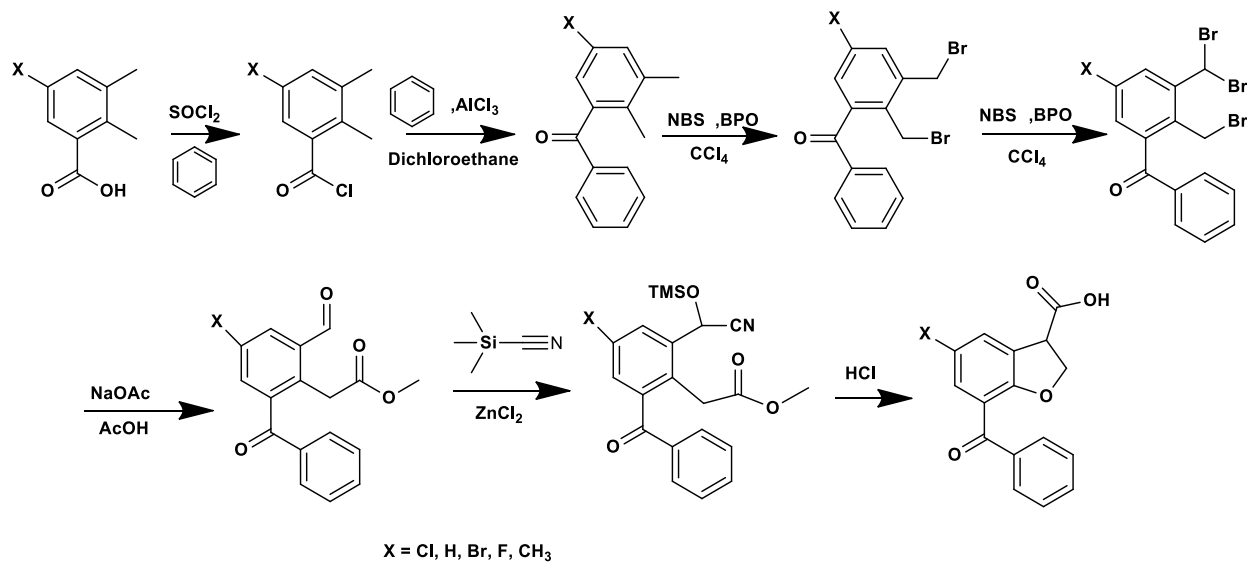
Scheme 4: Direct Friedel-Crafts benzoylation of 5-chlorobenzofuran-3-ethyl ester

Yield: 20%
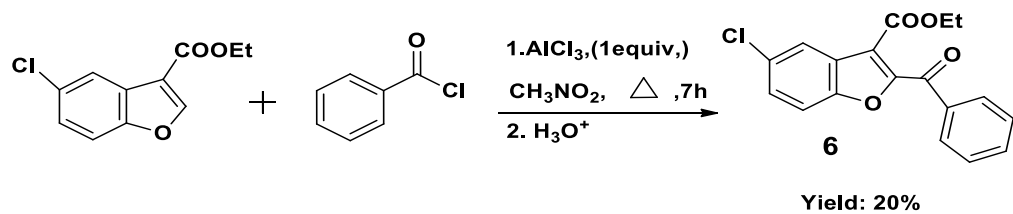
Scheme 5: Sharghis method of acylation

N.R.
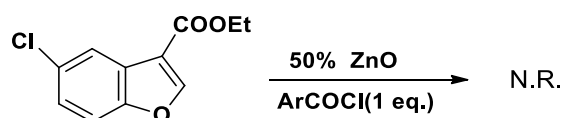
Approach 1: Formylation
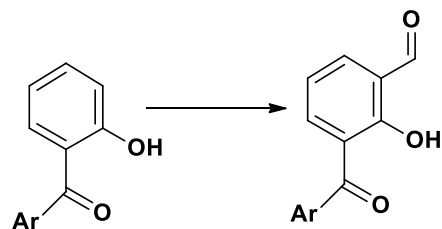
Approach 2: Benzoylation
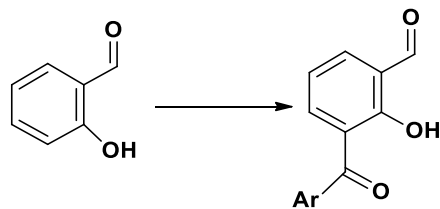
Figure 35- Two possible approaches to produce BRL-37959

Scheme 6: Fries rearrangement
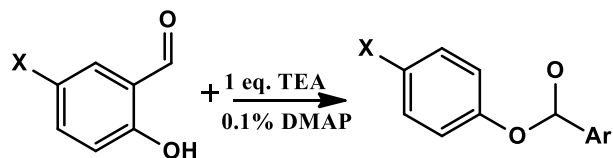
X = Cl, 5-chlorosalicylaldehyde

X = H, salicylaldehyde

X = Cl, 5-chlorosalicylaldehyde benzoic acid ester

> 90%

X = H, salicylaldehyde benzoic acid ester

> 90%

AlCl$_3$
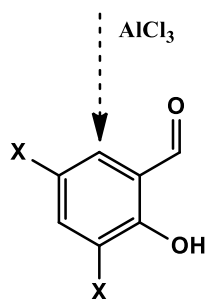
X = 5-Cl, 3-COAr; 4-chloro-2-hydroxy-3-formyl- benzophenone

N.R

X = 3-H, 5-COAr; 3-hydroxy-4-formyl- benzophenone

5%

Scheme 7: The Duff formylation of salicylic acid

hexamine   salicylicacid

3-formylsalicylic acid
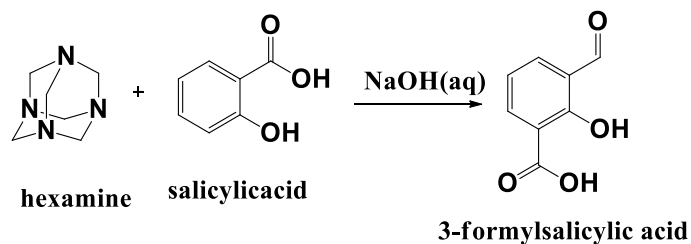
The second method showed difficult when using the Fries rearrangement and besides required protection of the aldehyde functional group. Several protection approaches were investigated using salicylaldehyde as the prototypical substrate. Some of these protected salicylaldehyde derivatives were tried using diethanolamine, glycol, or methanol to give the corresponding acetal or oxazolidine derivatives. Remarkably, the addition of diethanolamine to salicylaldehyde gave a high yield (>90%) after azeotropic distillation of oxazolidine. Attempted protection with ethylene diamine gave an imine. Furthermore, protection of the phenolic group by replacement with methoxy was active using o-anisaldehyde. In addition to, complete reduction of salicylaldehyde to salicyl alcohol (i.e., 2-hydroxybenzyl alcohol) was also attempted using sodium borohydride, followed by treatment with acetone in the presence of a catalytic amount of aluminum chloride (AlCl$_3$). This reaction created a protected dioxin compound which subsequently polymerized heavily on treatment under the resulting Friedel-Crafts conditions employed duringbenzoylation. The overall structures of the protecting groups and the final reaction scheme are illustrated in Figure 24 below. None of the protection plans outlined in Figure 24 gave benzoylation.
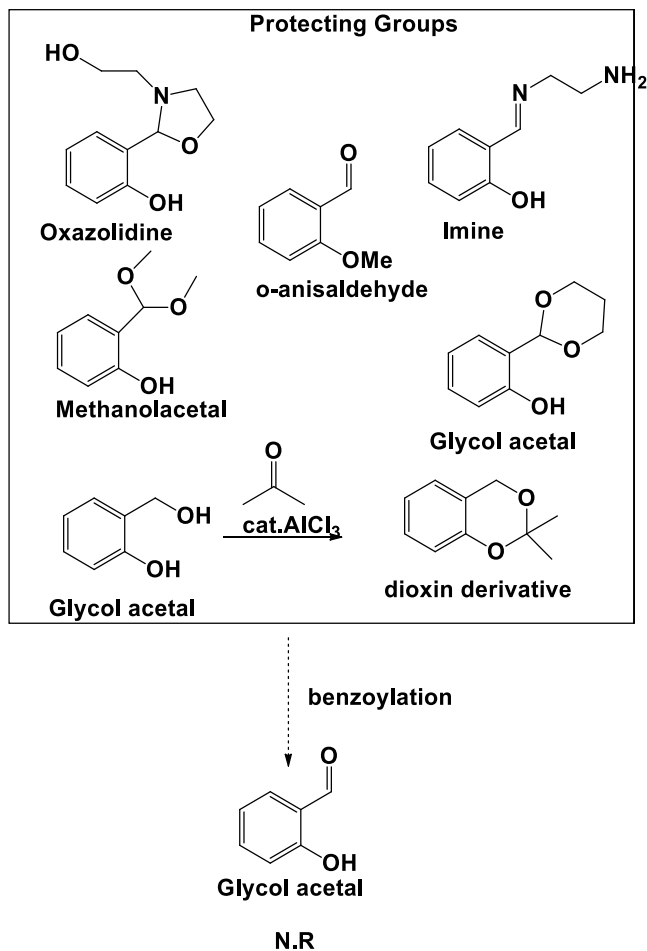
Figure 36-Protecting group employed in unsuccessful o-benzoylations.

1.8.4. Negative results for acylation at the ortho position.

It seems that there still does not exist a cheap method to produce acylation at the ortho position of salicylaldehyde derivatives. Later a review of the literature, only two potential literature methods were found. Both procedures were investigated with no positive outcome. Details of each of these methods are included in Figure 37.
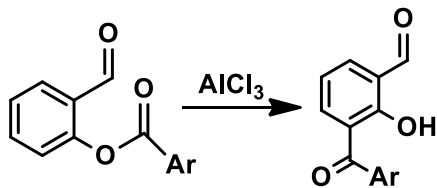
Figure 37- Known literature methods to synthesize 3-formyl-2-hydroxybenzophenones.
Elizalde-Herrera's method.

Elizalde-Herrera's method is straightforward and inexpensive. It is like the Fries rearrangement above. The method seemed to be the same as that did in the Fries rearrangement. Discussion with Elizalde himself produced no help in attaining the compound. The only proof of benzoylation at the para-position of salicylaldehyde occurs. Unfortunately, several attempts at using Elizalde-Herrara's method gave no ortho product - only substitution at the para-position. The utility in the investigation of Elizalde-Herrara's method ensured to have one positive outcome as it allowed for improvement in yield for acylation at the para-position as shown in Scheme 8.

Scheme 8: Improvements upon Elizalde-Herrara's method of p-aroylation of Salicylaldehydes

~50%
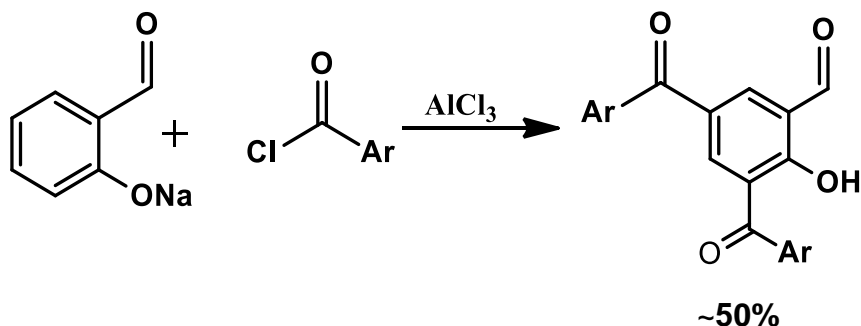
The method of Dey was, unfortunately, not found to be passable either. Dey's method initially looked to be promising, though more complicated and expensive. Dey's process was nevertheless, concluded as suitable to produce a valid reference sample for ongoing

research. The method needed the use of 3-formyl-salicylic acid from the formylation as mentioned earlier procedure of Duff and Bills[217] (Scheme 7). Per the method of Kida[218] et. al., 3-Formyl-salicylic acid is then allowed to react in the presence of warm aqueous Na2C03 and ethylenediamine in the presence of 1 equivalent Ni(ll) acetate tetrahydrate for approximately one hour as shown in Scheme 8. Difficulty rises in this procedure from the formation of the highly stable (and unreactive) binuclear complex also shown Scheme 9.

Scheme 9: Preparation of the Nickel complex used by Dey
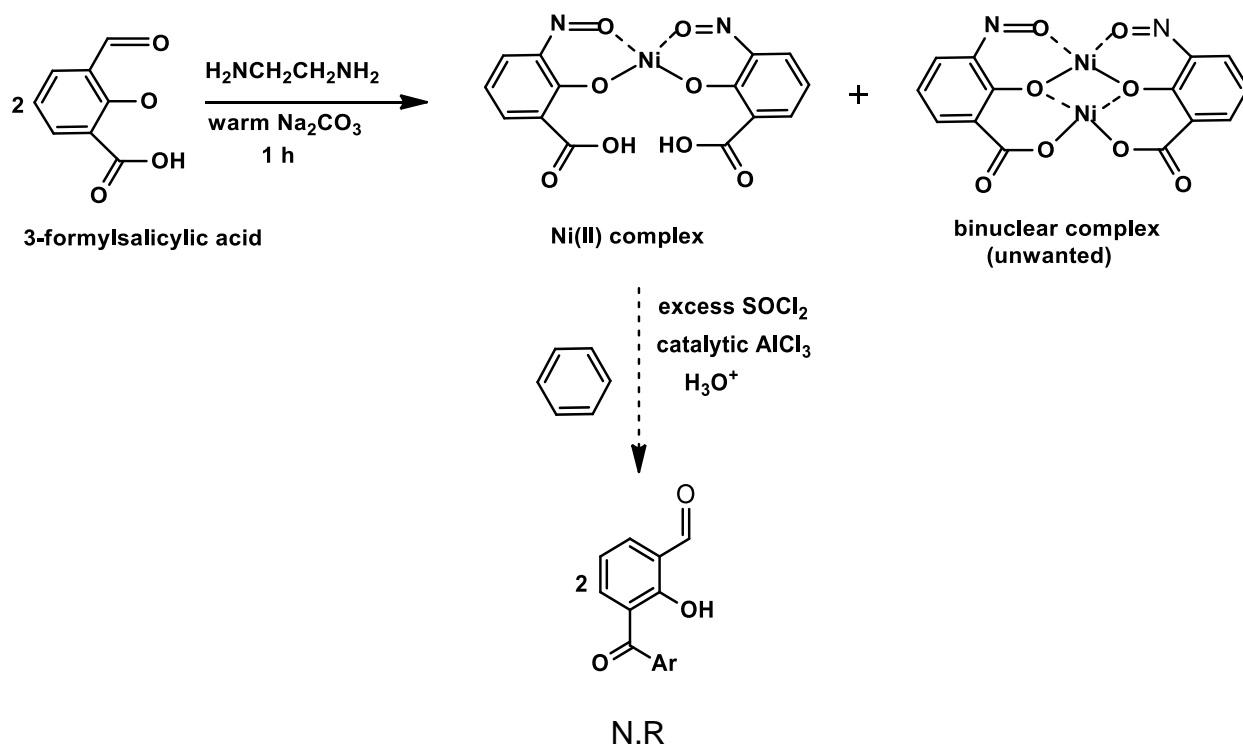
1.8.5 Improved methodology

A developed methodology utilized the use of 2-benzyl-4-chloro-6-formyl-phenol (i.e. Chlorophene) as a substrate (Figure 38). This method proved convenient as it completely avoids the use of acylation and instead relies on a strategy of benzylic oxidation. The

Figure 38-Route to BRL37959 showing proposed oxidation
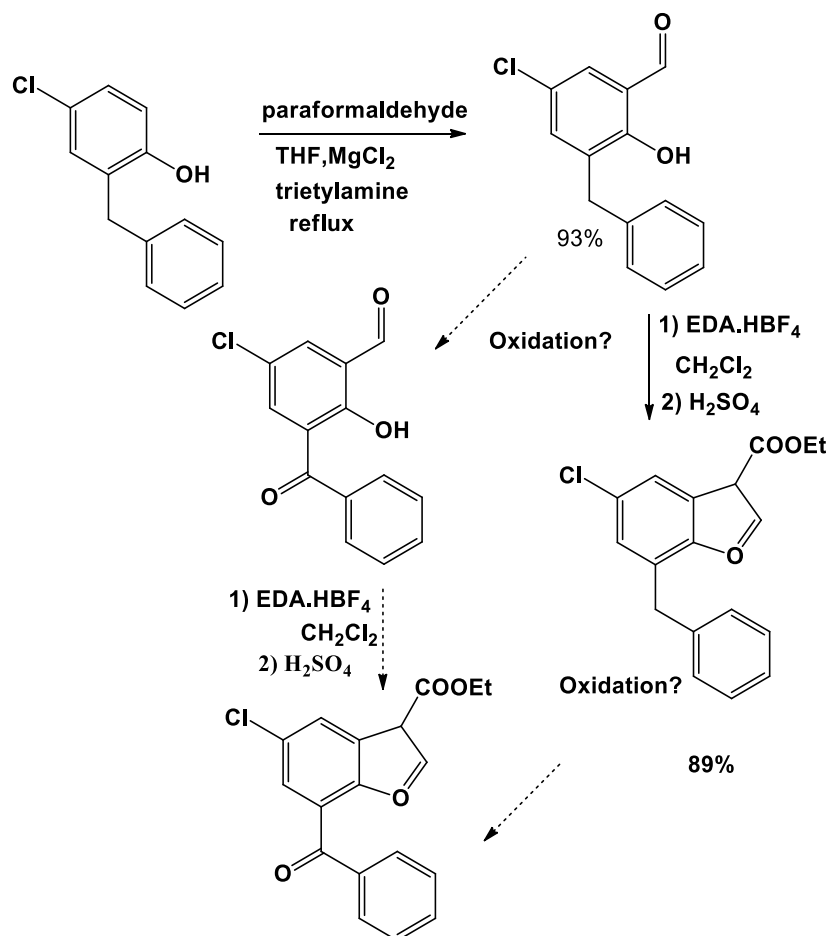
improved methodology is also cheap and high-yielding, although it is apparently limited in comparison to the acylation approach due to the requirement of para-substituted phenol derivatives. As shown in Figure 17, the reaction is high-yielding and successful up to oxidation of the benzylic carbon. No oxidation was observed at the benzylic carbon

despite several strategies using oxidizing methods such as phase transfer catalysis (PTC) with NaOH and ambient air (O_2); NaOCl; H_2O_2; and MnO_2.

1.8.6. Synthesis of Chiral BRL-37959

In 2012, Bongen, Patrick, and his co-workers synthesized chiral BRL-37959 by direct Friedel-Crafts benzoylation of 5-choro benzofuran-3-ethyl ester (scheme- 9) and found benzoylation exclusively at the Ortho-position (i.e., 33) in 30% yield. They followed Hossain et al. to synthesize racemic 5-chlorobenzofuran-3-ethyl ester.
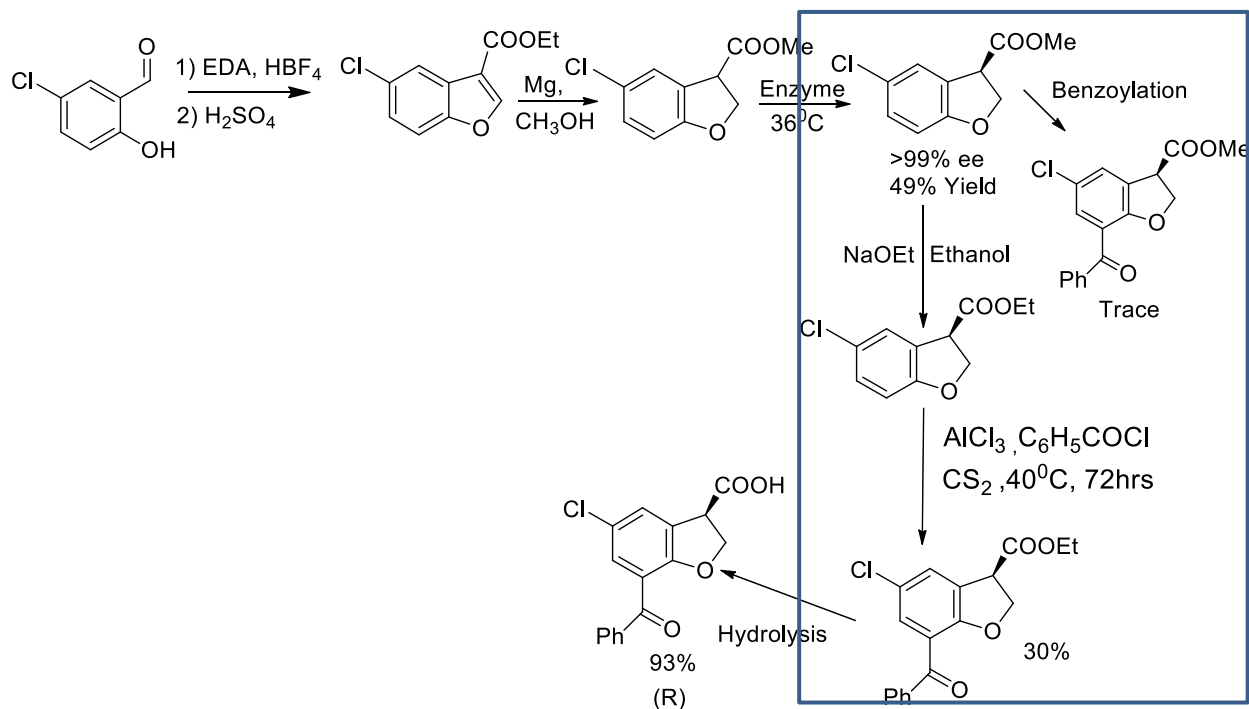
Results and Discussion

2.1. Previous work

2.1.1. Synthesis of BRL-37959

In 1986, Boyle[32] and her co-worker synthesized BRL-37959 (**5**) and found that the compound was active as a Non-Steroidal Anti-Inflammatory Drug (NSAID). The overall yield of the method was only 5%(Scheme 9). In the First Step, 6-chloro-4-chromanone (**1**) was treated with thallium trinitrate {Tl(NO$_3$)$_3$} on K-10 clay. Then obtained yellow solid was dissolved in MeOH and reacted with Na$_2$CO$_3$ followed by the treatment with EtOH and HCl to form Ethyl 5-chloro-benzo[b]furan-3-carboxylate (**2**) in a 15% yield. In reduction, **2** was treated with Mg in MeOH to give methyl 5-chloro-2,3-dihydrobenzo[b]furan-3-carboxylate (**3**). Trans-esterification of **3** produced ethyl 5-chloro-2,3-dihydrobenzo[b]furan-3-carboxylate (**4**). In benzoylation, **4** was treated with powdered
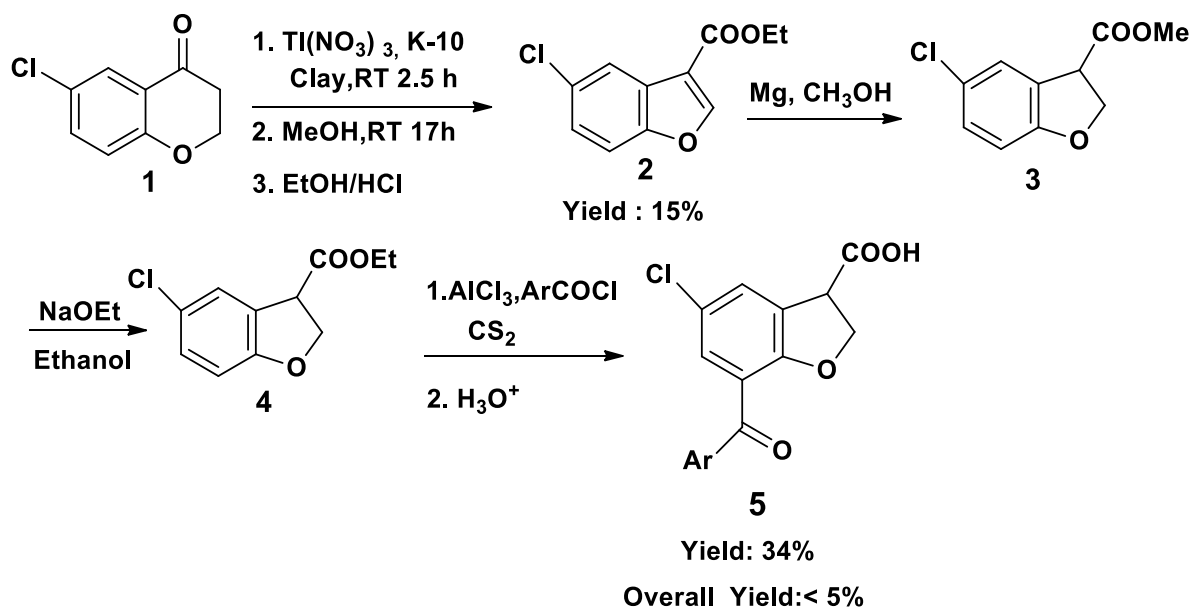
Scheme 1. First Method introduced by Boyle et.al to produce BRL 37959.

88

AlCl₃ in CS₂ at 0⁰C and followed by hydrolysis to give the desired product BRL-37959{7-Benzoyl- 5-chloro-2,3-dihydrobenzo[b]furan-3-carboxylic acid (5)} and of 34% in yield. They did not able to benzoylate **3** and thus one step was increased. The overall yield of the synthesis was only < 5%.
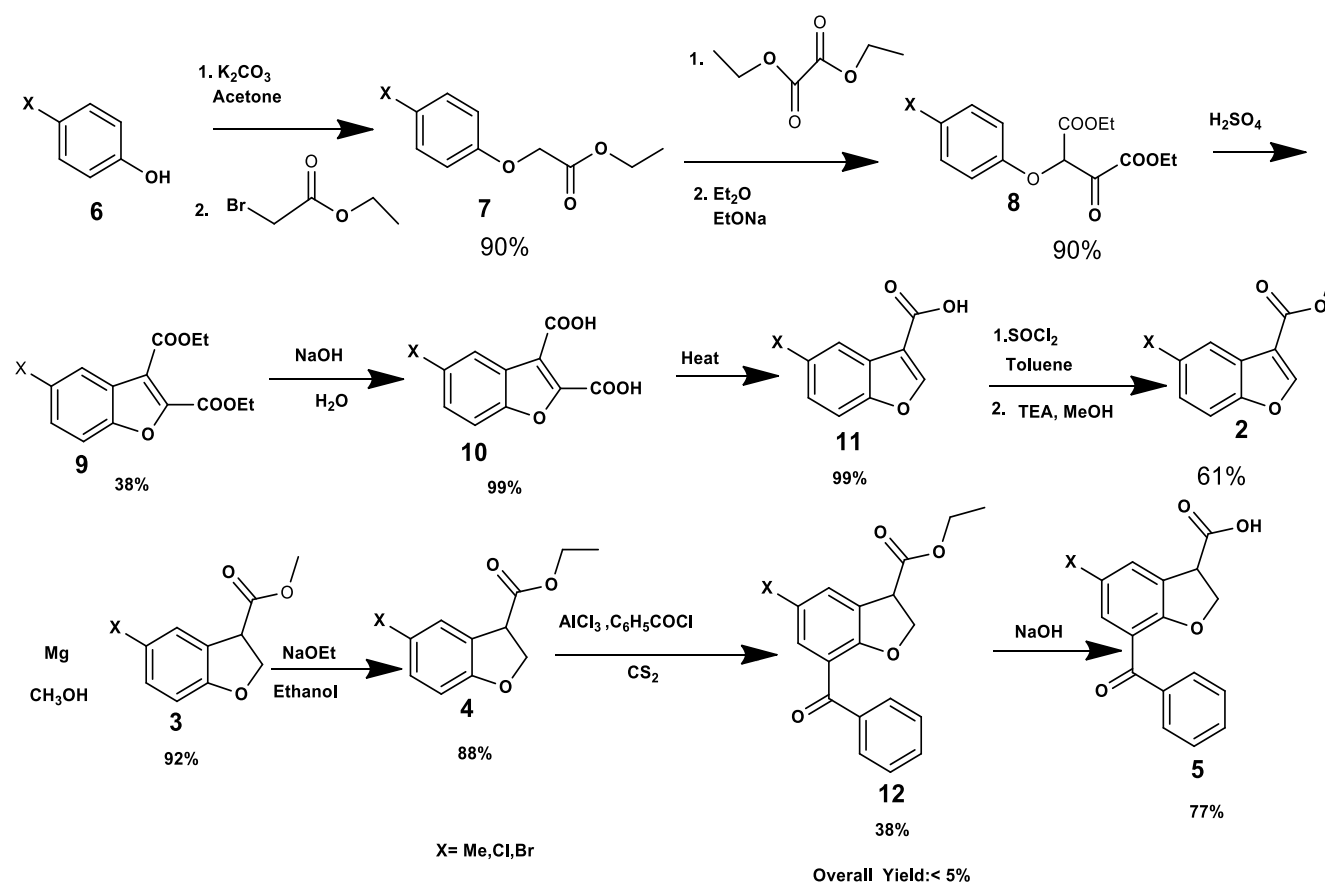
Scheme 2. Second Method developed by Boyle et.al to produce BRL -37959.

Since the compound seemed a potent NSAID, Beckham Research Laboratory(BRL) developed the second method(scheme-2) to produce BRL-37595. The overall yield of the process was also ≤ 5%. The most crucial step is benzoylation reaction(step-8), and yield of the step is only 38% that reduced the overall yield. Then they developed also the third method to (scheme-10) synthesize the compound, but yield was not improved (≤ 5%).
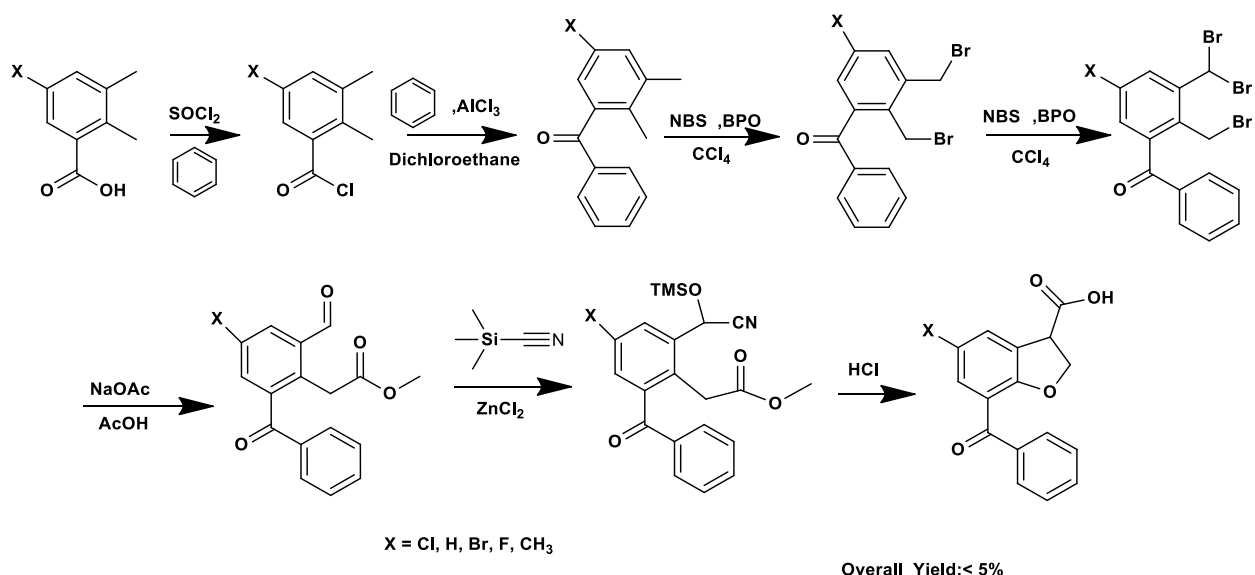
Scheme 3. Third Method developed by Boyle et.al to produce BRL -37959.

2.1.2. Synthesis of Chiral BRL-37959

In 2012, Bongen, Patrick, and his co-workers synthesized chiral BRL-37959 by direct
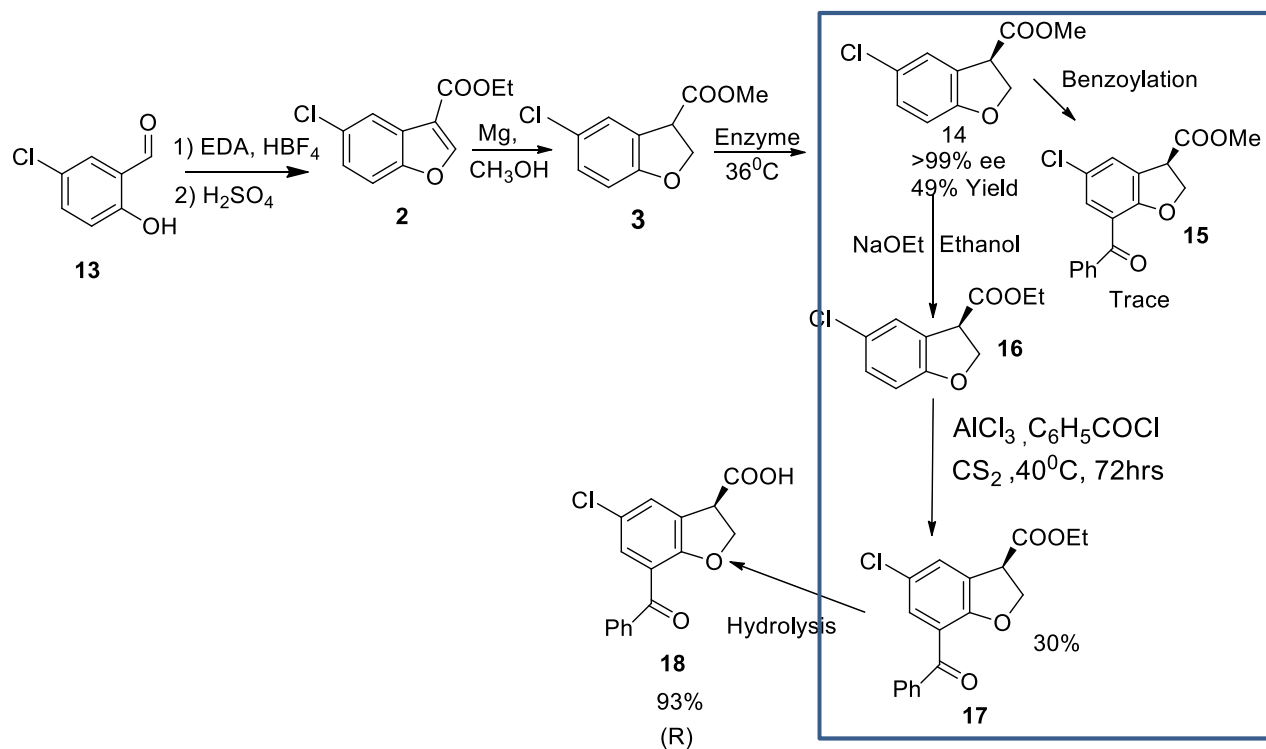
Scheme 10. Method introduced by Bongen et.al to make chiral BRL-37959.

Friedel-Crafts benzoylation of 5-choro benzofuran-3-ethyl ester (scheme- 12) and found benzoylation exclusively at the Ortho-position (i.e., 33) in 30% yield. They followed Hossain et al. to synthesize racemic 5-chlorobenzofuran-3-ethyl ester. Bongen, Patrick, and his co-workers were not able to solve the problem, i.e., to improve the benzoylation step. After benzoylation of (R) methyl 5-chloro-2,3-dihydrobenzo[b]furan-3-carboxylate (**14**) they obtained only trace amount of (R) BRL-37959{7-Benzoyl- 5-chloro-2,3-dihydrobenzo[b]furan-3-carboxylic acid (**15**)}.

2.2. Our Contribution.

2.2.1. Method development for the short synthesis of BRL-37959

Benzofuran is an essential building block of BRL 37959. In Dr. Hossain's lab, Matt Dudley[33] had discovered a novel, unique, one-pot procedure to synthesize various benzofuran derivatives. We intended to follow the efficient, more cost-effective, large-scale potential, selective, high yield and simple process to synthesize benzofuran and designed a synthetic route (Scheme-11) to synthesize BRL-37959 with higher yield. First step is the SN2 and ring closing reaction of starting material 5-chloro- salicylaldyde
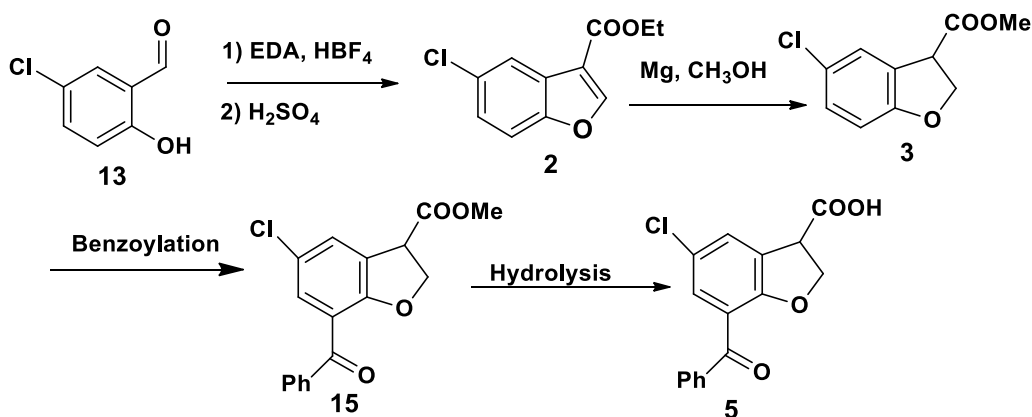
Scheme11. Proposed synthesis of BRL-37959

.

with Ethyl diazo acetate (EDA) and HBF$_4$ at room temperature(RT) to yield Ethyl 5-chloro-benzo[b]furan-3-carboxylate (**2**) in 94%[33]. Next, reduction[209-210] of (**2**) with Mg at RT in CH$_3$OH formed Methyl 5-chloro-2,3-dihdrobenzo[b]furan-3-carboxylate (**3**) in good yield of 99%(Scheme 12).
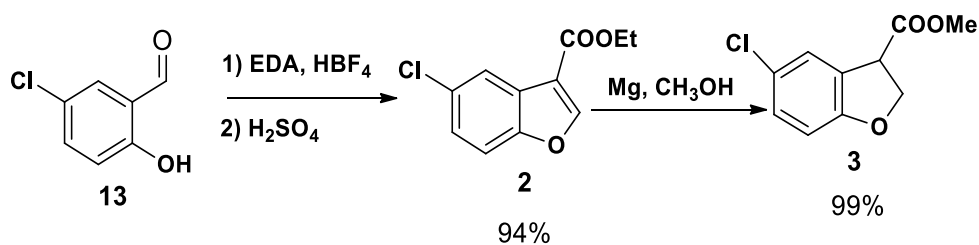
Scheme 12. Preparation of Ethyl 5-chloro-benzo[b]furan-3-carboxylate (**2**) and Methyl 5-chloro-2,3-dihdrobenzo[b]furan-3- carboxylate (3)

In Boyle, et al. and Bongen et al. benzoylation of ethyl 5-chloro-2,3-dihydrobenzo[b]furan-3-carboxylate (4) was done, and yield was 38% and 30% respectively. The major challenging step was benzoylation upon which overall yield of the method depended. We used up a much of time to improve the benzoylation of (Scheme-15) methyl 5-chloro-2,3 dihydrobenzo[b]furan-3-carboxylate (3). In benzoylation (step-3), we tried with Lewis Acid catalyst AlCl$_3$ along with different solvents and keeping AlCl$_3$, benzoyl chloride, temperature fixed. We obtained only 16% conversion in CH$_3$NO$_2$ (**Table 4. entry:1**).
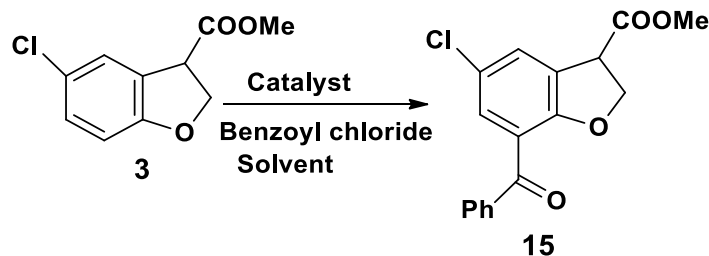
Scheme 13. Friedel-Craft benzoylation of **3**.

Next, we decided to keep benzoyl chloride and solvent fixed but vary AlCl$_3$ and temperature. Conversion is good,51% of yield in nitromethane at 80^{0}C (**Table 5. entry 13**).

Table 4. Effects of solvent.

Entry	Temperature (^{0}C)	Benzoyl Chloride	AlCl3	Solvent	Time	% of Conversion
1	**50**	**2 eq**	**1.2 eq**	**Nitromethane**	**16h**	**16**
2	50	2 eq	1.2 eq	1,2-dichloroethane	3-days	0
3	50	2 eq	1.2 eq	Dichloromethane	3-days	2
4	r.t	2 eq	1.2 eq	Carbon disulfide	3-days	8
9	70	2 eq	1.2 eq	Acetonitrile	3-days	0

We attempted to do Friedel-crafts benzoylation reactions without any solvent (Scheme-16), but the conversion was not good at all (**Table 6.**). Meanwhile, we found that researchers are using microwave radiation[211] in organic synthesis for higher yield and saving time. Generally, in most organic reactions, traditional heat transfer equipment such as oil bath, sand bath, and the heating jacket is used to provide heat to the reaction mixture. These heating systems are still rather slow, and temperature gradients can develop within the sample. Additionally, local overheating can lead to product, reagent and substrate decomposition. In compare, in microwave dielectric heating, the associate microwave energy is initiated by the chemical reaction remotely, and direct access to the

energy sources to the give reaction vessels is obtained. The microwave radiation disseminates through the walls of the vessels and heats only reactants and solvents and not the reaction vessel itself. If the device is appropriately designed, the temperature increase will be even though the sample, which can bring about fewer by-products and decomposition products. In pressurized systems, it is likely to fast increase the temperature far above the general boiling point of the solvents used. So, we decided to apply microwave radiation in our reactions. Before, we optimized $AlCl_3$ loading (1.6 eq.) (**Table 5. entry 13**). In case of microwave-assisted reaction (Scheme 17), we kept solvent and catalyst loading fixed, varied benzoyl chloride, temperature as well as time to yield 67% conversion ((**Table 7. entry 6**). Next, we attempted to use Zn^{212} as a catalyst for Friedel-craft benzoylation reaction (Scheme 16).

Table 5. Effects of $AlCl_3$ and Temperature

Entry	Temperature (^{0}C)	Benzoyl Chloride	AlCl3	Solvent	Time	% of Conversion
1	67	2 eq	1.2 eq	Nitromethane	16h	No-product
2	67	2 eq	1.3 eq	Nitromethane	24h	No-product
3	67	2 eq	1.4 eq	Nitromethane	48h	No-product
4	75	2 eq	1.2 eq	Nitromethane	16h	No-product
5	67	2 eq	1.2 eq	Dry-Nitromethane	16h	6.33
6	67	2 eq	1.3eq	Distilled Nitromethane	16h	19.5
7	67	2 eq	1.5eq	Distilled Nitromethane	16h	30
8	60	2 eq	1.5 eq	Distilled Nitromethane	16h	19
9	r.t	2 eq	1.5 eq	Distilled Nitromethane	3-days	8
10	r.t	2 eq	1.5 eq	Distilled Nitromethane	10-days	18
11	70	2 eq	1.5 eq	Distilled Nitromethane	16h	39
12	80	2 eq	1.5 eq	Distilled Nitromethane	16h	42
13	**80**	**2 eq**	**1.6 eq**	**Distilled Nitromethane**	**16h**	**51**
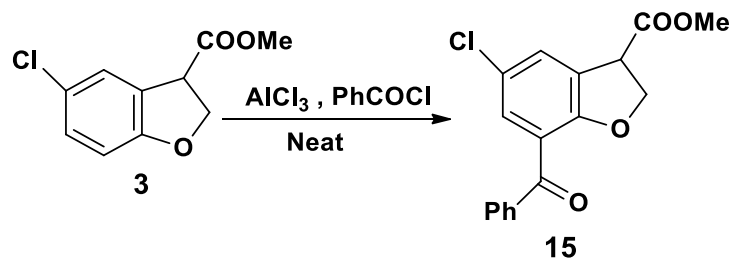
Scheme 14. Neat benzoylation reaction.

Table 6. Optimization of Neat Reaction.

Entry	Temperature (⁰C)	Benzoyl Chloride	AlCl₃	Time	% of Conversion
1	50	2 eq	1.6 eq	3-days	8
2	70	3 eq	1.6 eq	3-days	9
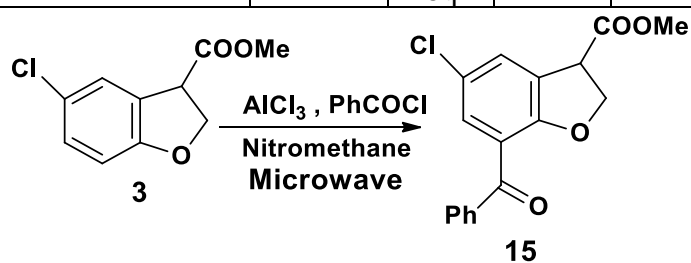
Scheme 15. Benzoylation reaction with Microwave radiation.

Table 7. Effect of Temperature on Microwave reaction.

Entry	Temperature (⁰ C)	Benzoyl Chloride	AlCl₃	Time	% of Conversion
1	75	2 eq	1.6 eq	1h	15
2	75	3 eq	1.6 eq	1h	30
3	75	4 eq	1.6 eq	1h	40
4	75	4.5 eq	1.6 eq	1h	44
5	75	5.5 eq	1.6 eq	1h	51
6	**80**	**5.5 eq**	**1.6 eq**	**1h**	**67**
7	90	5.5 eq	1.6 eq	1h	49
8	80	5.5 eq	1.6 eq	2h	27
9	100	5.5 eq	1.6 eq	1h	0

but the conversion was unsatisfactory. We found that ionic liquids[213] is used as an additive

to increase the catalytic activity of AlCl$_3$ that leads to greater yield. We exploited ionic

liquid (Scheme 17) and obtained 37% conversion.
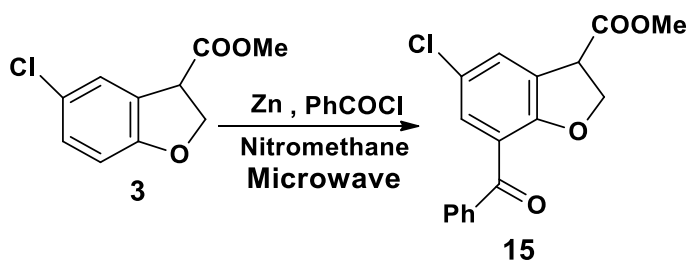
Scheme 16. Microwave -assisted benzoylation reaction with Zn catalyst.

Table 8. Zn catalyzed Microwave reaction.

Entry	Temperature (^{0}C)	Benzoyl Chloride	Zn	Time	% of Conversion
1	100	1 eq	10 eq	10 min	0
2	140	1 eq	10 eq	30 min	5
3	140	10 eq	10 eq	1h	10
4	140	10 eq	10 eq	1h	10
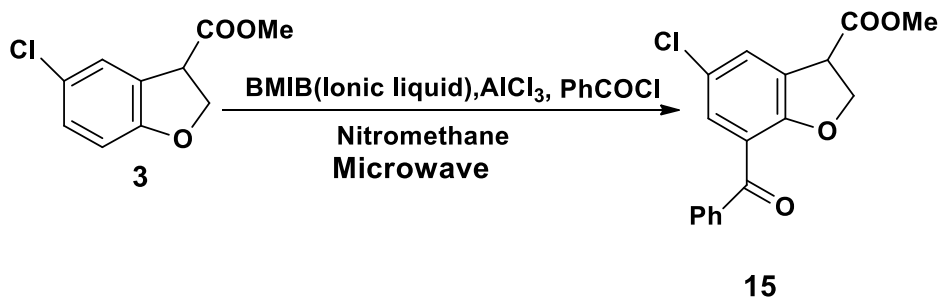
Scheme 17. Microwave- assisted reaction with additive.

Table 9. Microwave reaction with additive.

Entry	Temperature (^{0}C)	Benzoyl Chloride	AlCl$_3$	BMIB	Time	% of Conversion
1	**80**	**14.7 eq**	**5.40 eq**	**2.85 eq**	**1h**	**37**
2	100	14.7 eq	5.40 eq	3.88 eq	1h	15
3	100	14.7 eq	5.40 eq	-	1h	22

Since in benzoylation reaction (Scheme 13), we obtained only 51% conversion, and overall yield would not be high, we proposed another route (Scheme 20). We used 5-chloro-2-hydroxy benzophenone as a starting material to avoid benzoylation (**20**). We did Reimer-Tiemann reaction (Scheme 19) to convert **19** to 7-benzoyl-5-chloro-salicylaldehyde (**20**), but unfortunately, no product was formed.
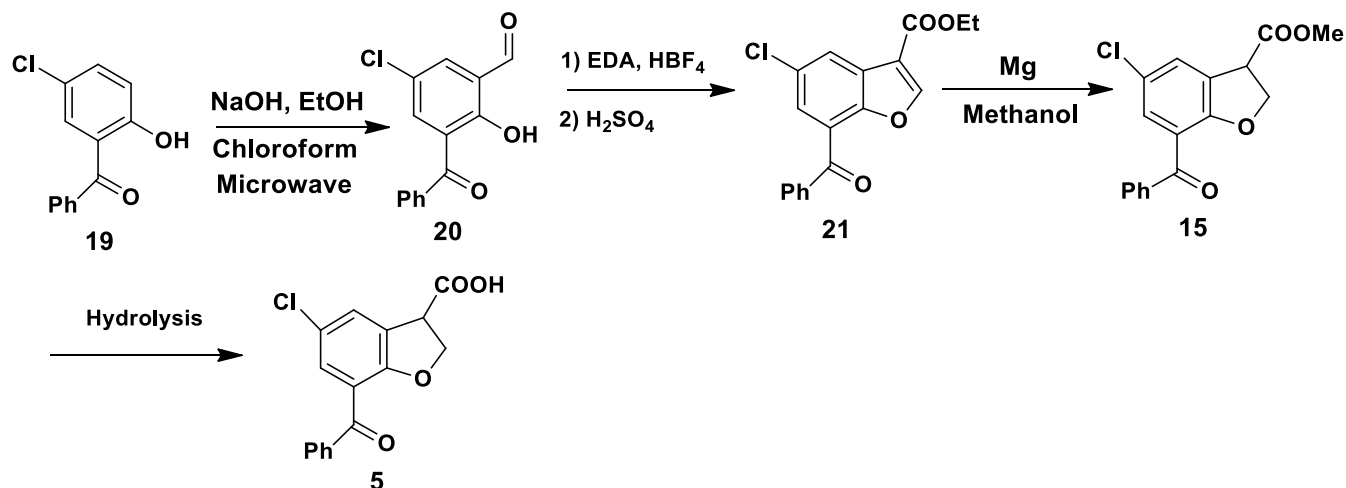
Scheme 18. Proposed synthesis of BRL-37959
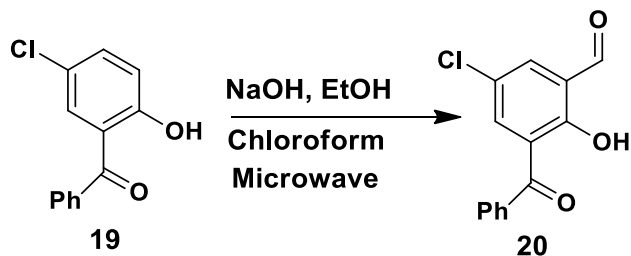
Scheme 19. Reimer-Tiemann reaction of 5-chloro-2-hydroxy benzophenone (**20**).

Table10. Reimer-Tiemann reaction.

Entry	Temperature (^{0} C)	NaOH	CHCl$_3$	Time	% of Conversion
1	110	7.5 eq	2 eq	5 min	0
2	110	7.5 eq	2 eq	10 min	0
3	120	7.5 eq	6 eq	5 min	0
4	170	10 eq	30 eq	5 min	0
5	170	10 eq	30 eq	10	0
6	90	10 eq	30 eq	1h	0
7	120	10 eq	30 eq	4h	0

We continuously persuaded to search a suitable catalyst for increasing conversion of benzoylation step and found that J.R. Desmur and his co-workers used Bi(OTf)$_3$ catalyst in Friedel-Craft benzoylation reaction as well as obtained 80-98% yield[214]. Next, we decided to use the super catalyst in our benzoylation reaction. First, we applied the great catalyst in microwave irradiation reaction (Scheme 20). We kept benzoyl chloride, catalyst Bi(OTf)$_3$, time fixed and varied temperature and achieved excellent yield of 77% (**Table 11, entry 3**)
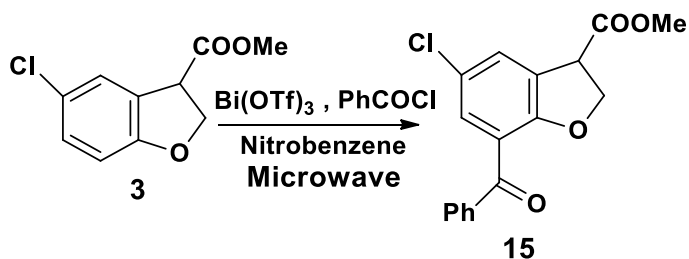
Scheme 20. Microwave- assisted reaction with Bi catalyst

Table 11. Effect of Temperature on Bi(OTf)$_3$ catalyzed Microwave Benzoylation reaction

Entry	Temperature(^{0}C)	Benzoyl Chloride	Bi(OTf)$_3$	Time	% of Conversion	% of Yield
1	100	2.2 eq	0.1 eq	30 min	55	-
2	120	2.2 eq	0.1 eq	30 min	67	-
3	**140**	**2.2 eq**	**0.1 eq**	**30 min**	**87**	**77**

Being inspired by the super activity of the catalyst, we planned to utilize Bi(OTf)$_3$ in traditional Friedel-Craft benzoylation reaction (Scheme 21). We optimized benzoyl chloride, catalyst loading, and temperature to obtain a higher yield of 70%(**Table: 12, entry 3**)
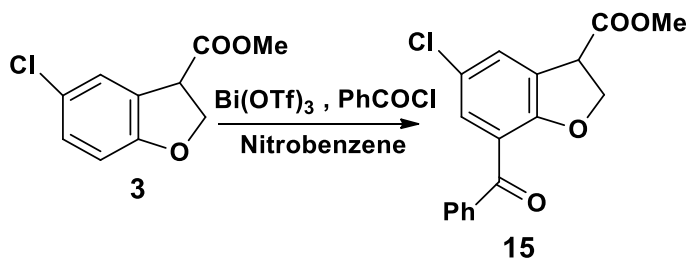
Scheme 21. Conventional benzoylation reaction with Bi catalyst.

Table 12. Effect of Catalyst loading and Temperature

Entry	Temperature (^{0}C)	Benzoyl Chloride	Bi(OTf)$_3$	Time	% of Conversion	% of Yield
1	90	0.5 eq	0.1 eq	3 days	64	-
2	100	0.5 eq	0.1 eq	3 days	59	-
3	90	2.3 eq	0.2 eq	3 days	87	70
4	90	2.3 eq	0.2 eq	3 days	90	70
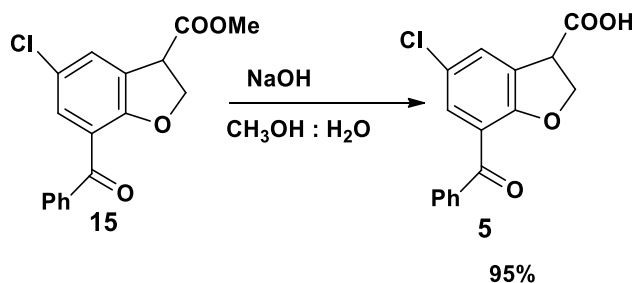
Scheme 22. Hydrolysis of Methyl-7-Benzoyl -5-Chloro-2,3-dihydrobenzo [b] furan-3-carboxylate (15)

Next, hydrolysis of **15** with NaOH in methanol and water at RT (Scheme 22) formed final product BRL-37959 (5-chloro-7-benzoyl-2,3-dihdrobenzo[b]furan-3-carboxyllic acid) (5) in the great yield of 99%.

Total Synthesis of BRL-37959:
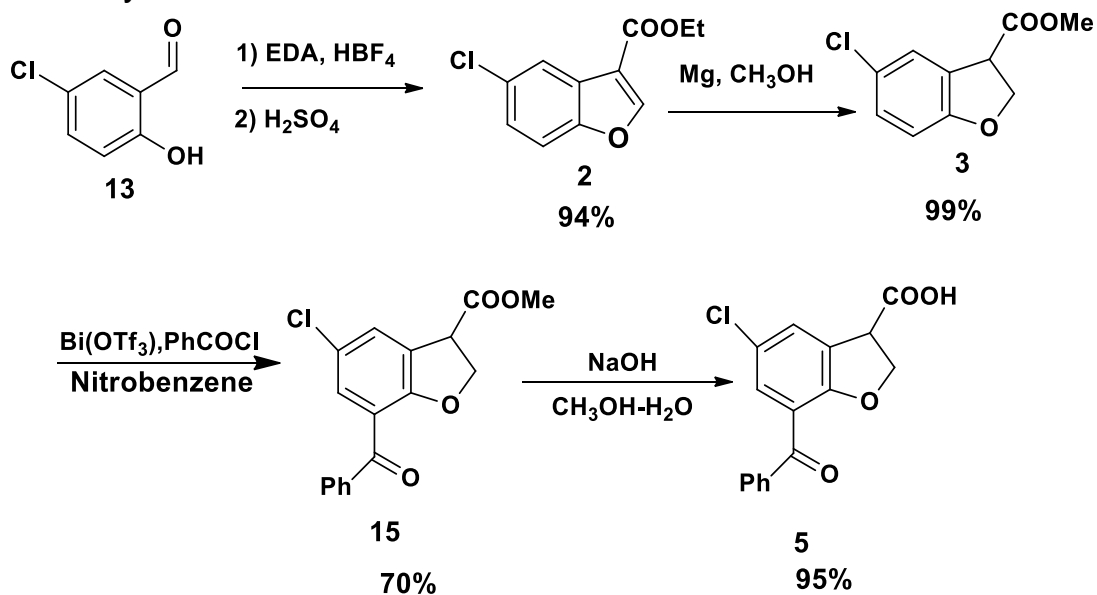
Overall Yeild : 62%

2.2.2. Synthesis of analogs of BRL-37959

Now, we developed the methodology of benzoylation reaction; we planned to apply the developed method to synthesize some analogs of BRL-37959. First, we intended to make Fluoro-analog of BRL-37959 (**26**) and followed our established synthetic route (Scheme 25). The step:1 is the SN2 and ring closing reaction[33] of starting material 5-Fluoro-
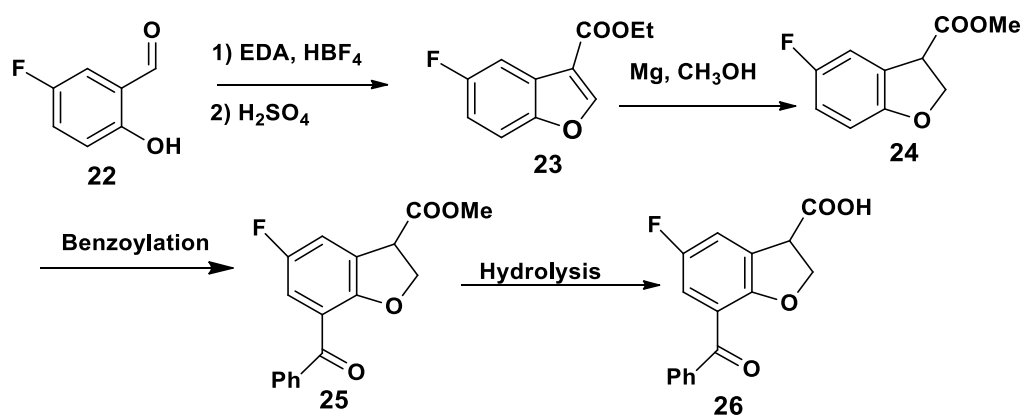
Scheme 23. Proposed synthesis of 7-Benzoyl- 5-Fluoro-2,3-dihydrobenzo[b]furan-3-carboxylic acid **(26)**

salicylaldyde with Ethyl diazo acetate(EDA) and HBF$_4$ at room temperature (RT) to yield Ethyl 5-Fluoro-benzo[b]furan-3-carboxylate **(23)** in 74%. Subsequently, reduction[209-210]
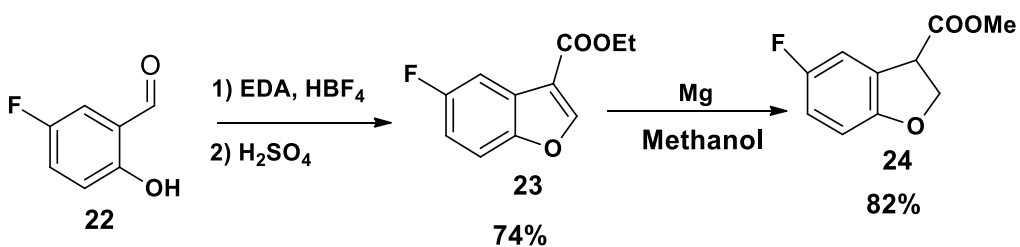
Scheme 24. Synthesis of Methyl 5-fluoro-2,3-dihydrobenzo[b]furan-3-carboxylate **(24)**

of (**23**) with Mg at RT in CH$_3$OH formed Methyl 5-Fluoro-2,3-dihdrobenzo[b]furan-3-carboxylate (**24**) in the good yield of 82% (Scheme 24). In microwave-assisted benzoylation reaction (Scheme 25) of **(24)** hold catalyst loading, benzoyl chloride fixed and changed temperature as well as time to yield 78% (**Table 13, entry 3**). After that, we focused on typical benzoylation (Scheme 26) of **24**. We fixed temperature, time and altered catalyst as well as benzoyl chloride to get 50% in yield. (**Table 14, entry 3**).
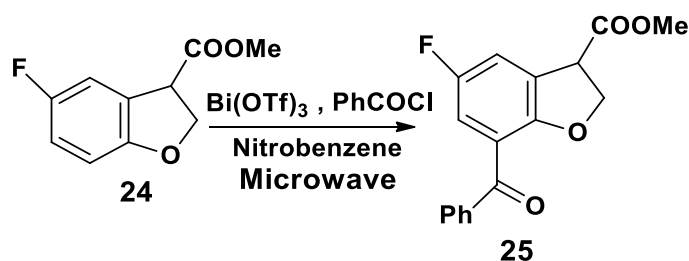
Scheme 25. Microwave- assisted reaction with Bi catalyst.

Table13. Effect of Temperature on Bi(OTf)$_3$ catalyzed Microwave benzoylation reaction

Entry	Temperature (^{0}C)	Benzoyl Chloride	Bi(OTf)$_3$	Time	% of Yield
1	100	2.2 eq	0.1 eq	20 min	45
2	120	2.2 eq	0.1 eq	30 min	56
3	**140**	**2.2 eq**	**0.1 eq**	**20 min**	**78**
4	150	2.2 eq	0.1 eq	30 min	63
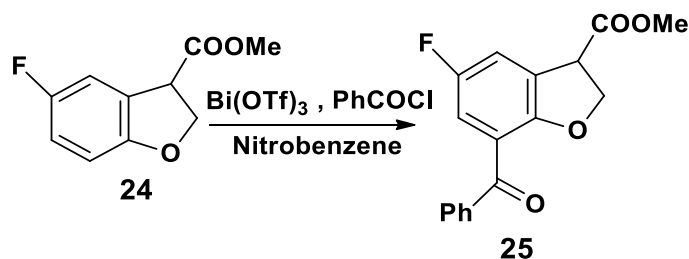
Scheme 26. Conventional benzoylation reaction with Bi catalyst

Table14. Effect of catalyst loading on traditional benzoylation reaction.

Entry	Temperature(^{0}C)	Benzoyl Chloride	Bi(OTf)$_3$	Time	% of Yield
1	90	2.3 eq	0.05 eq	3 days	30
2	90	2.3 eq	0.1 eq	3 days	50
3	**90**	**2.3 eq**	**0.2 eq**	**3 days**	**50**
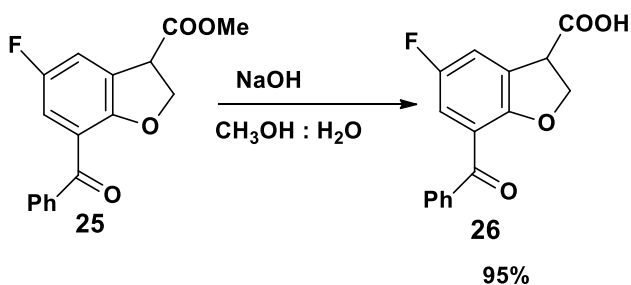
Scheme 27. Hydrolysis of Methyl-7-Benzoyl -5-Fluoro-2,3-dihydrobenzo [b] furan-3- carboxylate (26).

Total Synthesis of 5-Fluoro- 7-Benzoyl -2,3-dihydrobenzo [b] furan-3- carboxylic acid (26)

Overall Yeild : 40%

103
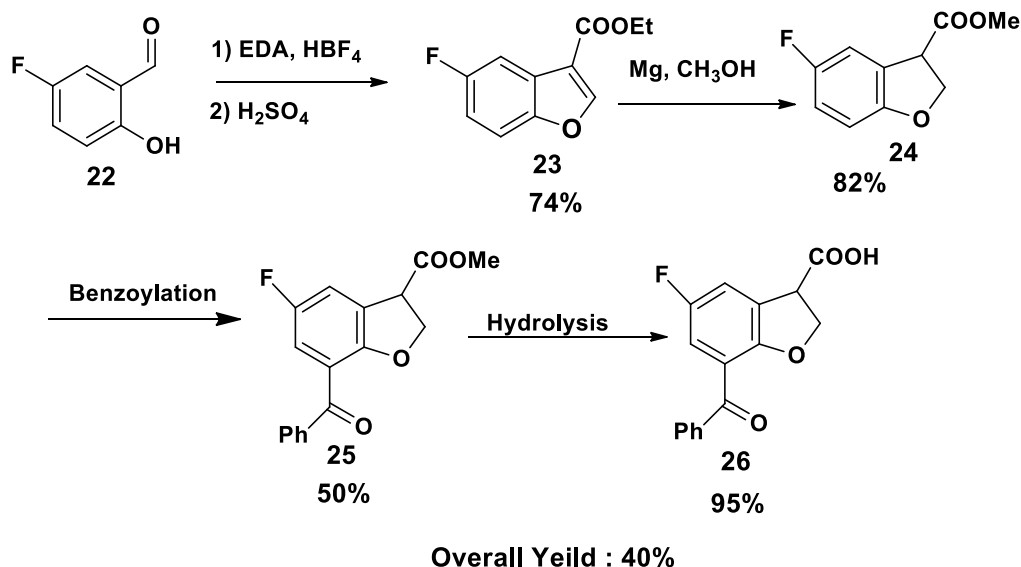
Next, we decided to synthesize methyl-analog of BRL-37959 (5-Methyl-7-Benzoyl- 2,3-dihydrobenzo[b]furan-3-carboxylic acid (**31**) by following our developed synthetic route (Scheme 28).
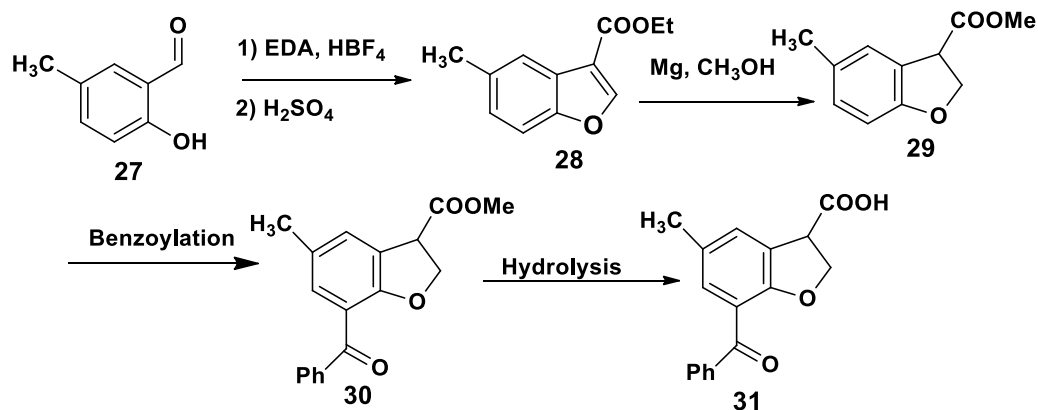
Scheme 28. Proposed synthesis of 7-Benzoyl- 5-Methyl-2,3-dihydrobenzo[b]furan-3-carboxylic acid (**31**).

The first step is the SN2 and ring closing reaction of starting material 5-Methyl-salicylaldyde with Ethyl diazo acetate(EDA) and HBF$_4$ at room temperature (RT) to yield Ethyl 5-Methyl-benzo[b]furan-3-carboxylate (**28**) in 81%[33]. After that, reduction[209-210] of (**28**) with Mg at RT in CH$_3$OH formed Methyl 5-Fluoro-2,3-dihdrobenzo[b]furan-3-carboxylate (**29**) in a good yield of 91% (Scheme 29). We pursued our optimized
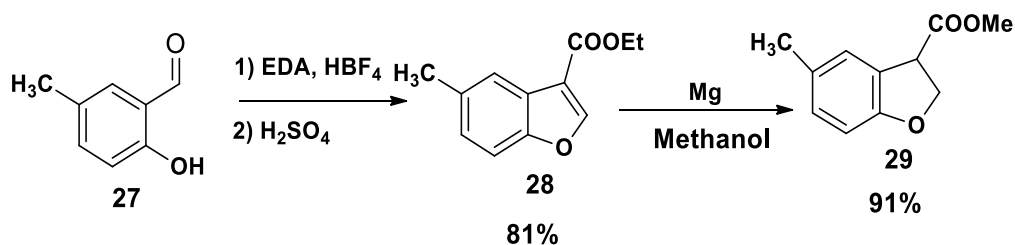
Scheme 29. Synthesis of Methyl 5-methyl-2,3-dihdrobenzo[b]furan-3-carboxylate (**29**)

microwave benzoylation reaction (Scheme 30) and formed **30** to yield in 72%(**Table15, entry 3**). Consequently, we augmented traditional Friedel-craft benzoylation (scheme 30) and achieved 77 % in yield (**Table 16, entry 3**).
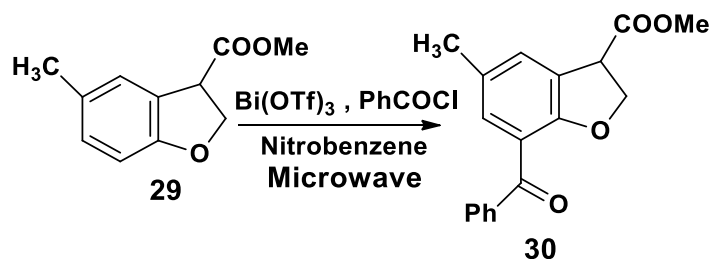
Scheme 30. Microwave -assisted reaction with Bi catalyst.

Table 15. Effect of temperature on microwave -mediated benzoylation reaction.

Entry	Temperature(^{0}C)	Benzoyl Chloride	Bi(OTf)$_3$	Time	% of Yield
1	100	2.2 eq	0.1 eq	30 min	45
2	**120**	**2.2 eq**	**0.1 eq**	**30 min**	**60**
3	140	2.2 eq	0.1 eq	30 min	72
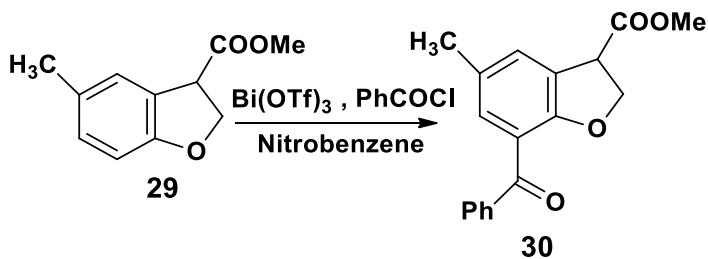
Scheme 31. Conventional benzoylation reaction with Bi catalyst

Table 16. Optimization of traditional benzoylation reaction with Bi(OTf)$_3$

Entry	Temperature (^{0}C)	Benzoyl Chloride	Bi(OTf)$_3$	Time	% of Yield
1	90	2.3 eq	0.1 eq	3 days	59
2	100	2.3 eq	0.1 eq	3 days	63
3	90	2.3 eq	0.15 eq	3 days	67
4	**90**	**2.3 eq**	**0.2 eq**	**3 days**	**77**
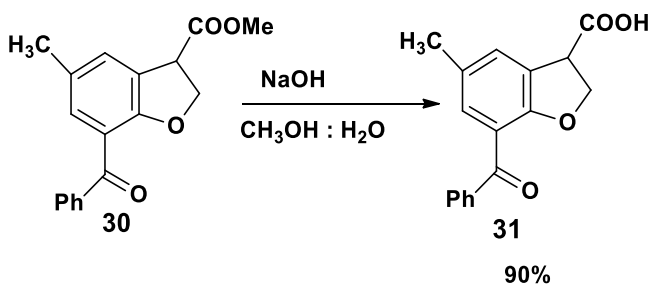
Scheme 32. Hydrolysis of Methyl-7-Benzoyl -5-Methyl-2,3-dihydrobenzo [b] furan-3-carboxylate (30)

Total Synthesis of 7-Benzoyl -5-Methyl-2,3-dihydrobenzo [b] furan-3-carboxylic acid (31)

Overall Yeild : 51%
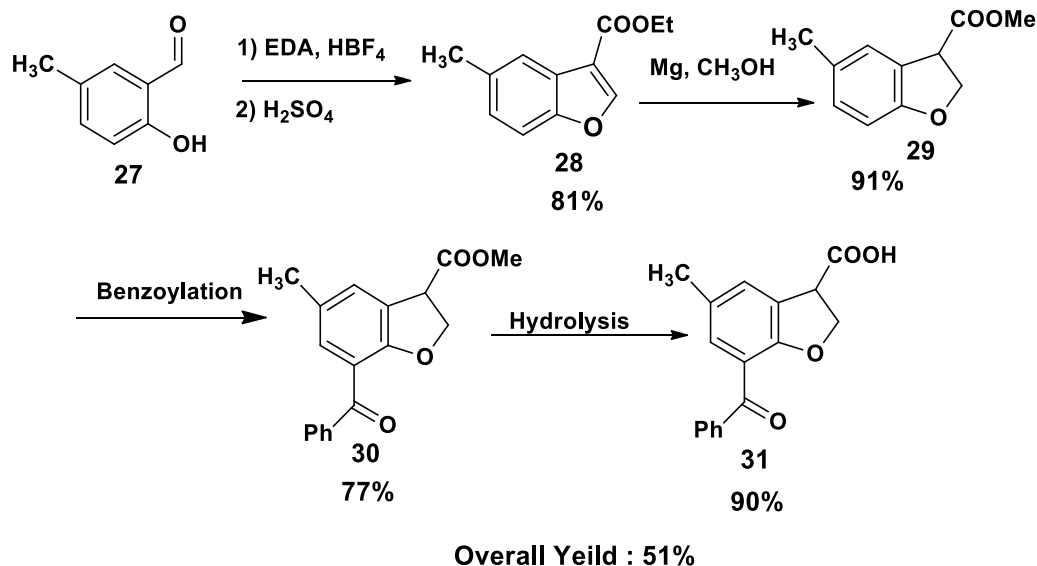
Afterwards, we designed to prepare methoxy analog of BRL-37959(7-Benzoyl- 5-Methoxy-2,3-dihydrobenzo[b]furan-3-carboxylic acid) (**36**) and stuck to our improved synthetic route (Scheme 33). The first step is the SN2 and ring closing reaction of starting
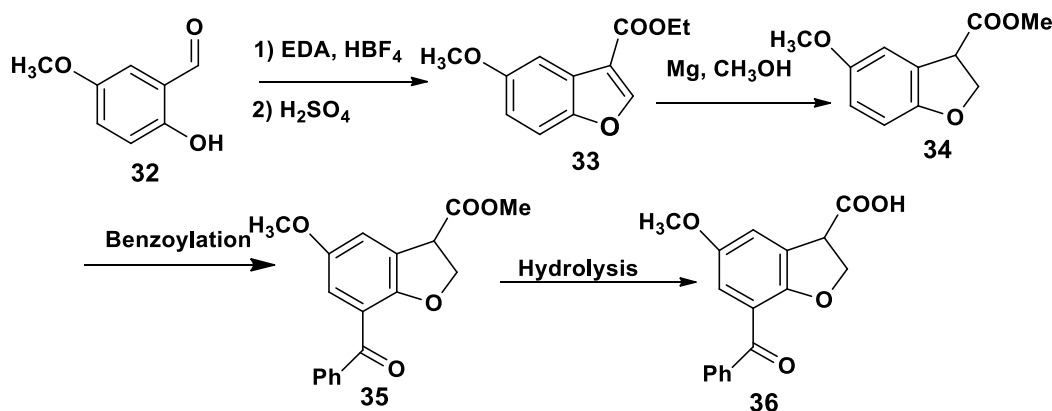
Scheme 33. Proposed synthesis of 7-Benzoyl- 5-Methoxy-2,3-dihydrobenzo[b]furan-3-carboxylic acid (**36**).

material 5-Methoxy- salicylaldyde with Ethyl diazo acetate(EDA) and HBF_4 at room temperature (RT) to yield Ethyl 5-Methoxy-benzo[b]furan-3-carboxylate (**33**) in 81%[33]. Next, reduction[209-210] of (**33**) with Mg at RT in CH_3OH formed Methyl 5-Methoxy-2,3-

dihdrobenzo[b]furan-3-carboxylate (**34**) in a good yield of 91%(Scheme-34). Microwave-assisted benzoylation reaction (Scheme 35) was carried out with noble catalyst Bi(OTf)$_3$ to yield 50%(**Table 17, entry 4**) Subsequently, we kept on our optimized standard Friedel-craft benzoylation (Scheme-36) and obtained 65% in yield (**Table 18, entry 2**).
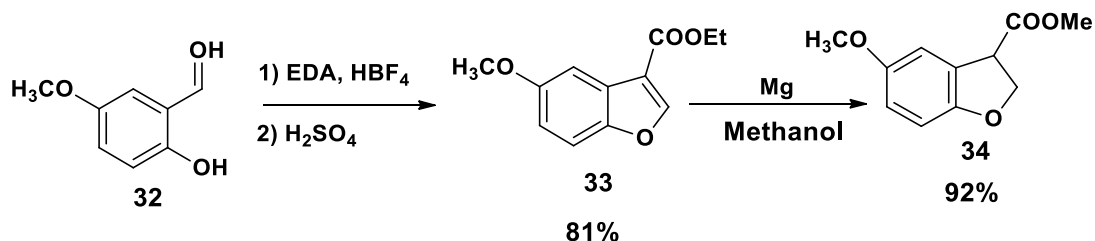
Scheme 34. Reduction of Ethyl 5-methyl-benzo[b]furan-3 carboxylate (**33**)
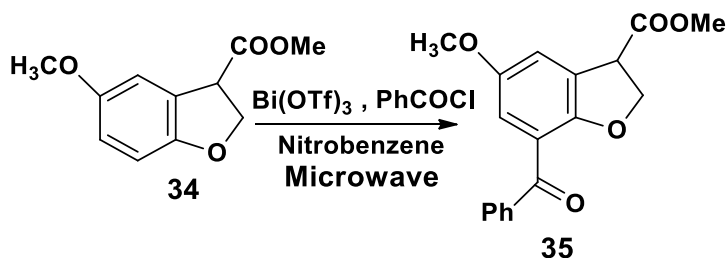
Scheme 35. Microwave -assisted reaction with Bi catalyst.

Table 17. Effect of temperature on microwave benzoylation reaction.

| Entry	Temperature (^{0}C)	Benzoyl Chloride	Bi(OTf)$_3$	Time	% of Yield
1	100	2.2 eq	0.1 eq	30 min	31
2	120	2.2 eq	0.1 eq	35 min	36
3	120	2.2 eq	0.1 eq	30 min	40
4	**140**	**2.2 eq**	**0.1 eq**	**30min**	**50**
5	140	2.2 eq	0.1 eq	35 min	42
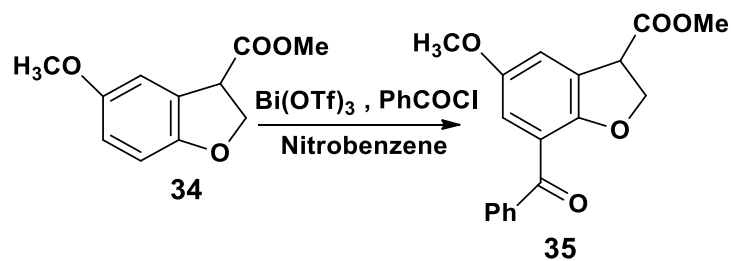
Scheme 36. Traditional benzoylation reaction with Bi catalyst

Table18. Effect of catalyst loading on conventional benzoylation reaction.

| Entry	Temperature (^{0}C)	Benzoyl Chloride	Bi(OTf)$_3$	Time	% of Yield
1	90	2.3 eq	0.1 eq	3 days	50
2	90	2.3 eq	0.2 eq	3 days	65
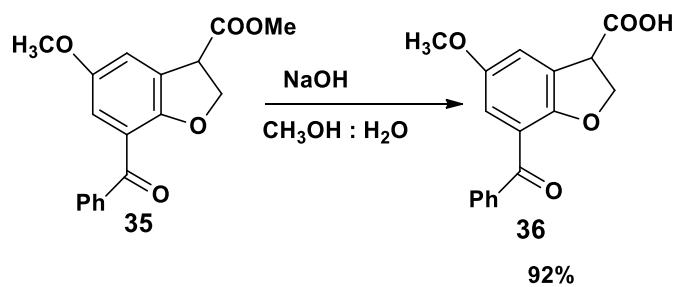
Scheme 37. Hydrolysis of Methyl-7-Benzoyl -5-Methoxy-2,3- dihydrobenzo [b] furan-3- carboxylate (36)

## Total Synthesis of 5-Methoxy 7-Benzoyl --2,3-dihydrobenzo [b] furan-3-carboxylic acid (36).
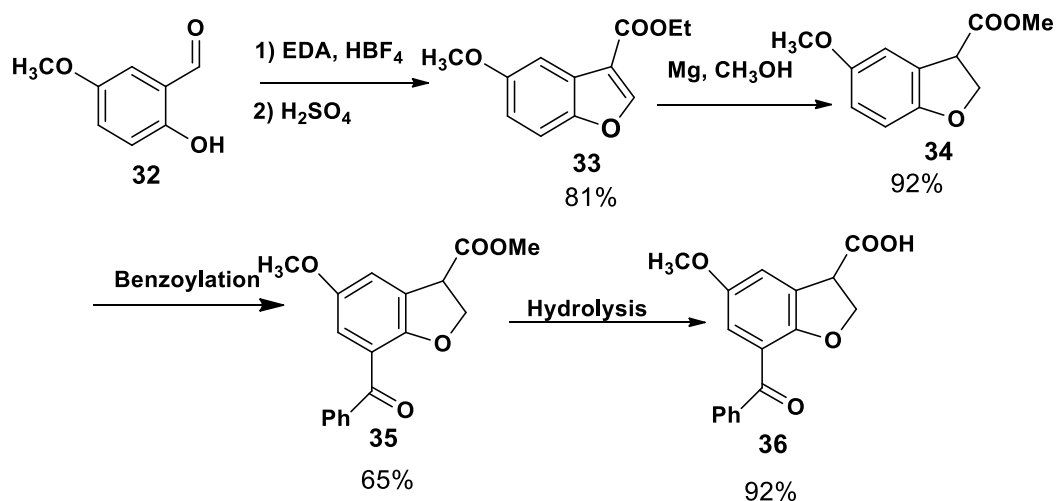
Overall Yeild : 45%

We performed Molecular Modeling Study of BRL-37959, and p-hydroxy analog of BRL-37959 {7-(4-hydroxy) Benzoyl- 5-Chloro-2,3-dihydrobenzo[b]furan-3-carboxylic acid} and found that both bind with the COX-2 enzyme (Figure- 18,19), but later bind tightly to the enzyme. Because of the hydroxyl group in p-hydroxy analog of BRL-37959 forms hydrogen bond with amino acid of the COX-2 enzyme. Now, we planned to make more analogs by placing different substituents in para-position of benzoyl group in BRL-37959. First, we decided to synthesize 7-(4-tri-fl..romethyl) Benzoyl- 5-Chloro-2,3-dihydrobenzo[b]furan-3-carboxylic acid (**38**). We followed our developed synthetic method (Scheme 38) and in benzoylation reaction (Scheme-39) p- trifluoromethyl benzoyl
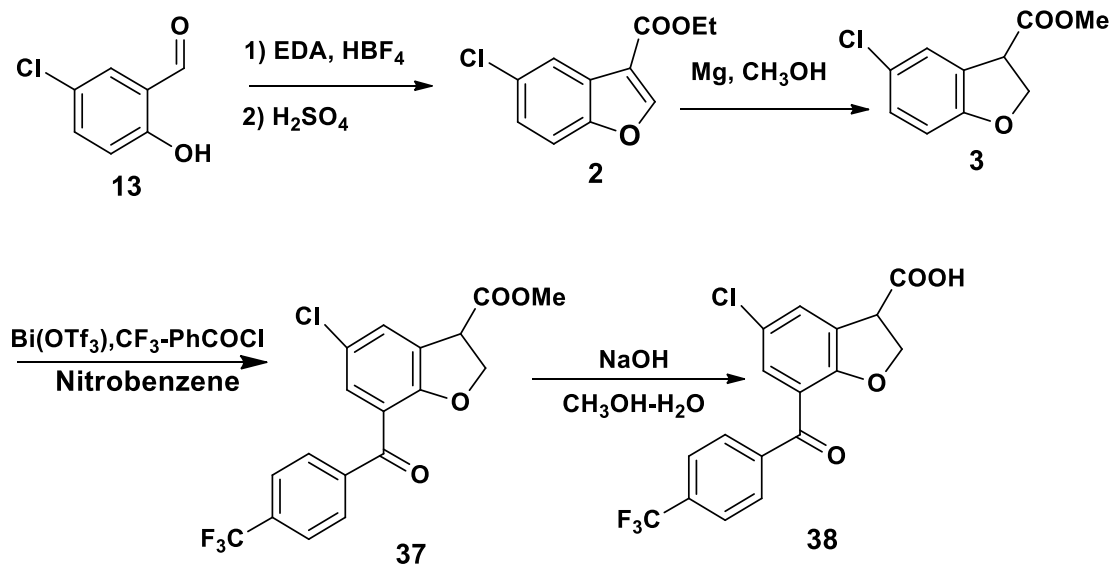
Scheme 38. Proposed synthesis of 7-(4-tri-fluromethyl) Benzoyl- 5-Chloro-2,3-dihydrobenzo[b]furan-3-carboxylic acid (**38**).
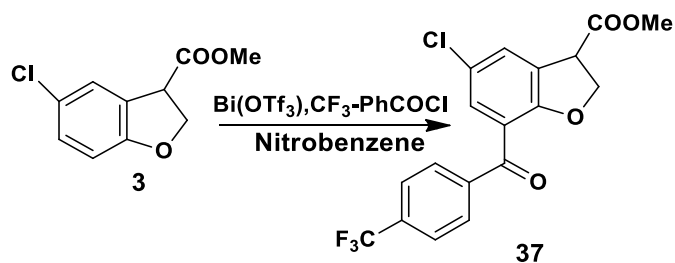
Scheme 39. Microwave -assisted reaction with Bi catalyst

Table 19. Effect of benzoylation reaction with Bi(OTf)$_3$

Entry	Temperature (⁰C)	7-(4-tri-fluromethyl) benzoyl Chloride	Bi(OTf)$_3$	Time	% of Yield
1	140	1 eq	0.1 eq	20 min	22
2	140	8.6 eq	0.1 eq	30 min	76
3	120	7.5 eq	0.1 eq	30 min	70
4	**120**	**8.6 eq**	**0.1 eq**	**1h**	**79**
5	120	4 eq	0.1 eq	1h	51

chloride was treated with 3 and super catalyst Bi(OTf)₃ to produce 7-(4-trifluromethyl) Benzoyl -5-Chloro-2,3- dihydro benzo [b] furan-3- carboxylate (**37**) 79% in yield **Table 19, entry 4**). Next, hydrolysis of **37** with NaOH in methanol and water at RT (Scheme 40) formed the final product, 7-(4-trifluromethyl) Benzoyl -5-Chloro-2,3- dihydro benzo [b] furan-3-carboxylic acid) (**38**) in the high yield of 94%.
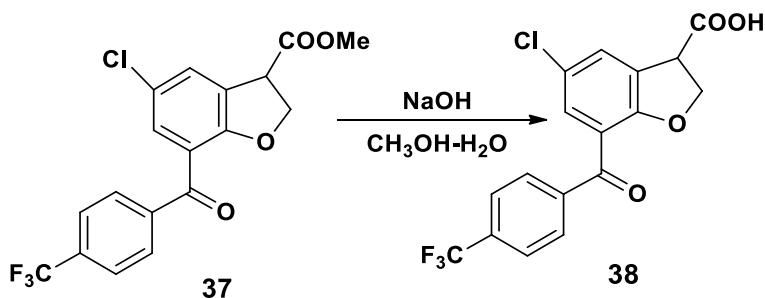
Scheme 40. Hydrolysis of 7-(4-trifluromethyl) Benzoyl -5-Chloro-2,3-
dihydrobenzo [b] furan-3- carboxylate (38)

Total Synthesis of 7-(4-trifluromethyl) Benzoyl -5-Chloro-2,3-dihydro benzo[b] furan-3- carboxylic acid (38).

Overall Yeild : 70%

After that, we worked out to make of 7-(4-fluro) Benzoyl- 5-Chloro-2,3-dihydro benzo [b]furan-3-carboxylic acid (**40**) (Scheme 41). We retained catalyst loading, as fixed, varied temperature, and benzoyl chloride as well as time in benzoylation (Scheme 42) to yield of 48% (**Table 18, entry 4**). Next, the final product, 7-(4-fluro) benzoyl -5-Chloro-2,3-dihydro benzo [b] furan-3-carboxylic acid (**40**) formed (yield 99%) after hydrolysis of **39** with NaOH in methanol and water at RT (Scheme-43).
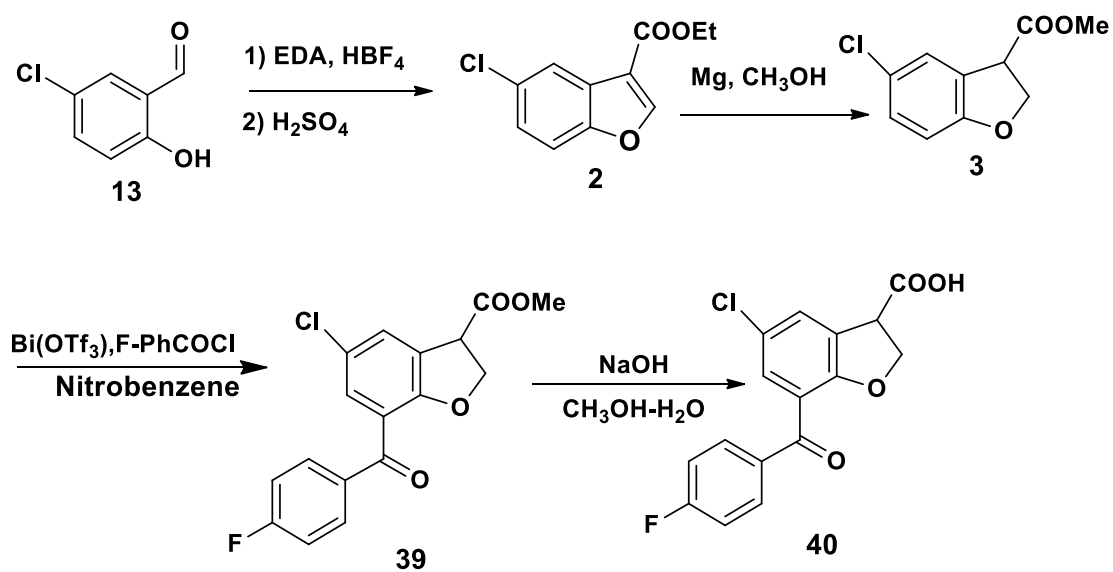
Scheme 41. Proposed synthesis of 7-(4-fluro) Benzoyl- 5-Chloro-2,3-dihydro benzo[b]furan-3-carboxylic acid (**40**).
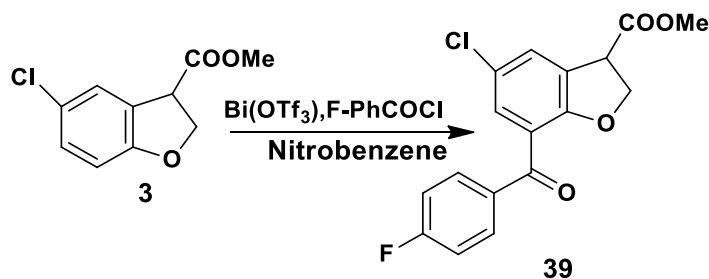
Scheme 42. Microwave assisted reaction with Bi catalyst.

Table 20. Effect of temperature benzoylation reaction.

Entry	Temperature (^{0}C)	4-Fluro Benzoyl Chloride	Bi(OTf)$_3$	Time	% of Yield
1	140	8.5 eq	0.1 eq	20 min	38
2	140	10.8 eq	0.1 eq	1h	48
3	100	10.8 eq	0.1 eq	1h	45
4	**120**	**10.8 eq**	**0.1 eq**	**1h**	**48**
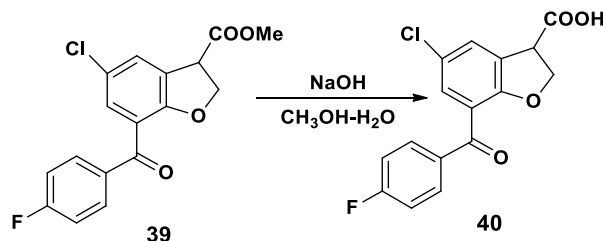
Scheme 43. Hydrolysis of 7-(4-fluro) Benzoyl -5-Chloro-2,3- dihydrobenzo [b] furan-3- carboxylate (40).

Thus, Total Synthesis of 7-(4-fluro) Benzoyl -5-Chloro-2,3- dihydrobenzo[b] furan-3- carboxylic acid (41)
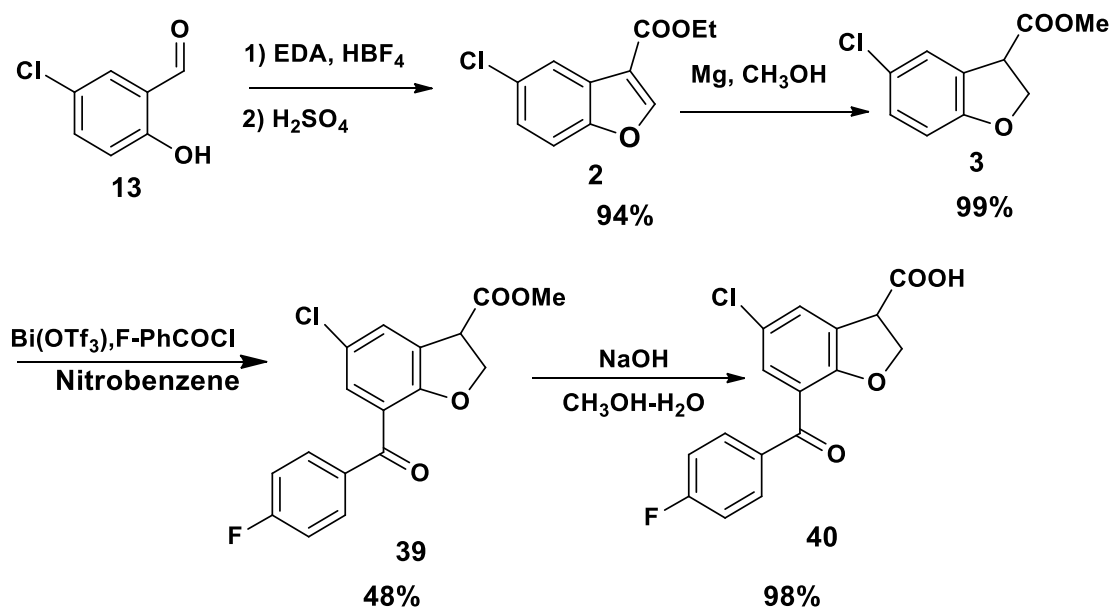
Overall Yeild: 44%

Later, we planned to synthesize 7-(4-chloro) Benzoyl- 5-Chloro-2,3-dihydro benzo[b] furan-3-carboxylic acid (42) by following our established synthetic route (**Scheme 44**). We kept benzoyl chloride and time as fixed, but altered catalyst loading and temperature in benzoylation reaction (Scheme 45) to form **41** yield in 70% (**Table19. entry 6**). Subsequent, hydrolysis (Scheme 46) we obtained target compound with 99 % in yield.

Scheme 44. Proposed synthesis of 7-(4-Chloro) Benzoyl- 5-Chloro-2,3-dihydrobenzo b] furan-3-carboxylic acid (**42**).
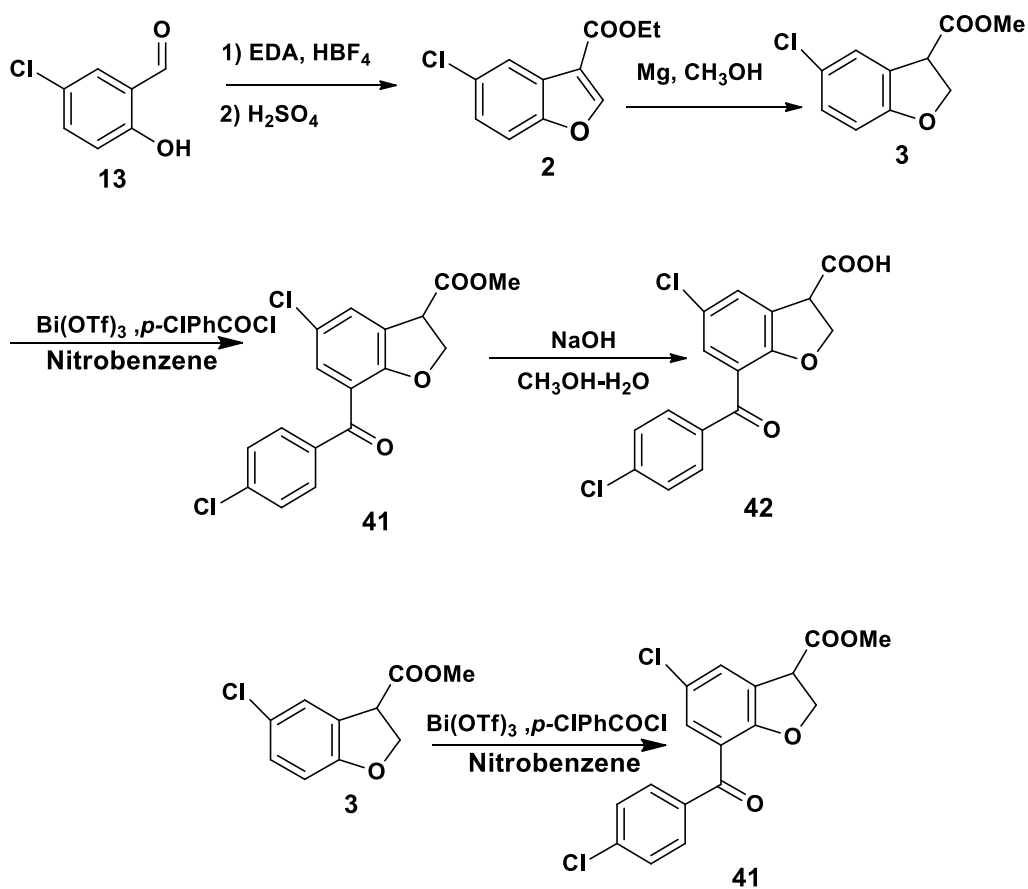
Scheme 45. Microwave assisted reaction with Bi catalyst.
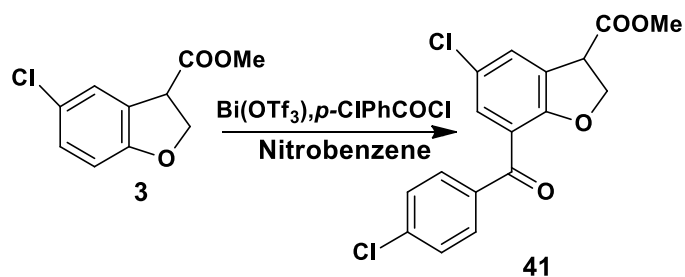
Table 21. Effect of catalyst loading on benzoylation reaction.

Entry	Temperature (^{0}C)	Benzoyl Chloride	Bi(OTf)$_3$	Time	% of Yield
1	100	2.2 eq	0.2 eq	1h	41
2	120	2.2 eq	0.2 eq	1h	47
3	140	2.2 eq	0.2 eq	1h	49
4	120	2.2 eq	0.3 eq	1h	51
5	120	2.2 eq	0.3 eq	1h	69
6	**120**	**2.2 eq**	**0.3 eq**	**1h**	**70**
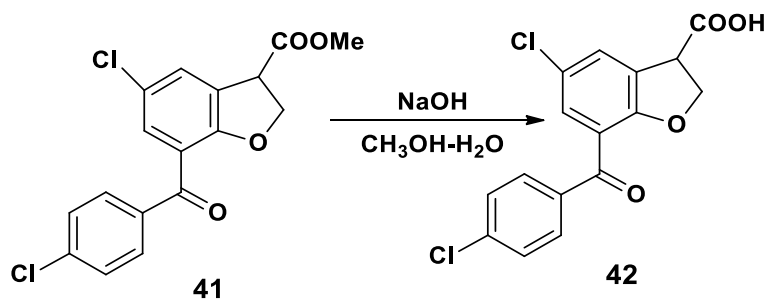
Scheme 46. Hydrolysis of 7-(4-Chloro) Benzoyl -5-Chloro-2,3- dihydrobenzo [b] furan-3- carboxylate (41).

Total Synthesis of 7-(4-chloro) Benzoyl -5-Chloro-2,3- dihydrobenzo[b] furan-3- carboxylic acid (42)

Overall Yeild : 65%
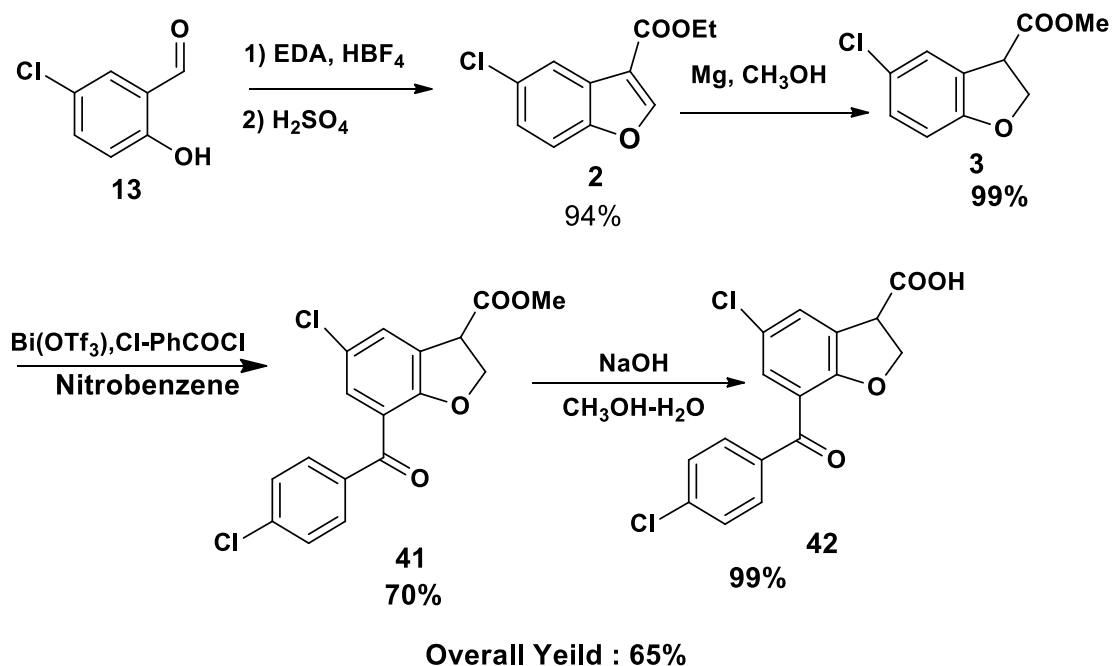
Next, we decided to make 7-(4-Notro) Benzoyl- 5-Chloro-2,3-dihydro benzo[b] furan-3-carboxylic acid (**44**). We did benzoylation reaction by pursuing our established synthetic route (Scheme 47) to form **43** (Scheme 48) yield in 56% (**Table:20, entry 4**).
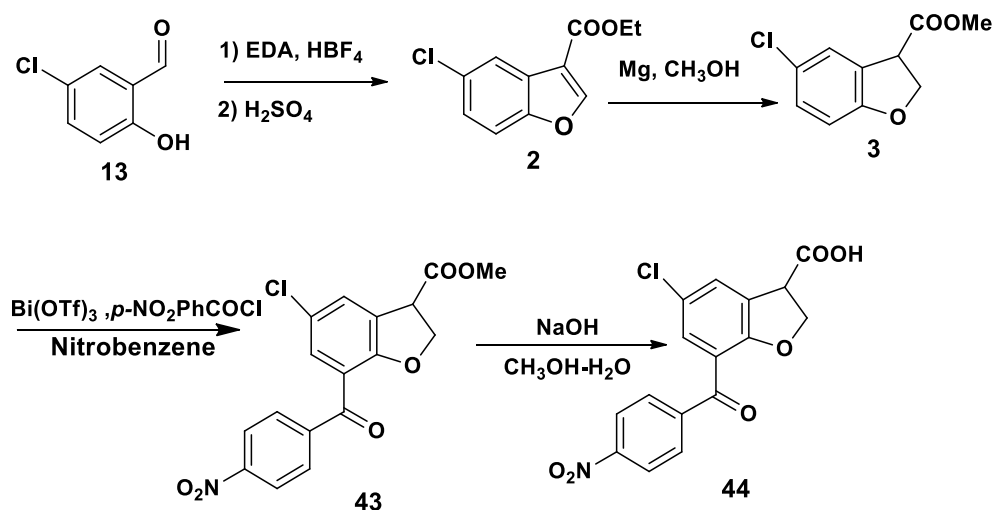
Scheme 47. Proposed synthesis of 7-(4-Nitro) Benzoyl- 5-Chloro-2,3- dihydrobenzo [b]furan -3-carboxylic acid (44).

Consequent, hydrolysis (Scheme 49) we found final product **45** with 95 % in yield.
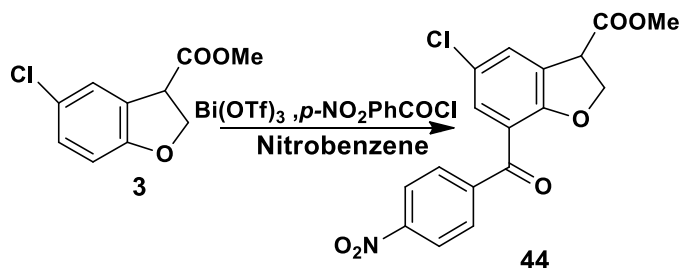
Scheme 48. Microwave-assisted reaction with Bi catalyst

Table 22. Optimization of benzoylation reaction with Bi(OTf)$_3$

Entry	Temperature (^{0}C)	Benzoyl Chloride	Bi(OTf)$_3$	Time	% of Yield
1	80	2.2 eq	0.2 eq	1h	43
2	90	2.2 eq	0.2 eq	1h	46
3	100	2.2 eq	0.2 eq	1h	53
4	**120**	**2.2 eq**	**0.2 eq**	**1h**	**56**
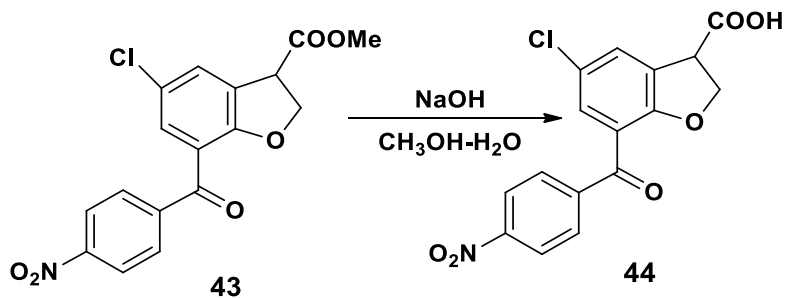
Scheme-49. Hydrolysis of 7-(4-Nitro) Benzoyl -5-Chloro-2,3- dihydrobenzo [b] furan-3- carboxylate (43)

Thus, Total Synthesis of 7-(4-Nitro) Benzoyl -5-Chloro-2,3-dihydrobenzo[b] furan-3- carboxylic acid (44)

Overall Yeild : 50%
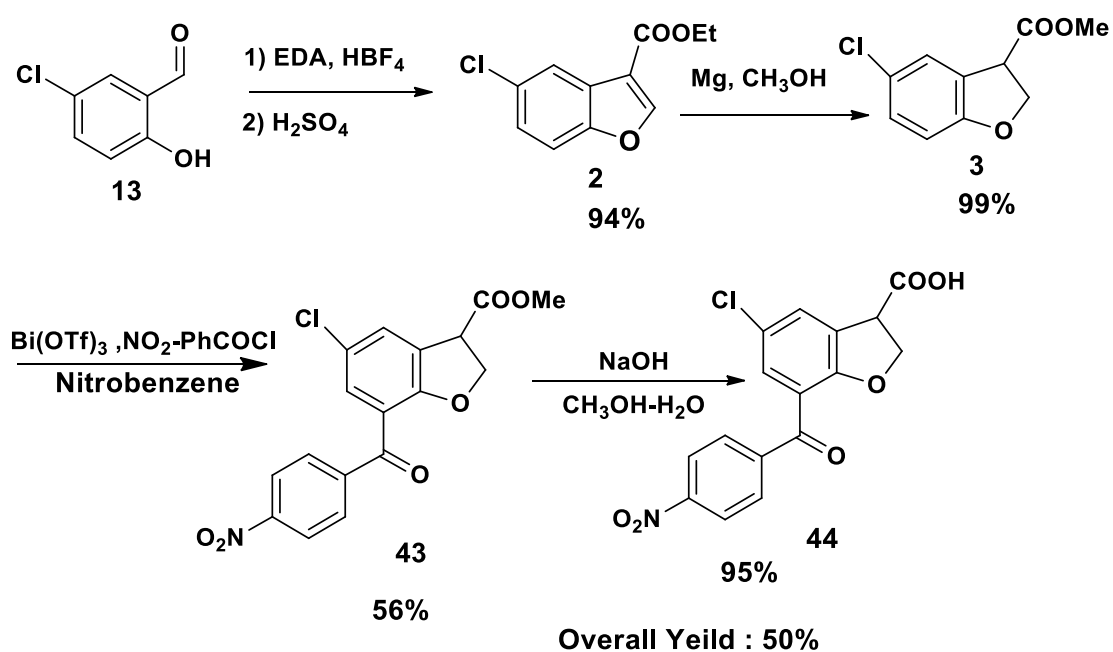
Afterwards, we designed to the synthesis of 7-(4-Methyl thiol) Benzoyl- 5-Chloro-2,3-dihydrobenzo[b]furan-3-carboxyllate (**45**) and stuck to our improved synthetic route
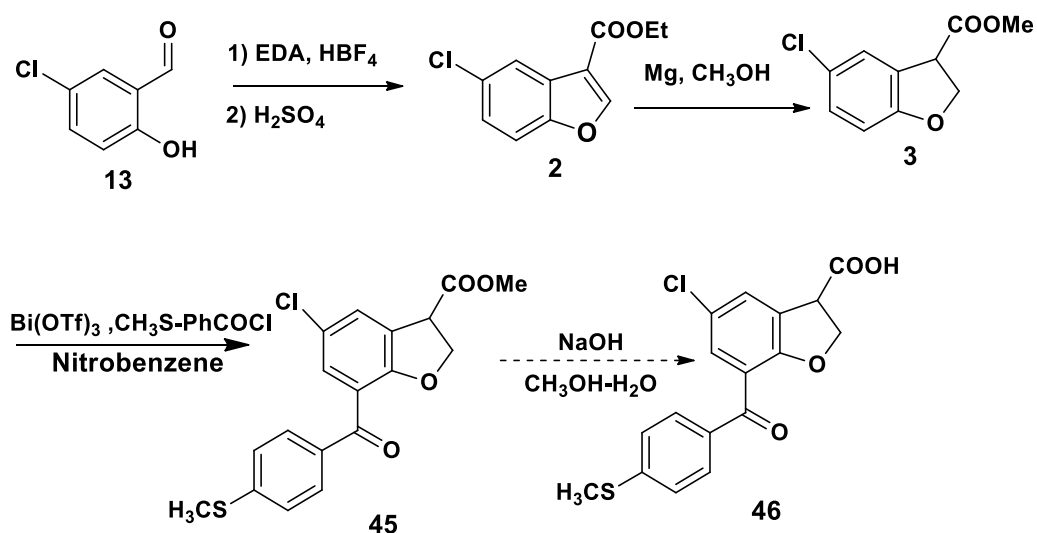
Scheme 50. Proposed synthesis of 7-(4-Methyl thiol) Benzoyl- 5-Chloro-2,3-dihydrobenzo[b]furan-3-carboxyllate (**45**).

(Scheme 50). Microwave-assisted benzoylation reaction (Scheme-51) was carried out with great catalyst Bi(OTf)$_3$ to yield 48%(**Table:21, entry 4**).
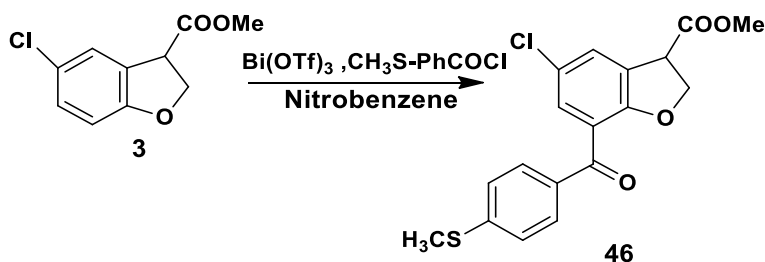
Scheme 51. Microwave assisted reaction with Bi catalyst

Table 23. Effect of Temperature on benzoylation reaction with Bi(OTf)$_3$.

Entry	Temperature (^{0}C)	7-(4-Methyl thiol) Benzoyl Chloride	Bi(OTf)$_3$	Time	% of Yield
1	100	1 eq	0.2 eq	1h	40
2	100	2.2 eq	0.2 eq	1h	45
3	120	2.2 eq	0.2 eq	1h	48
4	**140**	**2.2 eq**	**0.2 eq**	**1h**	**54**

Next, we planned to synthesis of 7-(4-hydroxy) Benzoyl- 5-Chloro-2,3-dihydro benzo[b]furan-3-carboxyllate (**47**) and followed to our developed synthetic route (Scheme 51). Microwave-assisted benzoylation reaction (Scheme 56) was carried out with noble
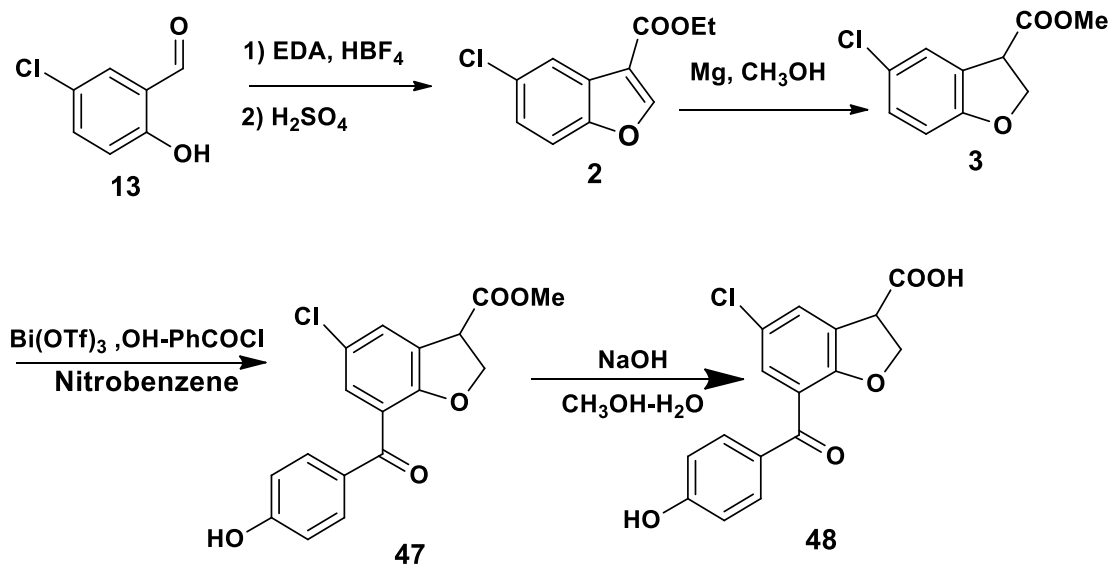
Scheme 52. Proposed synthesis of 7-(4-hydroxy) Benzoyl- 5-Chloro-2,3-dihydrobenzo[b]furan-3-carboxyllate (**47**).

catalyst Bi(OTf)$_3$, but unfortunately, the reaction did not happen.
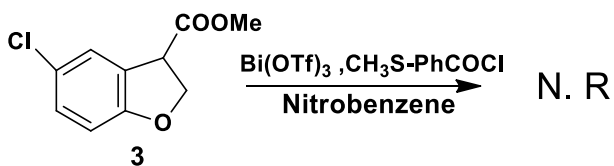
Scheme-53. Microwave assisted reaction with Bi catalyst

Afterwards, we decided to synthesis of 7-(4-Methyoxy) Benzoyl- 5-Chloro-2,3-dihydrobenzo[b]furan-3-carboxyllate (45) and followed our improved synthetic route
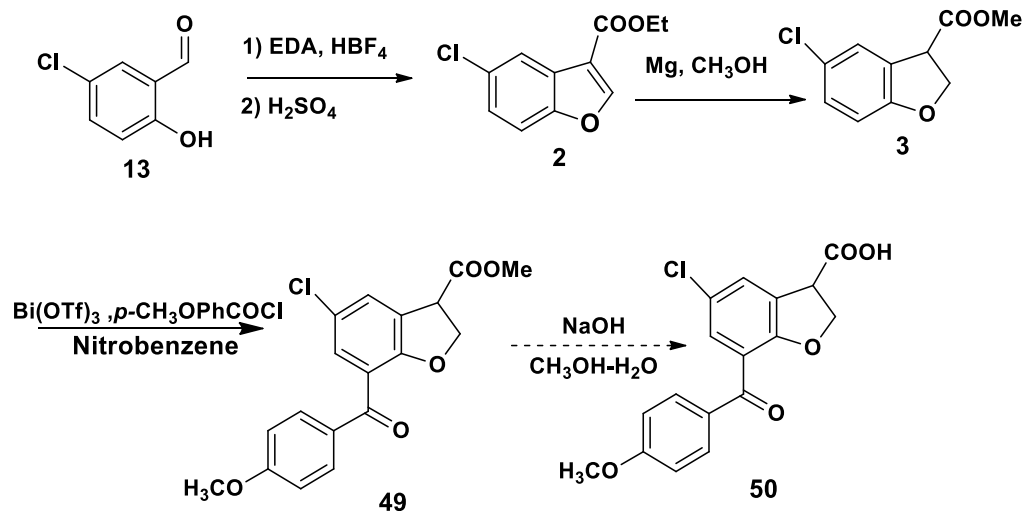
Scheme 54. Proposed synthesis of 7-(4-Methoxy) Benzoyl- 5-Chloro-2,3- dihydrobenzo

[b]furan -3-carboxylic acid (50).

(Scheme-54). Microwave-assisted benzoylation reaction (Scheme-55) was carried out

with great catalyst Bi(OTf)$_3$ to yield 45%(Table:22, entry 3).
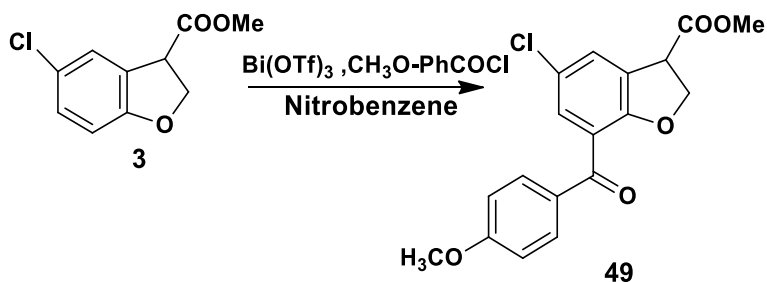
Scheme-55. Microwave assisted reaction with Bi catalyst.

Table 24. Effect of Temperature on benzoylation reaction with Bi(OTf)$_3$.

Entry	Temperature (^{0}C)	7-(4-Methoxy) Benzoyl Chloride	Bi(OTf)$_3$	Time	% of Yield
1	90	1 eq	0.2 eq	1h	38
2	100	2.2 eq	0.2 eq	1h	44
3	**120**	**2.2 eq**	**0.2 eq**	**1h**	**45**
4	140	2.2 eq	0.2 eq	1h	42

2.3. Enzyme Inhibition studies.

2.3.1. Enzymes

The expression and purification of murine COX-2 (mCOX-2) from insect cells and of ovine COX-1 (oCOX-1) from ram seminal vesicles were done by following published methods[218-220] All activity or inhibition studies were performed in 100 mM Tris-HCl buffer containing 500 μM phenol. Inhibitors were dissolved in dimethyl sulfoxide. Reaction mixtures contained hematin-reconstituted proteins at final enzyme concentrations adjusted to give approximately 30-35% substrate consumption (mCOX-2 = 77 nM, oCOX-1 = 22.5 nM). Fig-18 shows that BRL-37959 is a selective COX-1 inhibitor with IC_{50} value of 245nM.
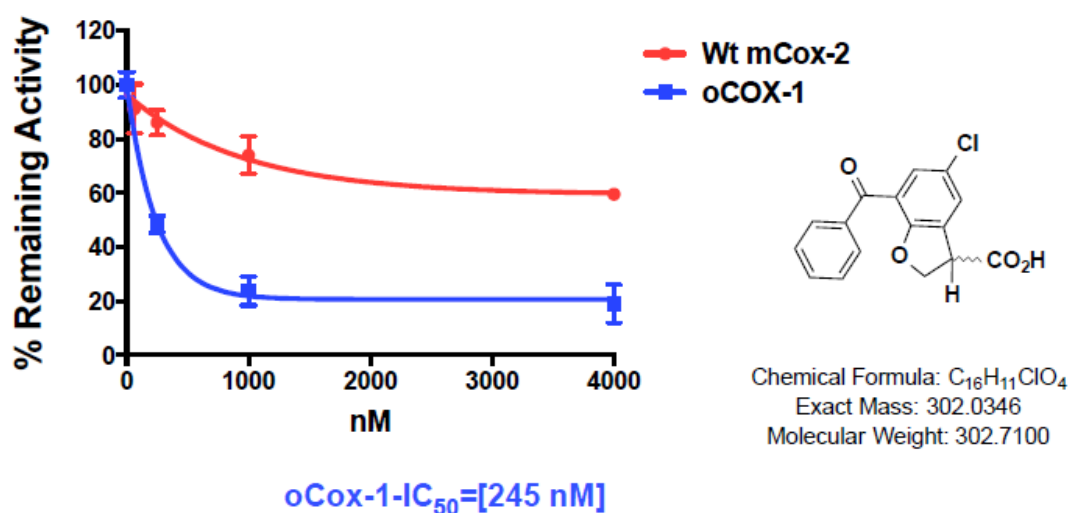
Figure-40: Inhibition of purified Wt mCOX-2 and oCOX-1, by BRL-37959.

2.4. Cellular Assays (Proliferation Assay)

The anti-proliferative activities of the BRL-37959 was verified against colon, breast, ovarian and prostate cancer cell lines in an MTT using the Indomethacin as a positive control. The MTT assay is a colorimetric assay for measuring cell viability[221]. NAD(P)H-dependent cellular oxidoreductase enzymes indicate the number of viable cells present. These enzymes can reduce the tetrazolium dye MTT, 3-(4,5-dimethylthiazol-2-yl)-2,5 diphenyltetrazolium bromide to its insoluble formazan, which has a purple color. The absorbance of this colored solution can be quantified by measuring at a certain wavelength (normally between 500 to 600 nm) by a spectrophotometer. The degree of light absorption depends on the solvent and how many living cells reduced MTT (yellow) to formazan (purple)[222].
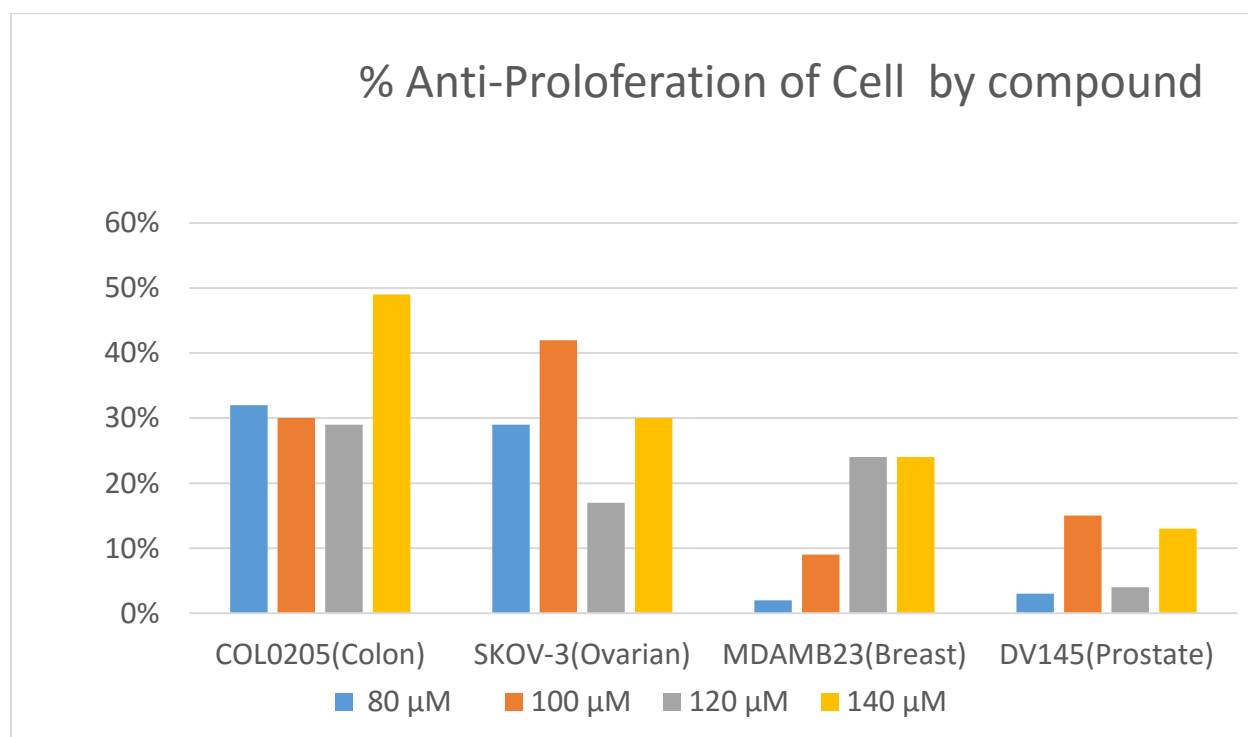
Figure 41: Proliferation Assay of BRL-37959.

3. General Methods and Experimental

3.1. General considerations

All reactions were performed under a nitrogen atmosphere in oven-dried glassware with

magnetic stirring. Air and moisture-sensitive liquids and solutions were transferred via an

oven-dried, stainless steel syringe and were introduced into the reaction vessel through

rubber septa. CH_2Cl_2 was distilled from calcium hydride. Other solvents used were

distilled from sodium-benzophenone ketyl. Freshly distilled solvents were then degassed

for Pd-catalyzed reactions by freeze-pump-thaw techniques under vacuum. Previously

reported compounds were identified by 1H NMR (nuclear magnetic resonance) spectra.

All new compounds were characterized by additional 13C NMR and high-resolution mass

spectroscopy. Analytical thin layer chromatography (TLC) was performed on silica gel

plates (Merck 60F254) visualized either with a UV lamp (254 nm) or by using an iodine

chamber. Flash chromatography was performed using 40-60 µm silica gel (Silicycle).

The eluent employed for flash chromatography is reported as volume/volume ratios.

Organic extracts were dried over anhydrous Na_2SO_4. The 1H and 13C NMR Spectra were

performed on a Bruker NMR at 300 and 75 MHz, or 500 and 125 MHz respectively. The1H

NMR spectral data are reported as follows: chemical shift (δ) in parts per million (ppm)

from tetramethylsilane as an internal standard ($CDCl_3$ δ7.26 ppm), multiplicity (s = singlet,

d = doublet, t = triplet, q = quartet, m = multiplet), intégration. ^{13}C data were reported as

follows: chemical shifts (δ) are reported in parts per million (ppm) from tetramethylsilane

with the solvent as an internal standard (CDCl₃ δ77.16 ppm). HPCL analysis was[115]

performed using a Waters 1500 Series HPLC equipped with a Regis Technologies Pirkle.

High-resolution mass spectra were done in the MS Shimadzu Laboratory for Advanced

and Applied Analytical Chemistry at the University of Wisconsin –Milwaukee.

3.2. Experimental Procedures

3.2.1.1. Preparation of Ethyl 5-chloro-benzo[b]furan-3-carboxylate[33] (**2**)

5-chlorosalicylaldehyde (1g, 6.39 mmol) was added to a 100 mL 3-neck round bottom

flask fitted with an addition funnel along with 2 mL dichloromethane (DCM). The mixture

was stirred at room temperature to make a slurry. After this,0.1mL $HBF_4 \cdot OEt_2$ (0.734

mmol) was added by a syringe directly to the solution and it was stirred for 15 min for

protonation of the aldehyde. 2 mL ethyl diazoacetate(EDA) (10.41 mmol) was added to

the addition funnel along with 1mL DCM. The EDA solution was added dropwise over a

period of 5-6 hours. The dark yellow colored solution was allowed to stir for 12 hrs. under

a nitrogen atmosphere. After that, the addition funnel was removed and the reaction

mixture was concentrated under rotary evaporation to remove free EDA. Then 0.4 mL of

99.99% H_2SO_4 was added dropwise to the viscous solution. The round bottom flask was

placed in an ice-bath and 10 min later the solution was diluted with 2 ml of DCM. The

acidic reaction mixture was neutralized by adding saturated of $NaHCO_3$ solution. The

reaction mixture was extracted by DCM. The organic layers were combined and dried

over anhydrous Na_2SO_4 and the solvent was removed by rotovaporation as well as yellowish white solid crude product obtained.

The crude product was dissolved in anhydrous ethanol and 0.183 g NaOH was added. The solution was stirred at 38^0C for 1h. After this, the solution cooled down to room temperature and deionized water was added dropwise until no precipitate formed. The round bottom flask was placed in an ice-bath for 5-10 minutes and then filtered on a Buchner funnel. The off white solid material was allowed to dry on the Buchner Filter for 1 hr. After that, the material was sublimed under high vacuum and clear white crystals of product (99% purity) was obtained.

^{1}H NMR (300 MHz, CDCl$_3$): δ 8.24(s, 1H), 8.00 (d, 1H), 7.42 (d, 1H), 7.29 (dd, 1H),4.41 (q, 2H), 1.43 (t, 3H).

The analytical data matched with that of previously reported[33] data.

3.2.1.1a. Preparation of Ethyl 5-fluroro-benzo[b]furan-3-carboxylate[33] (**23**)

 5-Fluorosalicylaldehyde (1g, 7.14 mmol) was added to a 100 mL 3-neck round bottom flask fitted with an addition funnel along with 6 mL dichloromethane (DCM). The mixture was stirred at r.t. to make a slurry. After this, 0.1mL HBF$_4$·OEt$_2$ (0.735 mmol) was added by a syringe directly to the solution and stirred for 15 min for protonation of the aldehyde. Then, 1.01 mL ethyl diazoacetate(EDA) (9.55 mmol) was added to the addition funnel along with 1mL DCM. The EDA solution was added dropwise over a period of 5-6 hrs. The dark yellow colored solution was allowed to stir for 12 hrs. under a nitrogen

atmosphere. After that, the addition funnel was removed and the reaction mixture was concentrated on a rotary evaporation to remove the remaining EDA. Then 0.5 mL of 99.99% H_2SO_4 was added dropwise to the viscous solution. The round bottom flask was placed in an ice-bath and 10 min later the solution was diluted with 2 mL of DCM. The acidic reaction mixture was neutralized by adding saturated of $NaHCO_3$ solution. The reaction mixture was then extracted by DCM. The organic layers were combined and dried over anhydrous Na_2SO_4 and the solvent was removed by rotovaporation and a yellowish white colored solid crude product was obtained.

The crude product was dissolved in anhydrous ethanol and 0.2 g NaOH was added. The solution was stirred at 38^0C for 1h. After this, the solution was cooled down to r.t. and deionized water was added dropwise until no precipitate formed. The round bottom flask was placed in ice-bath for 5-10 min. and the mixture filtered on a Buchner funnel. The off white solid material was allowed to dry on the Buchner filter for 1 hr. After that, the material was sublimed under high vacuum and clear white crystals of product (99% purity) was obtained. The analytical data matched with previously reported[33] data.

3.2.1.1b. Preparation of Methyl 5-methyl-benzo[b]furan-3-carboxylate[33] (**28**)

5-methylsalicylaldehyde (1g, 7.34 mmol) was added to a 100 mL 3-neck round bottom flask fitted with an addition funnel along with 4 mL dichloromethane (DCM). The mixture was stirred at r.t. to make a slurry. After this,0.1mL $HBF_4 \cdot OEt_2$ (0.734 mmol) was added by a syringe directly to the solution and stirred for 15 min for protonation of the aldehyde. Then,1.07 mL of Ethyl diazoacetate(EDA) (10.12 mmol) was added to the addition funnel along with 2 mL DCM. The EDA solution was added dropwise over a period of 5-6 hrs.

The dark yellow colored solution was allowed to stir for 12 hrs. under a nitrogen atmosphere. After that, the addition funnel was removed and the reaction mixture was concentrated under a rotary evaporatory to remove the remaining EDA. After this,0.4 mL of 99.99% H_2SO_4 was added dropwise to the viscous solution. The round bottom flask was placed in an ice-bath and 10 min later the solution was diluted with 2 mL of DCM. The acidic reaction mixture was neutralized by adding saturated of $NaHCO_3$ solution. The reaction mixture was extracted by DCM. The organic layers were combined and dried over anhydrous Na_2SO_4 and the solvent was removed by rotary evaporation and a yellowish white solid crude product was obtained.

The crude product was dissolved in anhydrous ethanol and 0.2 g NaOH was added. The solution was stirred at 38^0C for 1h. After this, the solution was cooled to r.t. and deionized water was added dropwise until no precipitate formed. The round bottom flask was placed in an ice-bath for 5-10 min. and filtered on a Buchner funnel. The off white solid material allowed to dry on the Buchner filter for 1 hr. After that, the material was sublimed under high vacuum and clear white crystals of product (99% purity) was obtained. The analytical data matched with previously reported[33] data.

3.2.1.1c. Preparation of Ethyl 5-Methoxy-benzo[b]furan-3-carboxylate[33] (**33)**

5-methoxysalicylaldehyde (1g, 6.57 mmol) was added to a 100 mL 3-neck round bottom flask fitted with an addition funnel along with 5 mL dichloromethane (DCM). The mixture was stirred at r.t. to make a slurry. After this, 0.1mL HBF$_4$·OEt$_2$ (0.734 mmol) was added by a syringe directly to the solution and stirred for 15 min for protonation of the aldehyde. 0.85 mL Ethyl diazoacetate(EDA) (7.80 mmol) was added to the addition funnel along

with 1mL DCM. The EDA solution was added dropwise over a period of 5-6 hrs. The dark yellow colored solution was allowed to stir for 12 hrs under a nitrogen atmosphere. After that, the addition funnel was removed and the reaction mixture was concentrated under a rotary evaporatory to remove the remaining EDA. After this,0.4 mL of 99.99% H_2SO_4 was added dropwise to the viscous solution. The round bottom flask was placed in an ice-bath and 10 min later the solution was diluted with 2 mL of DCM. The acidic reaction mixture was neutralized by adding saturated of $NaHCO_3$ solution. The reaction mixture was extracted by DCM. The organic layers were combined and dried over anhydrous Na_2SO_4 and the solvent was removed by rotary evaporation and a yellowish white solid crude product was obtained.

The crude product was dissolved in anhydrous ethanol and 0.2 g NaOH was added. The solution was stirred at 380C for 1h. After this, the solution was cooled to r.t. and deionized water was added dropwise until no precipitate formed. The round bottom flask was placed in an ice-bath for 5-10 min. and filtered on a Buchner funnel. The off white solid material allowed to dry on the Buchner filter for 1 hr. After that, the material was sublimed under high vacuum and clear white crystals of product (99% purity) was obtained. The analytical data matched with previously reported[33] data.

3.2.1.2. Preparation of Methyl 5-chloro-2,3-dihdrobenzo[b]furan-3-carboxylate (3)

Ethyl 5-chloro-benzo[b]furan-3-carboxylate (**2**) (1g, 4.45mmol) was dissolved in methanol(35mL) followed by addition of magnesium powder of ~300 mesh (1.2g,0.05 mol). The reaction mixture was stirred for 3 days under a nitrogen atmosphere at r.t. After

that, the reaction mixture was poured to 35 mL of deionized water to quench the reaction and ash colored solid material formed. Then, the Erlenmeyer flask containing the reaction mixture was placed in an ice bath and 5M HCl was added dropwise until P^H would be 1.0. The solution was extracted with diethyl ether. The organic layers were combined, washed with brine and dried over anhydrous Na_2SO_4 and the solvent was removed by rotary evaporation as well as pale yellow oily product obtained (1.42g, 99% yield).

^1H NMR (300 MHz, CDCl$_3$): δ 7,41(d, J=2Hz,1H), 7.17 (dd, J=8& 2Hz 1H), 6.67 (d, J=8Hz,1H), 4.99 -4.37 (m, 3H), 3.82(s,3H).

3.2.1. 2.a. Methyl 5-Fluoro 2,3-dihdro benzo[b]furan-3-carboxylate (24).

Ethyl 5-fluoro-benzo[b]furan-3-carboxylate (**2**) (1.2g, 5.71mmol) was dissolved in methanol (20 mL) followed by addition of magnesium powder of ~300 mesh (1.44g,0.06 mol). After that, the reaction mixture was allowed to stir for 3 days under a nitrogen atmosphere at r.t. Then the reaction mixture was poured to 20 mL of deionized water to quench the reaction and ash colored solid material was formed. After that, the Erlenmeyer flask containing the reaction mixture was placed in an ice bath and 5M HCl was added dropwise until P^H would be 1.0. Then, the solution was extracted with diethyl ether. The organic layers were combined, washed with brine and dried over anhydrous Na_2SO_4 and the solvent was removed by rotary evaporation and pale yellow oily product was obtained (0.90g, 81% yield). The analytical data matched with previously reported[33]data.

3.2.1. 2.b. Methyl- 5-Methyl -2,3-dihdro benzo[b]furan-3-carboxylate (29)

Ethyl 5-methyl-benzo[b]furan-3-carboxylate (**2**) (1g, 4.85mmol) was dissolved in methanol (35mL) followed by addition of magnesium powder of ~300 mesh (1.1g,0.05

mol). Then, the reaction mixture was allowed to stir for 3 days under a nitrogen atmosphere at r.t. After this, reaction mixture was poured to 35 mL of deionized water to quench the reaction and ash colored solid material formed. Then, the Erlenmeyer flask containing the reaction mixture was placed in an ice bath and 5M HCl was added dropwise until P^H would be 1.0. After that, the solution was extracted with diethyl ether. Then, the organic layers were combined, washed with brine and dried over anhydrous Na_2SO_4 and the solvent was removed by rotary evaporation and yellow oily product was obtained (0.85g, 91% yield.

The analytical data matched with previously reported[33] data.

3.2.1. 2.c. Methyl- 5-Methoxy -2,3-dihdro benzo[b]furan-3-carboxylate (34).

Methyl 5-methoxy-benzo[b]furan-3-carboxylate (**2**) (1g, 4.45mmol) was dissolved in methanol (35mL) followed by addition of magnesium powder of ~300 mesh (1.2g,0.058 mol). Then, the reaction mixture was allowed to stir for 3 days under nitrogen a atmosphere at r.t. After this, the reaction mixture was poured to 35 mL of deionized water to quench the reaction and ash colored solid material formed. Then, the Erlenmeyer flask containing the reaction mixture was placed in an ice bath and 5M HCl was added dropwise until P^H would be 1.0. The solution was extracted with diethyl ether. After that, the organic layers were combined, washed with brine and dried over anhydrous Na_2SO_4 and the solvent was removed by rotovaporation as well as pale yellow oily product obtained (0.85g, 92% yield.

 Analytical data matched with previously reported[33]data.

3.2.1.3. Method A: Synthesis of Methyl-7-benzoyl 5-chloro-2,3-dihdrobenzo[b]furan-3- carboxylate (15)

$AlCl_3$ (1g.,7.45 mmol) was added to a 100 mL 3-neck round bottom flask fitted with condenser and septum connected to a nitrogen line. 10 mL nitromethane was charged into the flask. Benzoyl chloride (1 mL,8.79 mmol) was added by a syringe followed by the addition of solution of Mthyl-7-benzoyl 5-chloro-2,3-dihdrobenzo[b]furan-3- carboxylate (1g.,4.2 mmol, in 10 mL nitromethane). Then, the reaction mixture was heated to 67^0 C with constant stirring for 3 days. Excess nitromethane was removed by rotary evaporator. After that, the round bottom flask was placed in an ice-bath and the dark oil residue was quenched with concentrated HCl (7 mL) .15 ml of H_2O was added to the flask and aqueous layer was removed. Then, 15 ml of H_2O was added to the flask and extracted with 30 mL of CH_2Cl_2. The organic layers were combined and dried over anhydrous Na_2SO_4 and the solvent was removed by rotovaporation as well as black crude product was obtained. [1]NMR indicated that roughly 51% of the mixture contained Mthyl-7-benzoyl 5-chloro-2,3-dihdrobenzo[b]furan-3- carboxylate (15).

^{1}H NMR (300 MHz, CDCl$_3$): δ 7.83 (d,J= 5Hz,2H), 7.62(t,J=5Hz,1H), 7.55(S,1H,),7.49(t, J=5Hz, 2H), 7.44(S, 1H), 4.99 (t,J=10Hz,1H),4.76(t,J=10Hz,1H),4.40(t,J=10Hz,1H), 3.86(s,3H).

3.2.1.4 Method B: Microwave-assisted synthesis of Methyl-7-benzoyl 5-chloro-2,3-dihdrobenzo[b]furan-3- carboxylate (15)

AlCl$_3$ (144 mg., 1.0 mmol) was added to a 10-mL pressurized tube fitted with a magnet bar and septum connected to a nitrogen line. Then, benzoyl chloride (0.4 mL,3.75 mmol) was added by a syringe followed by the addition of 1mL of nitromethane. After this, the reaction was stirred for 20 min and catalyst was dissolved. Then, the solution of Mthyl-7-benzoyl 5-chloro-2,3-dihdro benzo [b]furan-3- carboxylate (100 mg.,0.47 mmol, in 1 mL nitromethane) was added to the tube and quickly septum was removed as well as sealed with the high -pressure tolerance septum. After that, the glass tube was placed into a CEM microwave at the temperature 80^0 C, pressure 40 PSI with high steering for 1h. The reaction mixture could cool to the room temperature in the MW oven. After cooling, the mixture was transferred to the Elamnary flask by CH$_2$Cl$_2$. The flask was placed in an ice-bath and the dark oil residue was quenched with concentrated HCl (3 mL). 5 mL of CH$_2$Cl$_2$ and 5 mL of H$_2$O was added to the flask and aqueous layer was removed. Then, 15 ml of H$_2$O was added to the flask and extracted with 30 mL of CH$_2$Cl$_2$. The organic layers were combined and dried over anhydrous Na$_2$SO$_4$ and the solvent was removed by rotovaporation as well as black crude product obtained. [1]NMR indicated that roughly 67% of the mixture contained Mthyl-7-benzoyl 5-chloro-2,3-dihdrobenzo[b]furan-3-carboxylate (15).

^{1}H NMR (300 MHz, CDCl$_3$): δ 7.83 (d,J= 5Hz,2H), 7.62(t,J=5Hz,1H), 7.55(S,1H,),7.49(t, J=5Hz, 2H), 7.44(S, 1H), 4.99 (t,J=10Hz,1H),4.76(t,J=10Hz,1H),4.40(t,J=10Hz,1H), 3.86(s,3H).

3.2.1.5 Microwave-assisted synthesis of Methyl-7-benzoyl 5-chloro-2,3-dihdrobenzo [b]furan-3- carboxylate (15) using Zn and Zn with BMIB (ionic liquid).

We followed the same procedure of 3.2.1.4. to synthesize Methyl-7-benzoyl 5-chloro-2,3-dihdrobenzo[b]furan-3- carboxylate (15).

3.2.1.6 Method C: Microwave-assisted synthesis of Methyl-7-benzoyl 5-chloro-2,3-dihydro benzo [b] furan-3- carboxylate (15) using Bi(OTf)$_3$ as a catalyst.

Methyl 5-chloro-2,3-dihydrobenzo[b]furan-3- carboxylate (3) (100 mg.,0.47 mmol) was added to a 10mL pressurized glass tube fitted with a septum connected to a nitrogen line. Next, Bi(OTf)$_3$ (60 mg,0.046 mmol) was added to the tube followed by the addition of 1.5mL of nitrobenzene. Benzoyl chloride (0.08 mL,0.01 mmol) was added by a syringe and quickly septum was removed as well as sealed with the High -pressure tolerance septum. The microtube was placed in the microwave for 1 hour to react at 80^0 C, temperature, 40 PSI pressure with high steering. The reaction mixture was transferred to the Elamnary flask. The dark oil residue was quenched with 15 ml of H_2O and 10 ml CH_2Cl_2 was added to the flask. Next the solution was passed through the silica plug. The filtrate was extracted with 30 mL of CH_2Cl_2 and organic layer was washed with $NaHCO_3$ and brine. The organic layers were combined and dried over anhydrous Na_2SO_4 and the solvent was removed by rotovaporation as well as black oily crude product obtained. [1]NMR indicated that roughly 85% of the mixture contained Mthyl-7-benzoyl 5-chloro-2,3-dihdrobenzo[b]furan-3- carboxylate (15). Next, the crude product was placed on the silica plug and washed with hexane followed by washed with ethyl acetate /hexane (5: 95) solvent. Nitrobenzene and unreacted starting material was remove. Mixture of product and starting material was separated from the silica plug with CH_2Cl_2 followed by

rotovaporation to remove CH_2Cl_2. After that, Hexane was added to the mixture and heated to 70^0 C and cooled down to RT and crystal of pure product was started to form. This crystallization process was repeated for several times and 102 mg (76% yield) of pure solid Methyl-7-benzoyl 5-chloro-2,3-dihdrobenzo[b]furan-3- carboxylate (15) was obtained.

^{1}H NMR (300 MHz, CDCl$_3$): δ 7.83 (d,J= 5Hz,2H), 7.62(t,J=5Hz,1H), 7.55(S,1H,),7.49(t, J=5Hz, 2H), 7.44(S, 1H), 4.99 (t,J=10Hz,1H),4.76(t,J=10Hz,1H),4.40(t,J=10Hz,1H), 3.86(s,3H).

3.2.1.7 Method D: Traditional synthesis of Methyl-7-benzoyl 5-chloro-2,3- dihydro benzo [b] furan-3- carboxylate (15) using Bi(OTf)$_3$ as a catalyst.

Methyl 5-chloro-2,3-dihdrobenzo[b]furan-3- carboxylate (3) (2.47g,10.44 mmol) was added to a 250 mL 3-neck round bottom flask fitted with condenser and septum connected to a nitrogen line. Then, Bi(OTf)$_3$ (1.5g, 2.28 mmol) was added to the flask followed by the addition of 30 mL of nitrobenzene. After that, benzoyl chloride (2.7 mL,23.24 mmol) was added by a syringe. Then, the reaction mixture was heated to 90^0C with constant stirring for 3 days. After that, the reaction mixture was cooled down to r.t. and transferred to the Elamnary flask. The dark oil residue was quenched with 50 ml of H_2O and 20 ml CH_2Cl_2 was added to the flask. Then, the solution was passed through the silica plug and the filtrate was extracted with 250 mL of CH_2Cl_2 and organic layer was washed with NaHCO$_3$ and brine. After this, the organic layers were combined and dried over anhydrous Na$_2$SO$_4$ and the solvent was removed by rotovaporation as well as black oily crude product obtained. [1]NMR indicated that roughly 87% of the mixture contained Mthyl-7-benzoyl 5-chloro-2,3-dihdrobenzo[b]furan-3- carboxylate (15). Then, the crude product

was placed on the silica plug and washed with hexane followed by washed with ethyl acetate /hexane (5: 95) solvent. Nitrobenzene and unreacted starting material was remove. Mixture of product and starting material was separated from the silica plug with CH_2Cl_2 followed by rotovaporation to remove CH_2Cl_2. After that, Hexane was added to the mixture and heated to 70^0 C and cooled down to RT and crystal of pure product was started to form. This crystallization process was repeated for several times and 2.32g (70% yield) of pure solid Methyl-7-benzoyl 5-chloro-2,3-dihdrobenzo[b]furan-3-carboxylate (15) was obtained.

^{1}H NMR (300 MHz, CDCl$_3$): δ 7.83 (d,J= 5Hz,2H), 7.62(t,J=5Hz,1H), 7.55(S,1H,),7.49(t, J=5Hz, 2H), 7.44(S, 1H), 4.99 (t,J=10Hz,1H),4.76(t,J=10Hz,1H),4.40(t,J=10Hz,1H), 3.86(s,3H).

3.2.1.8. Preparation of Methyl-7-benzoyl 5-Fluoro-2,3-dihdrobenzo[b]furan-3-carboxylate (25): Method C was followed for the preparation of **25**. A 10-mL pressurized glass tube with High -pressure tolerance septum equipped with a magnet bar was charged with Methyl 5-Fluoro-2,3-dihdrobenzo[b]furan-3- carboxylate (24) (0.1g,0.51 mmol), Bi(OTf)$_3$ (30mg mg,0.046 mmol) and Benzoyl chloride (0.08 mL, 0.1 mmol) in 1 mL of Nitrobenzene. Then, glass tube was placed into CEM microwave for 1 hr. to react at 140^0 C, temperature, 40 PSI pressure with high steering. The title compound (0.12 mg, 78 % of yield) isolated as a solid after crystallization in hexane.

For Traditional synthesis of **25** Method D was followed. To a 250 mL 3-neck round bottom flask fitted with condenser and septum connected to a nitrogen line was charged with Methyl 5-Fluoro-2,3-dihdrobenzo[b]furan-3- carboxylate (**24**) (2.86g,14.58 mmol),

Bi(OTf)₃ (1.8g,2.74 mmol), Benzoyl chloride (3.19 mL, 27.46 mmol) and 35 mL of Nitrobenzene. Then, the reaction mixture was heated at 90^0 C with constant steering for 3-days. The title compound (2.19 g, 50% of yield), was isolated as a solid after crystallization in hexane.

^{1}H NMR (300 MHz, CDCl₃): δ 8.10(s,1H),7.80(s,1H),7.59(dd,J=6Hz,2H),7.10(t,J=3Hz, 1H),6.89(t,J=3Hz,1H),6.76(dd,J=9Hz,1H),4.96 (t,J=10Hz,1H),4.71(t,J=10Hz,1H), 4.35 (t, J=10Hz,1H), 3.81(s,3H).

3.2.1.9. Preparation of Methyl-7-benzoyl 5-Methyl-2,3-dihdrobenzo[b]furan-3-carboxylate (30): Method C was followed for the preparation of **30**. A 10-mL pressurized glass tube with High -pressure tolerance septum equipped with a magnet bar was charged with Methyl 5-Methyl-2,3-dihdrobenzo[b]furan-3- carboxylate (**29**) (0.1g,0.50 mmol), Bi(OTf)₃ (30mg mg,0.046 mmol) and Benzoyl chloride (0.08 mL, 0.10 mmol) in 2 mL of Nitrobenzene. Then, glass tube was placed into CEM microwave for 1 hour to react at 140^0 C, temperature, 40 PSI pressure with high steering. The title compound (0.107g, 72 % of yield) isolated as a solid after crystallization in hexane.

For Traditional synthesis of **25** Method D was followed. To a 250 mL 3-neck round bottom flask fitted with condenser and septum connected to a nitrogen line was charged with Methyl 5-methyl-2,3-dihdrobenzo[b]furan-3- carboxylate (**24**) (1.2g,6.02 mmol), Bi(OTf)₃ (0.82g, 1.25 mmol), Benzoyl chloride (1.6 mL, 13.77 mmol) and 25 mL of Nitrobenzene. After that, the reaction mixture was heated at 90^0 C with constant steering for 3-days. The title compound (1.37 g, 77% of yield), isolated as a solid after crystallization in hexane.

138

¹H NMR(500 MHz, CDCl₃):δ 7.81(d,2H),7.58(t,J=9Hz,1H),7.46(t,J=9Hz,2H),7.28(s,2H) 4.95(dd, J=9Hz,1H), 4.69(t, J=9Hz, 1H), 4.35(t, J=9Hz,1H), 3.82 (s,3H).

3.2.1.10. Preparation of Methyl-7-benzoyl 5-Methoxy-2,3-dihdrobenzo[b]furan-3-carboxylate (36): Method C was followed for the preparation of **36**. A 10-mL pressurized glass tube with Teflon-coated septum equipped with a magnet bar was charged with Methyl-5-methoxy-2,3-dihdrobenzo[b]furan-3-carboxylate (**35**) (0.1g,0.48 mmol), Bi(OTf)₃ (30mg mg,0.046 mmol) and Benzoyl chloride (0.12 mL, 1.06 mmol) in 1.0 mL of Nitrobenzene. Then, glass tube was placed into CEM microwave for 30 min to react at 140⁰ C, temperature, 40 PSI pressure with high steering. The title compound (0.075g, 50 % of yield) was isolated as a solid after crystallization in hexane.

 For Traditional synthesis of **36** Method D was followed. To a 250 mL 3-neck round bottom flask fitted with condenser and septum connected to a nitrogen line was charged with Methyl-5-methoxy-2,3-dihdrobenzo[b]furan-3-carboxylate (**35**) (1.5g,7.2mmol), Bi(OTf)₃ (0.94g, 1.43 mmol), Benzoyl chloride (1.8 mL, 15.84 mmol) and 20 mL of Nitrobenzene. Then, the reaction mixture was heated at 90⁰ C with constant steering for 3-days. The title compound (1.46 g, 65% of yield), was isolated as a solid after crystallization in hexane.

¹H NMR(500 MHz, CDCl₃):δ 7.60(dd,J=2H),7.48 (t,J=9Hz,1H),7.45(t,J=9Hz,2H), 7.28(s,2H) 4.92(dd, J=9Hz,1H), 4.72(t, J=9Hz, 1H), 4.38(t, J=9Hz,1H), 3.82 (s,3H).

3.2.1.11. Preparation of 7-(4-tri-fluromethyl) Benzoyl- 5-Chloro-2,3-dihydrobenzo [b]furan-3- carboxylate (37):

Method C was followed for the preparation of **37**. A 10-mL pressurized glass tube with High -pressure tolerance equipped with a magnet bar was charged with 5-chloro-2,3-dihdrobenzo[b]furan-3- carboxylate (3) (100 mg.,0.47 mmol) Bi(OTf)$_3$ (60mg mg,0.092 mmol) and 7-(4-tri-fluromethyl) benzoyl chloride (0.3mL, 2.02 mmol) in 1.0 mL of Nitrobenzene. Then, glass tube was placed into CEM microwave for 1hr to react at 120^0 C, temperature, 40 PSI pressure with high steering. The title compound (0.143g, 79 % of yield) was isolated as a solid after crystallization in hexane.

^{1}H NMR (500 MHz, CDCl$_3$): δ 8.02 (d,J=5Hz,1H),7.91(d,J=5Hz, 1H),7.80(dd, J=5hz, 1H), 7.59(s,1H) 7.48 (s,1H), 7.49(s,1H),7.34(d,J=5Hz,1H) 4.98(t,J=5Hz,1H),4.73(t, J=5Hz,1H),4.40(t,J=5Hz,1H), 3.87(s,3H)

3.2.1.12. Preparation of 7-(4-fluro) Benzoyl- 5-Chloro-2,3-dihydrobenzo [b]furan-3-carboxylate (39):

Method C was followed for the preparation of **39**. A 10-mL pressurized glass tube with High -pressure tolerance equipped with a magnet bar was charged with 5-chloro-2,3-dihdrobenzo[b]furan-3- carboxylate (3) (100 mg.,0.47 mmol) Bi(OTf)$_3$ (60mg mg,0.092 mmol) and 7-(4-fluromethyl) benzoyl chloride (0.3mL, 5.06 mmol) in 1.0 mL of Nitrobenzene. Then, glass tube was placed into CEM microwave for 1hr to react at 120^0 C, temperature, 40 PSI pressure with high steering. The title compound (75mg, 48 % of yield) was isolated as a solid after crystallization in hexane.

^{1}H NMR(500 MHz, CDCl$_3$):δ 7.78(d,J=10Hz,2H),7.62 (s,1H),7.45(t,J=10Hz,2H), 7.29(s,2H) 4.99(t,J=5Hz,1H), 4.76(t, J=5Hz, 1H), 4.44(t, J=5Hz,1H), 3.86 (s,3H)

3.2.1.13. Preparation of 7-(4-Chloro) Benzoyl- 5-Chloro-2,3-dihydrobenzo [b]furan-3- carboxylate (41):

Method C was followed for the preparation of **41**. A 10-mL pressurized glass tube with High -pressure tolerance equipped with a magnet bar was charged with 5-chloro-2,3-dihdrobenzo[b]furan-3- carboxylate (3) (100 mg.,0.47 mmol) Bi(OTf)$_3$ (60mg mg,0.092 mmol) and 7-(4-fluromethyl) benzoyl chloride (0.06mL, 0.47 mmol) in 0.5 mL of Nitrobenzene. Then, glass tube was placed into CEM microwave for 1hr to react at 120^0 C, temperature, 40 PSI pressure with high steering. The title compound (0.115g, 70 % of yield) was isolated as a solid after crystallization in hexane.

^{1}H NMR(500 MHz, CDCl$_3$):δ 7.77(d,J=9Hz,2H),7.55 (s,1H),7.74(t,J=9Hz,2H), 7.28(s,2H) 4.98(t,J=15Hz,1H), 4.77(t, J=15Hz, 1H), 4.41(t, J=15Hz,1H), 3.85 (s,3H)

3.2.1.14. Preparation of 7-(4-Nitro) Benzoyl- 5-Chloro-2,3-dihydrobenzo [b]furan-3-carboxylate (43):

Method C was followed for the preparation of **43**. A 10-mL pressurized glass tube with High -pressure tolerance equipped with a magnet bar was charged with 5-chloro-2,3-dihdrobenzo[b]furan-3- carboxylate (3) (100 mg.,0.47 mmol) Bi(OTf)$_3$ (60mg mg,0.092 mmol) and 7-(4-nitro) benzoyl chloride (0.174g, 0.94 mmol) in 2 mL of Nitrobenzene. Then, glass tube was placed into CEM microwave for 1hr to react at 120^0 C, temperature, 40 PSI pressure with high steering. The title compound (86.70mg, 56 % of yield) was isolated as a solid after crystallization in hexane.

^{1}H NMR (300 MHz, CDCl$_3$): δ 7.86 (s,1H),7.81(dd,J=15Hz,2H)7.40(s,1H), 6.81(d,2H), 4.93(t,J=6Hz),4.73(t, j=12Hz,1H),4.66(t,1H), 3.89(s,3H).

3.2.1.15. Preparation of 7-(4-Methyl thiol) Benzoyl- 5-Chloro-2,3-dihydrobenzo [b]furan-3- carboxylate (45):

Method C was followed for the preparation of **45**. A 10-mL pressurized glass tube with High -pressure tolerance equipped with a magnet bar was charged with 5-chloro-2,3-dihdrobenzo[b]furan-3- carboxylate (3) (100 mg.,0.47 mmol) Bi(OTf)$_3$ (60mg mg,0.092 mmol) and 7-(4-Methyl thiol) benzoyl chloride (0.16ml, 1.03 mmol) in 2 mL of Nitrobenzene. Then, glass tube was placed into CEM microwave for 1hr to react at 140^0 C, temperature, 40 PSI pressure with high steering. The title compound (92.02mg, 54 % of yield) was isolated as a solid after crystallization in hexane.

^{1}H NMR (500MHz, CDCl$_3$):δ 8.35 (s,2H),8.16(d,J=6Hz,2H),7.84(d,J=9Hz,2H), 7.51(dd, J=9Hz, 7.44(t,J=2Hz, 1H),4.98(t, J=9Hz,1H), 4.76(t, J=9Hz, 1H),4.16(t,J=9Hz,1H), 3.82 (s,3H).

3.2.1.16. Preparation of 5-Chloro -7-Benzoyl -2,3-dihydrobenzo [b] furan-3- carboxylic acid (5).

Methyl-7-Benzoyl- 5-chloro-2,3-dihydro benzo[b]furan-3-carboxylate (**15**) (1g, 3.15mmol) was dissolved in 30mL methanol:H$_2$0(1:1) solution followed by addition of sodium hydroxide (1.26g,31.5mmol). The reaction mixture was stirred for overnight at RT.

30 mL of deionized water was poured to the reaction mixture to quench the reaction and the solution was extracted with ethyl acetate. The Erlenmeyer flask containing the aqueous layer was placed in an ice bath and 5M HCl was added dropwise until P^H would be 1.0. The solution was extracted with ethyl acetate. The organic layers were combined, washed with brine and dried over anhydrous Na_2SO_4 and the solvent was removed by rotovaporation as well as pale yellow solid product obtained (0.94g, 99% yield).

^{1}H NMR (300 MHz, CDCl3): δ 7.84 (d,J= 5Hz,2H), 7.62(t,J=5Hz,2H), 7.51(t, J=5Hz, 2H), 7.47(S,1H,), 7.29(S, 1H), 4.95(t,J=10Hz,1H),4.78(t,J=10Hz,1H),4.46(t,J=10Hz,1H).

Analytical data was matched with the previous data[33].

3.2.1.17.a. 5-Fluoro- 7-Benzoyl -2,3-dihydrobenzo [b] furan-3- carboxylic acid **(26)**, 5-Methyl- 7-Benzoyl -2,3-dihydrobenzo [b] furan- carboxylic acid (**31**), 5-Methoxy 7-Benzoyl --2,3-dihydrobenzo [b] furan-3- carboxylic acid (**36**), 7-(4-trifluromethyl) Benzoyl -5-Chloro-2,3-dihydro benzo[b] furan-3- carboxylic acid (**38**), 7-(4-fluro) Benzoyl -5-Chloro-2,3- dihydrobenzo[b] furan-3- carboxylic acid (**41**),7-(4-chloro) Benzoyl -5-Chloro-2,3- dihydrobenzo[b] furan-3-carboxylic acid (**42**),7-(4-Nitro) Benzoyl- 5-Chloro-2,3-dihydrobenzo [b]furan -3-carboxylic acid (**44**) were prepared by following procedure in 3.2.1.16.

Analytical data:

5-Fluoro- 7-Benzoyl -2,3-dihydrobenzo [b] furan-3- carboxylic acid **(26)**

 ^{1}H NMR (300 MHz, CDCl3): δ 11.16 (s, 1H), 7.83(d,J=10Hz,2H), 7.61(t,J=10Hz,1H), 7.45(s,1H), 4.98(t,J=10Hz,1H),4.75(t,J=10Hz,1H),4.44(t,J=10Hz,1H).

5-Methyl- 7-Benzoyl -2,3-dihydrobenzo [b] furan-3- carboxylic acid (**31**)

^{1}H NMR (300 MHz, CDCl$_3$): δ 7.78(d,J=5Hz,2H), 7.62(t,J=5Hz,2H),7.51(t,J=15Hz ,3H), 4.86(t,J=10Hz,1H),4.65(t,J=5Hz,1H),4.39(t,J=5Hz,1H).

7-(4-fluro) Benzoyl -5-Chloro-2,3- dihydrobenzo[b] furan-3- carboxylic acid (**41**)

^{1}H NMR (500 MHz, CDCl$_3$): δ 7.78(d,J=10Hz,2H), 7.62(s,J=10Hz,1H),7.49(d,J=10Hz ,2H), 4.99(t,J=5Hz,1H),4.76(t,J=5Hz,1H),4.44(t,J=5Hz,1H).

7-(4-chloro) Benzoyl -5-Chloro-2,3- dihydrobenzo[b] furan-3-carboxylic acid (**42).**

^{1}H NMR (500 MHz, CDCl$_3$): δ 7.61(d,J=15Hz ,2H),7.56 (s,1H) ,7.45(t,J=10Hz,2H),7.29 (s,1H),4.96(t,J=10Hz,1H),4.73(t,J=10Hz,1H),4.40(t,J=10Hz,1H).

7-(4-trifluromethyl) Benzoyl- 5-Chloro-2,3-dihydrobenzo [b]furan-3- carboxylic acid (**38**)

^{1}H NMR (500 MHz, CDCl$_3$): δ 7.78 (d,J=10Hz,1H),7.62(s,1H) 7.48 (s,1H), 7.29(s,1H), 4.99(t,J=5Hz,1H),4.76(t, J=12Hz,1H),4.45(t,J=10Hz,1H).

4. Biological Evaluations.

4.1. COX Inhibition Screening Assay at Vanderbilt University, Nashville, Tennessee.

Concentration-dependent inhibition reactions were completed by pre-incubating the inhibitor and enzyme for 17 min at 25^0C, followed by 3 min at 37^0C prior to the addition of 50 µM [1-14C]-AA (~55 mCi/mmol, Perkin Elmer, Waltham, MA) for 30 sec. at 37^0C. Reactions were terminated, and the resulting mixtures were analyzed for substrate consumption by thin-layer chromatography as previously described[194]. Inhibitor concentrations required for 50% inhibition of enzyme activity (IC_{50}) were determined graphically using Prism (GraphPad Software, La Jolla, CA) and were the average of at least two independent determinations.

4.2. Time-Dependent COX Inhibition Assays at Vanderbilt University, Nashville, Tennessee.

 Time-dependent inhibition assays were conducted by pre-incubating increasing concentrations of the inhibitor with m/hCOX-2, oCOX-1, or the active site mCOX-2 mutants for various time points (0, 0.125, 0.25, 0.5, 1, 3, 5, 15, 30 and 60 min) at 37^0C prior to the addition of 50 µM [1-14C]-AA for 30 sec. at 37^0C. Reactions were terminated and analyzed by thin layer chromatography as described above. The values were the average of at least three independent determinations.

4.3. COX Inhibition Screening Assay by Cayman Chemical, MI.

All reactions were performed in 100 mM Tris (pH 8.0), 5 mM EDTA, 2 mM phenol, and 1 µM heme. Compounds were diluted in DMSO and incubated with enzyme for 10 minutes

at 37^{0}C, followed by the initiation of the reaction with 100 µM arachadonic acid. Reactions proceed at 37^{0}C for 2 minutes, then quenched with 120 mM HCl containing 29 mM stannous chloride. SnCl2reduced PGH2 was measured using Cayman Chemical's Prostaglandin Screening ELISA Kit (Item No 514012). The amount of prostaglandin product produced from each reaction was calculated using non-linear regression (four-parameter fit) using Graph Pad Prism V.6.07. Percent inhibition for each compound was calculated using the vehicle and inhibited control compound wells. From the studies it is found that BRL-37959 and it's the analogs do not bind with COX-2 enzymes.

4.4. Anti-proliferative assay

The cytotoxicity of the BRL-37959 against the COLO-205 (colon cancer, ATCC), MDA-MB-231 (breast cancer, ATCC), SKOU-3(ovarian cancer, ATCC), and DU-145 (prostate cancer, ATCC), cell lines was tested using the MTT assay as previously described.[221, 222] Concisely, the tumor cells (1x104cells/well) were seeded in 96-well microtiter plates and incubated for 24 h at 37°C. Following incubation, the media was replaced with fresh media containing the above compound at concentrations ranging from 1 µM to 1 pM diluted in DMSO and incubated for an additional 48 h. Drug was run in duplicate or triplicate and control cells received fresh media with DMSO concentration equivalent to the treatment groups. Then, the wells were washed twice with warm PBS and incubated for another 4 h with RPMI 1640 media containing 250 µg/mL of MTT. Later, aspirating the culture medium, 200 µL of DMSO was added to dissolve the precipitate and the resulting solution

was measured for absorbance at 570 nm with a reference wavelength of 690 nm using a microplate reader 56 (Infinite M200 Pro TECAN). Results were used to find out the growth inhibition- 50% (GI50) of the compound.

References

1. Dawood, K.M. *Expert Opin Ther Pat*. **2013**, *23*,1133–1156.

2. Habtemariam, S. *Phytother Res.* **2001**,*15*,687–690.

3. Pauletti, P.M.; Araújo, A.R.; Young, M.C.; Giesbrecht, A.M; Bolzani, V.D. *Phyto chemistry*. **2000**,*55*,597–601.

4. Masubuchi, M.; Kawasaki, K.; Ebiike, H.; Ikeda, Y.; Tsukiji, S.; Sogabe, S. *Bioorg Med Chem. Lett.* **2001**,*11*,1833–1837.

5. Wrobel, J.E.; Dietrich, A.J.; Antane, M.M. *US Patent* **2001**,*1–57*, 6,251,936.

6. Kayser, O.; Chen, M.; Kharazmi, A.; Kiderlen, A.F. Z Naturforsch C. **2002**,57,717–20.

7. Hayakawa, I.; Shioya, R.; Agatsuma, T.; Furukawa, H.; Naruto, S.; Sugano, Y. *Bioorg Med Chem. Lett*.**2004**,*14*,455–458.

8. Vane, J.R.; Botting, R.M. *Am J Med*. **1998**, *104* (Suppl 3A), 2S-8S.

9. Antman, E.M.; DE Mets, D.; Loscalzo, J. *Cyclooxygenase inhibition and cardiovascular risk. Circulation*. **2005**,*112*, 759-770.

10. Grosser, T.; Fries S.; FitzGerald, G.A. *J Clin Invest*. **2006**, 116, 4-15.

11. Topper, J.N.; Cai, J.; Falb, D.; Gimbrone, M.A. Jr. *Proc Natl Acad Sci USA*. **1996**,*93*,10417-10422.

12. (a) FitzGerald, G.A.; Smith, B.; Pedersen, A.K.; Brash, A.R.*N Engl J Med*. **1984**, *310*,1065-1068.
    (b) FitzGerald GA. *N Engl J Med*. **2004**,*351*,1709-11.

13. Antman, E.M.; Bennett, J.S.; Daugherty, A.; Furberg, C.; Roberts H.; Taubert. K.A. *American Heart Association. Circulation* **2007**,115, 12,1634-1642.

14. Batlouni, *Arq Bras Cardiol* **2010**, 94(4),522-529.

15. Fitzgerald, G.A, Austin, YCS. Clin Exp Rheumatol. **2001**,*19* (Suppl 25): S31-6.

16. Abraham, N.S.; El-Sereg, H.B.; Hartman, C. Richardson P.; Deswal, A. *Aliment Pharmacol Ther.* **2007**,*25*, 913-924.

17. Bhatt, D.L.; Scheiman, J.; Abraham, N.S.; Antman E.M.; Chan, F.K.; Furberg, C.D. *A report of the American College of Cardiology Foundation Task Force on Clinical Expert Consensus Documents. Circulation.* **2008**, *118*,909-1894.

18. Mkherjee, D. *Thromb Haemost.* **2006***, 96*,407-412.

19. Whelton, A. *Am J Med.* **1999**, *106* (5B),13S-24S.

20. Oates, J.A.; FitzGerald, G.A; Branch, R.A.; Jackson, E.K; Knapp, H.R.; Roberts, L.J. *N. Engl J Med.* **1998**, *319* (12), 761-767.

21. *MSP, BCC Research - The Global Market for Pain Management Drugs and Devices, September 2015.*

22. Evaluate Pharma LLC.

23. *Transparency Market Research LLC*.

24. *Persistence Market research*

25. Rudd, R. A.; Seth, P.; David, F.; Scholl, L.; Increases in Drug and Opioid-Involved Overdose Deaths — United States, 2010–2015. MMWR Morb Mortal Wkly Rep. **2016**;*65*. doi:10.15585/mmwr.mm655051e1.

26. Florence, C.S.; Zhou, C.; Luo, F.; Xu, L. The Economic Burden of Prescription Opioid Overdose, Abuse, and Dependence in the United States, 2013. *Med Care.* **2016**,*54(10*),901-906. doi:10.1097/MLR.0000000000000625.

27. Center for Behavioral Health Statistics and Quality (CBHSQ). *2015 National Survey on Drug Use and Health: Detailed Tables*. Rockville, MD: Substance Abuse and Mental Health Services Administration; 2016.

28. Vowles, K.E.; McEntee, M.L.; Julnes, P.S.; Frohe, T.; Ney, J.P, *Pain.* **2015**,*156(4)*,569-576.

29. Muhuri, P.K; Gfroerer, J.C. Davies, M.C. Associations of Nonmedical Pain Reliever Use and Initiation of Heroin Use in the United States. CBHSQ Data Rev. August **2013**.

30. Cicero, T.J.; Ellis, M.S.; Surratt, H.L.; Kurtz, S.P. *JAMA Psychiatry.* **2014**,*71(7)*,821-826.

31. Carlson, R.G.; Nahhas, R.W; Martins, S.S.; Daniulaityte, R. *Drug Alcohol Depend*. **2016**,*160*,127-134.

32. Elizabeth, A**.** Boyle; Frank, R. Mangan; Roger, E. Markwell; Stephen, A. Smith; Michael, J. Thomson; Robert, W. Ward; Paul, A**.** Wyma; *Journal of Medicinal Chemistry*, **1986**, 29*, 6.*

33. Dudley, M.E.; Morshed, M.M.; Hossain, M.M. *Synthesis.* **2006**, *10*, 1711-1714.

34. Nathan, C., *Nature*, **2002**, *420*,846–885.

35. Smith, W.L.; DeWitt, D.L.; Garavito, R.M., *Annu Rev Biochem*. **2000**, *69*,145–182.

36. Dubois, R.N.; Abramson, S.B.; Crofford, L.; Gupta, R.A.; Simon, L.S.; Van, De Putte, L.B. Lipsky, P.E. FASEB J. 1998; *12*:1063–1073.

37. Smyth, E.M.; Grosser, T; Wang, M. Yu. Y.; FitzGerald, G.A.; *J. Lipid Res.* **2009**,*50*, S423–428.

38. Tilley, S.L.; Coffman, T.M; Koller, B. H ;J Clin Invest. **2001**,*108*,15–23.

39. Narumiya, S.; FitzGerald, G.A. *J Clin Invest*. **2001**,*108*,25–30.

40. Breyer, R.M, Bagdassarian, C.K, Myers, S.A, Breyer, M.D. *Annu Rev Pharmacol Toxicol*. **2001**,*41*,661–690.

41. Hirai H.; Tanaka K.; Yoshie, O. Ogawa, K, Kenmotsu, K.; Takamori, Y.; Ichimasa, M.; Sugamura, K.; Nakamura, M.; Takano, S.; Nagata, K;J Exp Med. 2001; 193:255–261. [PubMed: 11208866]

42. Pierce, K.L.; Fujino, H.; Srinivasan, D.; Regan, J.W. *J. Biol. Chem*. **1999**,*274*,35944–35949.

43. Hatae, N.; Sugimoto, Y.; Ichikawa, A.*J Biochem.* **2002**,*131*,781–784.

44. Wilson, S.J; McGinley, K.; Huang, A.J.; Biochem Biophys Res Commun. 2007; 352:397–403.

45. Wilson, S.J.; Roche, A.M.; Kostetskaia, E.; Smyth, E.M. *J Biol Chem*. **2004**, *279*,53036–53047.

46. McGraw, D.W.; Mihlbachler, K.A; Schwarb, M.R.; Rahman, F.F; Small, K.M.; Almoosa, K.F.; Liggett, S.B. *J Clin Invest*. **2006**,*116*,1400–1409.

47. Yuan, C.; Sidhu, R.S.; Kuklev, D.V.; Kado, Y.; Wada, M.; Song, I.; Smith, W.L. *J Biol Chem*. **2009**,*284*,10046–10055.

48. Funk, C.D. *Science.* **2001**,*294*,1871–1875.

49. Noda, M. Kariura; Y. Pannasch. U; Nishikawa, K.; Wang, L.; Seike, T.; Ifuku, M. Kosai, Y.; Wang, B.; Nolte, C.; Aoki, S.; Kettenmann, H.; Wada, K. *J. Neurochem.* **2007**,*101*,397–410

50. Kawabe J, Ushikubi F, Hasebe N. Circ J. **2010,**74,836–843.

51. Liou, J.Y, Shyue, S.K, Tsai, M.J, Chung, C.L, Wu, K.K. *J Biol Chem*. **2000**,*275*,15314–15320.

52. Miyata, A.; Hara, S.; Yokoyama, C.; Inoue, H.; Ullrich, V.; Tanabe, T. *Biochem Biophys Res Commun.* **1994**, *200*,1728–1734.

53. Caughey, G.E, Cleland L.G, Gamble J.R, James, M.J. *J Biol Chem*. **2001**; *276*,37839–37845.

54. Libby, P. Warner, S.J, Friedman, G.B. *J Clin Invest.***1988**; *81*,487–498.

55. Smyth, E.M.; FitzGerald, G.A. Vitam Horm. **2002**, *65*,149–165.

56. Bombardieri, S.; Cattani, P.; Ciabattoni, G.; Di, Munno, O.; Pasero, G.; Patrono, C.; Pinca, E.; Pugliese, F. *Br J Pharmacol*. **1981**,*73*,893–901

57. Higgs, G.A, Moncada, S.; Salmon, J.A.; Seager, K. *Br J Pharmacol*. **1983**, *79*,863–868.

58. Berkenkopf, J.W; Weichman, B. M. *Prostaglandins*.**1988**, *36*,693–709.

59. Jowsey, I.R; Thomson, A.M.; Flanagan, J.U.; Murdock, P.R.; Moore, G.B.; Meyers, D.J. *Biochem J*. **2001**,*359*,507–516.

60. Urade, Y.; Hayaishi, O. *Biochim. Biophys Acta*, **1999**,*1436*, 606–615.

61. Eguchi, N.; Minami, T.; Shirafuji, N.; Kanaoka, Y.; Tanaka, T.; Nagata, A. Yoshida, N.; Urade, Y.; Hayaishi, O. *Proc Natl Acad Sci USA*,**1999**,*96*, 726–730.

62. Lewis, R.A.; Soter, N.A.; Diamond, P.T.; Austen, K.F.; Oates, J.A.; Roberts II, L.J. *J Immunol.***1982**,*129*,1627–1631.

63. Urade, Y.; Ujihara, M.; Horiguchi, Y.; Ikai, K.; Hayaishi, O. *J Immunol.***1989**, *143*,2982–2989.

64. Tanaka, K.; Ogawa, K.; Sugamura, K; Nakamura, M; Takano, S.; Nagata, K.; *J Immunol.* **2000**,*164*,2277–2280.

65. Herlong, J.L.; Scott, T.R.; *Immunol Lett.* **2006**, *102*,121–131.

66. (a) Fitzpatrick, F.A.; Wynalda, M.A.*J Biol Chem.***1983**,*258*,11713–11718.

    (b) Shibata, T.; Kondo, M.; Osawa, T.; Shibata, N.; Kobayashi, M.*J Biol Chem.* **2002**,*277*,10459–10466.

67. Sugimoto, Y.; Yamasaki, A.; Segi, E.; Tsuboi, K, Aze, Y.; Nishimura, T.; Oida, H.; Yoshida, N.; Tanaka, T.; Katsuyama, M.; Hasumoto, K.; Murata, T.; Hirata, M.; Ushikubi, F.; Negishi, M.; Ichikawa, A.; Narumiya, S. *Science.***1997**, *277*,681– 683.

68. Saito, O.; Guan, Y.; Qi, Z.; Davis, L.S. *Am. J. Physiol-Renal.* **2003**, *284*,1164– 1170.

69. Breyer, M.D.; Breyer, R.M. *Annu Rev, Physiol.***2001**, *63*,579–605.

70. Nakahata, K.; Kinoshita, H.; Tokinaga, Y.; Ishida, Y.; Kimoto, Y.; Dojo M, Mizumoto, K.; Ogawa, K.; Hatano, Y. *Anesth Analg.***2006**,*102*.571–576.

71. Takayama, K.; Yuhki, K.; Ono, K.; Fujino, T.; Hara, A.; Yamada, T.; Kuriyama, S.; Karibe, H.; Okada, Y.; Takahata, O.; Taniguchi T, Iijima, T.; Iwasaki, H. Narumiya, S.; Ushikubi, F. *Nat Med.***2005**,*11*,562–566.

72. Jovanovic, N.; Pavlovic, M.; Mircevski, V.; Du, Q.; Jovanovic, A. *Lipid Mediat.* **2006**, *80*,110– 119.

73. Saleem S, Ahmad, A.S.; Maruyama, T.; Narumiya, S.; Doré, *Neurotox Res.***2009** ,*15(1),*62–70.

74. Kunori, S.; Matsumura, S.; Mabuchi, T.; Tatsumi, S. Sugimoto, Y.; Minami, T. *Neuroscience.***2009**, *163*,362–71

75. Basu, S.; Whiteman, M.; Mattey, D.L, Halliwell, B. Ann Rheum Dis.**2001**, *60*,627–631.

76. Helmersson, J.; Larsson, A.; Vessby, B. Basu, S. *Atherosclerosis*.**2005**,*181*,201–207.

77. Helmersson, J.; Vessby, B.; Larsson, A.; Basu, S. *Circulation.***2004**,*109*,1729–1734.

78. Funk, C.D.; FitzGerald, G.A.; *Pharmacol*.**2007**,*50*,470–479.

79. Félétou, M. Verbeuren, T.J, Vanhoutte, P.M. *Br J Pharmacol*.**2009**,*156*,563–574.

80. Félétou M, Vanhoutte P.M, Verbeuren, T.J.*J Cardiovasc Pharmacol*.**2010**, *55*,317–32.

81. Villain. J.; Nakahata, N. *Pharmacol Ther*. **2008**,*118*,18–35.

82. Gluais, P.; Lonchampt, M.; Morrow, J.D.; Vanhoutte, P.M.; Félétou, M. *Br J Pharmacol.***2005**,*146*,834–845.

83. Cheng, Y.; Austin, S.C.; Rocca, B.; Koller, B.H.; Coffman, T.M.; Grosser, T.; Lawson, J.A.; FitzGerald, G.A. *Science*, **2002**, *296*,539– 541.

84. Kobayashi, T.; Tahara, Y.; Matsumoto, M.; Iguchi, M.; Sano, H.; Murayama T, Arai H, Oida H, Yurugi, Kobayashi, T. Yamashita, J.K, Katagiri, H., Majima, M.; Yokode, M.; Kita, T.; Narumiya, S.*J Clin Invest*.**2004**, *114*:784–794

85. Francois, H. Athirakul, K. Mao, L.; Rockman, H.; Coffman, T.M. *Hypertension.* 2004, *43*,364–369.

86. Francois H.; Makhanova, N.; Ruiz, P.; Ellison, J.; Mao, L.; Rockman, H.A.; Coffman, T.M. *Am J Physiol Renal Physiol*.**2008**, *295*,1096– 1102.

87. Hamberg, M.; and Samuelsson, B. *Proc. Natl. Acad. Sci*. U.S.A. *70*, 899- 903.

88. Ohki, S., Ogino, N., Yamamoto, S., and Hayaishi, O. J. Biol. Chem.**1979**,*254*, 829-836.

89. Dietz, R.; Nastainczyk, W.; Ruf., H. H. Eur. J. Biochem.**1988**,*171*, 321-328.

90. Landino, L. M.; Crews, B. C.; Gierse, J. K.; Hauser, S. D.; Marnett, L. J. *J. Biol. Chem.***1997**, *272*, 21565-21574

91. Smith, W. L.; and Lands, W. E.; Biochemistry ,**1972**,*11*,3276-3285.

92. Mizuno, K.; Yamamoto, S.; Lands, W. E. *Prostaglandins* .**1982**, *23*, 743-757

93. Koshkin, V.; Dunford, H. B. *Biochim. Biophys. Acta.***1999**,*1431*, 47-52

94. Picot, D.; Loll, P. J.; Garavito, R. M. *Nature*,1994, *367*, 243-249.

95. Kurumbail, R. G., Stevens, A. M., Gierse, J. K., McDonald, J. J., Stegeman, R. A., Pak, J. Y., Gildehaus, D., Miyashiro, J. M., Penning, T. D., Seibert, K., Isakson, P. C., and Stallings, W. C. Nature,**1996**. *384*, 644-648

96. Rouzer, C. A. ; Marnett, L. J. J. Lipid. Res.**2009**,*50*, S29 - S34.

97. Vander Ouderaa, F. J.; Buytenhek, M.; Nugteren, D. H., Van Dorp, D. A. *Biochim. Biophys. Acta.* **1977**, *487*, 315-331.

98. Shimokawa, T.; Smith, W. L. *J. Biol. Chem*.**1991**, *266*, 6168-6173.

99. Liu, J.; Seibold, S. A.; Rieke, C. J.; Song, I.; Cukier, R. I.; Smith, W. L. *J. Biol. Chem*. **2007,** *282*, 18233-18244.

100.   Gupta, K.; Selinsky, B. S.; Loll, P. J. *Acta. Crystallogr. D. Biol. Crystallogr*. **2006**,*62*, 151-156.

101.   Chubb, A. J.; Fitzgerald, D. J.; Nolan, K. B., and Moman, E. Biochemistry, **2006**, *45*, 811-820.

102.   Luong, C.; Miller, A.; Barnett, J.; Chow, J.; Ramesha, C.; Browner, M. F. *Nat. Struct. Biol,***1996**. *3*, 927-933.

103. Malkowski, M. G.; Ginell, S. L.; Smith, W. L., and Garavito, R. M. Science,**2000** *, 289*, 1933-1937.

104. Rowlinson, S. W.; Crews, B. C.; Lanzo, C. A.; Marnett, L. J.*J. Biol. Chem*.**1999**, *274*, 23305-23310.
   a) Blobaum, Anna, L.; Marnett, Lawrence, J. *J Med Chem*. **2007**, *5*,50(7),1425-41.

105. Meade, E. A.; Smith, W. L.; DeWitt, D. L. J. Biol. Chem. **1993**, *268*, 6610-6614.

106. Vane, J. R.; Botting, R. M. *Scand. J. Rheumatol*., Suppl. **1996**,*102*,9-21.

107. Lecomte, M.; Laneuville, O.; Ji, C.; DeWitt, D. L.; Smith, W. L. *J. Biol. Chem*. **1994**, *269*, 13207-13215.

108. Xiao, G.; Tsai, A. L.; Palmer, G.; Boyar, W. C.; Marshall, P. J.; Kulmacz, R. J. *Biochemistry*, **1997**, *36*, 1836-1845.

109. Holtzman, M. J.; Turk, J.; Shornick, L. P. *J. Biol. Chem.* **1992**, *267*, 21438-21445.

110. Rowlinson, S. W.; Crews, B. C.; Goodwin, D. C.; Schneider, C.; Gierse, J. K.; Marnett, L. J. *J. Biol. Chem*. **2000**, *275*, 6586-6591.

111. Loll, P. J.; Picot, D.; Garavito, R. M. *Nat. Struct. Biol.* **1995**, *2*, 637-643.

112. Hochgesang, G. P. Jr.; Rowlinson, S. W.; Marnett, L. J. *J. Am. Chem. Soc.* **2001**, *122*, 6514-6515.

113. Loll, P. J.; Sharkey, C. T.; O'Connor, S. J.; Dooley, C. M.; O'Brien, E.; Devocelle, M.; Nolan, K. B.; Selinsky, B. S.; Fitzgerald, D. *J. Mol. Pharmacol*. **2001**, *60*, 1407-1413.

114. Rowlinson, S. W.; Kiefer, J. R.; Prusakiewicz, J. J.; Pawlitz, J. L.; Kozak, K. R.; Kalgutkar, A. S.; Stallings, W. C.; Kurumbail, R. G.; Marnett, L. J. *J. Biol. Chem.* **2003**, *278*, 45763-45769.

115. Menard, R.; Storer, A. C. *Biol. Chem. Hoppe-Seyler*, **1992**, *373*, 393-400.

116. Chen, Y. N.; Marnett, L. J. *FASEB J*. **1989**, *3*, 2294-2297.

117. Aronoff, D. M.; Boutaud, O.; Marnett, L. J.; Oates, J. A. *J. Pharmacol. Exp. Ther*. **2003**, *304*, 589-595.

118. Selinsky, B. S.; Gupta, K.; Sharkey, C. T.; Loll, P. J. **Biochemistry,** 2001, *40*, 5172-5180.

119. Hashimoto, Y.; Naito, C.; Kume, S.; Kato, H.; Watanabe, T., Kawamura, M., Teramoto, T.; Oka, H. *Biochim. Biophys. Acta*. **1985**, *841*, 283-291.

120. Prusakiewicz, J. J.; Felts, A. S.; Mackenzie, B. S.; Marnett, L. J. *Biochemistry* **2004**, *43*, 15439-15445.

121. Mancini, J. A.; Vickers, P. J.; O'Neill, G. P.; Boily, C.; Falgueyret, J. P.; Riendeau, D. *Mol. Pharmacol*.**1997**,*51*,52-60.

122. Houtzager, V.; Ouellet, M.; Falgueyret, J. P.; Passmore, L. A.; Bayly, C.; Percival, M. D. *Biochemistry*.**1996**,*35*, 10974-10984.

123. Guo, Q.; Wang, L. H.; Ruan, K. H.; Kulmacz, R. J. *J. Biol. Chem.***1996**,*271*, 19134-19139.

124. Gierse, J. K.; McDonald, J. J.; Hauser, S. D.; Rangwala, S. H.; Koboldt, C. M.; Seibert, K. A. *J. Biol. Chem.* **1996**, *271*, 15810-15814.

125. Elizabeth R.; Rayburn, Scharri J. Ezell; Ruiwen, Zhang, *Mol Cell Pharmacol*, **2009,** *1*,1, 29-43.

126. Lubet, R.A.; Steele, V.E.; Juliana, M.M.; Grubbs, C.J. *J. Urol.***2010**,*183*,1598–1603.

127. Ray, W.A.; Varas-Lorenzo, C.; Chung, C.P.; Castellsague, J.; Murray, K. T.; Stein, C.M.; Daugherty, J.R.; Arbogast, P.G.; García-Rodríguez, L.A. *Circ. Cardiovasc. Qual. Outcomes2*, **2009**,*155*–163 5.

128. Kearney, P. M.; Baigent, C.; Godwin, J.; Halls, H., Emberson, J. R.; Patrono, C. *BMJ*, **2006**, *332*,1302–1308 6.

129. Capone, M.L.; Tacconelli, S.; Sciulli, M.G.; Anzellotti, P; Di Francesco, L.; Merciaro, G.; Di Gregorio, P.; and Patrignani, P. *J. Pharmacol. Exp. Ther* 2007, *322*,453–460.

130. Kelsey C. Duggan; Matthew J. Walters; Joe Musee; Joe M. Harp; James R. Kiefe; John A. Oates; Lawrence J. Marnett. *Journal of Biological Chemistry*, **2010**, *285*, 45, 34950–34959.

131. Kurumbail, R.G. Stevens; A.M. Gierse; J.K. McDonald; J.J. Stegeman; R. A. Pak; J.Y.; Gildehaus, D.; Miyashiro, J.M.; Penning, T. D.; Seibert, K., Isakson, P.C.; Stallings, W.C. Nature, 1996, *384*,644–648.

132. Vagin, A.; Teplyakov, A. *J. Appl. Crystallogr*. **1997**,*30*,1022–1025 22.

133. Murshudov, G.N.; Vagin, A.A.; Dodson, E.J. Acta. Crystallogr. D Biol. Crystallogr., **1997,** *53*,240–255, 23.

134. Emsley, P.; Cowtan, K., Acta Crystallogr. D. Biol.Crystallogr.60, **2004,** *24*,2126–2132.

135. Rome, L.H.; Lands, W.E. *Proc. Natl. Acad. Sci.***1975**,*72*,4863–4865 25.

136. Blobaum, A.L.; Marnett, L.J., J.Biol.Chem. **2007**, *282*, 26, 16379–16390.

137. Gierse, J. K.; Koboldt, C.M.; Walker, M.C.; Seibert, K.; Isakson, P.C. *Biochem. J.***1999,** *339*, 27, 607–614.

138. Picot, D.; Loll, P.J.; Garavito, R.M. *Nature*, **1994**, *367*,243–249.

139. Rowlinson, S.W.; Kiefer, J.R.; Prusakiewicz, J.J.; Pawlitz, J. L; Kozak, K.R.; Kalgutkar, A. S.; Stallings, W. C.; Kurumbail, R. G., and Marnett, L. J. *J.Biol.Chem.* **2003**, *278*,45763–45769

140. Gupta, K.; Selinsky, B. S; Loll, P. J. *Acta Crystallogr. D Biol. Crystallogr.* **2006**, *62*,151–156.

141. Colloc' h, N.; Gabison, L.; Monard, G.; Altarsha, M.; Chiadmi, M., Marassio, G. Sopkova-de, Oliveira Santos, J., El Hajji, M., Castro, B., Abraini, J.H., Prange, T. *Biophys.* J. **2008**, *95*,2415–2422 30.

142. Peretto, I.; Radaelli, S.; Parini, C.; Zandi, M.; Raveglia, L. F., Dondio, G. Fontanella; L., Misiano.; P., Bigogno, C.; Rizzi, A.; Riccardi, B.; Biscaioli, M.; Marchetti, S.; Puccini, P.; Catinella, S, S.; Rondelli, I.; Cenacchi, V, V.; Bolzoni, P.T.; Caruso, P.; Villetti, G.; Facchinetti, F.; Del Giudice, E.; Moretto, N.,Imbimbo, B.P. J.Med.Chem.**2005,** *48*,5705–5720

143. Steiner, R. A., Janssen, H.J., Roversi, P., Oakley, A.J., and Fetzner, S., *Proc. Natl. Acad. Sci*. **2010,** *107*,657–662.

144. Thuresson, E.D., Lakkides, K.M., Smith, W.L. J.Biol.Chem. **2000**, *275*,8501–8507.

145. Rieke, C. J., Mulichak, A. M., Garavito, R. M., and Smith, W. L. *J.Biol.Chem.* **1999**,*274*,17109–1711.

146. Selinsky, B.S.; Gupta, K., Sharkey, C.T.; Loll, P.J., *Biochemistry,* **2001**, *40*,5172–5180

147. Prusakiewicz, J.J.; Felts, A.S. Mackenzie,; Marnett, L.J. *Biochemistry*, **2004**,*43*,15439–1544.

148. Shu Xu; Daniel J. Hermanson, Surajit Banerjee; Kebreab Ghebreselasie; Gina M. Clayton; R. Michael; Garavito; Lawrence J. Marnett, *Journal of Biological Chemistry*,**2014**, *289*,10, 6799–6808.

149. Coote, Ho, J.; Franco-Perez, M. L. M.; Gomez, Balderas, R. *J. Phys.Chem. A.* **2010** ,*114*,11992–1200.

150. Windsor, M.A.; Hermanson, D.J.; Kingsley, P.J.; Xu, S. Crews; B.C. Ho,; W. Keenan, ; C.M. Banerjee,; S.Sharkey,K.A.; Marnett, L.J. *ACSMed.Chem. Lett*.**2012**, *3*,759–763.

151. Luong, C.; Miller, A.; Barnett, J.; Chow, J.; Ramesha, C.; Browner, M.F.; Nat. Struct. Biol. **1996**, *3*,927–933.

152. Loll, P. J.; Picot, D.; Garavito, R. M.*Nat.Struct.Biol*.**1995**, *2*,637–643.

153. Vecchio, A.J.; Orlando, B.J.; Nandagiri, R, ; Malkowski,M.G. *J. Biol. Chem.* **2012**, *287*, 24619–24630.

154. Forli, S.; Olson, A. J. *J. Med. Chem*. **2012**, *55*,623–638

155. Groot, D.J.A. de; Vries, E.G.E. de.; Groen, H.J.M.; Jomg, S. de, *Critical Reviews in Oncology/Hematology*, **2007,** *61*,52-69.

156. Wang, Hong-Mei, Zhang, Gui-Ying, *World J Gastroenterol*. **2005**, *11(3),* 340– 343.

157. Alexander, Greenhough, Helena, J.M. Smartt, Moore, Amy E., Heather, R. Roberts, Christos, Ann C. Williams,

158. Paraskeva, Kaidi, Abderrahmane*, Carcinogenesis*, **2009**, *30*, 3,377–386.

159. Fu, Suo-Lin; Wu, Yun-Lin; Zhang, Yong-Ping, Qiao, Min-Min, Chen, Ying; *World J Gastroenterol* **2004**,*10*,13,1971-1974.

160. Basu, Gargi D.; Pathangey, Latha B; Tinder, Teresa L; Gendler, Sandra J; Mukherjee, Pinku. *Breast Cancer Research*, *2005*, *7*, R422-R435

161. Dai, Zhi- Jun; Ma, Xiao-Bin; Kang, Hua-Feng, Gao. Jie, Wei-Li Min, Hai-Tao Guan, Diao, Yan; Lu Wang-Feng; Wang Xi- Jing*, Cancer Cell International* **2012**, *12*, 53.

162. Sahin, Halil, Ibrahim., Hassan, Manal M. Garrett, Christopher R, *Cancer Letters*, **2014**,*345*,249–257.

163. Korbut, Teicher B.A; Menon, T.T. K, *Chemother Pharmacol* **1994**, *33*,515–522.

164. Soriano, A.F; Helfrich, B.; Chan, D.C, *Cancer Res*. **1999**,*59*, 6178–84.

165. Kishi, K.; Petersen, S.; Petersen, C.; *Cancer Res*, **2000**,*60*,1326–31.

166. Pyo, H.; Choy, H.; Amorino, G.P. *Clin Cancer Res*.**2001**,*7*,2998–3005.

167. Hida, T.; Kozaki K.; Muramatsu, H. Clin, *Cancer Res*. **2000**,*6*,2006–2011.

168. Mann, M.; Sheng, H; Shao, J*.; Gastroenterology*, **2001**, *120*, 1713–1719.

169. Lin E.; Morris J.S.; Ayers, G.D. *Oncology,* **2002**, *16*, 31–7.

170. Reed, J.C. *J Clin Oncol* **1999**;*17*:2941–2953.

171. Campos, L.; Rouault, J.P; Sabido, O. *Blood* **1993**,*81*,3091–3096.

172. Bargou, R. C. ; Daniel, P. ; T, Mapara, M.Y, *Int. J. Cancer* **1995**,*60*,854–859.

173. Prokop, A.; Wieder, T.; Sturm, I. *Leukemia* **2000**,*14*,1606–1613.

174. SturmI, Kohne; Wolg, C.H. *J Clin Oncol*. **1999**; *17*,1364–1374.

175. Lima, R.T.; Martins, L.M.; Guimaraes, J.E, Sambade, C, Vasconcelos, M.H. *Cancer Gene Ther* 2004,*11*, 309–16.

176. Zangemeister, Wittke U. *Ann N Y Acad Sci,* **2003**,*1002*,90–94.

177. Nita, M. E; Nagawa, H.; Tominaga, O. *Br J Cancer* **1998**, *78*,986–992.

178. Liu, X.H.; Yao, S.; Kirschenbaum, A.; Levine, A.C. *Cancer Res* **1998**,*58*,4245–4249.

179. Zhang L, Yu. J.; Park, B.H; Kinzler, K. W; Vogelstein, *Science* **2000**, *290*, 989–992.

180. Zhou, X.M.; Wong, B.C.; Fan, X.M.; *Carcinogenesis* **2001**,*22*,1393–1397.

181. Ding, H.; Han, C.; Zhu, J.; Chen, C.S.; D'Amboise, S.M.; *Int J Cancer* **2005**,*113*,803–810.

182. Narayanan, B.A.; Condon, M.S.; Bosland, M.C. Narayanan, N.K.; Reddy, B.S. *Clin Cancer Res* **2003**,*9*,3503–3513.

183. Gajewski, T.F.; Thompson, C.B; *Cell* ,**1996,** *87*,589–592.

184. Cardone, M.H.; Roy, N.; Stennicke, H.R. *Science* .**1998**,*282*,1318–1321.

185. Hsu, A.L.; Ching, T.T.; Wang, D.S; Song, X.; Rangnekar, V.M.; Chen, C.S. *J Biol Chem* **2000**,*275*,11397–11403.

186. Basu, G.D.; Pathangey, L.B.; Tinder, T.L.; Lagioia, M.; Gendler, S.J; Mukherjee, P. *Mol Cancer Res* **2004**,*2*, 632–42.

187. Zhang, Z.; Lai, G.H; Sirica, A.E. *Hepatology*. **2004**, *39*,1028–1037.

188. Olayioye, M.A.; Neve, R.M; Lane, H.A; Hynes, N.E.; *EMBO J* **2000**,*19*,3159–3167.

189. Yarden, Y. *Eur J Cancer* **2001**,*37*(Suppl 4): S3–8.

190. Buchanan, F.G.; Wang, D. Bargiacchi F.; DuBois, R.N. *J Biol Chem* **2003**,*278*,35451–35457.

191. Pai, R. Soreghan. B, Szabo, I.L, Pavelka, M.; Baatar, D.; Tarnawski, A.S. *Nat Med* **2002**,*8*,289–93.

192. Dannenberg, A.J.; Lippman, S.M.; Mann, J.R.; Subbaramaiah, K.; DuBois, R.N. *J Clin Oncol* **2005**,*23*,254–66.

193. Shao, J.; Lee, S.B; Guo. H; Evers. B.M.; Sheng, H; *Cancer Res* **2003**;*63*,5218–5223.

194. Ozoren, N.; El Deir, W.S.; *Cancer Biol.***2003**,*13*,135–47.

195. De Jong, S; Timmer, T; Heijenbrok, F.J.; De Vries, E.G.E.; Cancer Metastasis Rev. **2001**,*20*,51–56.

196. Hengartner, M. O. *Nature* **2000**, *407*:770–776.

197. Zhang, Z. Lai, G.H, Sirica, A.E. *Hepatology* **2004**,*39*,1028–1037.

198. HanZ, Pantazis, P.; Wyche, J.H.; Kouttab, N.; Kidd, V.J.; Hendrickson, E.A. A. *J Biol Chem.* **2001**,*276*,38748–38754.

199. Groot, De, D.J.; Timmer, T.; Spierings, D.C.; Le, T.K.; Jong, De S, Vries, De. E.G. *Br J Cancer,* **2005**, *92*,1459–1466.

200. Cheng, A.S.; Chan, H.L, Leung, W.K.; Wong, N. Johnson P.J, Sung, J. J. *Int J Oncol* **2003**,*23*, 113–9.

201. Liu, X.; Yue. P.; Zhou. Z, Khuri, F.R, Sun, S.Y. *J Natl Cancer Inst*. **2004**, *96*,1769–1780.

202. Huang Y.; He, Q.; Hillman, M.J.; Rong, R, ; Sheikh, M.S. *Cancer Res* **2001**,*61*,6918–24.

203. Martin, S.; Phillips, D.C.; Szekely, Szucs, K; Elghazi, L. Desmots F, Houghton, J.A. *Cancer Res*. **2005**, *65*,11447–11458.

204. He, Q.; Luo, X.; Huang Y.; Sheikh, M.S. *Oncogene*, 2002,*21*:6032–40.

205. Huang Y, He Q, Hillman MJ, Rong R, Sheikh M.S; *Cancer Res*.**2001**,*61*,6918–6924.

206. Tang, X.; Sun, Y.J, Half E, Kuo, M.T, Sinicrope, F. *Cancer Res*.**2002**,*62*,4903–4908.

207. Ravi, R.; Bedi, A. *Cancer Res*.,**2002**, *62*,1583–1587.

208. Brettle, R.; Shibib, S. M. *Tetrahedron Lett*. **1980**, *21*, 2915.

209. Profitt, J. A.; Ong, H. H.; *J. Org. Chem*. **1979**, *44*, 3972.

210. Pelle, Lidstrom; Jason, Tierney; Bernard, Wathey; *Tetrahedron.***2001**. *57* A. 9225-9283.

211. Sarvari, M. H.; Sharghi, H. *J. Org. Chem.,* **2004**, *69*, 6953-6956.

212. Nicholas, E. Leadbeater; Hanna M. Torenius, *J. Org. Chem*.**2002**,*67*,3145-3148.

213. Earle, Martyn, Wasserscheid, Peter Schulz, Bourbigou, Héléne Olivier; Favre, Frederic, Vaultier, Michel, Organic Synthesis, Ionic Liquids in Synthesis, Second Edition. Pages:**2008**, *265*– 568.

214. Desmurs, J. R. ; Labrouillre, M. ; Roux, C. Le, Gaspard, H. Laporterie. A.; Dubac. J. *Tetrahedron Letters*. **1997**, *38*,51, 8871-8874.

215. Cagniant, P ; Cagniant, D. *Adv. Het Chem. **1975, 18,237.*

216. Katrizky, AR.; Taylor, R. *Advances in Heterocyclic* Chemistry,**1990**, *47*,181-239.

217. Duff, J.C.; Bills, E. J. Chem. Soc. **1932,** *1987*-1,988.

218. Rowlinson, S. W.; Crews, B. C.; Lanzo, C. A.; Marnett, L. J. *J.Biol.Chem.* **1999**, *274*, 23305-23310

219. Odenwaller, R.; Chen, Y.-N. P.; Marnett, L. J. *Methods.Enzymol.* **1990**, *187*, 479-485.

220. Kalgutkar, A. S.; Crews, B. C.; Rowlinson, S. W.; Marnett, A. B.; Kozak, K. R.; Remmel, R. P.; Marnett, L. J., *Proc.Natl.Acad.Sci.USA* **2000**, *97*, 925-930

221. De Ruijter, A. J.; Van Gennip, A. H.; Caron, H. N.; Kemp, S.; *Biochem. J.* **2003**, *370*, 737−749

222. Weichert, W.; Röske, A.; Gekeler, V.; Beckers, T.; Stephan, C.; Jung, K.; Fritzsche, F. R.; Niesporek, S.; Denkert, C.; Dietel, M.; Kristiansen, G Br. *J. Cancer* **2008**, *98*, 604

APPENDIX A:

NMR Data

5

(^{1}HNMR, 500MHz, CDCl$_3$)

4.44
4.46
4.46
4.47
4.76
4.78
4.80
4.98
5.00
5.00
5.01
7.29
7.47
7.47
7.49
7.51
7.52
7.62
7.63
7.83
7.84

1.00
1.00
0.99

0.70
0.90
2.11
2.13
2.10

ppm

0

5

10

15

(¹HNMR, 500 MHz, CDCl₃)

3.86
4.38
4.40
4.41
4.74
4.76
4.78
4.97
4.99
4.99
5.00

7.29
7.44
7.48
7.49
7.51
7.55
7.55
7.60
7.62
7.63
7.82
7.83

2.96
0.98
1.00
1.00

0.20
0.96
2.02
0.95
1.03
1.94

ppm

26

(^{1}HNMR, 300MHz, CDCl$_3$)

1.29
1.31
1.45

2.22
2.50
2.71

4.42
4.44
4.46
4.73
4.75
4.77
4.96
4.97
4.98
4.99
5.30
7.29
7.45
7.45
7.47
7.49
7.50
7.60
7.61
7.63
7.81
7.83
8.10
8.11
8.25
8.29
8.29
8.37

11.16

H₃CO — COOMe

35

(^{1}HNMR, 300MHz, CDCl$_3$)

0.88
0.90

1.28

1.57

3.51
3.56
3.70
3.77
3.81
3.83
3.85
4.00
4.34
4.37
4.39
4.66
4.69
4.72
4.88
4.91
4.91
4.94
5.32
6.83
7.00
7.01
7.08
7.11
7.19
7.20
7.28
7.45
7.48
7.50
7.57
7.60
7.63
7.84

Integrations (right, vs ppm axis):

1.05 — 1.0
1.75
1.38 — 1.5

2.0

2.5

0.69 — 3.0
0.24
0.38 — 3.5
0.83
2.77
2.09 — 4.0
0.22
0.24
0.98 — 4.5
1.08
1.00 — 5.0

0.30 — 5.5

6.0

6.5
0.12
0.85
0.39 — 7.0
0.82
2.31
2.51 — 7.5
0.36
1.57
2.35 — 8.0
0.25

ppm

(^{1}HNMR, 300MHz, CDCl$_3$)

30

1.27

2.06
2.34

3.82
4.12
4.15
4.26
4.32
4.35
4.38
4.66
4.69
4.72
4.89
4.91
4.92
4.95

7.26
7.28
7.38
7.44
7.46
7.49
7.55
7.58
7.81

0.91

0.51
3.37

0.50
3.00

0.19
1.14

1.15

1.07

1.43
1.36
2.42
1.48
2.06

ppm

H3C

COOH

31

(^{1}HNMR, 300MHz, MeOD)

2.18
2.35

3.34

4.37
4.38
4.39
4.40
4.64
4.65
4.67
4.84
4.86
4.86
4.88
4.97

7.21
7.48
7.49
7.51
7.61
7.62
7.77
7.78

0.47
3.10

1.17

1.00
1.03
1.16
2.07

1.00
3.03
1.18
2.07

ppm
2.5
3.0
3.5
4.0
4.5
5.0
5.5
6.0
6.5
7.0
7.5
8.0

(1HNMR, 300 MHz, CDCl₃)

1.28

2.07
2.20

3.86
4.13
4.16
4.39
4.40
4.76
4.98

7.28
7.44
7.44
7.51
7.65
7.81
7.84
8.14
8.16
8.33
8.35
8.61

2.12

0.81

3.00
0.62
1.13
1.18
1.01

1.09
7.69
3.57
2.03
3.78
4.42
0.12

ppm

(1HNMR, 300 MHz, CDCl$_3$)

1.28

2.07
2.20

3.86
4.13
4.16
4.39
4.40
4.76
4.98

7.28
7.44
7.44
7.51
7.65
7.81
7.84
8.14
8.16
8.33
8.35
8.61

2.12

0.81

3.00
0.62
1.13
1.18
1.01

1.09
7.69
3.57
2.03
3.78
4.42
0.12

ppm

0.90

1.29

2.53
2.55

3.89
4.52
4.56
4.66
4.66
4.69
4.74
4.78
4.91
4.93
5.02
5.15
5.19
5.61

6.79
6.81
7.20
7.28
7.40
7.40
7.75
7.78
7.81
7.83
7.86

Cl

COOMe

O

H₃CO

O

48

(1HNMR, 300 MHz,CDCl₃)

15.36
1.81
16.47

4.62

3.00
0.72

1.52
2.32
0.55

72.09

0.43

2.14

1.07

4.79
0.82

ppm

1.0
1.5
2.0
2.5
3.0
3.5
4.0
4.5
5.0
5.5
6.0
6.5
7.0
7.5
8.0
8.5

COOMe

Cl

O

F

39

$(^1\text{HNMR},500\text{MHz},\text{CDCl}_3)$

0.87
0.89
0.90
0.91
1.28

2.21

3.86

4.44
4.46
4.75
4.76
4.78
4.97
4.98
4.99
5.00

7.29
7.46
7.47
7.49
7.62
7.76
7.78

1.34
1.64
0.15
0.43
1.02
1.01
1.00
1.04
2.82
0.87
1.92

ppm
1.0
1.5
2.0
2.5
3.0
3.5
4.0
4.5
5.0
5.5
6.0
6.5
7.0
7.5
8.0

40

(^{1}HNMR,500MHz,CDCl$_3$)

1.29
1.31
1.45

2.22
2.50
2.71

4.42
4.44
4.46
4.73
4.75
4.77
4.96
4.97
4.98
4.99
5.30
7.29
7.45
7.45
7.47
7.49
7.50
7.60
7.61
7.63
7.81
7.83
8.10
8.11
8.25
8.29
8.29
8.37

11.16

41

(^{1}HNMR, 300MHz, CDCl$_3$)

1.61

3.85

4.36
4.39
4.41
4.70
4.74
4.77
4.95
4.97
4.98
5.00

7.28
7.44
7.44
7.47
7.55
7.74
7.77

0.82
2.99
0.97
1.02
1.00
0.34
2.80
0.92
1.94

ppm 2.0 2.5 3.0 3.5 4.0 4.5 5.0 5.5 6.0 6.5 7.0 7.5 8.0

175

COOH

42

(^{1}HNMR,500MHz,CDCl$_3$)

0.10

0.87
0.90
0.91
1.28
1.61

3.87
4.38
4.40
4.41
4.73
4.74
4.76
4.97
4.98
5.00

37

(¹HNMR,500MHz,CDCl₃)

7.29
7.33
7.34
7.48
7.59
7.75
7.77
7.79
7.80
7.90
7.91
8.01
8.02

0.61
1.84
0.54

0.66
0.23
0.21
0.20

0.64
0.46
0.53
1.94
0.74
1.00

ppm
1.0
1.5
2.0
2.5
3.0
3.5
4.0
4.5
5.0
5.5
6.0
6.5
7.0
7.5
8.0
8.5

38

(^{1}HNMR,500MHz,CDCl$_3$)

1.00
1.16
1.18
1.23
1.24
1.26
1.29
1.31
1.33
1.35

3.53
3.54

3.86

4.43
4.45
4.46
4.74
4.76
4.78
4.97
4.98
4.99
5.00

7.29
7.47
7.48
7.62
7.76

46.26

73.48
76.62
77.05
77.26
77.47

COOMe

Cl

O

15

(^{13}CNMR, 300 MHz, CDCl$_3$)

122.31
125.67
127.32
128.43
129.17
129.91
130.54
133.31
136.99

157.26

175.29

193.06

50
60
70
80
90
100
110
120
130
140
150
160
170
180
190

(¹³CNMR, 300 MHz, CDCl₃)

46.35
52.97
73.77
76.63
77.05
77.47
122.35
125.51
127.92
128.38
128.94
129.86
130.25
133.17
137.11
157.20
170.41
192.81

15

ppm
60 70 80 90 100 110 120 130 140 150 160 170 180 190

180

30.88

46.31
52.99

73.81
76.59
77.01
77.44

128.73
129.32
130.13
131.19

206.84

42

(^{13}CNMR, 300MHz, CDCl$_3$)

20.64

46.37

73.07
77.01
77.43

131.25
125.38
128.22
129.77
129.90
130.26
131.25
132.75
137.79

156.68

175.51

194.40

31

(^{1}HNMR, 300MHz, MeOD)

ppm

200
180
160
140
120
100
80
60
40

APPENDIX B:

HPLC Data

Sample Name: Cl-ester
Sample Type: Unknown
Vial: 1
Injection #: 1
Injection Volume: 10.00 ul
Run Time: 60.00 Minutes

Acquired By: Breeze
Date Acquired: 4/19/2017 3:03:55 PM CDT
Acq. Method: 95% A
Date Processed: 6/20/2017 11:29:06 AM CDT
Channel Name: 249.3nm
Sample Set Name: DJH041917
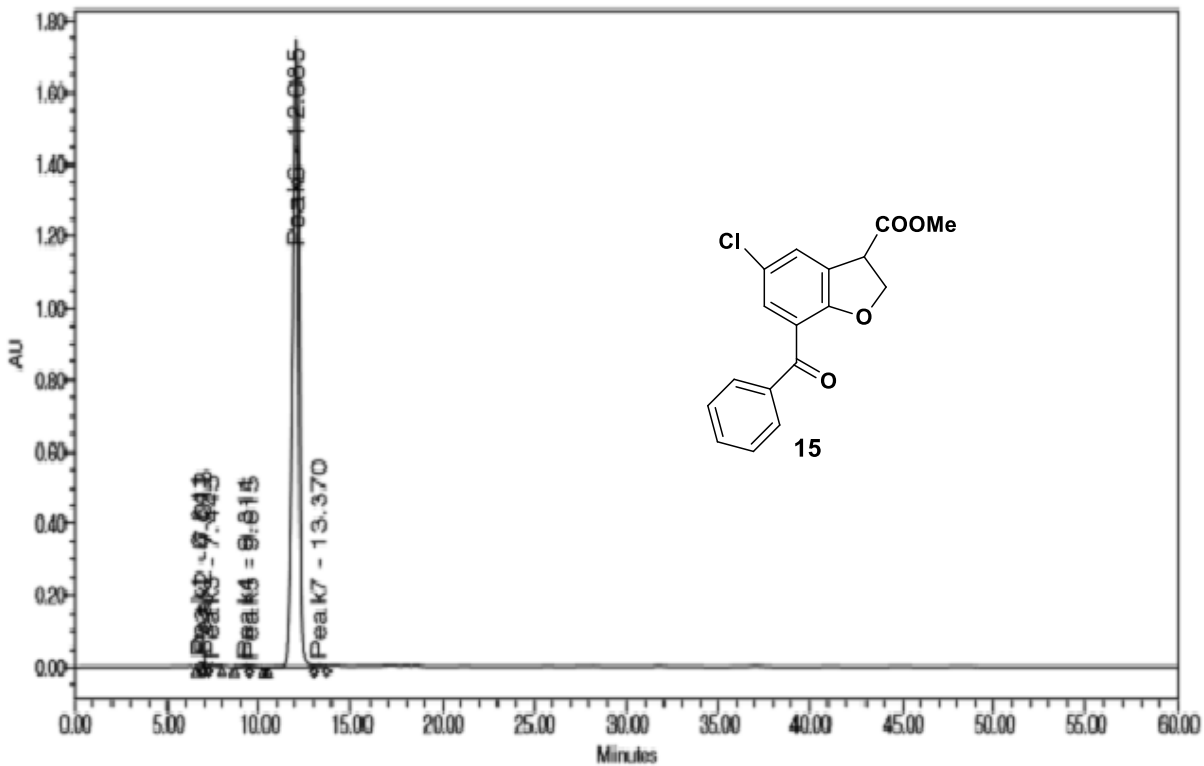
	Peak Name	RT (min)	Area (µV*sec)	% Area	Height (µV)	% Height
1	Peak1	6.841	107445	0.28	12623	0.70

Breeze 2
HPLC System

SAMPLE INFORMATION

Sample Name:	042017-Chloro acid
Sample Type:	Unknown
Vial:	1
Injection #:	1
Injection Volume:	10.00 ul
Run Time:	60.00 Minutes

Acquired By:	Breeze
Date Acquired:	4/20/2017 9:26:13 AM CDT
Acq. Method:	90% A
Date Processed:	6/20/2017 11:26:02 AM CDT
Channel Name:	250.6nm
Sample Set Name	042017 DJH Chloro acid 10%EtOH
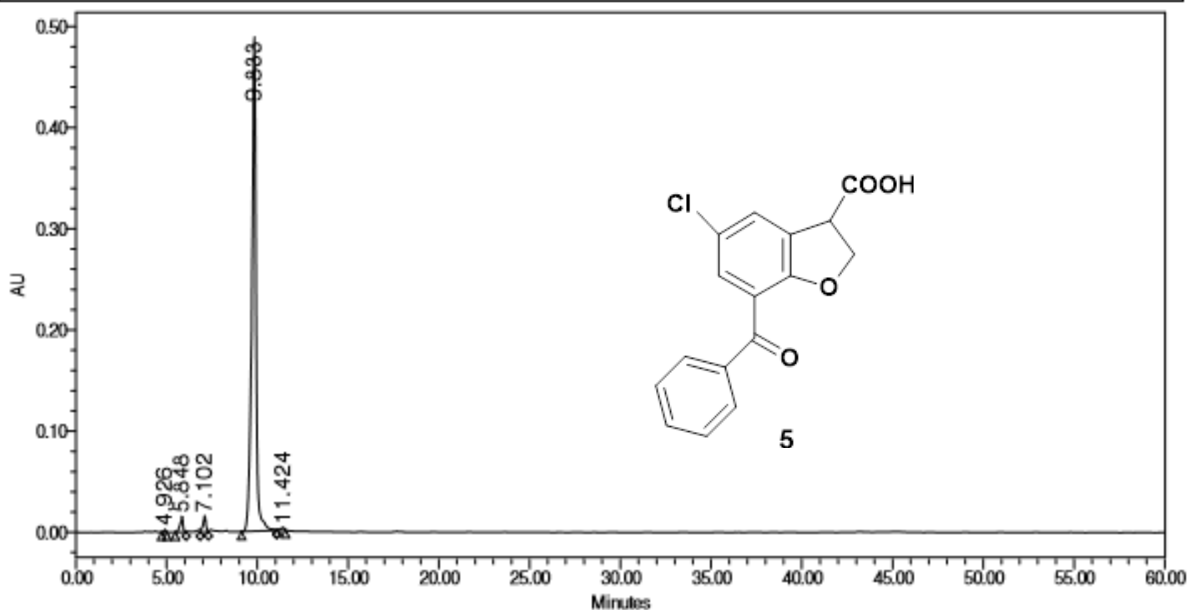
	RT (min)	Area (µV*sec)	% Area	Height (µV)	% Height
1	4.926	15333	0.19	2230	0.43
2	5.848	161714	1.96	15373	2.93
3	7.102	180987	2.19	15755	3.01
4	9.833	7867131	95.27	488361	93.23
5	11.424	32594	0.39	2133	0.41

185

SAMPLE INFORMATION

Sample Name:	Fluoro	Acquired By:	Breeze
Sample Type:	Unknown	Date Acquired:	7/19/2017 12:43:00 PM CDT
Vial:	1	Acq. Method:	90% A
Injection #:	1	Date Processed:	7/19/2017 1:42:40 PM CDT
Injection Volume:	10.00 ul	Channel Name:	324.2nm
Run Time:	60.00 Minutes	Sample Set Name	Fluoro acid
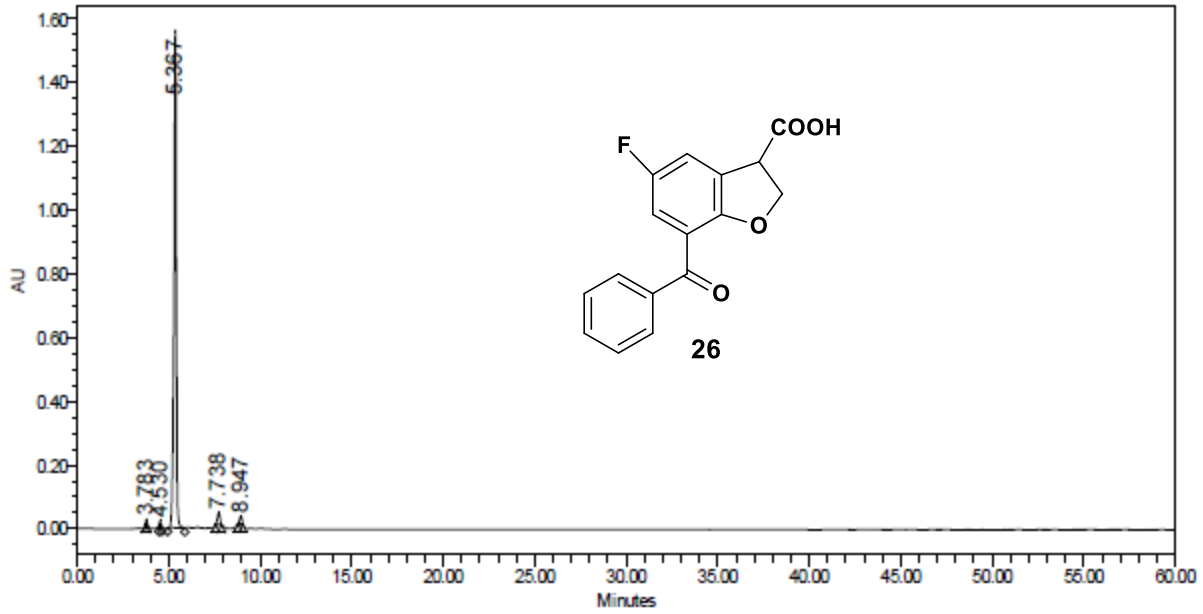
	RT (min)	Area (µV*sec)	% Area	Height (µV)	% Height
1	3.783	53776	0.38	16393	0.99
2	4.530	121139	0.86	21080	1.27
3	5.367	13411243	94.70	1560877	94.07
4	7.738	363971	2.57	37000	2.23
5	8.947	211025	1.49	24002	1.45

SAMPLE INFORMATION

Sample Name:	042017-methyl ester	Acquired By:	Breeze
Sample Type:	Unknown	Date Acquired:	4/20/2017 10:27:50 AM CDT
Vial:	1	Acq. Method:	90% A
Injection #:	1	Date Processed:	6/20/2017 11:21:22 AM CDT
Injection Volume:	10.00 ul	Channel Name:	250.6nm
Run Time:	60.00 Minutes	Sample Set Name	042017 methyl ester
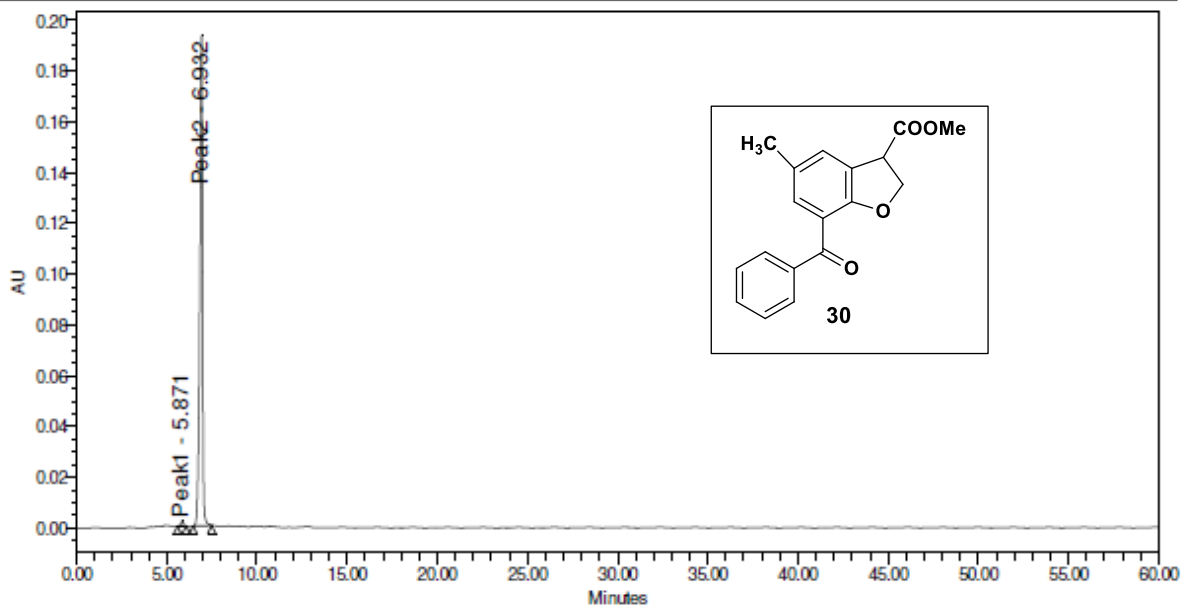
	Peak Name	RT (min)	Area (µV*sec)	% Area	Height (µV)	% Height
1	Peak1	5.871	20459	1.05	2302	1.18
2	Peak2	6.932	1936172	98.95	193186	98.82

187

S A M P L E   I N F O R M A T I O N

Sample Name:	DJH-070617-2.64-MeAcid	Acquired By:	Breeze
Sample Type:	Unknown	Date Acquired:	7/6/2017 4:02:32 PM CDT
Vial:	1	Acq. Method:	90% A
Injection #:	1	Date Processed:	7/7/2017 10:36:15 AM CDT
Injection Volume:	10.00 ul	Channel Name:	2998 Ch1 254nm@1.2nm
Run Time:	60.00 Minutes	Sample Set Name	DJH070617_2_64_MeAcid
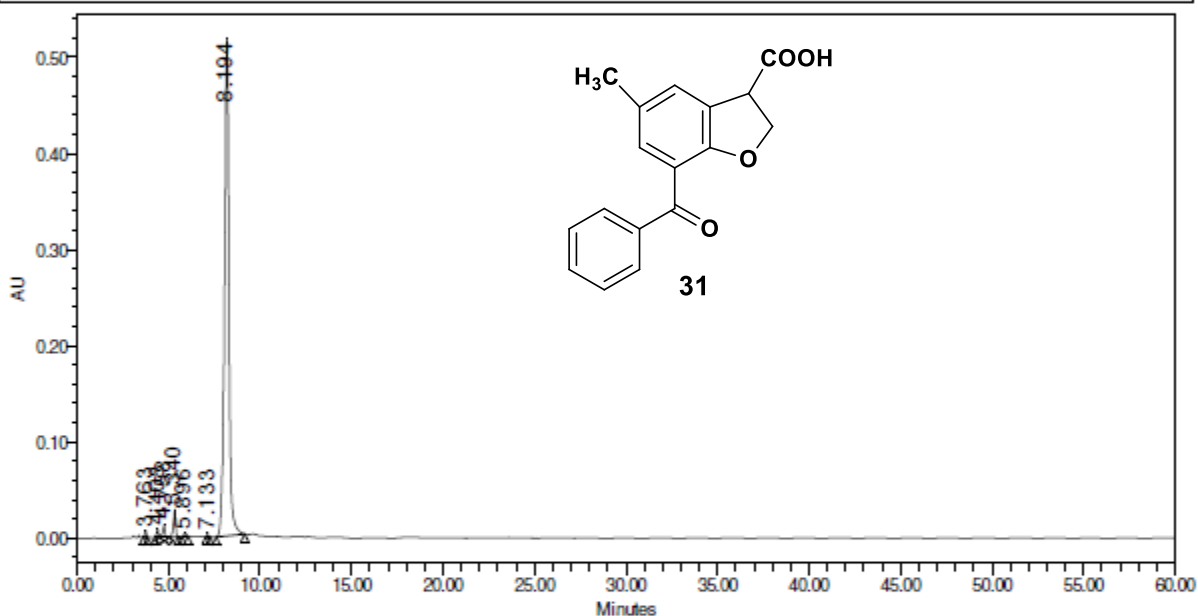
	RT (min)	Area (µV*sec)	% Area	Height (µV)	% Height
1	3.763	40080	0.44	6651	1.14
2	4.408	50541	0.55	8495	1.46
3	4.758	100770	1.10	12975	2.23
4	5.340	221607	2.41	28402	4.88
5	5.896	31988	0.35	3882	0.67
6	7.133	10626	0.12	4059	0.70
7	8.194	8726461	95.04	517022	88.91

SAMPLE INFORMATION

Sample Name:	Shamsul p-CF3	Acquired By:	Breeze
Sample Type:	Unknown	Date Acquired:	6/7/2017 3:41:53 PM CDT
Vial:	1	Acq. Method:	90% A
Injection #:	1	Date Processed:	6/7/2017 4:55:24 PM CDT
Injection Volume:	10.00 ul	Channel Name:	224.2nm
Run Time:	60.00 Minutes	Sample Set Name	p_CF3 10% EtOH
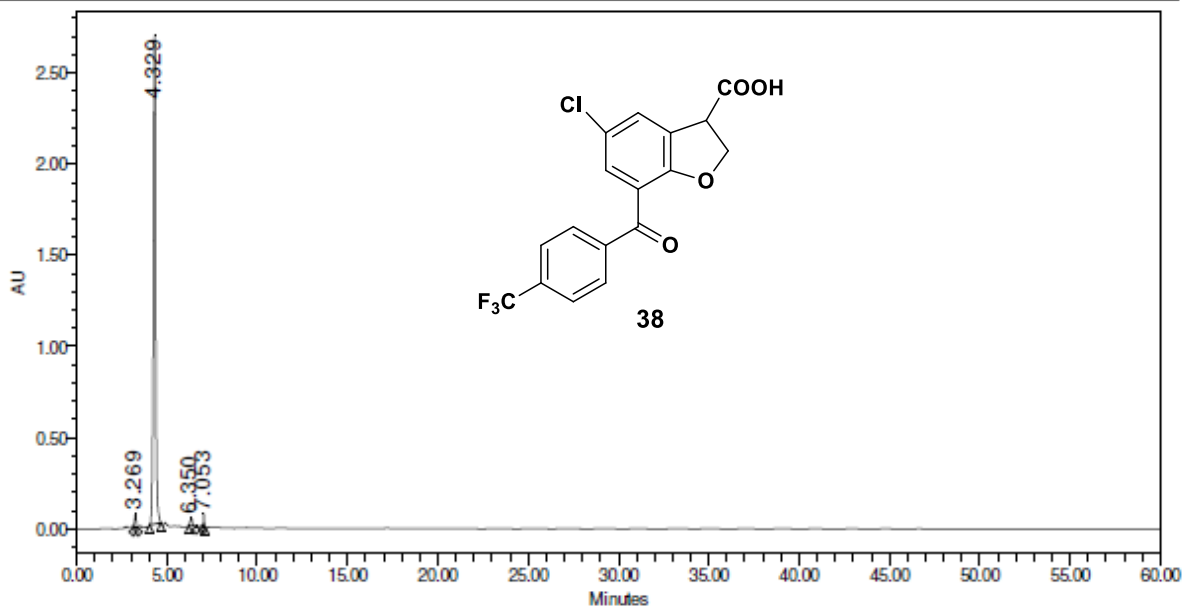
	RT (min)	Area (µV*sec)	% Area	Height (µV)	% Height
1	3.269	506049	1.91	79287	2.76
2	4.329	25507981	96.03	2680287	93.30
3	6.350	366159	1.38	42127	1.47
4	7.053	183146	0.69	70990	2.47

Breeze 2
HPLC System

SAMPLE INFORMATION

Sample Name:	DJH-070717p-cl acid	Acquired By:	Breeze
Sample Type:	Unknown	Date Acquired:	7/7/2017 1:13:26 PM CDT
Vial:	1	Acq. Method:	90% A
Injection #:	1	Date Processed:	7/19/2017 1:36:36 PM CDT
Injection Volume:	10.00 ul	Channel Name:	255.1nm
Run Time:	60.00 Minutes	Sample Set Name	DJH070717 p cl acid
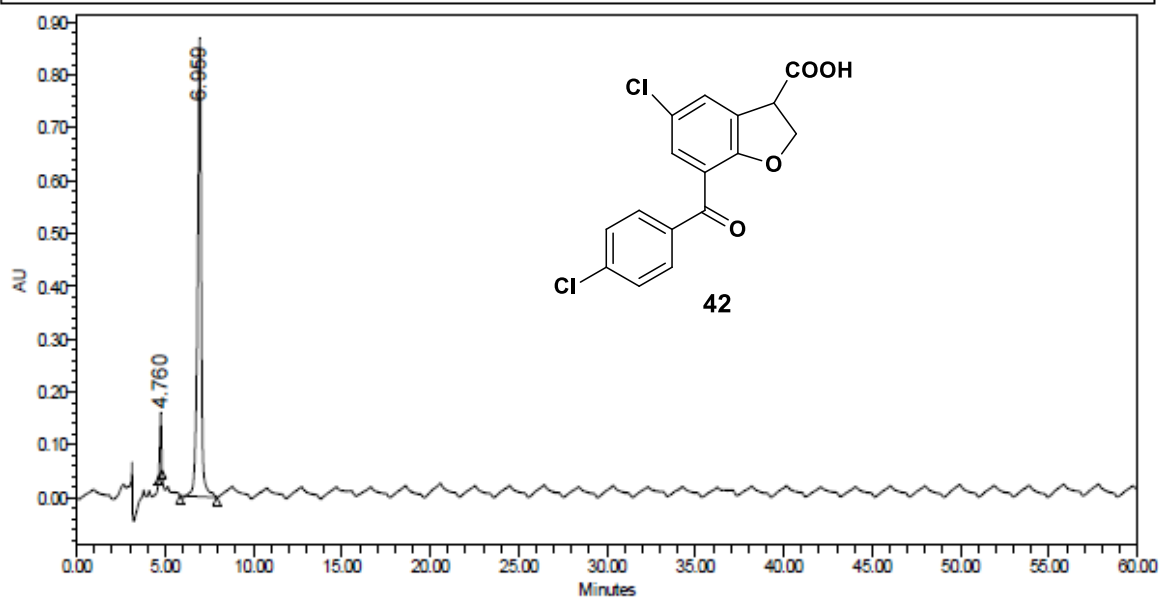
	RT (min)	Area (µV*sec)	% Area	Height (µV)	% Height
1	4.760	701250	5.17	115038	11.71
2	6.959	12866964	94.83	867423	88.29

SAMPLE INFORMATION

Sample Name:	DJH-070617-2.64	Acquired By:	Breeze
Sample Type:	Unknown	Date Acquired:	7/6/2017 3:01:07 PM CDT
Vial:	1	Acq. Method:	90% A
Injection #:	1	Date Processed:	7/7/2017 10:32:45 AM CDT
Injection Volume:	10.00 ul	Channel Name:	2998 Ch1 254nm@1.2nm
Run Time:	60.00 Minutes	Sample Set Name	DJH_070617_2_64
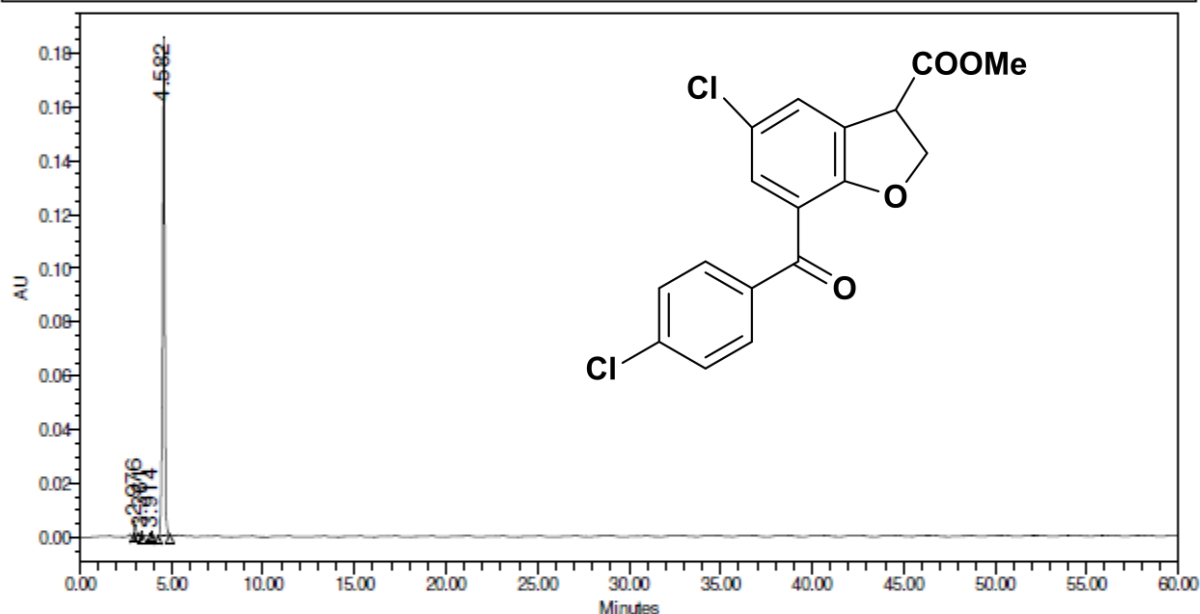
	RT (min)	Area (µV*sec)	% Area	Height (µV)	% Height
1	2.976	28718	1.95	5242	2.72
2	3.361	5803	0.39	1203	0.62
3	3.914	4231	0.29	1016	0.53
4	4.582	1434160	97.37	185220	96.13

SAMPLE INFORMATION

Sample Name:	p-Fluoro acid	Acquired By:	Breeze
Sample Type:	Unknown	Date Acquired:	7/12/2017 1:23:42 PM CDT
Vial:	1	Acq. Method:	80% A
Injection #:	1	Date Processed:	7/19/2017 10:39:45 AM CDT
Injection Volume:	10.00 ul	Channel Name:	250.9nm
Run Time:	60.00 Minutes	Sample Set Name	p Fluoro acid
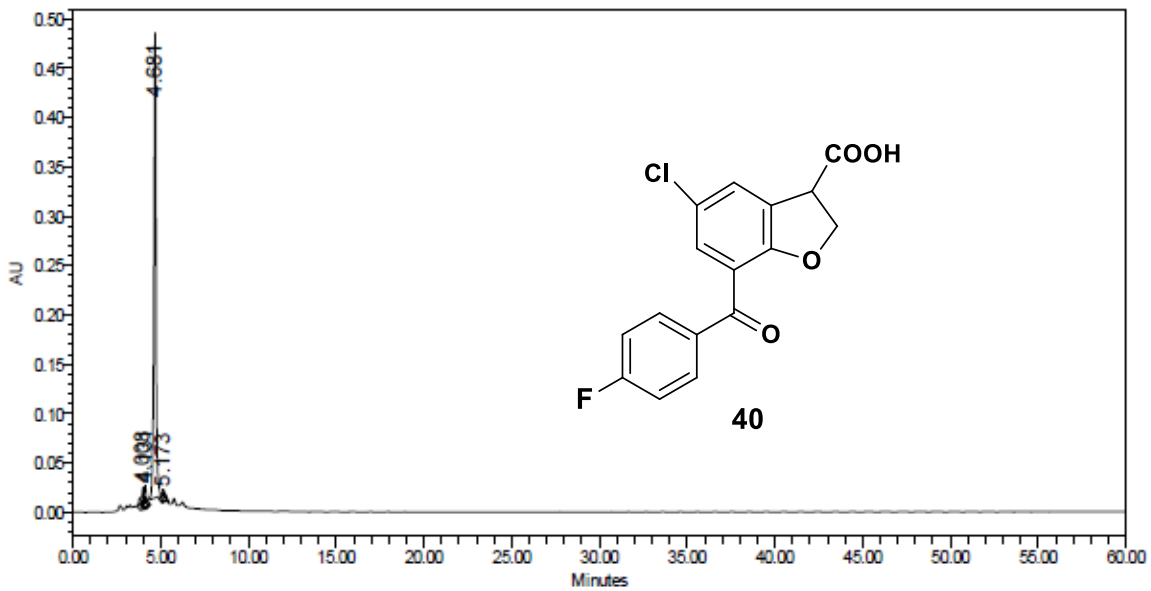
	RT (min)	Area (μV*sec)	% Area	Height (μV)	% Height
1	4.008	111167	2.70	14877	2.93
2	4.131	79717	1.94	15741	3.10
3	4.681	3896269	94.77	471175	92.94
4	5.173	24272	0.59	5162	1.02

APPENDIX C:

HRMS Data
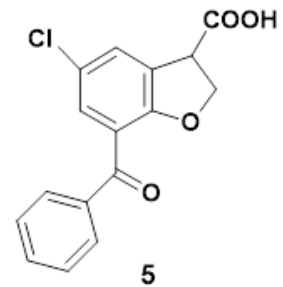
Data File: C:\LabSolutions\Data\Revathi\DJH\DJH Data from Batch file\DJH_Vial2.lcd

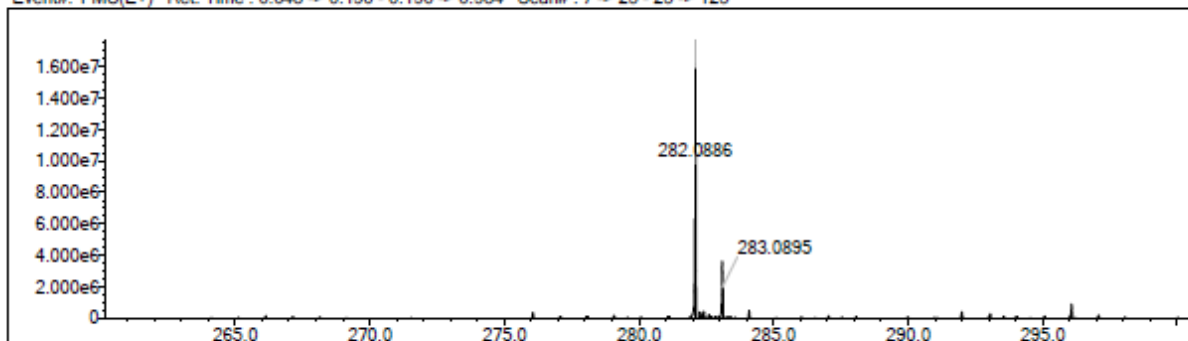| Elmt	Val.	Min	Max	Use Adduct
H	1	0	50	H
C	4	0	30	Na
N	3	0	0	K
O	2	0	5	NH4
Cl	1	0	5	CH3OH
				H2O
				HCOO
				CH3CN

Error Margin (mDa): 10.0
HC Ratio: 0.0 - 3.0
Max Isotopes: all
MSn Iso RI (%): 75.00

DBE Range: -100.0 - 100.0
Apply N Rule: no
Isotope RI (%): 1.00
MSn Logic Mode: OR

Electron Ions: both
Use MSn Info: no
Isotope Res: 10000
Max Results: 4

Event#: 1 MS(E+) Ret. Time : 0.048 -> 0.206 - 0.174 -> 0.982 Scan# : 7 -> 27 - 23 -> 125
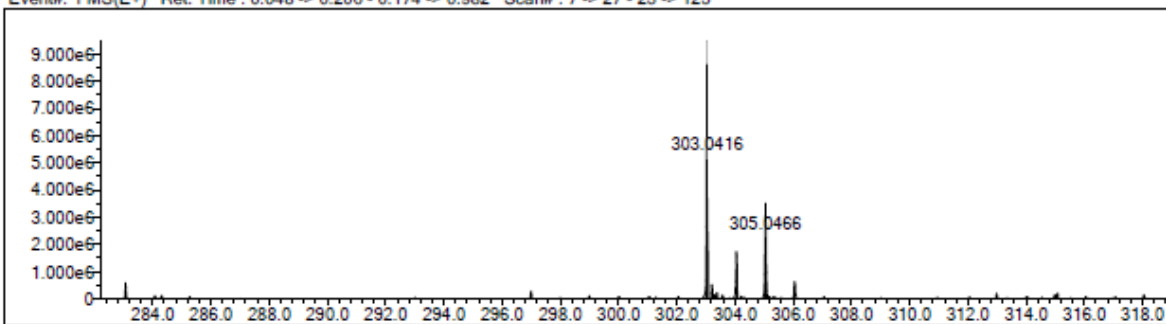
Measured region for 303.0416 m/z
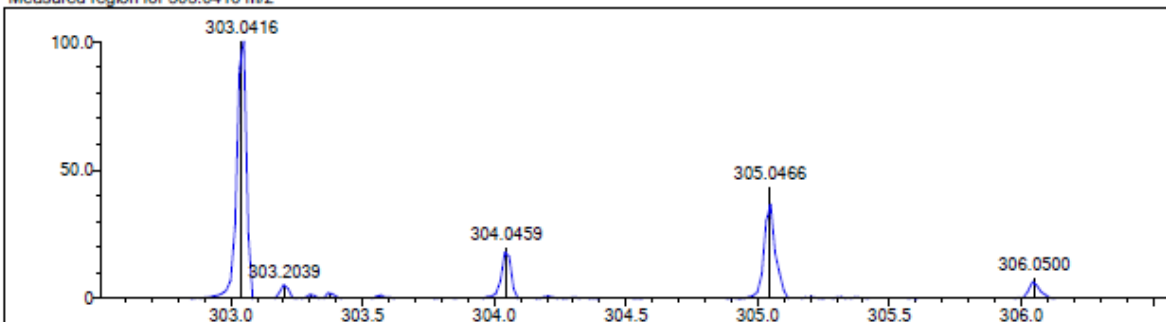
C16 H11 O4 Cl [M+H]+ : Predicted region for 303.0419 m/z
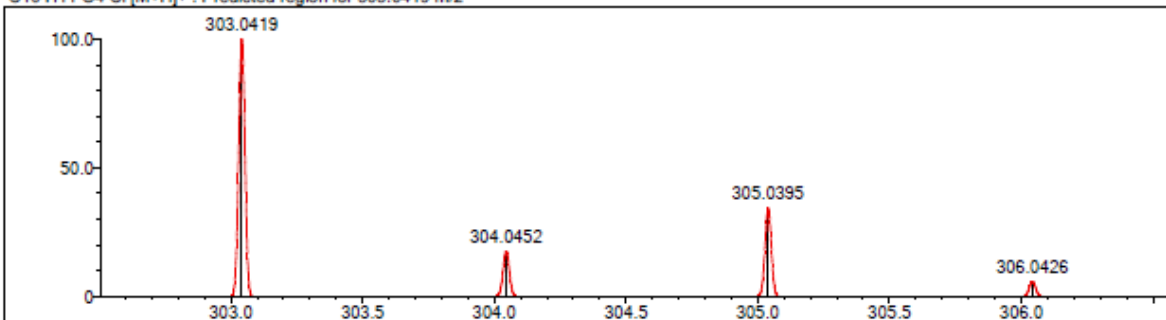
Rank	Score	Formula (M)	Ion	Meas. m/z	Pred. m/z	Df. (mDa)	Df. (ppm)	Iso	DBE
1	87.53	C16 H11 O4 Cl	[M+H]+	303.0416	303.0419	-0.3	-0.99	87.53	11.0
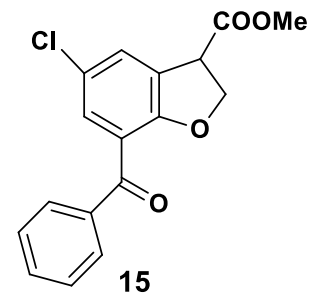
Data File: C:\LabSolutions\Data\Revathi\DJH\DJH Data from Batch file\DJH_Vial1.lcd

Elmt	Val.	Min	Max	Use Adduct
H	1	0	50	H
C	4	0	30	Na
N	3	0	0	K
O	2	0	5	HCOO
Cl	1	0	5	CH3CN

Error Margin (mDa): 10.0
HC Ratio: 0.0 - 3.0
Max Isotopes: all
MSn Iso RI (%): 75.00

DBE Range: -100.0 - 100.0
Apply N Rule: yes
Isotope RI (%): 1.00
MSn Logic Mode: OR

Electron Ions: both
Use MSn Info: no
Isotope Res: 10000
Max Results: 3

Event#: 1 MS(E+) Ret. Time : 0.048 -> 0.190 - 0.174 -> 0.986 Scan# : 7 -> 25 - 23 -> 125
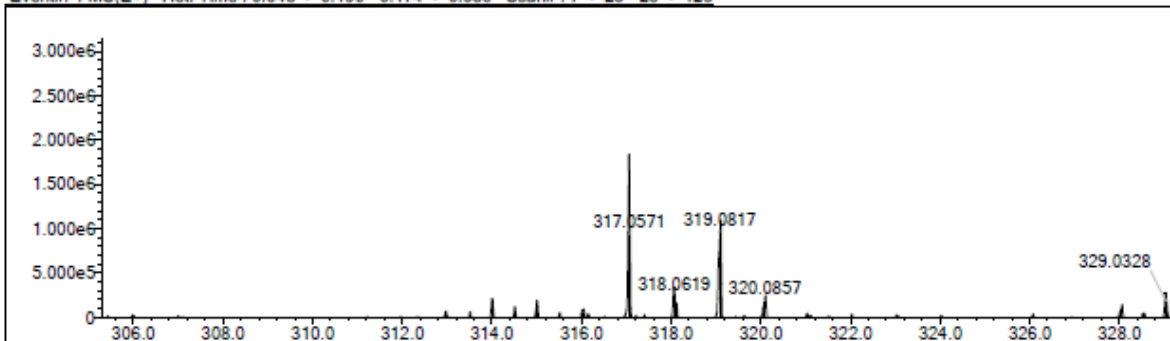
Measured region for 317.0571 m/z
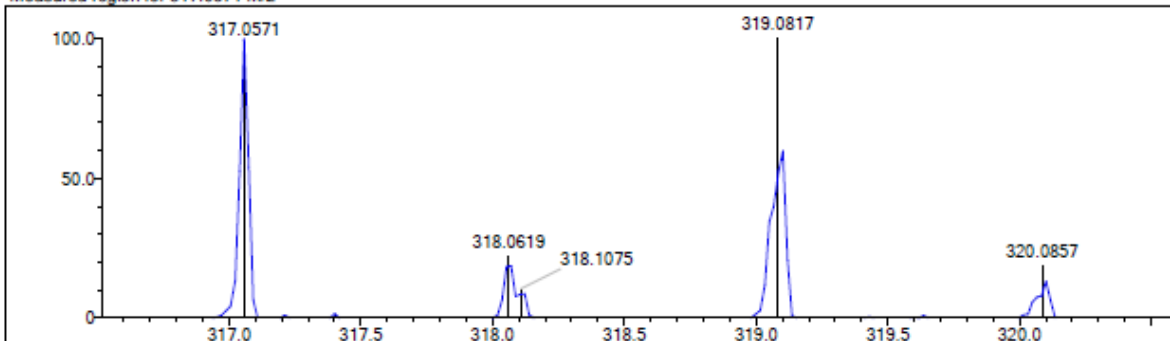
C17 H13 O4 Cl [M+H]+ : Predicted region for 317.0575 m/z
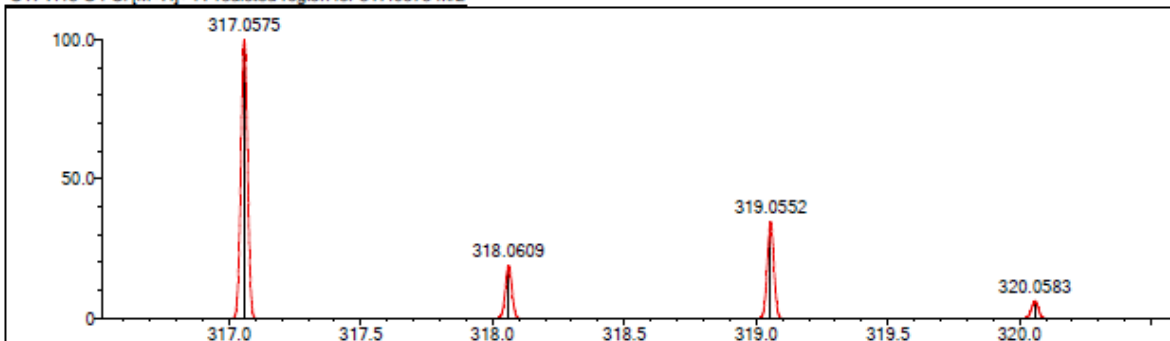
Rank	Score	Formula (M)	Ion	Meas. m/z	Pred. m/z	Df. (mDa)	Df. (ppm)	Iso	DBE
1	61.65	C17 H13 O4 Cl	[M+H]+	317.0571	317.0575	-0.4	-1.26	62.05	11.0

Data File: C:\LabSolutions\Data\Revathi\DJH\vial 5 DJH.lcd

Elmt	Val.	Min	Max
H	1	0	50
C	4	0	30
N	3	0	0
O	2	4	5
F	1	0	5

Elmt	Val.	Min	Max
Cl	1	0	5

| Use Adduct |
|------------|
| H |
| Na |
| K |
| HCOO |
| CH3CN |

Error Margin (mDa): 10.0
HC Ratio: 0.0 - 3.0
Max Isotopes: all
MSn Iso RI (%): 75.00

DBE Range: -100.0 - 100.0
Apply N Rule: yes
Isotope RI (%): 1.00
MSn Logic Mode: OR

Electron Ions: both
Use MSn Info: no
Isotope Res: 10000
Max Results: 4

26
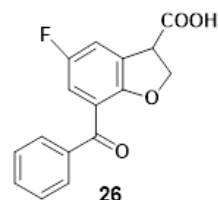
Event#: 1 MS(E+) Ret. Time : 0.048 -> 0.174 - 0.143 -> 0.838 Scan# : 7 -> 23 - 19 -> 107

271.8897
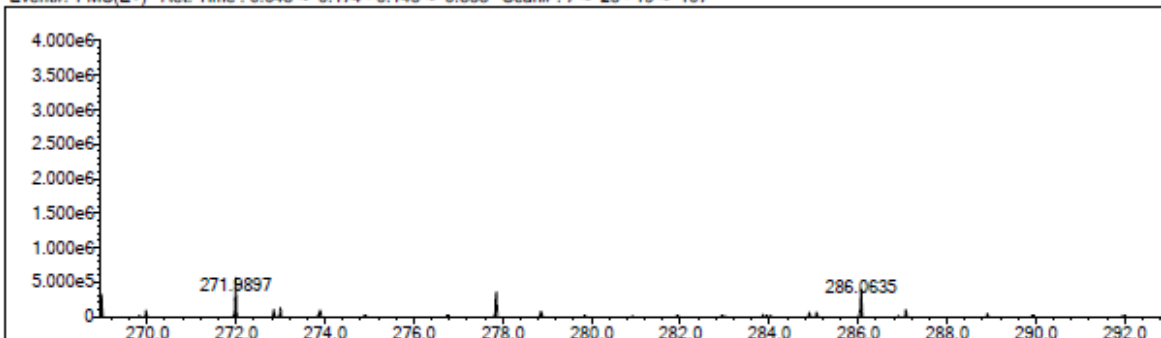
286.0635

Measured region for 286.0635 m/z

286.0635

287.0734
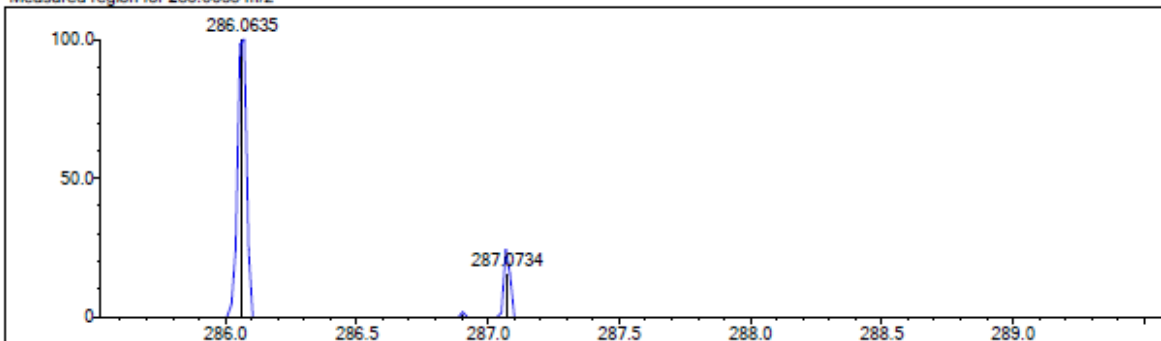
C16 H11 O4 F M+ : Predicted region for 286.0636 m/z

286.0636

287.0670
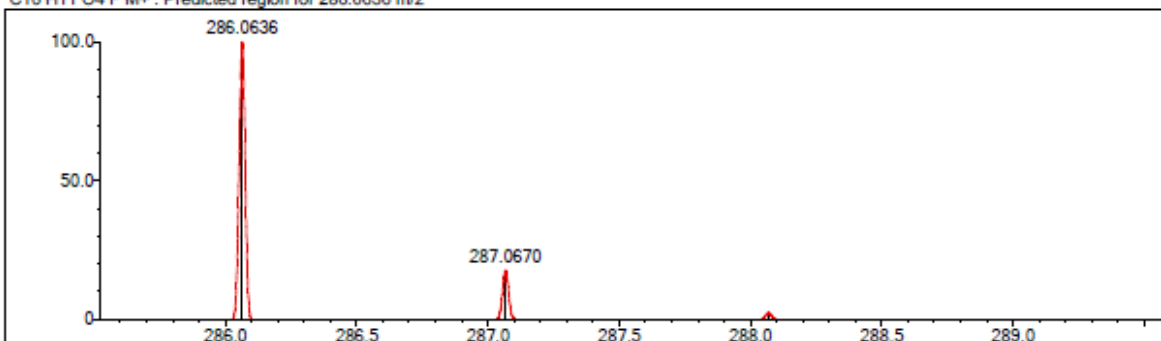
Rank	Score	Formula (M)	Ion	Meas. m/z	Pred. m/z	Df. (mDa)	Df. (ppm)	Iso	DBE
1	58.70	C16 H11 O4 F	M+	286.0635	286.0636	-0.1	-0.35	58.70	11.0

Data File: C:\LabSolutions\Data\Revathi\DJH\DJH Data from Batch file\DJH_Vial4.lcd

Elmt	Val.	Min	Max	Use Adduct
H	1	0	50	H
C	4	0	30	Na
N	3	0	0	K
O	2	0	5	NH4
Cl	1	0	0	HCOO
				CH3CN

Error Margin (mDa): 10.0
HC Ratio: 0.0 - 3.0
Max Isotopes: all
MSn Iso RI (%): 75.00

DBE Range: -100.0 - 100.0
Apply N Rule: yes
Isotope RI (%): 1.00
MSn Logic Mode: OR

Electron Ions: both
Use MSn Info: no
Isotope Res: 10000
Max Results: 20

30
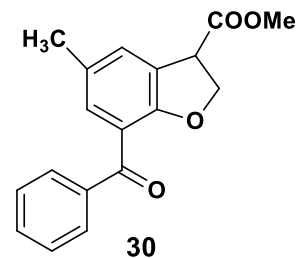
Event#: 1 MS(E+)   Ret. Time : 0.048 -> 0.190 - 0.190 -> 0.984   Scan# : 7 -> 25 - 25 -> 125

Measured region for 282.0890 m/z
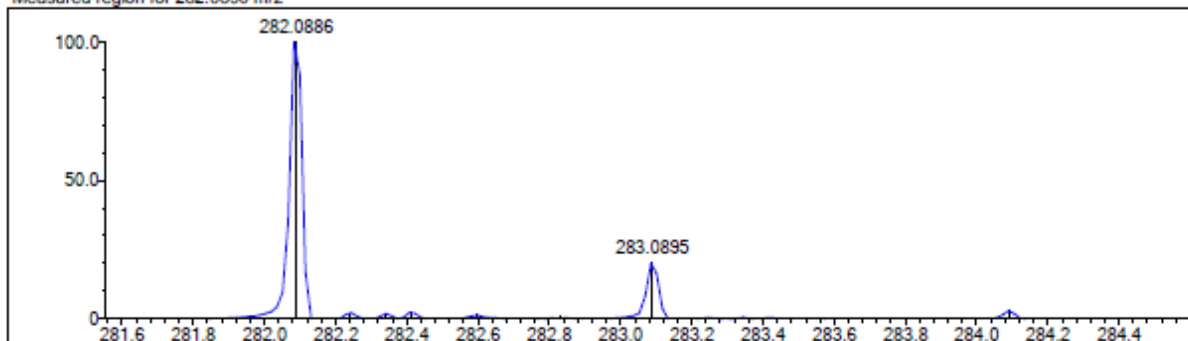
C17 H14 O4 M+ : Predicted region for 282.0887 m/z
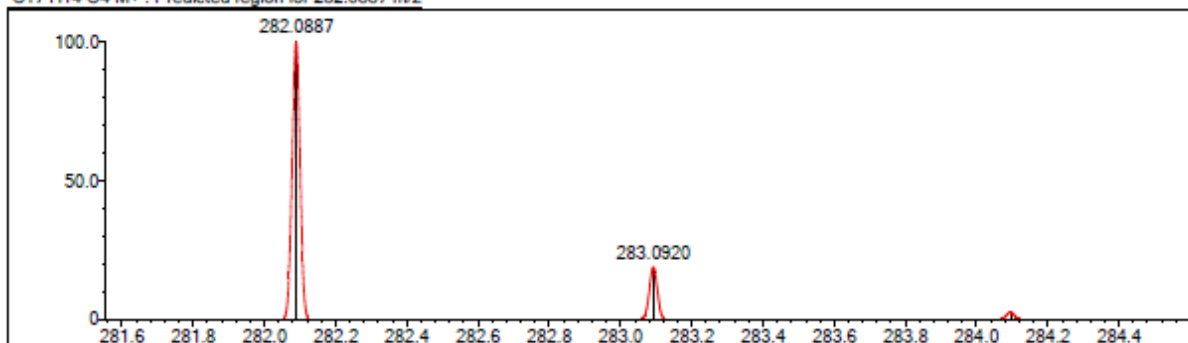
Rank	Score	Formula (M)	Ion	Meas. m/z	Pred. m/z	Df. (mDa)	Df. (ppm)	Iso	DBE
1	85.42	C17 H14 O4	M+	282.0890	282.0887	0.3	1.06	85.55	11.0
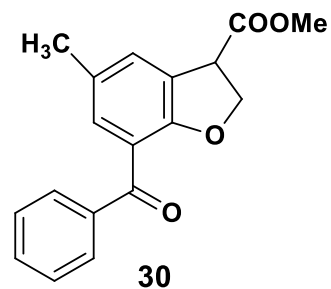
30

| Elmt	Val.	Min	Max	Use Adduct
H	1	0	50	H
C	4	0	30	Na
N	3	0	0	K
O	2	0	5	NH4
Cl	1	0	0	HCOO
				CH3CN

Error Margin (mDa): 10.0
HC Ratio: 0.0 - 3.0
Max Isotopes: all
MSn Iso RI (%): 75.00

DBE Range: -100.0 - 100.0
Apply N Rule: yes
Isotope RI (%): 1.00
MSn Logic Mode: OR

Electron Ions: both
Use MSn Info: no
Isotope Res: 10000
Max Results: 20

Event#: 1 MS(E+) Ret. Time : 0.063 -> 0.222 - 0.222 -> 0.976 Scan# : 9 -> 29 - 29 -> 125
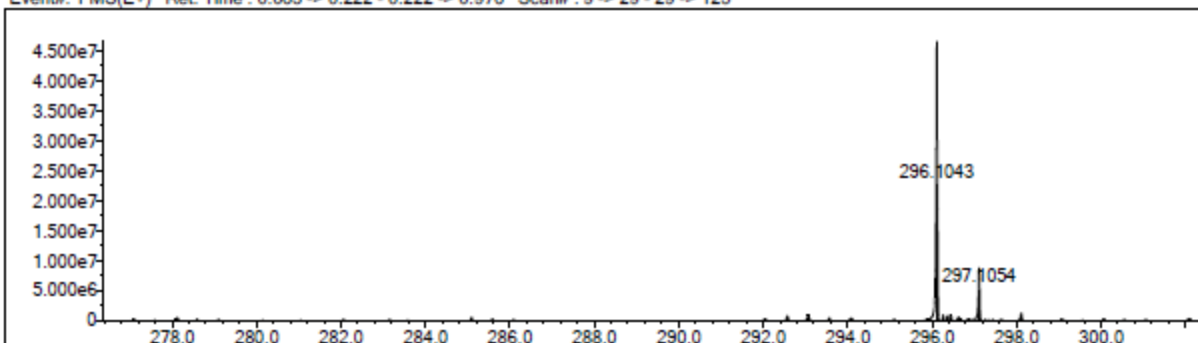
Measured region for 296.1040 m/z
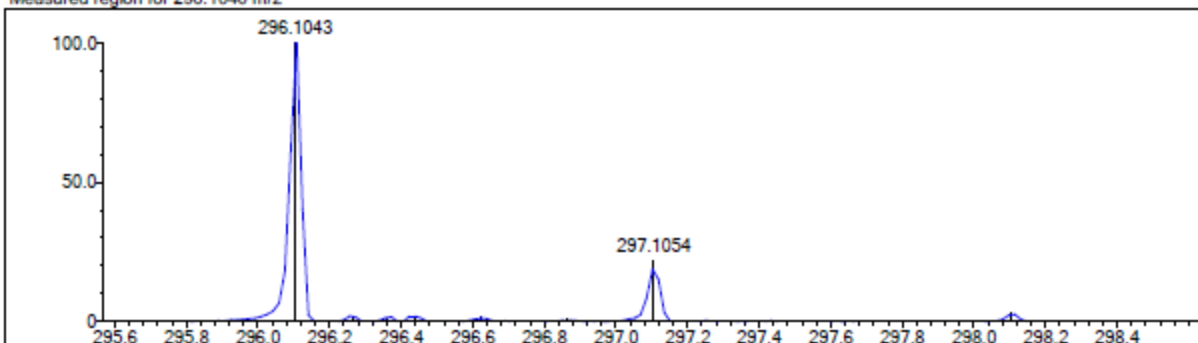
C18 H16 O4 M+ : Predicted region for 296.1043 m/z
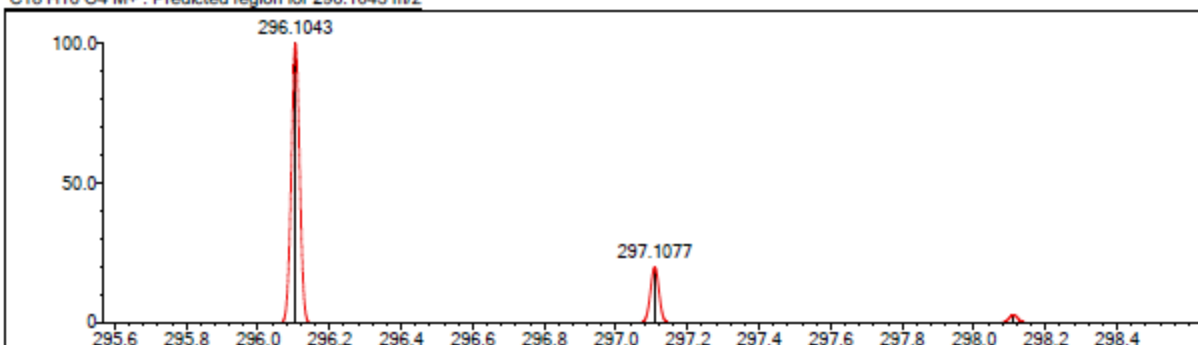
Rank	Score	Formula (M)	Ion	Meas. m/z	Pred. m/z	Df. (mDa)	Df. (ppm)	Iso	DBE
1	75.19	C18 H16 O4	M+	296.1040	296.1043	-0.3	-1.01	75.20	11.0

Data File: C:\LabSolutions\Data\Revathi\CF3.lcd

Elmt	Val.	Min	Max	Use Adduct
H	1	0	50	H
C	4	0	30	Na
N	3	0	0	K
O	2	0	5	NH4
F	1	0	10	CH3OH
Cl	1	0	5	H2O
				HCOO
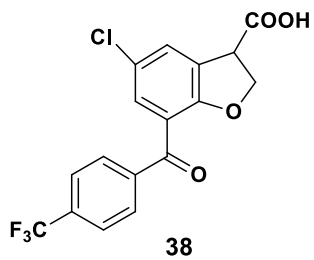
Error Margin (mDa): 10.0
HC Ratio: 0.0 - 3.0
Max Isotopes: all
MSn Iso RI (%): 75.00

DBE Range: -100.0 - 100.0
Apply N Rule: yes
Isotope RI (%): 1.00
MSn Logic Mode: OR

Electron Ions: both
Use MSn Info: no
Isotope Res: 10000
Max Results: 5

Event#: 1 MS(E+) Ret. Time : 0.048 -> 0.253 - 0.253 -> 0.976 Scan# : 7 -> 33 - 33 -> 125
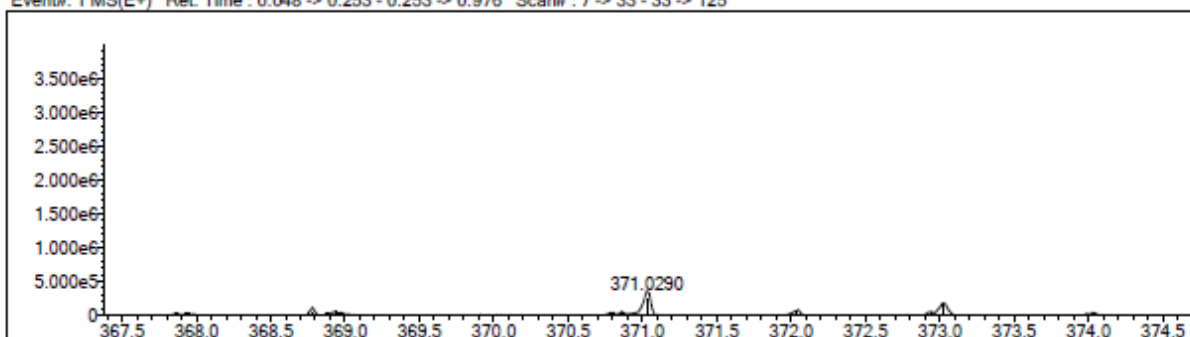
Measured region for 371.0290 m/z
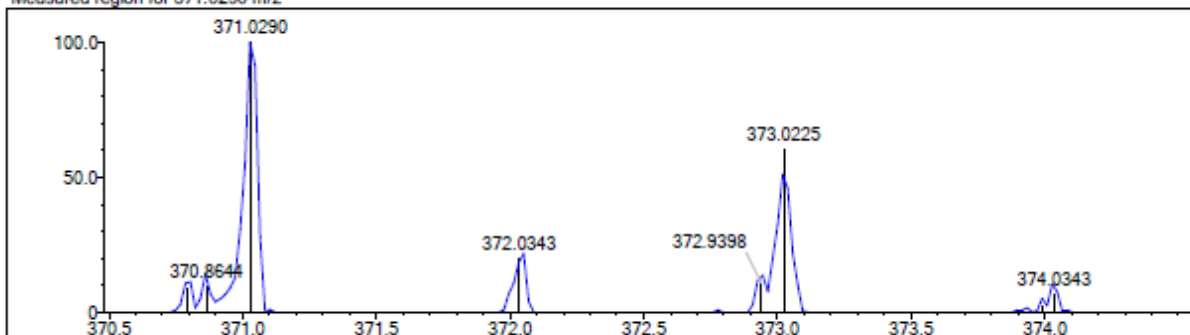
C17 H10 O4 F3 Cl [M+H]+ : Predicted region for 371.0292 m/z
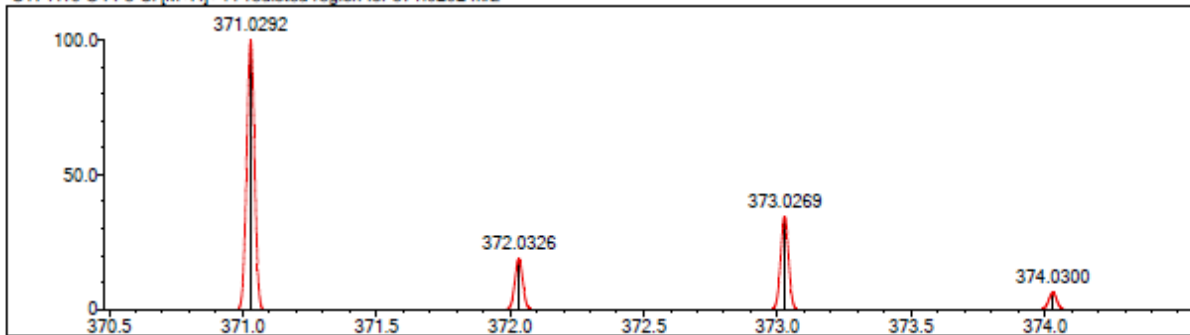
Rank	Score	Formula (M)	Ion	Meas. m/z	Pred. m/z	Df. (mDa)	Df. (ppm)	Iso	DBE
1	52.50	C17 H10 O4 F3 Cl	[M+H]+	371.0290	371.0292	-0.2	-0.54	52.50	11.0

199

Data File: C:\LabSolutions\Data\Revathi\DJH\DJH Data from Batch file\DJH_Vial6.lcd

| Elmt	Val.	Min	Max	Use Adduct
H	1	0	50	H
C	4	0	30	Na
N	3	0	0	K
O	2	0	5	NH4
F	1	0	5	HCOO
Cl	1	0	5	CH3CN

Error Margin (mDa): 10.0
HC Ratio: 0.0 - 3.0
Max Isotopes: all
MSn Iso RI (%): 75.00

DBE Range: -100.0 - 100.0
Apply N Rule: yes
Isotope RI (%): 1.00
MSn Logic Mode: OR

Electron Ions: both
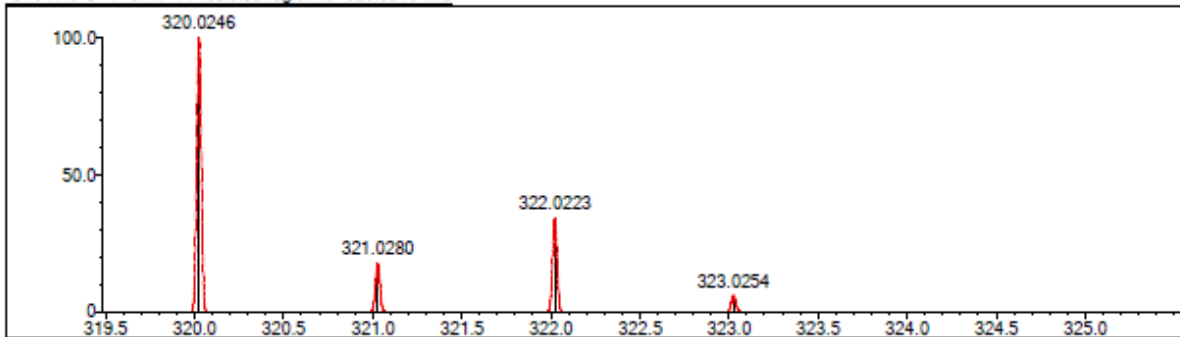Use MSn Info: no
Isotope Res: 10000
Max Results: 4

41
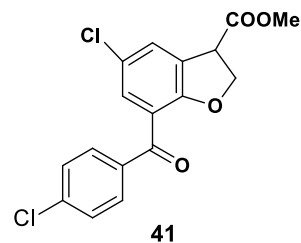
Event#: 1 MS(E+)   Ret. Time : 0.048 -> 0.174 - 0.174 -> 0.903   Scan# : 7 -> 23 - 23 -> 115
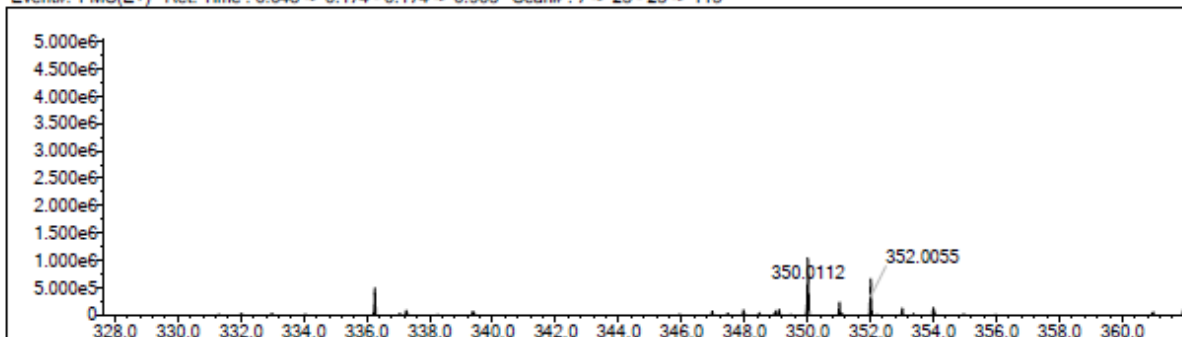
Measured region for 350.0112 m/z
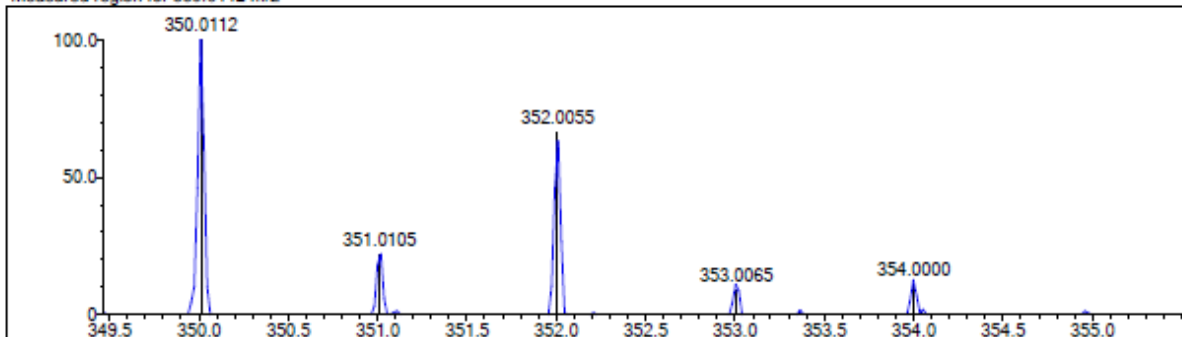
C17 H12 O4 Cl2 M+ : Predicted region for 350.0107 m/z
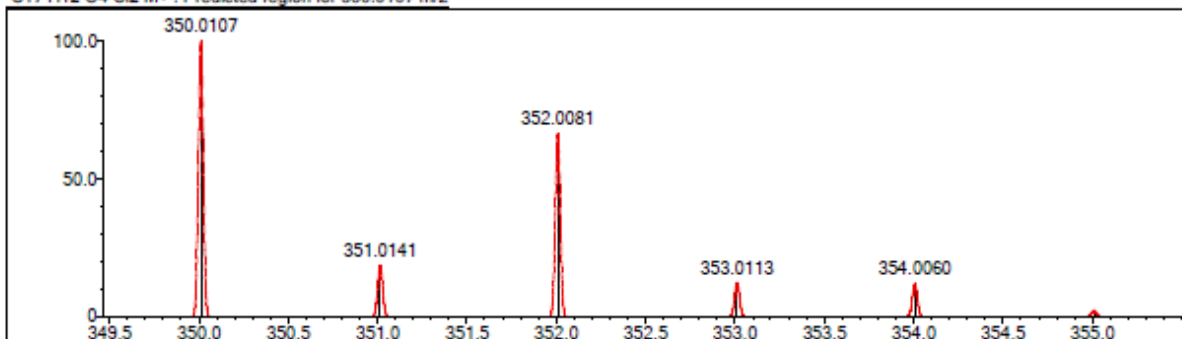
Rank	Score	Formula (M)	Ion	Meas. m/z	Pred. m/z	Df. (mDa)	Df. (ppm)	Iso	DBE
1	88.84	C17 H12 O4 Cl2	M+	350.0112	350.0107	0.5	1.43	89.81	11.0
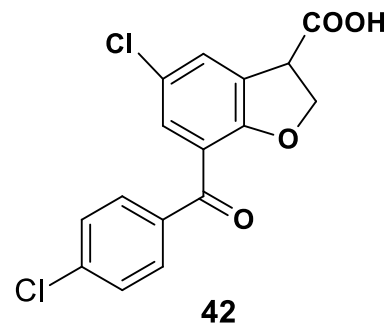
Data File: C:\LabSolutions\Data\Revath\DJH\DJH Data from Batch file\DJH_Vial7.lcd

Elmt	Val.	Min	Max	Use Adduct
H	1	0	50	H
C	4	0	30	Na
N	3	0	0	K
O	2	0	5	NH4
F	1	0	5	HCOO
Cl	1	0	5	CH3CN

Error Margin (mDa): 10.0
HC Ratio: 0.0 - 3.0
Max Isotopes: all
MSn Iso RI (%): 75.00

DBE Range: -100.0 - 100.0
Apply N Rule: yes
Isotope RI (%): 1.00
MSn Logic Mode: OR

Electron Ions: both
Use MSn Info: no
Isotope Res: 10000
Max Results: 4

Event#: 1 MS(E+)   Ret. Time : 0.048 -> 0.190 - 0.174 -> 0.993   Scan# : 7 -> 25 - 23 -> 127
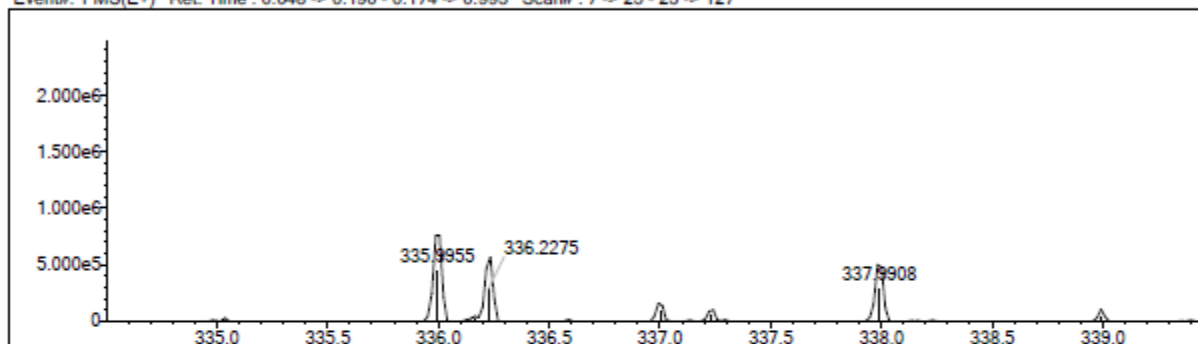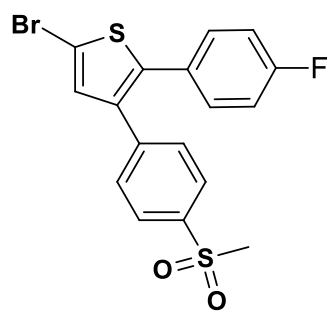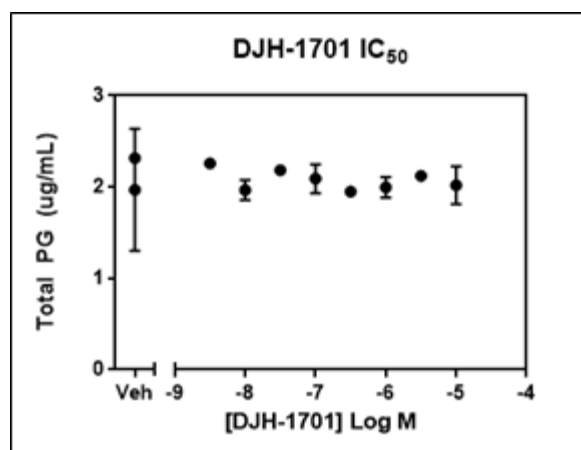
Measured region for 335.9955 m/z
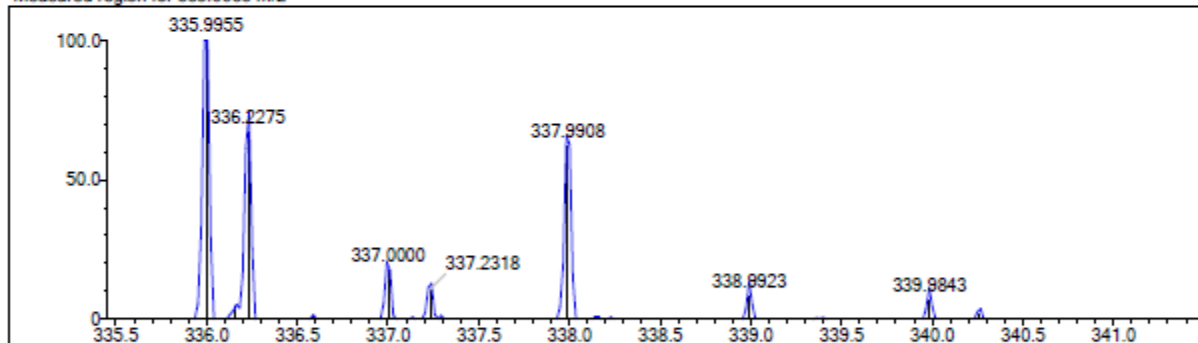
C16 H10 O4 Cl2 M+ : Predicted region for 335.9951 m/z
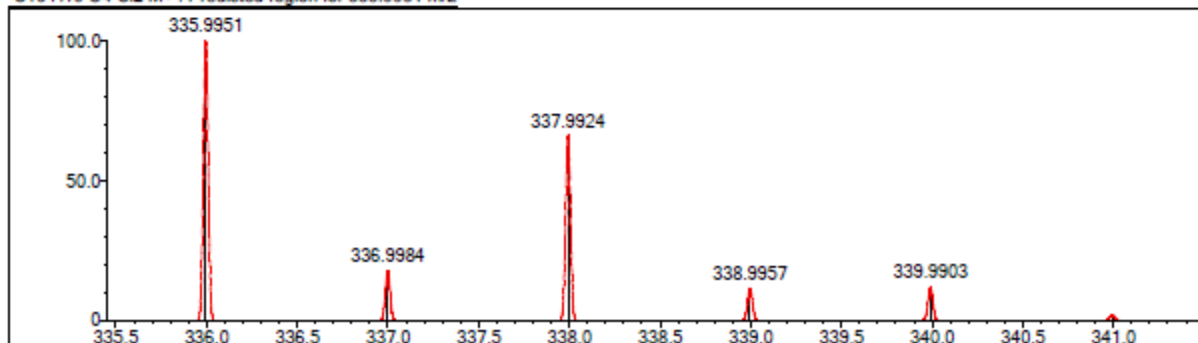
Rank	Score	Formula (M)	Ion	Meas. m/z	Pred. m/z	Df. (mDa)	Df. (ppm)	Iso	DBE
1	99.53	C16 H10 O4 Cl2	M+	335.9955	335.9951	0.4	1.19	100.00	11.0

201

Data File: C:\LabSolutions\Data\Revathi\DJH\DJH Data from Batch file\DJH_Vial9.lcd

Elmt	Val.	Min	Max	Use Adduct
H	1	0	50	H
C	4	0	30	Na
N	3	0	0	K
O	2	0	5	NH4
F	1	0	5	HCOO
Cl	1	0	5	CH3CN

Error Margin (mDa): 10.0
HC Ratio: 0.0 - 3.0
Max Isotopes: all
MSn Iso RI (%): 75.00

DBE Range: -100.0 - 100.0
Apply N Rule: yes
Isotope RI (%): 1.00
MSn Logic Mode: OR

Electron Ions: both
Use MSn Info: no
Isotope Res: 10000
Max Results: 4

40
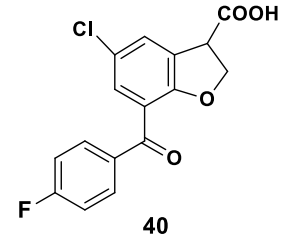
Event#: 1 MS(E+)   Ret. Time : 0.048 -> 0.174 - 0.158 -> 0.979   Scan# : 7 -> 23 - 21 -> 125
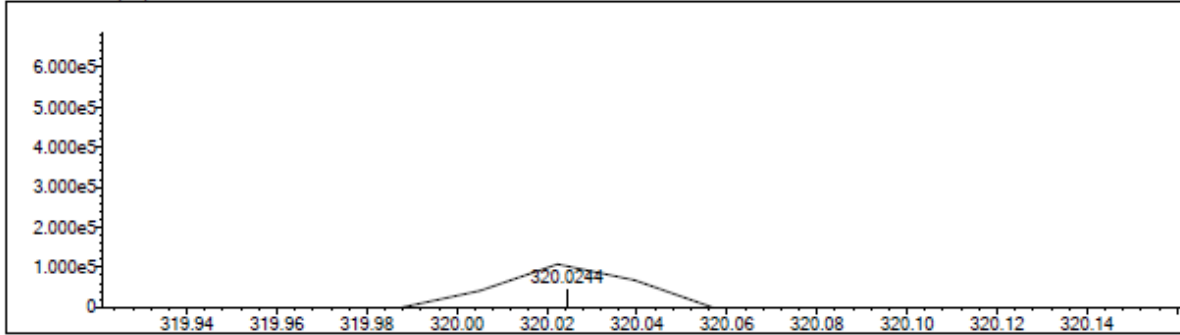
320.0244

Measured region for 320.0244 m/z

320.0244
322.0213
322.3108
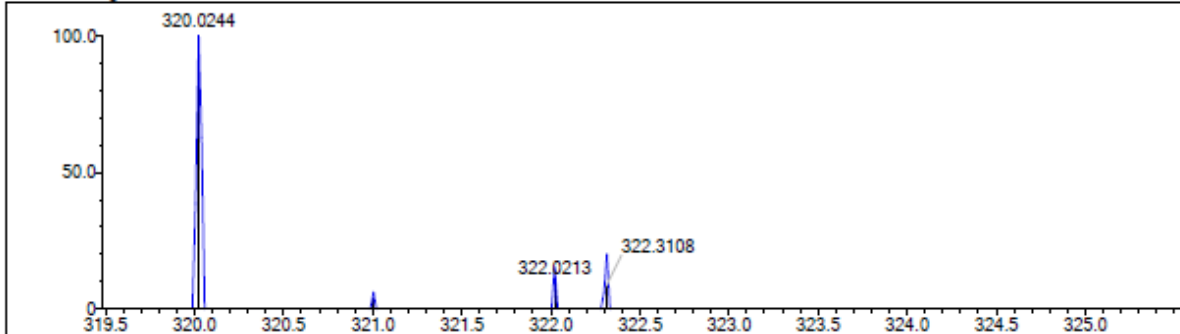
C16 H10 O4 F Cl M+ : Predicted region for 320.0246 m/z

320.0246
321.0280
322.0223
323.0254

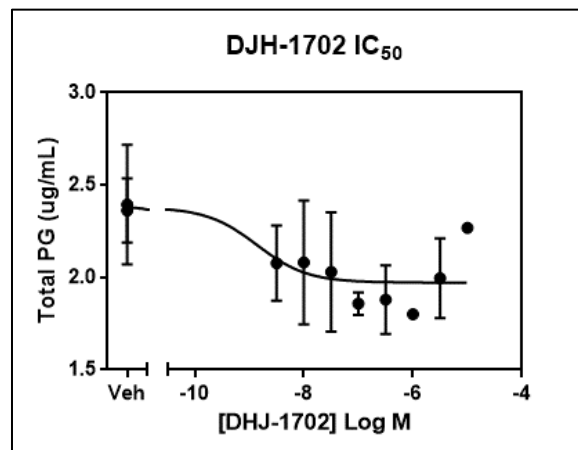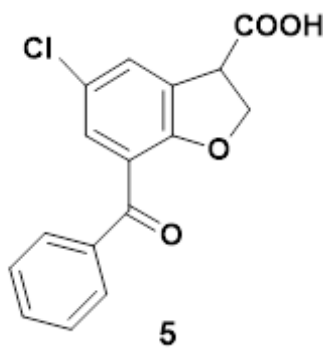| Rank	Score	Formula (M)	Ion	Meas. m/z	Pred. m/z	Df. (mDa)	Df. (ppm)	Iso	DBE
1	51.66	C16 H10 O4 F Cl	M+	320.0244	320.0246	-0.2	-0.62	51.66	11.0

APPENDIX D:

Biological Data

COX -2 Inhibition Studies

15

DJH-1701 IC$_{50}$

DuP-697

Control

DuP-697 IC$_{50}$

5

DJH-1702 IC$_{50}$

26

DJH-1707 IC$_{50}$

205

30

DJH-1703 IC$_{50}$

31

DJH-1704 IC$_{50}$

41

40

38
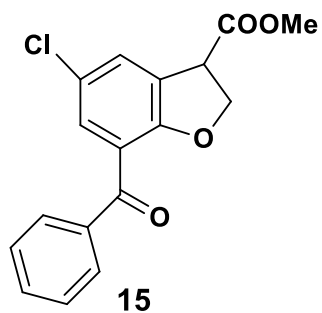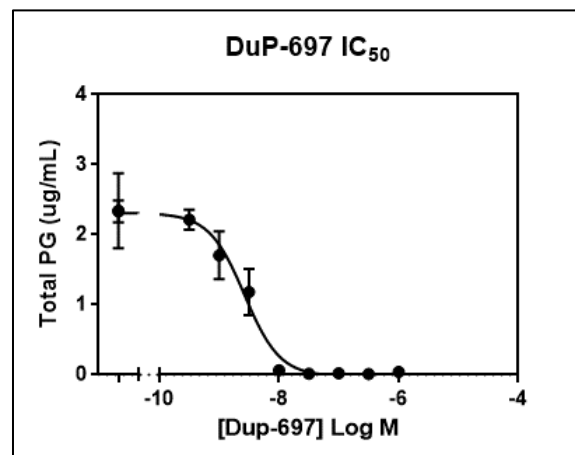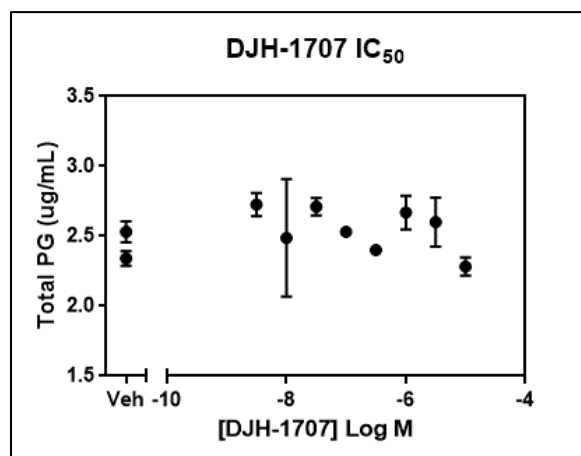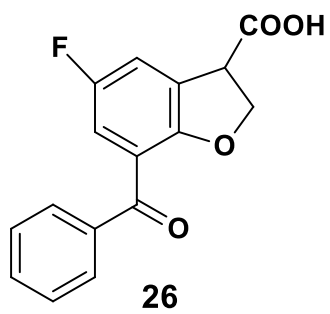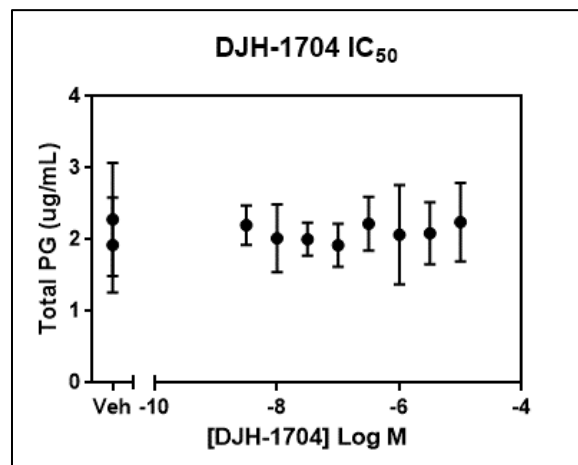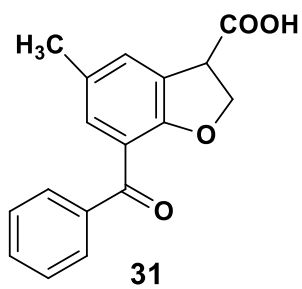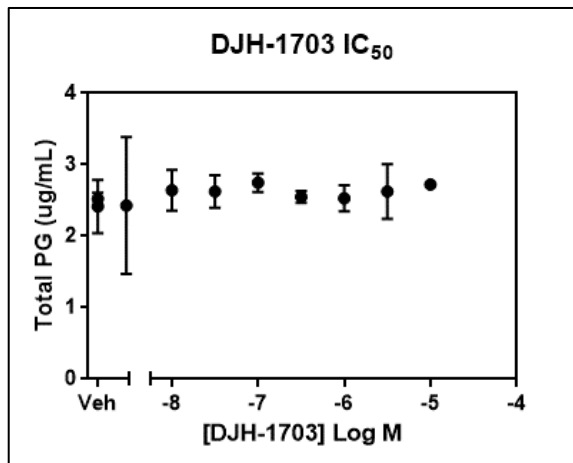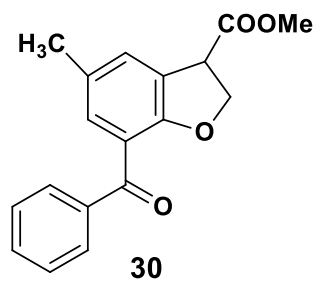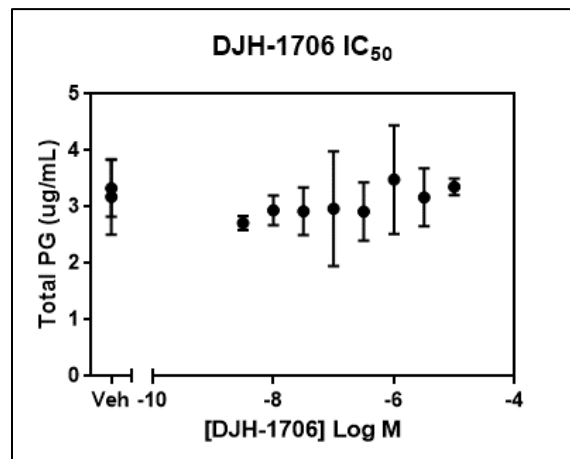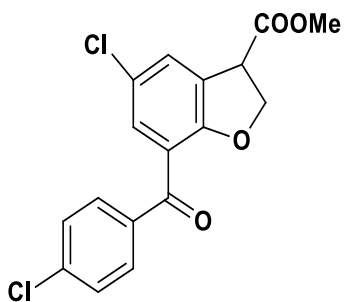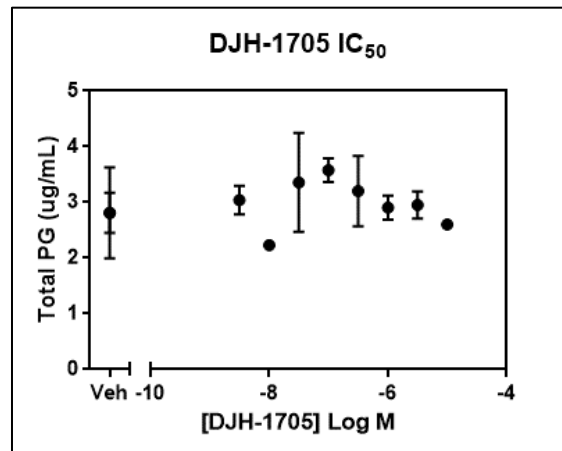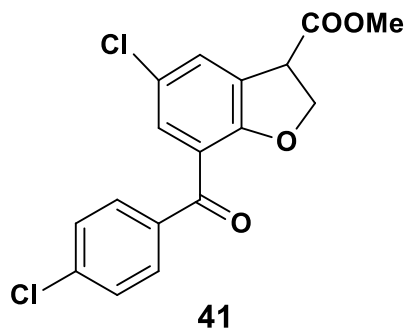
CURRICULUM VITAE

SHAMSUL AREFIN AHMED

Highlights

- Extensive experience in multi-steps organic synthesis and method development.
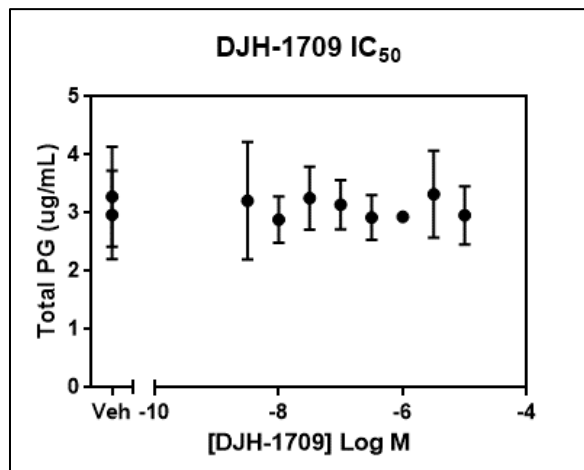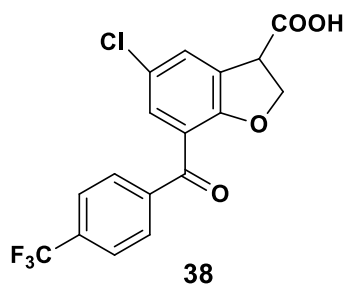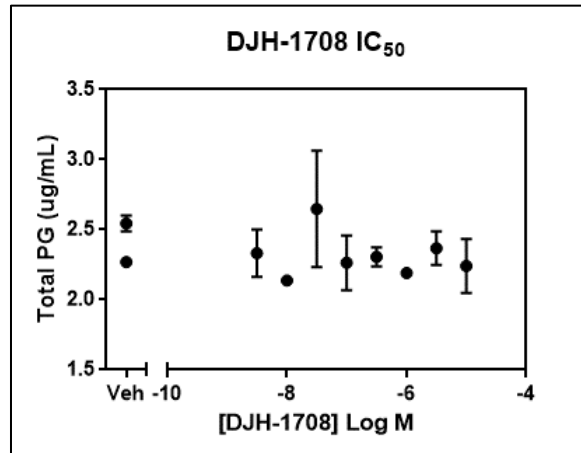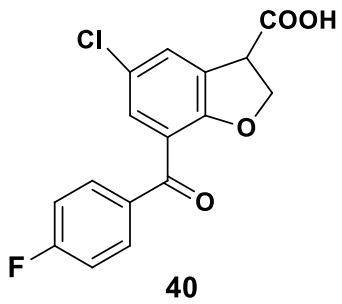- Asymmetric synthesis and analysis of enantiomeric excess using HPLC.
- Analysis of organic compounds using NMR (e.g., ^{1}H, ^{13}C, DEPT, COSY, NOESY, HSQC, HMBC etc.), LC-MS, MALDI-TOF, HPLC, FT-IR, GC, UV-visible spectroscopy and Polarimetry.
- Well-versed and experienced in the principles of drug design, synthesis, and evaluation of biological activity.
- Scale-up organic reactions on from milligram to kilogram scale, and conduct multiple reactions at the same time.
- Team builder and motivator.
- Hands-on experience with moisture and air-sensitive reaction techniques.
- Strong written, oral communication and interpersonal skill.
- Computer skills: MS Office, ChemDraw, literature searching via ACS SciFinder and Reaxys, Topspin NMR software, as well as Breeze Waters HPLC software

Education

Ph.D. Organic Chemistry, University of Wisconsin-Milwaukee, Milwaukee, WI 53211
December '2017

MS, Applied Chemistry & Chemical Technology, University of Dhaka, Bangladesh, 1996

BS, Applied Chemistry & Chemical Technology, University of Dhaka, Bangladesh, 1994

Employment

September,2009 – Present   Research/Teaching Assistant, Department of Chemistry
            & Biochemistry, University of Wisconsin- Milwaukee.

- Designed and developed a short and effective procedure for the synthesis of benzofuran ring containing compound BRL-37959 and its analogs.
- Designed and discovered that BRL-37959 and its analogs are anticancer drugs.
- Experienced in the design, synthesis, functionalization, characterization and biological evaluation of BRL-37959 as a COX1 inhibitor.
- Proficient in laboratory techniques, including crystallizations, reagent preparation, titrations, spectrophotometric determinations.
- Led discussions and lab class for Chemistry: Introductory General Chemistry, General Chemistry, Introductory Organic Chemistry & Survey of Biochemistry, General Chemistry & Qualitative Analysis, Introductory to Organic Chemistry and Organic Chemistry labs.

  The main responsibilities in a problem-solving discussion classes and laboratories are:
  - Prepare and deliver lectures to students.
  - Evaluate and grade students' class work, laboratory performance, assignments, and exam papers.

June,2016 – Augest,2016   Summer Internship (R&D Chemistry), Millipore-Sigma,
            Milwaukee, Wisconsin.

- Scale up multi-steps (5-8 steps) organic synthesis from milligram scale to gram scale and run multiple reactions at the same time.
- Large scale purification process of desired products.
- Safety and Hazardous training for Industrial R& D
- Hands on experience of Electronic lab book writing, SOP and ordering chemicals.

2007– 2009   Shift-In Charge, Mohadevi INC. New York

2004 – 2007   Assistant Chief, Planning   Commission, Govt. of the People's Republic
            of Bangladesh.

2001 – 2004   Assistant Chief, Ministry of Civil Aviation & Tourism, Govt. of the

People's Republic of Bangladesh.

1999 – 2001   Assistant Chief, Ministry of Industries, Govt. of the People's Republic
                       of Bangladesh.

1996 – 1999   Quality Control Chemist, Pragati Pharmaceuticals, Dhaka, Bangladesh.

1994 – 1996   Researcher, University of Dhaka, Bangladesh.

- Studies on Color Removal of Textile-Dying Effluents with Activated Carbons Produced From   Various Indigenous Vegetable Sources.

Publications and Presentations

- '' New COX Inhibitors as Anticancer Agents" **Shamsul Arefin Ahmed,** M. Mahmun Hossain**,** Patent application submitted.
- "BRL-37959 and its analogs: New COX inhibitors and Anticancer Agents" **Shamsul Arefin Ahmed,** Damon Hinz, M. Mahmun Hossain, Manuscript in preparation.
- "Short and Cost-effective method for the synthesis of Benzofuran ring containing compound BRL-37959 and its analogs" **Shamsul Arefin Ahmed,** Damon Hinz, M. Mahmun Hossain, Manuscript in preparation.
- **S.A. Ahmed**, D. Hinj, M. Jellen, M. Hossain." Synthesis and biological evaluation of benzofuran ring containing compound BRL-37959 and its analogs" Abstracts of Papers, 251st ACS National Meeting & Exposition, San Diego, California, USA, 2016, March 13-17 MEDI-369.
- **Shamsul Arefin Ahmed**, D. Hinj, M. Jellen, M. Hossain." Synthesis of COX 1 inhibitor: Benzofuran ring containing compound BRL-37959 and its analogs "ACS Milwaukee Section Meeting, Milwaukee, March 31, 2016.

- Presented research outcomes in Research Symposiums UW-Milwaukee, 2009-2017.
- Graduate Student Seminar, Department of Chemistry and Biochemistry, UW-Milwaukee.

Awards

- McFarland Graduate Research Award in Research Symposiums, Department of Chemistry and Biochemistry, UW-Milwaukee,2017.
- ACS Milwaukee Section Travel Award, 2016.
- Graduate School Travel Award, 2016, UW-Milwaukee,
- Graduate Student Travel Award, 2016, Department of Chemistry and Biochemistry, UW-Milwaukee.

- Chemistry and Biochemistry Graduate Student Council Travel Grant, 2016, UW-Milwaukee.
- UW- Milwaukee Chancellor's Fellowship, 2009-2014.
- University Merit and Govt. Scholarships both in BS and MS classes (University of Dhaka, Bangladesh).

Professional Affiliations

- Member of the American Chemical Society
- Member of the American Chemical Society, Milwaukee Section.